CRYSTALLIZATION ENGINEERING TECHNIQUES FOR DEVELOPING A NOVEL DRY POWDER INHALER FORMULATION FOR IBUPROFEN

Afrina Afrose

B. Pharm (Honours), M. Pharm

Submitted in fulfilment of the requirements for the degree of

Doctor of Philosophy

School of Clinical Sciences

Faculty of Health

Queensland University of Technology

2017

"Verily, with hardship, there is relief"

- Al Quran

Keywords

Anti-solvent precipitation crystallization (APC), Dry powder inhaler (DPI), D-mannitol, Water-Ethanol co-solvent, Hydroxypropylmethylcellulose (HPMC), Ibuprofen (IBP), Pluronic F127 (Pl F127), L-leucine, Solubility, UV spectrophotometry, Calibration, Dissolution equilibrium, Plackett-Burman design, Laser diffraction, Particle size, Density and flowability, Crystallinity, Particle morphology, Drug dispersibility, Scanning electron microscopy (SEM), Transmission electron microscopy (TEM), Differential scanning calorimetry (DSC), X-ray diffraction (XRD), Raman spectroscopy, Twin stage impinger (TSI).

Abstract

In recent years, there has been an upwelling in research into the aerosol systems projected for therapeutics that are conventionally not delivered via that route [1, 2]. The bioavailability of ibuprofen (IBP), a non-steroidal anti-inflammatory drug from the currently available dosage forms (oral and topical), is poor and these formulations are marketed with high dose which can produce significant adverse reactions in long term use [3-5]. This investigation aims to use IBP preparation by developing a controlled engineering method of producing fine (< 5 μm) crystals for pulmonary delivery from dry powder inhaler (DPI) formulation with very low dose. In the context of inhalation systems, IBP has been taken as a model drug.

The techniques of producing respirable size (< 5 μm) particles for dry powder inhaler (DPI) formulations mostly involve crystallization followed by high energy input size reduction systems like milling and homogenization. Particles produced in such processes have a very high surface energy and poor flow property which restricts the efficient dispersal of the DPI in to the deep lungs.

This investigation has used an anti-solvent precipitation crystallization (APC) method of producing fine IBP (< 5 μm) crystals for pulmonary delivery from DPI formulation with very low dose. In this process, the poorly water-soluble drug (IBP) was dissolved in a solvent (ethanol), and the solution was added into a miscible non-solvent (water) with additives (HPMC, Pluronic F127, D-mannitol & L-leucine) under agitation. The crystallization method, solvent, anti-solvent and additives were selected based on the evidence reported in currently available literature.

In the first phase of this dissertation, IBP solubility was investigated in the selected solvent-anti-solvent system, namely water-ethanol co-solvents at 10, 25 and 40 °C. It was found that the solubility of IBP increased considerably when ethanol contents were increased, and also increases with temperature. A correlation of fit of all measured data was established with published IBP solubility data at high aqueous ethanol (> 50 %). The experimental solubility data of IBP in the presence of additives as single component and in combination revealed the trend quantitatively.

The results allowed calculation of the minimum amount of initial drug to be used to precipitate IBP and to determine the drug yield value after the precipitation

crystallization to produce fine (< 5 µm) IBP crystals for DPI formulations. The solubility investigation also revealed that Pluronic F127 and L-leucine enhance IBP solubility, whereas HPMC and mannitol show little or no effect.

In the second phase of this research, the Plackett-Burman design revealed batch size, ultrasound and stirring speed as the significant process variables for particle size reduction in APC process. Optimised levels of temperature (25 °C), ultrasound (30 minutes), stirring duration (> 20 minutes) and the additive concentrations HPMC (0.2%), Pl F127(1.3%), leucine (1.2%) and mannitol (8.6%) were determined to produce IBP particles with a volume median diameter of 3.9 ± 0.4 µm.

In the third phase of this thesis, DPI formulations were prepared and characterized for density and flowability, size and aerodynamic diameter, crystallinity and drug dispersilibity in a twin stage impinger with respect to the composition, batch size and drug-additive concentrations. It was observed that the presence of leucine and mannitol in the formulation improved the flowability, lowered particle aerodynamic diameter and showed a higher percentage of FPF in the drug dispersibility test. Finally, all the formulation characterization results indicated that a high percentage of crystalline IBP phase in the formulation (by differential scanning calorimetry and X-ray diffraction) positively influenced the drug dispersibility in the *in vitro* aerosolization test. Surprisingly, the milled raw IBP powder dispersed a higher percentage of the drug due to the surface morphology (corrugated) than those of IBP particles produced in the APC process.

The maximum drug release from milled pure IBP was 81 % after 90 minutes of dissolution, whereas from the prepared formulations F4, F6 and F10 were 100, 87% and 96% at 90, 60 and 60 minutes respectively. The dissolution profile indicated F4 formulation achieves the 100% release of the drug and F6 formulation showed the faster dissolution which is 96% at 60 minutes comparing to other formulations. The outcomes of the dissolution test and the fine particle dose (FPD) of the prepared formulations (554 µg, 574.0 µg & 413.8 µg from the formulations F4, F6 and F10, respectively) indicated the future potential for inhalation to improve the IBP drug delivery by lowering the dose and increasing the bioavailability. Moreover, the faster dissolution performance of the prepared powder formulations will contribute to the development of other dosage form like tablet or capsule to achieve an improved bioavailability of IBP other than the currently marketed formulations.

Table of Contents

List of Figures

List of Tables

Nomenclature

List of Abbreviations

API	Active Pharmaceutical Ingredient
APC	Anti-solvent Precipitation Crystallization
BDP	Beclomethasone-17,21-dipropionate
BCS	Biopharmaceutics Classification System
COPD	Chronic obstructive pulmonary disease
CAB	Cohesive–adhesive balance
CM	Commercial mannitol
C_i	Solute concentration on the particle surface (w/w, g/g)
C^*	Saturation concentration (w/w, g/g)
C	Solute molar concentration (mol/L)
DPI	Dry powder inhaler
d	Particle diameter (μm)
d_{ae}	Aerodynamic diameter (μm)
dN/dt	Nucleation rate (g/min)
Dif	Diffusion coefficient
ED	Emitted dose
ER	Elongation ratio
EM	Drug emission
E	Ethanol
FPF	Fine particle fraction
FP	Fluticasone propionate
FIR	Flow increase rate

List of Abbreviations

GI	Gastrointestinal
g	Gravitational acceleration (m/s^2)
G	Growth rate (µm/min)
GSD	Geometric standard deviation
HPLC	High performance liquid chromatography
HPMC	Hydroxylpropylmethylcellulose
IBP	Ibuprofen
IPA	Isopropanol
IB	Ipratropium bromide
I_i	light intensity with the sample
I_0	light intensity with no sample
I	Ibuprofen
k	Boltzmann's constant (J/K)
K_d	Solute diffusion rate constant (m^2/s)
K_g	Particle growth rate constant
K_n	Solute nucleation constant
k_S	Correlation coefficient
k_G	Growth rate constant
kV	Kilovolt
Min	Minute
MMAD	Median aerodynamic diameter (µm)
MDI	Metered–dose inhaler
MSCI	Multistage cascade impactor
NSAID	Non-steroidal anti-inflammatory drug
nm	Nanometer.

List of Abbreviations

PIF	Peak inspiratory flow
PCL	Polycaprolactone
PVA	Polyvinyl alcohol
PEG	Polyethylene glycol
PCCA	Professional Compounding Chemists of Australia
PSD	Particle size distributions
ppm	Parts per million
R	Airway radius
RESS	Rapid expansion supercritical solutions
RH	Relative Humidity
SD	Standard deviation
SNT	Secondary nucleation threshold
SPG	Size proportional growth
SEM	Scanning electron microscopy
SS	Salbutamol sulphate
Stk	Stokes number
SX	Salmetrol xinofoate
Sol	Solubility
TSI	Twin-stage impinge
T	Absolute temperature (°C, K)
t_m	Micro-mixing time
UV	Ultraviolet
USP	United States Pharmacopoeia
UK	United Kingdom
VMD	Volume median diameter

List of Abbreviations

V	Air velocity
V_{ts}	Terminal settling velocity
W	Water
w/w	Weight by weight
XRD	X-ray diffraction
X_E	% ethanol content
ρ_p	Particle density (g/cm^3)
η	Air viscosity
ρ_a	Air density
ρ_0	Unit density of the media of particle settling
μm	Micrometre

Statement of Original Authorship

The work contained in this thesis has not been previously submitted to meet requirements for an award at this or any other higher education institution. To the best of my knowledge and belief, the thesis contains no material previously published or written by another person except where due reference is made.

Signature: QUT Verified Signature

Date: May 2017

Acknowledgements

First, I am very grateful to Almighty Allah who bestowed me with His enormous blessings to complete this PhD project.

I would like to acknowledge and sincerely thank my principal supervisor Dr Nazrul Islam for giving me the opportunity to pursue my PhD under him and for his constant support to overcome the hurdles and challenges in the completion of this project. I owe my deepest gratitude to my associate supervisor Prof. Edward Ted White, for his patient guidance, technical and analytical supports for the crystallization experiments, useful critiques of this research work and for being always there in need. My special thanks to Prof. Graeme George for his support to provide the lab space to conduct my experiments and his enthusiastic encouragement that charged me up during the critical stage of my research. I must also express my thanks to my associate supervisors A/Prof. Tony Howes and Dr Abdur Rashid for their worthy advice and guidance. Without their indispensable assistance, the completion of this thesis would not have been possible.

I wish to extend my acknowledgement and thanks to the technical staff who have provided instrumental training and inductions for the experimental assistances. I am particularly grateful for the assistance given by Dr Chris Carvalho for the UV and IR spectrophotometry, Dr Lauren Butler for the differential scanning calorimetry, Dr Henry Spratt for the X-ray diffraction training and data analysis, and Rachel Hancock for the help with SEM and TEM. I am also thankful to Tanya Rinas and Kelvin Henderson for helping with the necessary equipment to conduct the powder density and flow measurements.

I thank Dr Christina Houen of Perfect Words Editing for editing this thesis according to the guidelines of the Institute of Professional Editors (IPEd).

The dream of a PhD wouldn't have been accomplished without the financial support provided by QUT during my whole candidature for my living allowance and tuition fees. I gratefully acknowledge QUT for giving me the QUT postgraduate research award (QUTPRA) and QUT tuition fees waiver to make my research a success.

I would like to finish by expressing warm thanks to my family and my dear friends both in Australia and Bangladesh, whose indispensable moral support certainly led me towards completion of my PhD studies.

Dedication

I would like to dedicate my thesis to my loving parents, Md. Mosharraf Hossain and Nasreen Akter, my elder sister Sanjana Anjum, my younger brother Md. Nafiur Rahman and my husband Md. Rashidur Rahman, whose love, moral support, motivation and encouragement helped me to overcome all the difficulties that I encountered during the PhD candidature.

List of Publications

Published conference paper

1. Afrose, Afrina; White, Edward T.; Howes, Tony; George, Graeme; Rashid, Abdur; & Islam, Nazrul (2015). "Solubility of ibuprofen in aqueous ethanol at low ethanol contents". In Asia Pacific Confederation of Chemical Engineering Congress 2015 (APCChE 2015) incorporating CHEMECA 2015, Engineers Australia, Melbourne, Victoria; paper # 3126423.

Published conference abstracts and posters

1. Afrose, Afrina; White, Edward; Howes, Tony; George, Graeme; Rashid, Abdur; Islam, Nazrul (2013) . "Investigation of crystallization approaches to produce fine Ibuprofen crystals for Dry Powder Inhaler (DPI) formulation". IHBI inspires' 2013 postgraduate student conference, 28th - 29th November 2013, Royal in the Park hotel, Brisbane, Australia.
2. Afrose, Afrina; White, Edward; Howes, Tony; George, Graeme ; Rashid, Abdur; Islam, Nazrul (2014). "Precipitation crystallization technique for producing free flowing fine ibuprofen crystals (<5µm) to develop efficient Dry Powder Inhaler (DPI) formulation". IHBI Inspires Postgraduate Conference, November 23-24, 2014, Gold Coast, Australia.
3. Afrose, Afrina; White, Edward; Howes, Tony; George, Graeme; Rashid, Abdur; Islam, Nazrul (2014). "Solubility studies of ibuprofen in aqueous ethanol co-solvents at high water content". Australian Pharmaceutical Science Association (APSA) Annual Conference, December 5-7, 2014, Brisbane, Australia.
4. Afrose, Afrina; White, Edward; Howes, Tony; George, Graeme ; Rashid, Abdur; Islam, Nazrul (2015) **"**Effect of HPMC and Pluronic F127 on ibuprofen solubility in aqueous ethanol solvents". 2015 AAPS Annual Meeting and Exposition, October 25-29, 2015, Orlando, Florida, USA.

Manuscripts ready for submission

5. Afrose, Afrina; White, Edward; Howes, Tony; George, Graeme ; Rashid, Abdur; Islam, Nazrul "Solubility of ibuprofen in ethanol and water co-solvents at high water content". To be submitted in Journal of Chemical Thermodynamics.
6. Afrose, Afrina; White, Edward; Howes, Tony; George, Graeme ; Rashid, Abdur; Islam, Nazrul **"**Effect of pharmaceutical additives on ibuprofen solubility in aqueous ethanol solvents". To be submitted in International Journal of Pharmaceutics.

Manuscripts under preparation

7. Afrose, Afrina; White, Edward; Howes, Tony; George, Graeme ; Rashid, Abdur; Islam, Nazrul "Development of a novel dry powder inhaler formulation of ibuprofen prepared by anti-solvent precipitation crystallization process and characterization for in vitro lung delivery". For submission in International Journal of Pharmaceutical Science.

Chapter 1: Introduction

1.1 BACKGROUND

The pulmonary delivery of drugs is an alternative to other dosage forms and it has been considered to be the most promising non-intrusive route of drug administration [6]. Pulmonary route has several distinct advantages such as direct drug delivery to the tracheobronchial tree followed by fast and predictable onset of action [7, 8]. As the gastrointestinal tract is avoided no degradation of the delivered dose occurs. Thus, lower dosages than by the oral route can be administered with similar efficacy which is expected to mitigate undesirable side effects [7, 8]. Finally, when two or more medications are administered alongside, pulmonary route can be adopted as an alternative to avoid the possible drug interaction [7, 8].

The lungs have a large surface area (100 m^2), ultra – thin alveolar epithelium (0.1 - 0.5 μm) and low-metabolic enzyme activity and therefore drug delivery via this route ensures rapid absorption and onset of action with a very low dose [9, 10]. Drug deposition in the lung is mainly controlled by the particle's aerodynamic diameter [11]. Particles larger than 5 μm are mostly caught by oropharyngeal deposition and are unable to reach the lungs while particles smaller than 1 μm are generally exhaled without deposition [12, 13]. To expedite successful delivery by a dry powder inhaler (DPI), nanoparticles are usually converted to nano-aggregates, having a larger geometric diameter (>10 μm) and low particle density (<1 g/cm^3) due to their porous or hollow morphology, incorporating aerodynamic diameters within the 1–5 μm range [14, 15]. Alveolar or peripheral airways deposition of particles is critical because major drug absorption is possible in this region where the suitable particle size for deposition is 1-5 μm. So, the drug particles for deep lung delivery should have a narrow particle size distribution [16-18] in the range 1–5 μm.

DPIs can be defined as the devices through which a dry powder formulation of an active drug is encapsulated and delivered for local or systemic effect through the respiratory tract. DPI formulations are basically categorized in two types. In the first category, micronized drug particles with controlled flow property are formulated as loose agglomerates [19]. Another formulation type is the carrier-based interactive mixtures where micronized drug particles are adhered onto the surface of larger

carriers. This method is useful to increase the flow property of very cohesive micronized drug particles [19]. However, in case of carrier-based interactive mixtures, three main aspects are important for desired therapeutic effects. The first step involves the detachment of drug particles from the surface of the large carriers. The second step is the dispersion of the detached drug particles during aerosolization by an inhalation device. Finally, resulting deposition of the drug particles in the lower airways of the lungs [20].

In recent years, DPIs are taking over the arena in pulmonary drug delivery due to the apparent restrictions in metered dose inhalers (MDIs) and nebulizers. DPIs overcome the problems associated in the use of propellant gases and the requisite for coordination of inhalation and actuation in the use of MDIs. Moreover, DPIs are more handy and user friendly as spacers are not required [19]. The successful delivery of drug from DPI is comprised of the integration of drug formulations, design of the devices and patient's inhalation profile [16].

Most currently available carrier-based dry powder inhalers are comparatively inefficient, delivering of only 20 – 30% of the nominal dose to the lungs [21]. The sensitivity of the delivered dose at poor inhalation flow rates to particle adhesion and static charges are generally accountable for the low efficiency of the DPI formulations [22]. Subtle changes in powder characteristics such as size distribution, shape, surface roughness, surface energetic, electrostatics and other properties are suspected to be responsible for significant changes in powder cohesion/adhesion, mixing and flow [23-25]. This is the most challenging problems in pulmonary delivery. To overcome these problems direct controlled crystallization of the drug particle has been taken as a promising aspect. The challenge of particle size control in ibuprofen (IBP) crystallization techniques is that the product naturally tends to form relatively large crystals due to the advantage of growth over the nucleation mechanism [26].

This study approaches to develop IBP microparticles (1 - 5µm) for DPI formulation produced by controlled crystallization process. The conventional micronization process (i.e. milling, homogenization) with high energy input incorporates undesirable particle shape, size, surface charge modifications, decreased crystallinity and possible degradation that limit the inhalation efficiency of DPI formulations [27]. It is expected that a controlled crystallization process free from high shear

milling using suitable additives would overcome limitations in producing IBP microcrystals suitable for DPI formulations. The drug particles produced by direct controlled crystallization are expected to be free flowing and of better surface properties and therefore will lead to a better inhalation efficiency profile from the DPI formulation.

1.2 AIMS

This project aims to develop an alternative functional and economic method of producing fine crystals (1–5μm) of the model drug IBP for pulmonary delivery from DPI formulations. The project has three objectives:

- To investigate the IBP solubility profile in aqueous ethanol with the selected additives.
- To manufacture IBP particles with a required size (< 5 μm) by using an optimized APC process.
- To investigate the particle size, flow properties and surface morphology of the IBP particles produced and relate the outcome to the lung delivery of the drug.

1.3 SIGNIFICANCE

A crash precipitation crystallization technique mixing an organic solution of IBP with an aqueous solution containing additives (e.g. Pluronic F127 & HPMC) will produce nano/microcrystals [28]. The IBP recovery in this process is very high (near 100% of theoretical) which makes the process cheap and cost effective. However, the problem with this method is agglomeration of the crystals produced, giving a non-uniform and large particle size distribution. Though the use of additives addresses this problem to some extent, the problem has not been solved. The solubility of IBP in different compositions of the organic and aqueous phase with and without additives would provide the amount of IBP to be used and the degree of supersaturation for crystallization. IBP is very poorly soluble in aqueous media [29] and determining its solubility in highly aqueous ethanol solution will contribute to the knowledge. Figure 1.1 represents the overall project.

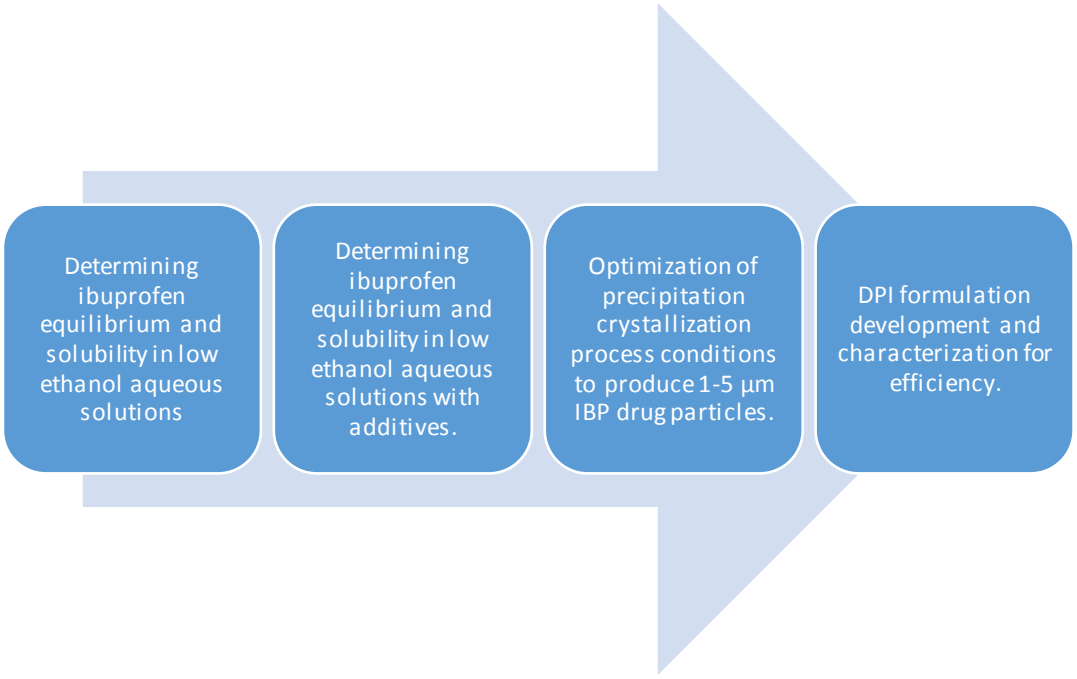

Figure 1.1 Steps in the project to develop the IBP dry powder inhaler formulation.

The key objective of particle engineering is to integrate necessary characteristics for example required size range and narrow particle size distribution with an improved dispersibility. This study will use racemic IBP particles as a model drug, which will provide a unique opportunity to develop a novel DPI formulation for pulmonary delivery of IBP for better therapeutic applications. However, this technique could be used for other API to produce fine (~5 µm) particles of other drugs.

Lately, inhalation therapy has remarked substantial bio-medical concern in the growth of innovative particle technologies for the dry powder inhaler (DPI) systems [22]. DPIs of the first generations, generally demonstrated a comparatively low efficacy (10-15%) in terms of the fine particle fraction (FPF) [30]. Many research efforts have looked to increase the percentage of fine particle fraction (%FPF) for DPI formulations of various drug products. No work has been done to make IBP DPI formulation with a one-step controlled crystallization technique to improve inhalation efficiency. This project results in the development of cost effective new DPI formulation strategies for lung delivery.

Improvement in industrial crystallization knowledge is of great interest to the pharmaceutical API manufacturing industry, which is under pressure from the regulatory authorities to develop a much more scientific approach to pharmaceutical manufacture. Therefore, a one-step direct controlled crystallization technique is an

exciting prospect for producing drug particles with the required size (1–5 μm) for DPI formulation.

1.4 THESIS OUTLINE

1.4.1 **Outline of Chapter 2**

This chapter reviews the literature on the anatomy of the pulmonary route of drug delivery, the mechanism of drug deposition into the deep lung, and different inhalation systems, and focuses on the lung delivery of drugs from a dry powder inhaler system. The existing particle engineering techniques and the challenges for dry powder inhaler formulations indicated that anti-solvent precipitation crystallization (APC) is promising, and its basic principles are demonstrated as the core methodology for this project. Then the selected additives used in this method are described in-depth in terms of their role in the particle manufacturing process. The chapter concludes with the justification for using IBP as the model drug in this project.

1.4.2 **Outline of Chapter 3**

This chapter describes the research methods used to achieve the aims and objectives stated in Chapter 1. IBP solubility was determined by the dissolution to equilibrium method, IBP concentration was determined by UV spectrophotometry, and the method of particle preparation suitable for inhalation was the APC process. Finally, the chapter describes the instruments and methodology used to characterize the prepared particles of the DPI formulation according to size, morphology, density, flow property, crystallinity and dispersibility in lungs.

1.4.3 **Outline of Chapter 4**

This chapter presents the initial investigation for the particle crystallization method development. The solubility of IBP was investigated in 0–50% of ethanol in water-ethanol co-solvents. The IBP solubility trend at three temperatures was determined and the correlations were compared with previous data at a higher ethanol range in previous work by Rashid [31]. Finally, the IBP solubility profile in water-ethanol co-solvents in the presence of selected additives (Pluronic F127, HPMC, L-leucine and mannitol) was determined and demonstrated.

1.4.4 **Outline of Chapter 5**

Chapter 5 involves the investigation of variables affecting the size of the IBP particles from anti-solvent precipitation crystallization (APC). The chapter first describes the experimental set up of a Plackett-Burman design studying nine variables and screening out the most effective ones. Then the effect of individual excipients, Pluronic F127, HPMC, leucine and mannitol, on the particles' size is discussed. An optimised formulation for preparing IBP particles < 5 μm and the method validation was done by characterization of particle size in Malvern Mastersizer 3000, scanning electron microscope (SEM) and transmission electron microscope (TEM).

1.4.5 **Outline of Chapter 6**

Chapter 6 demonstrates the DPI formulation development and characterization for density and flowability, size and aerodynamic diameter, particle morphology, crystallinity and aerosol performance using the methods described in Chapter 3. The outcome of the characterization results was correlated with the effect of the batch size, additive composition and crystallinity on the aerosol and dissolution performance of the developed DPI formulations.

1.4.6 **Outline of Chapter 7**

Chapter 7 summarises all the outcomes obtained from the research work in Chapters 3, 4, 5 and 6. The significant research findings and analysis are specified. The benefits and importance of the proposed methods are summarised. Finally, recommendations for future research directions are suggested.

Chapter 2: Literature Review

2.1 INTRODUCTION

This chapter begins with the anatomy of the pulmonary route of drug delivery and the mechanism of drug deposition into the deep lung. Then the different inhalation systems are discussed with a focus on the lung delivery of drugs from a dry powder inhaler system. The literature review of the existing particle engineering techniques and the challenges for dry powder inhaler formulations are outlined in next section. The anti-solvent crystallization technique and its basic principles are demonstrated as the core methodology for this project. Then the selected additives used in this method are described in-depth in terms of their structural configuration, mechanism of action and role in the particle manufacturing process. The chapter concludes with the justification for using ibuprofen (IBP) as the model drug in this project.

The pulmonary route of drug delivery is already a well-established route for treating respiratory diseases such as asthma and chronic obstructive pulmonary disease (COPD) [32]. More recently, this route of drug delivery is becoming attractive for commonly prescribed medications to reduce systemic exposure and decrease the associated side effects [33].

Although promising, delivery of drugs to the respiratory tract is encountered by a number of anatomical and physiological challenges [34]. The process and development of an inhalable formulation requires the knowledge of the physicochemical properties of the drug formulation components and the biological features of the respiratory tract [35]. So, this chapter will start with the mechanism of drug deposition into the deep lungs and its transport through the alveolar epithelia to the systemic circulation.

2.2 BIOLOGICAL TRANSPORT MECHANISMS OF PARTICLES IN PULMONARY EPITHELIAL CELLS

There are different particle uptake mechanisms in epithelial cells dependent upon the properties of cells and particles. *Figure 2.1* shows the diagram of the transport mechanisms across bronchial and alveolar epithelial cells.

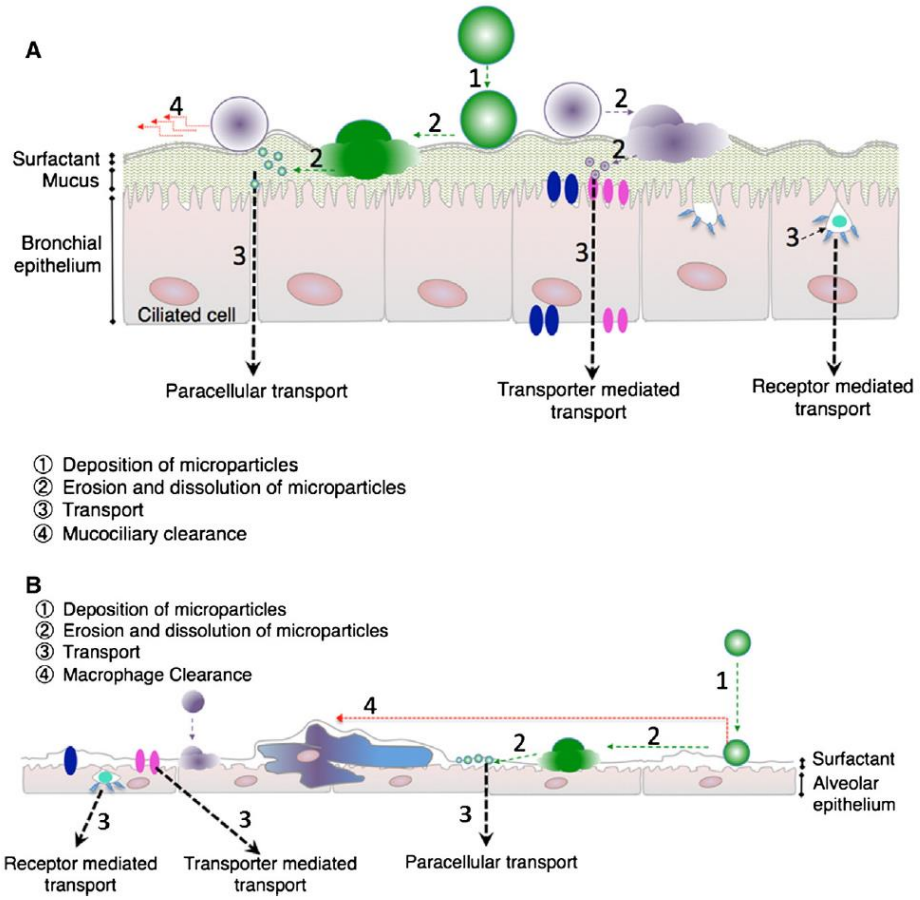

Figure 2.1 The mechanism of transport of microparticles after deposition on the (A) bronchial and (B) alveolar epithelium [35].

Before entering the epithelial cells, drug particles need to cross over the surfactant and mucus layers. The surfactant is the lung lining fluid comprising phospholipid and proteins. The mucus layer is a part of the mucociliary clearance system [36, 37]. This step is also aided by the alveolar macrophase and mucociliary escalator clearance systems. Alveolar macrophages act as the first-line host guard against the inhaled drug particles which are cleared from the alveoli to the bronchioles by the lining fluid and then by the mucociliary escalator [38]. The drug particle transport across these layers depends on the particle size, solubility, lipophilicity and charge [39, 40] which leads to the erosion and dissolution of the microparticles into the epithelial cells.

The epithelial cells regulate the transport of compounds, retaining the structural role, barrier integrity and the cellular communications. There are multi-protein complexes known as tight junctions which tie the apical membrane of the epithelial cells.

Lipophilic compounds are believed to be absorbed through the cell membranes and hydrophilic molecules through the tight junctions by passive diffusion [41, 42]. Moreover, hydrophilic compounds like carbohydrates, amino acids, neurotransmitters and vitamins are also known to be transported by carrier-mediated processes.

An active transport system uses cellular metabolic energy (e.g. sodium-potassium pump) and electrochemical gradient (coupled transport) to transport molecules across the cell membrane [43]. However, the active transporters in the lung's epithelial cells are believed to be responsible for affecting the residence time of drug molecules and uptake of drugs from the systemic circulations, causing pulmonary toxicity or the drug metabolism kinetics [44]. P-glycoprotein is considered to be the most notable transporter among the efflux transporters [35].

The receptor-mediated transport particularly involves the transcellular trafficking of biopharmaceuticals due to their large molecular size and poor permeability. Literature suggests that particles < 200 nm are mostly entrapped via clathrin-coated pits, while those > 200 nm are entrapped via caveolae-mediated endocytosis [45]. Macromolecules smaller than 40 kilodaltons in alveolar spaces are assumed to be absorbed through tight junctions and paracellular diffusion [46, 47].

The providence of an inhalation system is dependent on the physicochemical characteristics of the particle and anatomical structures of the pulmonary airways. Therefore, particle size plays an important role to influence the depth of penetration, site of deposition and bioavailability of the drug in the respiratory tract [48]. The next section will discuss the effect of the particle size on its deposition mechanism within the respiratory tract.

2.3 MECHANISMS OF PARTICLE DEPOSITION IN LUNGS

Alveoli deposition of particles is critical, because major drug absorption is allowed in this region and the suitable particle size for alveolar (peripheral airways) deposition is 1-5 μm in aerodynamic diameter. So, the drug particles for deep lung delivery should have a narrow particle size distribution [16-18, 49, 50].

The particle deposition in the lungs can be defined in five different mechanisms. They are inertial impaction, sedimentation, diffusion, interception and electrostatic precipitation. The two last mechanisms are related to particle shape and electrostatic

charges, respectively [51, 52]. It is evident in the available literature that smaller particles delivered to the lungs are deposited in the smaller airways as opposed to the larger airways (*Figure 2.2*).

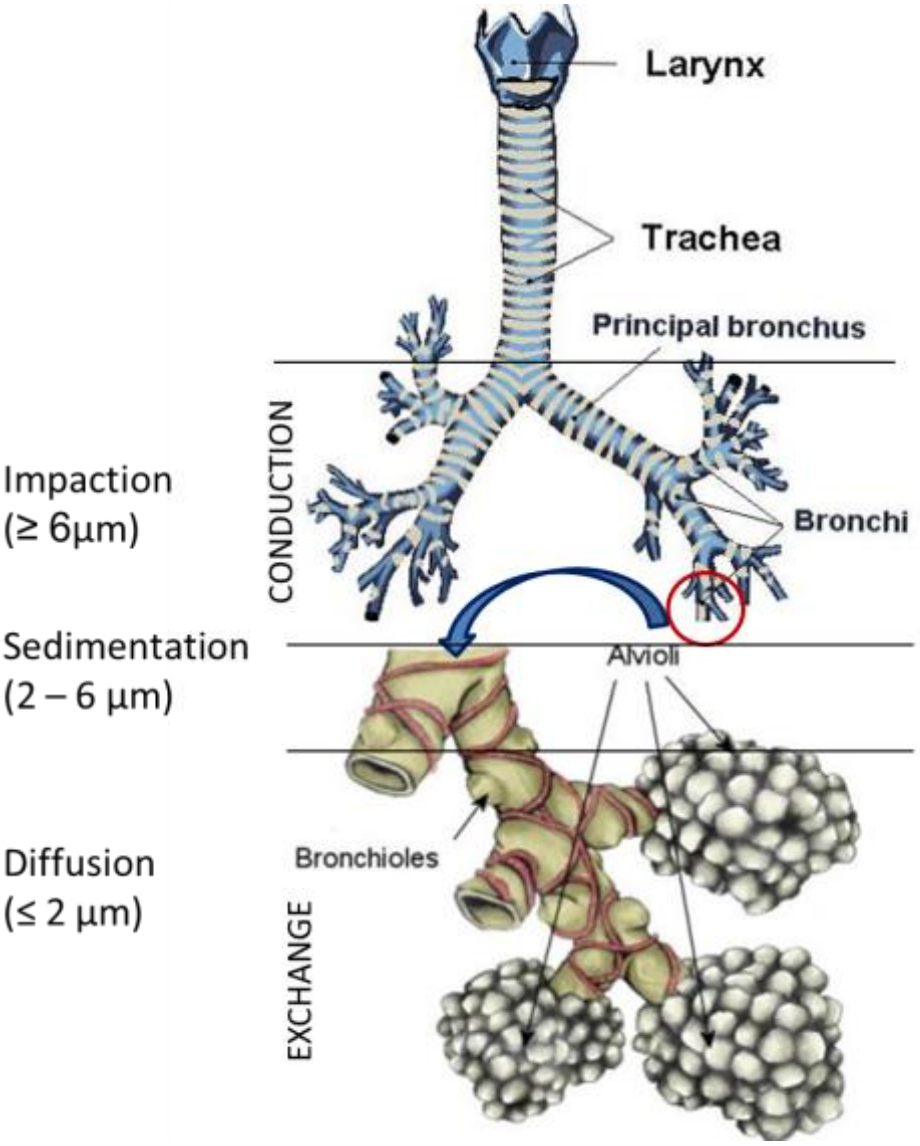

Figure 2.2 The diagram represents particle deposition in the lungs according to different mechanisms related to particle size: inertial impaction, sedimentation and diffusion. [53].

The mechanisms of deposition directly (or inversely) related to particle size are presented in *Figure 2.3*, where, *d*: particle diameter; *Stk*: Stokes number; ρ_p: particle density; *V*: air velocity; η: air viscosity; *R*: airway radius; V_{ts}: terminal settling velocity; ρ_a: air density; *g*: gravitational acceleration; *Dif*: diffusion coefficient; *k*: Boltzmann's constant; *T*: absolute temperature; d_{ae}: aerodynamic diameter; ρ_0: unity density [49, 50].

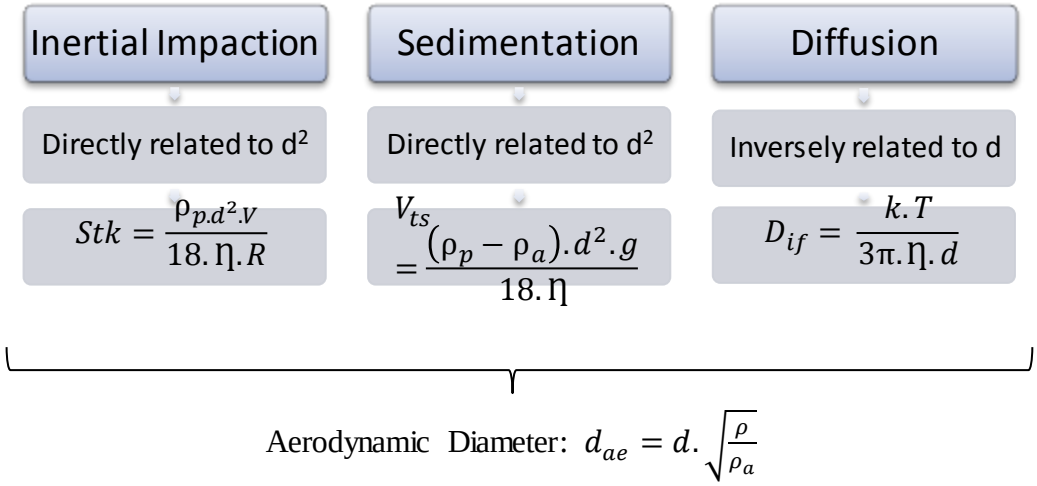

Figure 2.3 The influence of particle size on deposition [50].

A recent study has shown that particle charge effects deposition substantially, especially for smaller sizes where the impaction mechanism of deposition is less dominant. An empirical dimensionless relation is suggested to predict average deposition in the mouth-throat that includes the three relevant dimensionless numbers: Stokes number, Reynolds number and induced charge number [54].

The aerodynamic diameter, D_{ae} is defined by the diameter of an equivalent volume sphere D_{eq} of unit density with the same terminal settling velocity as the actual particle [55]. The following expression describes the relationship between these dimensions.

$$D_{ae} = D_{eq}\sqrt{\frac{\rho_p}{\rho_\circ \chi}}$$

where ρ_p represents the particle density and ρ_o represents the unit density of the air where the particles are dispersed and χ is the dynamic shape factor. Any deviation from the sphericity is called the dynamic shape factor [50, 55]. D_{eq} can be calculated using the volume mean diameter (D [4,3]) from the particle size distribution curves [56, 57].

In vitro determination of the aerodynamic size of inhaled medication can be done using cascade impactors or the twin stage impinger [58]. Usually, the aerosolization efficiency is evaluated in terms of different parameters, such as emitted dose (ED),

fine particle fraction (FPF), the geometric standard deviation (GSD) and mass median aerodynamic diameter (MMAD) [22].

MMAD is the median aerodynamic diameter (D_{ae}) of the entrained particles based on mass [59, 60] and also refers to the particle size, in which 50% of the mass of the aerosol is smaller and 50% larger than the referred parameter [61, 62].

2.4 PULMONARY DRUG DELIVERY SYSTEMS

The pulmonary drug delivery systems are commonly available in three dosage forms, the jet or ultrasonic nebulizer, metered–dose inhaler (MDI), and dry-powder inhaler (DPI). Nebulizers are not preferred for chronic drug treatment in the daily care of patients due to their administration and lack of portability. The pressurised MDIs were the most well-accepted inhalation system over decades due to the perceived ease of use [63]. But problems in the use of environmentally non-friendly propellant gases and the inherent difficulties in coordination of inhalation and actuation have created the need for developing new pulmonary drug delivery system to replace the propellant driven MDIs [64]. Dry powder inhalers (DPI) were premeditated with the aim of eliminating the limitations of MDI.

2.5 DRY POWDER INHALER (DPI) SYSTEM

DPIs deliver single doses of powder drug formulation contained in capsules that should be broken inside the device by patient's inspiratory flow before their administration [49]. They have several advantages over other pulmonary drug delivery systems; for example, direct delivery of the drug into the deep lungs utilising the patient's respiration [19], solid state stability of formulation, and no need to coordinate between inhalation and actuation.

The main drawbacks of the DPI system are that patients perceive the drug entering the airway to a lesser degree. They should be kept in a dry atmosphere, as humidity instigates the powder agglomeration deterring the stability of the inhalation system [65].

2.5.1 **Role of devices in inhalation efficiency of DPI system**

The role of the device in DPI is to redisperse the interactive powder mixtures into fine drug particle fractions by aerodynamic means [64]. The function of the device can be altered by the resistance to airflow, that directly influences parameters

such as the peak inspiratory flow (PIF), flow increase rate (FIR), and the total inhalation time [66]. At present, a wide range of devices is available on the market, but the desired clinical efficacy has not been achieved yet. The future improvement on DPI devices will have to emphasis on simplicity of use, dependability, suitability for products and doses variety, and most important on the cost-effectiveness [64]. With increasing demand for the pulmonary delivery of the systemic drugs there is a potential scope for developing new DPI delivery devices [19].

2.5.2 Role of patient's inhalation profile in drug delivery efficiency of DPI system

The variability of the drug dosage to different age group patients, delivered by inhalation, is a key concern as an older patient's breathing capacity would be different to the younger ones. It has been found that older patients are unable to reach adequate inspiratory flow in devices with high resistance to airflow [67]. Therefore, the device–patient interface has been given special attention for pulmonary drug delivery, since the patients vary in their skill and training to use the inhalation product [68, 69]. It has been demonstrated that, delivery of a drug either from DPI or MDI would be equally efficient if the inhalation technique is accurate [70].

2.6 DRY POWDER INHALER FORMULATIONS AND CHALLENGES

DPI products are formulated either as loose agglomerates of micronized drug particles with controlled flow property or as carrier-based interactive mixtures with micronized drug particles adhered onto the surface of large lactose carriers, which is used to increase the flow property of very cohesive micronized drug particles [19].

Particle surfaces are key factors in particle interactions, stability, and ease of dispersion. Due the very small particle size (<5 μm) requirement of the inhalation system, the total surface area of the powder formulation is very large, which possess greater potential for charging, moisture uptake and influencing the van der Waals forces [55]. A small amount of moisture present will also bring about capillary forces [71]. These factors are mostly responsible for causing stability issues in a DPI system.

In a study by Kaily et al. [72], it was found that carrier particles with higher elongation ratio (ER) can significantly increase the amounts of drug delivered to

lower airway regions [72]. They also found that, shape of carrier particles or the drug itself influenced the dynamics of drug dispersion and particles with different morphologies demonstrates different dispersive shear forces during the aerosolization [72].

The electrostatic charging behaviour of the drug product may also affect the dosing, aerosol performance and inhaler retention. So, a consistent charging of the drug in ambient conditions is desired from the dry powder inhaler preparation [54]. It is found that this electrostatic charging behaviour can be consistently maintained by the crystalline form rather than the amorphous form of the drug salbutamol sulphate, [73] and knowledge gained from the study may be useful for optimising the dry powder inhaler formulation development process.

2.7 TECHNOLOGIES OF PARTICLE ENGINEERING FOR THE DPI SYSTEMS

Most commercially available DPI formulations are shown to have low fine particle fraction (FPF), typically 10-30%, and research efforts have looked at conventional formations, particle properties and product performance to increase this low range of %FPF. The currently available mechanisms of preparing micronized particles for inhalation purposes are described in the following sections.

2.7.1 **Drug micronization and powder blending limitations**

Jet-milling micronization

This is the most commonly used method to get particles with inhalable size for DPI formulations. Nevertheless, micronization by milling requires high energy, excess duration of time and may produce contamination [27]. It also results in undesirable particle shape, size, decreased crystallinity and resulting instabilities from degradation, and therefore could be unsuitable for some DPI formulations [74, 75]. Moreover, during the milling micronization processs, the particles are not grown in natural process because it cleaves at the crystal face with little attachment energy on the surface [76]. A number of studies have been undertaken to investigate the influence of the primary crystallization and micronization of active pharmaceutical ingredients for dry powder inhaler formulations. The study by Kubavat et al. [77] shows that in different crystallization conditions the %FPF of budesonide was not more than 9.7 ± 0.3%, which is negligible in respect of dry powder inhalation

efficiency. So, it was concluded that mechanical micronization of the material after crystallization may affect their interfacial characteristics and dispersibility of the carrier based DPI formulations [77].

Air-jet micronization

Shur et. al. [78] used air-jet micronization to process anhydrous and monohydrate ipratropium bromide (IB) crystals and investigated the effects on the aerosolization performance in dry powder inhaler (DPI) formulations. The physicochemical and surface interfacial property data derived from the cohesive-adhesive balance (CAB) approach were correlated to the in-vitro aerosolization performance. The percentage FPF of the monohydrate and anhydrous IB formulations was 22.6 ± 1.3% and 23.3 ± 0.8%, respectively [78]. Therefore, no improvement in the inhalation efficiency was found on subsequent micronization of anhydrous ipratropium bromide crystals produced by using supercritical fluid technology and ipratropium monohydrate crystals produced by seed crystallization.

2.8 CONTROLLED CRYSTALLIZATION OF DRUG CARRIER TO IMPROVE THE INHALATION EFFICIENCY OF DPI

To improve the flow property of the dry powder inhaler formulations, various strategies have been applied for the modification of the drug carrier particles as well as to increase the FPF. A number of studies have been undertaken on the drug salbutamol sulphate using different carrier molecules produced by different engineering techniques [79-81]. Likewise, conventional anti-solvent crystallization with mechanical agitation [82] was investigated for the crystallization of lactose and use of the crystals to improve the dispersion and disaggregation of salbutamol sulphate. But a respirable size was not obtained, due to the poor mixing which gave heterogeneous growth of crystals, and to variations in the particle size and morphological features; for example, prismatic, pyramidal and tomahawk-shaped crystals were observed.

Unlike the lactose molecules or other sugar particles, surface modified biodegradable polymer microparticles of polycaprolactone (PCL) have been investigated as carriers for a dry powder inhaler formulation [60, 83]. This work explored the aerosolization profile of salbutamol sulphate (SS) from mixtures with polycaprolactone (PCL) microspheres and polyvinyl alcohol (PVA) pre-coated with magnesium stearate and

leucine [83]. However, the overall improvement in the FPF was not sufficiently significant compared with conventional DPI formulations.

The effect of particle size of an ideal carrier with uniform physical properties on the dry powder inhaler performance was investigated by Kaialy et al. [84] and it was concluded that if the carrier morphology, shape, true density and the solid carrier has a uniform spherical shape, the size of the carrier does not influence the dry powder inhaler performance significantly.

2.9 CONTROLLED CRYSTALLIZATION OF THE DRUG TO IMPROVE THE INHALATION EFFICIENCY OF DPI

At present micron-sized near-spherical particles in inhalable size are often prepared by spray-drying of a drug solution [85]. However, this technique can result in an amorphous product which is then thermodynamically unstable and could be susceptible to absorb moisture, to form agglomerates or to recrystallise on storage. An amorphous product may not flow well and eventually affects the FPF [85-87].

On the other hand, when melt sonocrystallization [88] was used, the product was unsuitable for inhalation due its larger size (100 μm to 1.1 mm) and unsuitable hardness and density. The concept of micro crystallization [89, 90] has been used in producing α-lactalbumin, using PEG-8000 as a stabilizer to overcome milling induced problems. The roughly spherical microcrystals were between 1 to 2 μm. Tests in pulmonary delivery showed the highest deposition was 36.3%, which is still a low level of FPF.

A seed zone crystallization method [90] was used for an insulin micro-crystallization process at pH 10.5, using an excess amount of seed in a supersaturated solution. But the crystals produced were too large (up to 20 μm) for pulmonary use. Microscystals of fluticasone propionate (FP) and salmeterol xinafoate (SX) from PEG solvents were prepared by aqueous crystallization. The highest FPF was 25.7 ±1.5%, which resulted from the formulation of fluticasone propionate (FP) microcrystals with the largest median diameter (FP PEG 400B: 6.1±0.2 mm), which is still considered to give a low efficiency of inhalation [91].

Rasenack et. al. [16, 92, 93] first introduced the direct controlled crystallization process for hydrophobic drugs to get respirable size range particles using antisolvent precipitation employing hydroxylpropylmethylcellulose (HPMC). The precipitated

drug crystals (budesonide, prednisolone, fluticasone and disodium cormatogycolate) exhibited a higher FPF than jet milled samples, for example: in the case of beclomethasone-17,21-dipropionate (BDP), the FPF of jet milled drugs was 9.5%, which increased to 25.6% by micro crystallization [94]. But the use of tailor made non-volatile additives can be highly restrictive due to toxicity issues, and the increased FPF was still not satisfactory. In addition, spherical agglomerates (200-300 μm) were produced using a conventional anti-solvent crystallization technique without additives, so the particles were deagglomerated by mixing with lactose. The results showed that the FPF was increased 2-3 times more than that of micronised materials [95, 96]. However, depending on the drug molecules, spherical agglomerates might not deagglomerate properly and the final FPF might be affected. A reactive precipitation crystallization technique was used for the protein molecule, sumatriptan succinate, without additives and followed by spray drying, and it gave a FPF value over 50% [96, 97]. However, depending on the drug compounds, spray drying may produce powders that are amorphous and hence physically unstable.

A spray drying method was applied to produce inhalable insulin powder suitable for dry powder formulation and it was capable of producing 83.6% FPF, [98] but the drug product is yet to be evaluated by the drug agency for market authorization.

These methods, however, exhibit some key issues like the presence of polymeric stabilising excipients on the surface of the particles that contributes to its amorphous content [92]. Ragab et al. [99], prepared progesterone crystals by antisolvent precipitation/ combined cooling and antisolvent crystallization from a water-isopropanol (IPA) mixture. He observed a significant effect of the antisolvent addition rate, initial drug concentration and the solvent composition of the crystallization process on the aerosol performance of progesterone microcrystals. Hence, the particle size for pulmonary deposition was possible to prepare and control by the process parameters alone. However, in the majority cases, the high size of the particles indicates a large portion would be unsuitable for pulmonary delivery [99]. In the case of the IBP crystallization, it was attempted to control the process parameters to achieve the desired narrow size distribution of particles (1-5 μm) in one step.

2.10 ANTISOLVENT PRECIPITATION CRYSTALLIZATION (APC) FOR DPI FORMULATION

Conventional crystallization processes mostly produce larger particles (>10 μm) which are not suitable for inhalation. As was discussed earlier, jet-milling micronization process requires high energy input that induces, several physicochemical instability of the product due to the contamination arising from the mechanical attrition during milling. Henceforth, a high-gravity precipitation (HGCP) technique has been used to produce salbutamol sulphate as a model anti-asthmatic drug, followed by spray drying [97]. The rotating packed bed (RPB) used in the HGCP method was the key component to producing particles within inhalable size range without using additives (*Figure 2.4*) [100].

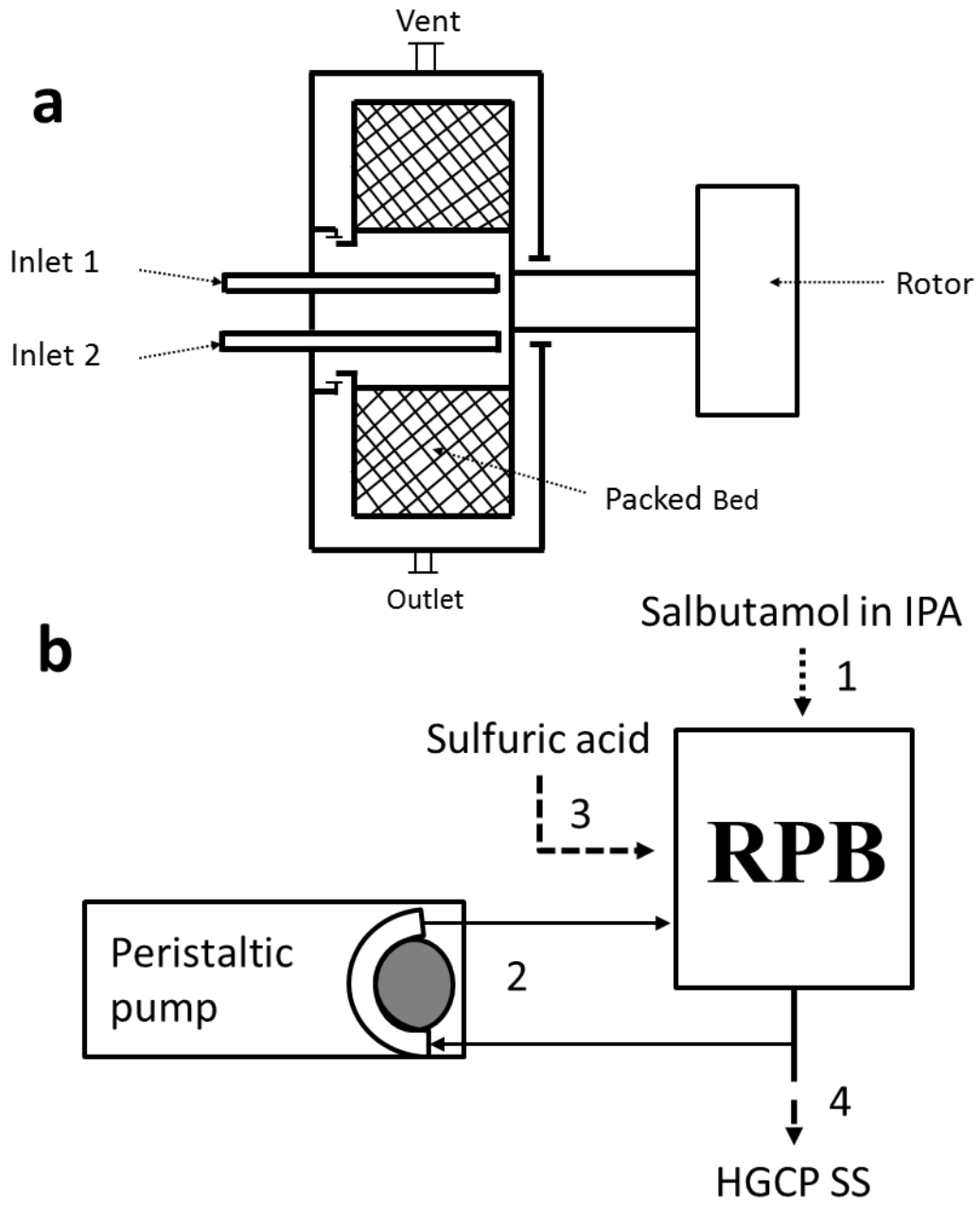

Figure 2.4 Schematic diagram of (a) the RPB and (b) the reactive HGCP process (re-drawn)[101].

A simple combination technology was used to prepare DPI formulation of salbutamol sulphate involving anti-solvent sonocrystallization followed by spray drying by Muhammad and co-workers (*Figure 2.5*) [102].

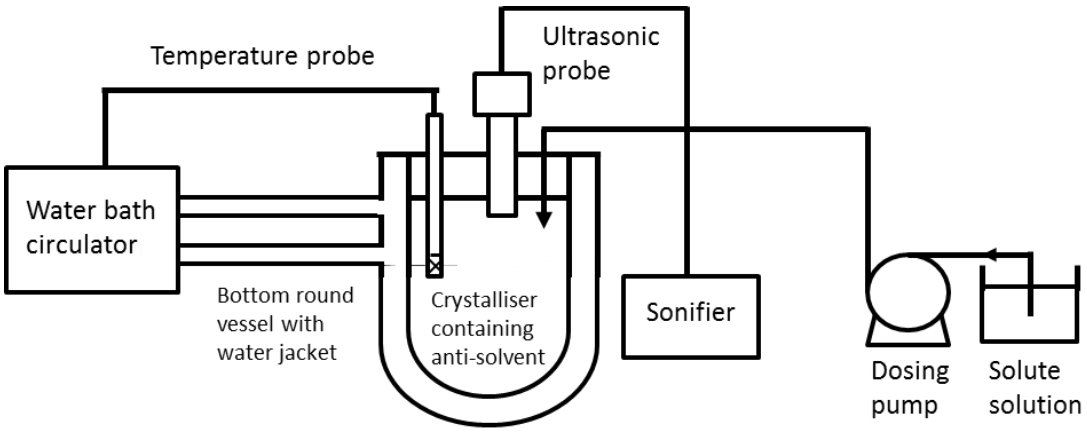

Figure 2.5 Schematic diagram of sonocrystallization technique (re-drawn) [102].

However, in both processes, spray drying was used for particle recovery which has been reported to produce amorphous powder leading to physical instabilities [97]. A limited number of studies report that the APC process has not been used so far to prepare a DPI formulation without involving a spray drying step. Moreover, according to recent reports, the method of particle recovery produced in the APC process by a suitable drying process is a challenge yet to overcome.

2.11 CRYSTALLIZATION

Crystallization is the process by which atoms, ions or molecules assemble to pack into an ordered three-dimensional arrangement under definite settings. Crystallization is driven by the excess concentration in solution above the solubility limit, which in solution equates to supersaturation. Hence it is necessary to know the solubility of a crystallising material in the solvent used.

2.11.1 Solubility and supersaturation

The solubility, C*, is defined as the amount of solute that can dissolve at equilibrium in the solvent to make a solution saturated at fixed conditions of temperature, pressure and pH. Supersaturation is a very important parameter in the crystallization processes. A supersaturated solution is one where the concentration of the dissolved solute exceeds the equilibrium. Supersaturation, which is the driving force for the nucleation and crystal growth processes, can be produced in a number of ways once a solvent is chosen. These include:

i) Solvent removal by evaporation or extraction. This is very useful when the solvent is non-aqueous and has a relatively high vapour pressure.

ii) By cooling or heating the solution depending on the solubility change with temperature. However, in many cases, this technique does not work if the solubility of material changes very little over the temperature ranges of interest, or if the solubility remains high at low temperatures.

iii) Salting out, by changing the properties of the solvent by the addition of a salt, an acid/base or an anti-solvent. Very good mixing is required for this method.

iv) Precipitation, when two soluble materials are mixed together in a solution that reacts quickly to form a product of low solubility. Since the solubility of the product is quickly surpassed, the solution reaches supersaturation and the material crystallizes [26].

Figure 2.6 shows the phase diagrams from the different crystallization techniques. It also shows how supersaturation is created and the relation between concentration, solubility and supersaturation ratio $S = c/c^*$.

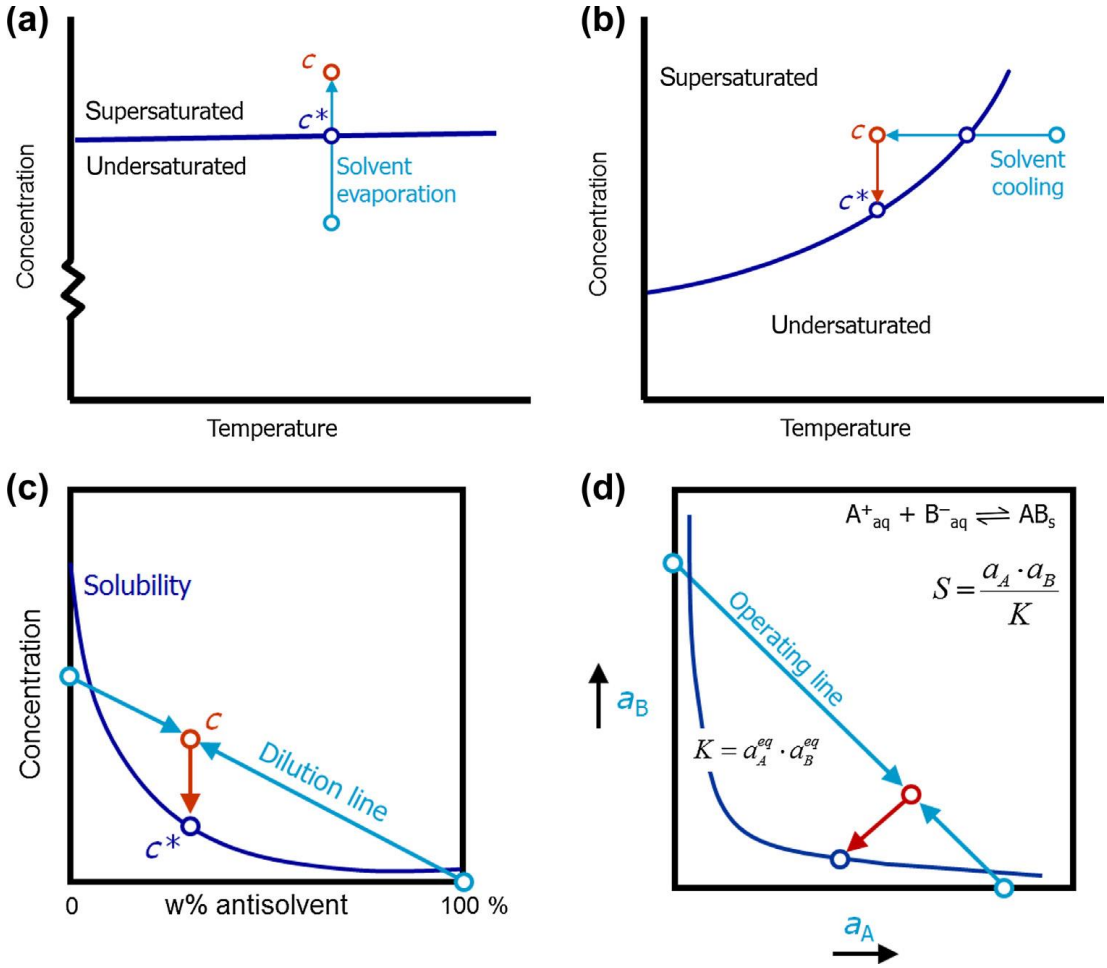

Figure 2.6 The phase diagrams, solubility lines, and operating points for the different crystallization techniques:

(a) evaporative crystallization; (b) cooling crystallization; (c) antisolvent crystallization; (d) precipitation [103].

2.11.2 **Anti-solvent (water) precipitation process of crystallization:**

Basic principles

Precipitation is comprised of a number of main steps: chemical reaction following supersaturation, nucleation, solute diffusion and particle growth [104]. The nucleation rate (dN/dt) can be correlated empirically with supersaturation as

$$\frac{dN}{dt} = K_n(C_i - C^*)^a \qquad (2.1)$$

where K_n is the solute nucleation constant, C_i and C^* are the solute concentration on the particle surface and saturation concentration, respectively.

The diffusion rate of solute to the particle surface is

$$\frac{dm}{dt} = K_d(C - C_i) \qquad (2.2)$$

where K_d is the solute diffusion rate constant and C is the bulk solution concentration. The growth rate of particle is

$$\frac{dl}{dt} = K_g(C_i - C^*)^b \qquad (2.3)$$

where K_g is the particle growth rate constant. The value of 'b' is usually between 1 and 3, and usually increases with temperature [105].

Particles in the nano-size range can be obtained by rapid micro-mixing of reactants to enhance nucleation while minimising the time for particle growth.

Eqs. (2.1) – (2.3) indicate that both the nucleation and particle growth depend on the level of supersaturation which needs to be controlled in various processes such as supercritical fluid, high-gravity, ultrasound, limited impacting jets or vortex mixing [105].

2.11.3 **Crystal structure of ibuprofen (IBP)**

During crystal formation, growth units (molecules, atoms or ions) prefer to pack into a vacancy in the exposed crystal lattice rather than form a new lattice layer. So crystals generally have plane faces linked to the inherent crystal lattice directions. Due to the difference in the growth rates of these faces, the sizes of the faces may change, resulting in different shapes (morphologies) for the crystals, but the angles between these faces are unique. Therefore, crystals are usually classified into systems based on three unique bond angles (**α**, **β**, **γ**) and three relative distances **a**, **b**, **c** in the directions of the chosen **x**, **y** and **z** axes. The smallest repeating lattice unit is known as the unit cell [106, 107].

Common racemic IBP contains an equal number of molecules of each enantiomer. But it is known the **S(+)** enantiomer has a different size of unit cell (cell dimensions **a**, **b**, **c**) and different space group from the racemic form [108]. The **RS (±)** racemic and **S (+)** form of IBP belong to the monoclinic system. *Figure 2.4* illustrates molecular structure obtained from neutron diffraction refinement of X-Ray diffraction of single IBP crystal. The structural data are reported in *Table 2.1*

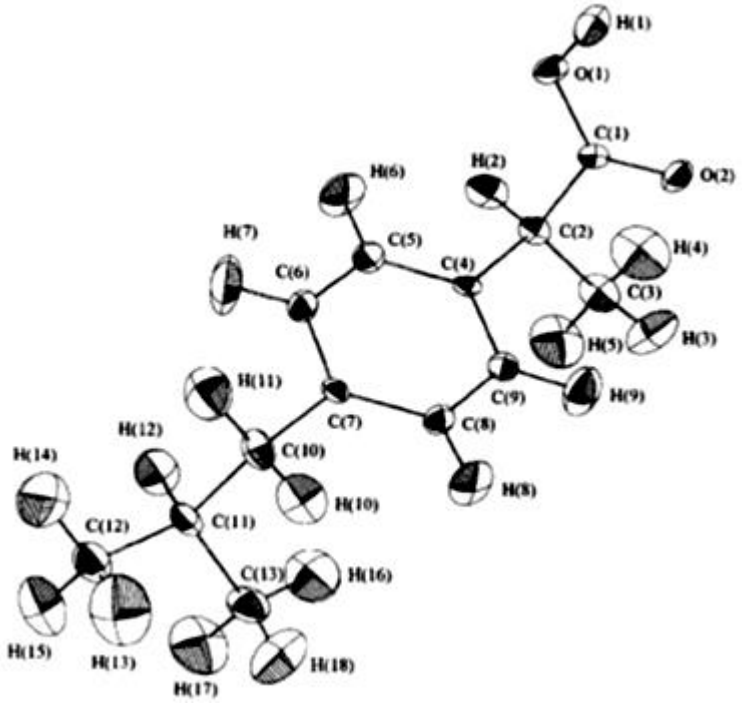

Figure 2.7 The molecular structure of IBP [109].

Table 2.1 Crystal structure of racemic and S-(+) form of ibuprofen [108, 110-113]

Parameter	**RS(±) ibuprofen**	**S(+) ibuprofen**
Formula	$C_{13}H_{18}O_2$	$C_{13}H_{18}O_2$
Molecular weight	206.3	206.3
Crystal system	Monoclinic	Monoclinic
Space group	$P2_{1/c}$	$P2_1$
a[Å]	12.67	12.46
b[Å]	7.88	8.03
c [Å]	10.73	13.53
ß[°]	99.3	112.95
No. of molecules in the cell	4	4
Density [g/cm3]	1.110	1.098

2.12 IBUPROFEN (IBP) CRYSTALLIZATION PREDICTION MODEL FROM HIGH ETHANOL SOLUTIONS

A crystallization chart for IBP in aqueous ethanol at 25°C has been generated and shows all the major properties required for a crystallization study. It is based on the results found by Rashid [26]. For 25°C, it shows: (i) the solubility; (ii) the metastable limits (for selected induction times); (iii) the growth rates; and (iv) the nucleation rates. The following sections will explain how *Figure 2.8* was prepared.

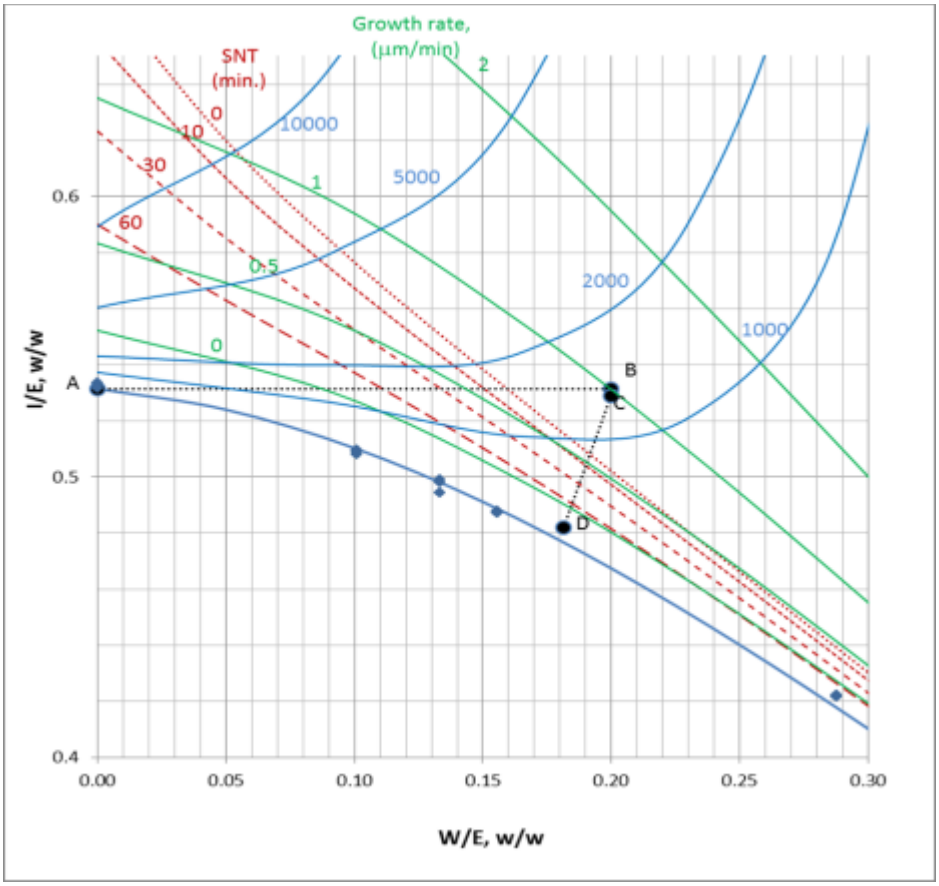

Figure 2.8 Enlarged crystallization diagram for ibuprofen (I) – ethanol(E) – water(W) at 25°C, showing the solubility curve and secondary nucleation threshold (SNT) lines (for various times). Also shown are growth rates (in μm/min) and nucleation rates (as #/min/g slurry). The nucleation rates are zero below the SNT. The lines ABCD correspond to a possible process for producing fine ibuprofen crystals. Water is added to a saturated solution of ibuprofen in ethanol (A) to give point B (above the nucleation limit) where nucleation (and growth) will occur. The supersaturation may fall a little (C) then ethanol is added to bring the solution back to a very low growth rate region (D).

The plot shows superimpositions on the phase diagram. This original plot from [26] has been enlarged to show details in the metastable zone. Also to put the new plot on a compatible basis for future work, the water concentration needed to be put on the same basis as the solubility. Now $\mathbf{X'_W = W/E}$ is used instead of the previous $\mathbf{X_W = W/(W+E)}$, where **W** is water and **E** is ethanol by weight. The range of $\mathbf{X'_W}$ from 0 to 0.3 was chosen as being the likely region for practical crystallizations. This allowed **I/E** (where **I** = ibuprofen) to run from 0.4 to 0.65 (*Figure 2.8*). Details of the calculation will now be shown.

i. Solubility

The 25°C solubility data of [26] are shown as the points on the plot. This data has been fitted using TableCurve 2D and the selected equation is

$$\ln(I^*/E) = 4.576 - 5.362*(X'_W) - 5.208*\exp(-X'_W) \qquad [2.4]$$

where **I*/E** is the solubility. This is the solubility curve shown in *Figure 2.8*. The three parameters of equation 2.4 have 95% uncertainties about ± 3%. The equation fits an estimated 95% of the **I*/E** data points within ± 0. 5%.

ii. Secondary Nucleation Threshold (SNT)

The 25°C SNT data of Rashid [26] has been refitted by exponentials to give the correlation

$$\sigma_{SNT} = 0.144*\exp(-X_W/0.117) * \exp(-t/1.1) \qquad [2.5]$$

where $\boldsymbol{\sigma_{SNT}}$ is the supersaturation [as $\mathbf{\Delta(I/E) = (I/E)_{SNT} - (I^*/E)}$] at which a solution, containing water with a solvent concentration $\mathbf{X_W = W/(E+W)}$, just nucleates at time **t** hours. The parameters have a 95% uncertainty of about ± 20% and the correlation

fits an estimated 95% of the data within ± 0.02 units of **I/E**. The fit of the correlation to the data is shown in *Figure 2.8*. SNT curves at selected induction times are shown in *Figure 2.9* [26].

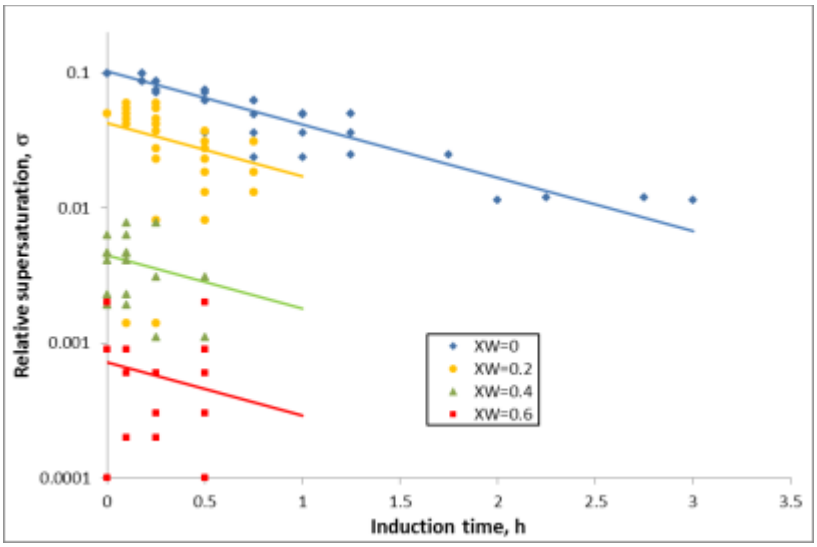

Figure 2.9 SNT supersaturation (on log supersaturation scale) against induction time, based on the data of Rashid [26]. The horizontal lines joining the pairs of experimental points have been omitted.

iii. Growth rate

Rashid [26] gives the following correlation for the growth rate at 25°C as a function of supersaturation s [as $\Delta(I/E) = (I/E) - (I^*/E)$] and water content $X_W = W/(E+W)$

$$G = 9.657 * \exp[1.95 * X_W] * s \qquad [2.6]$$

where G is the growth rate of a volume median size crystal in µm/min. The parameters have a 95% uncertainty of about ± 25% and the correlation fits an estimated 95% of the growth data within ± 40%. Rashid [26] showed that IBP crystallising from aqueous ethanol shows growth rate dispersion (GRD). For nucleated IBP crystals, the distribution is log normal in shape with a CV_G (= standard deviation/ mean) of ~ 0.5.

A procedure is needed for generating the constant growth rate lines (series of I/E vs. X'_W points) for *Figure 2.8*. An X_W (i.e. X'_W) value can be chosen for a selected G value. From equation 2.6 the supersaturation s can be evaluated. From equation 4 the

solubility can be calculated and adding s to it gives the required solution I/E concentration. Lines of selected constant growth rate are shown in *Figure 2.8*.

iv. *Nucleation rates*

Rashid [26] gives the following correlation for the secondary nucleation rates at 25°C in a seeded suspension where the solution has a supersaturation s

$B = 1.73 \times 10^5 * \exp[-X_W/0.12] * s$ for $s > s_{SNT}$

$B = 0$ for $s < s_{SNT}$ [2.7]

where **B** is the nucleation rate in #/min/g of the slurry. The nucleation rates are low. Equation 2.7 is not a very well defined correlation. The parameters have a 95% uncertainty of about ± 80% and the correlation fits an estimated 95% of the measured **B** data within a factor of 3.

The procedure for calculating curves of constant **B** is the same as that given above for **G**, except equation 2.7 is used instead of equation 2.6. The predicted nucleation curves for selected nucleation rates are shown in *Figure 2.8*.

2.12.1 **Predicted crystal contents**

The crystal content (mass of crystal per g of slurry) **CC** is calculated by

$$\mathbf{CC = \pi/6\ \rho_C\ N\ \mu_3} \qquad [2.8]$$

where ρ_C is the crystal density, **N** is the number of crystals present per g of slurry, μ_3 is the third moment of the size distribution $\mu_3 = \int L^3\ F(L)\ dL$, **L** is crystal size (as volume equivalent size) and **f(L)** is the number size distribution function. For the simplified processes considered, we will take **N = B*t**, where **B** is the nucleation rate, **t** the time the solution is held at that nucleating rate and $\mu_3 = L_m^3 * F$, **Lm** is the volume median size of the crystals and **F** (here taken as 2) a correction factor for the distribution shape.

From the data in *Figure 2.8*, *Figure 2.10* shows estimated crystal contents as a function of the selected water content of the solution. The parameter is the concentration of the initial solution (as w/w **I/E**) which does not have a great effect, except to allow operation at lower $\mathbf{X'_W}$ values, giving higher nucleation rates. Values have been restricted to operation above the t=0 SNT curve and initial solutions below

the t = 60 min SNT curve, so solutions can be prepared without nucleation. Growth times are those required to give a 3 µm volume median crystal size.

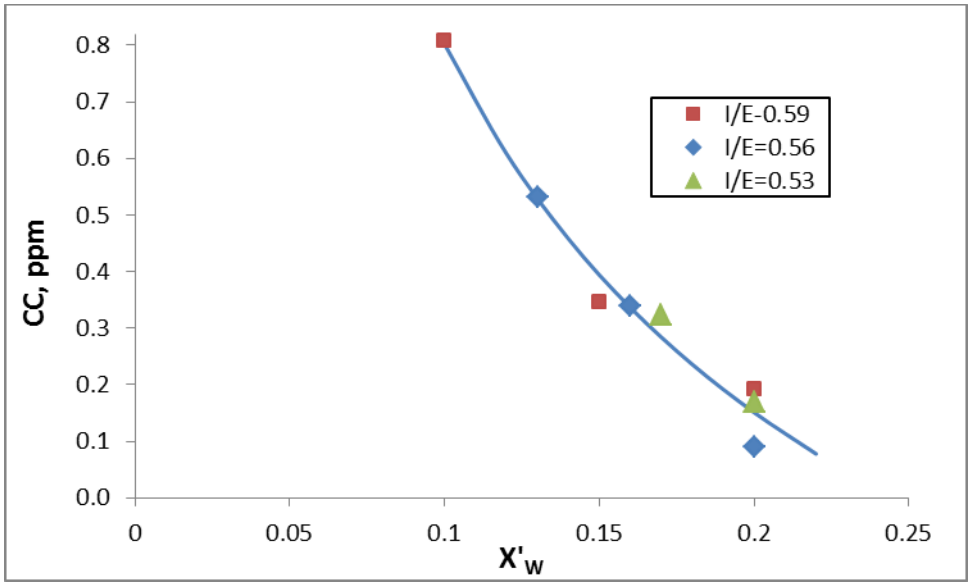

Figure 2.10. Predicted crystal contents from crystallization processes.

The estimated **CC** values were ridiculously small (< 1 ppm, which would not even be observable). To get a viable process, nucleation rates will need to be at least three or four orders of magnitude larger. This model was developed to produce IBP crystals in inhalable size. However, the predicted crystal content model showed that the process is not suitable, as the yield value is below the practical range. Hence, this process established from the solubility data from Rashid [26] could not be used for this work.

2.13 IBUPROFEN (IBP) PARTICLE SIZE REDUCTION TECHNIQUES FROM CURRENT LITERATURE

IBP has been used as a model drug to produce particles of micro and nanometer range by the rapid expansion of supercritical solutions (RESS) method, but critical conditions (temperature and pressure) and the complicated plant set up make it less suitable for bulk production [114]. Another combinative particle size reduction technology, based on solvent-antisolvent precipitation coupled high pressure homogenization (HPH), was adopted to produce IBP nanocrystals by Sinha and co-workers [115] in nanosuspension form. The generation of small crystals (nano-crystals) by crash nucleation of IBP has been proposed by Khan [28] with the use of the additives Pluronic F127 (Pl F127) and HPMC (hydroxypropyl

methylcellulose) respectively to restrict crystal growth and prevent agglomeration. Solvent diffusion and melt emulsification methods have also been used to produce IBP nanosuspension with polyvinylalcohol (PVA), polyvinylpyrrolidone (PVP) K25, Pluronic® F68, Tween 80 [116]. Verma and co-workers produced nanosuspension of IBP using sodium lauryl sulfate (SLS), PVP K30, Pluronic® F68, F127, Tween 80, HPMC in precipitation and microfluidization methods [117]. These studies focused on investigating the feasibility of the nanosuspension formulation for oral administration. IBP was also studied to develop the formulation for inhalation in aerosol suspension [118] and nebulizer dosage form [119]. However, it was evidenced in many reports that liquid dosage forms are very likely to show physical and chemical instability, caused by particle agglomeration and crystal growth in the Oswald ripening process [120]. In the case of pulmonary drug delivery, particle agglomeration could be a major issue, since it affects the amount of drug deposition in the site and thus the formulation efficacy [51]. *Table 2.2* shows a summary of the recent literature for IBP nanoparticle preparations.

Table 2.2 Literature summary of IBP nanoparticle preparations.

Manufacturing technique	**Delivery route**	**Dispersion medium**	**Stabilizers**	**Formulation type**	**Reference**
Solvent diffusion, melt emulsification	NA	Water	Polyvinylalcohol (PVA), Polyvinylpyrrolidone (PVP) K25, Pluronic® F68, Tween 80	Nanosuspension	[116]
Precipitation, microfluidization	NA	Water	Sodium lauryl sulfate (SLS), PVP K30, Pluronic® F68, F127, Tween 80, HPMC	Nanosuspension	[117]
Evaporation-condensation	Inhalation	Argon+vapor	None	Aerosol suspension	[118]
Self-nanoemulsufication	Inhalation	Oil-in-water	Tween 80,Cremophor RH 40, Transcutol P, Capryol 90, Polyethylene glycol (PEG) 400	Nebulizer	[119]
Rapid expansion of supercritical solutions (RESS)	NA	Supercritical CO_2	NA	Precipitated powder	[114]
Supercritical Antisolvent (SAS)	NA	Supercritical CO_2	Poly L-lactic acid (PLA), Eudragit L100	Precipitated powder	[121]
Anti-solvent precipitation	NA	Aqueous ethanol	Hydroxypropylmethylcellulose (HPMC), Pluronic F127 (Pl F127)	Nanosuspension	[28]

Manufacturing technique	Delivery route	Dispersion medium	Stabilizers	Formulation type	Reference
Solvent anti-solvent precipitation, High pressure homogenization (HPH)	NA	Water-Isopropanol (IPA)	Hydroxypropylmethylcellulose (HPMC), Sodium dodecylsulphate	Nanosuspension	[115]

The literature in *Table 2.2* shows that many researchers prepared IBP nanoparticles but none have investigated its feasibility as a dry powder inhaler formulation. Our research will attempt to produce IBP particles using an anti-solvent precipitation crystallization (APC) process by controlling particle size in the presence of additives. In most of the literature given in *Table 2.2*, the yield value of drug particles is very high (> 90%) in anti-solvent precipitation crystallization methods [18, 122, 123]. Moreover, Pl F127 and HPMC polymers have been successfully used as particle growth and agglomeration inhibitors in several formulation preparations [28, 117]. Pl F127 and HPMC polymeric additives were selected to control the IBP particle size in the anti-solvent precipitation crystallization process in the present work.

2.13.1 **Precipitation techniques**

Basically, in the antisolvent precipitation process, the solution of a poorly water-soluble drug, generally in an organic solvent is added into a miscible non-solvent or an aqueous solvent under agitation. A rapid high supersaturation occurs resulting in fast nucleation and precipitation (*Figure 2.11*). This method simply takes advantage of the change in the solubility of the same drugs in different but miscible liquids. However, due to the agglomeration tendency of the drug particles, it is hard to inhibit growth, which brings problems in production. Stabilizers/additives need to be added to the solvent or non-solvent phases to limit the particle growth and produce stable drug particles with desired size by the adsorption of the stabilizer at the particle surface in a fixed orientation [122, 124]. An illustration of the driving mechanism for the antisolvent precipitation (AP) process is shown in *Figure 2.11*.

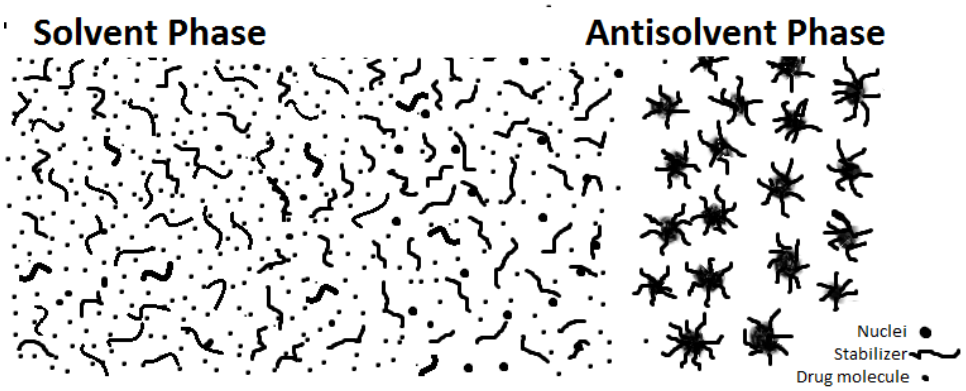

Figure 2.11. Representation of antisolvent precipitation (AP) of drug particles in the presence of amphiphilic stabilizers. Re-drawn from Matteucci et al. [122]

Optimization of the stirring rate, solvent-antisolvent ratio, drug content and temperatures are required to obtain uniform size nanoparticles in the AP process [125]. The drug precipitates as micro- or nanoparticles and the resulting dispersion is called a hydrosol [126]. A larger volume ratio of antisolvent to solvent leads to a higher supersaturation and rapid nucleation. But, a moderate drug content is considered, because a higher drug concentration will obstruct the diffusion process resulting a non-uniform supersaturation and also will increase the tendency of particle aggregation [127]. A lower temperature generally favours the decrease of particle size. This technique is cost-effective, avoids the use of high energy, increase the solubility and also enhance the drug dissolution rate due to the formation of slightly amorphous state [128, 129].

2.14 ROLE OF ADDITIVES IN CONTROLLING CRYSTAL GROWTH

It was mentioned that uncontrolled crystal growth and the particle aggregation are significant drawbacks for the anti-solvent APC process. Different parameters like stirring rate, the volume ratio of anti-solvent to solvent, temperature, drug solution addition rate and so on may be optimised, but the desired particle properties may still be out of reach. Use of additional substances (additives) in the anti-solvent crystallization system has been successful in inhibiting crystal growth and alleviating particle aggregation [130].

Additives can be classified into two types, tailor-made additives and polymeric additives where the first ones are not preferred due to their potential toxicities [131]. On the other hand, polymeric additives have been used conveniently in different

types of crystallization processes in different studies [123, 130, 132]. In the inhalation field, only excipients generally recognized as safe (GRAS) can be used [133]. The additives used in this work are already established as safe excipients for various pharmaceutical preparations, and *Figure 2.12* presents the molecular structure of the additives selected for this work.

a)

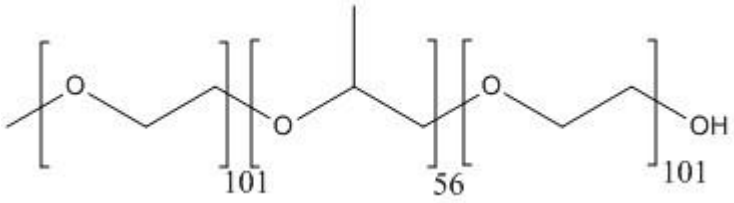

b)

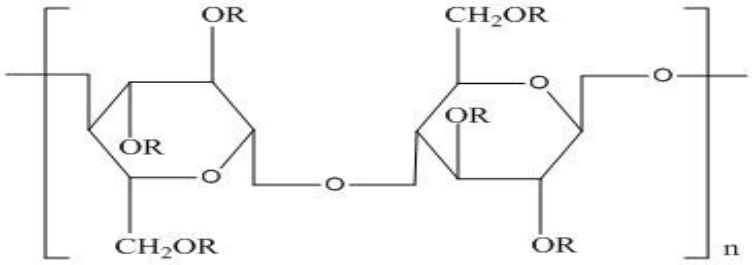

n= degree of polymerization, R= -H; $-CH_3$; $-(CH_2CH(CH_3)O)-H$; or $-(CH_2CH(CH_3)O)-CH_3$

c)

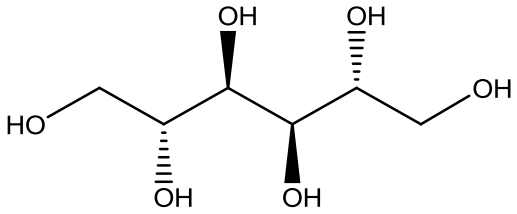

d)

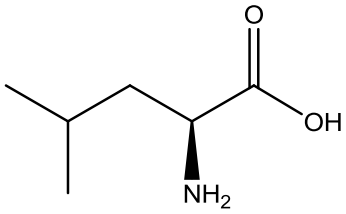

Figure 2.12 Molecular structures of additives used in this study a) Pluronic F127, b) HPMC, c) D-mannitol and d) L-leucine. (Drawn using Chemdraw Pro 11).

2.14.1 **Crystal growth inhibitor: Pluronic F127 (Pl F127)**

Pluronic F127 (Pl F127) (*Figure 2.12*a) is a triblock copolymer containing a hydrophobic propylene oxide (PO) polymer unit in the middle of two hydrophilic ethylene oxide (EO) polymer units. Literature reports suggest that a larger molecular weight with a more hydrophobic group in the polymer chain is suitable for inhibiting the growth of non-polar surface drug molecules like IBP [134]. Moreover, the quantitative effect of the Pl F127 in the growth of IBP crystals in anti-solvent precipitation process was investigated by Vetter and co-workers [124]. It was observed that the growth mechanism was surface integration controlled and the presence of the surfactant polymer reduces IBP crystal growth by its surface active properties. It was seen that the polymeric additive adsorbs isotropically on the surface of the crystals which hinders the diffusion of solute molecules resulting a slower rate of crystal growth. It was also shown that the Pl F127 used in the crystallization process is not incorporated into the structure of the crystals [124]. It has been reported that a mixture of surfactant Pl F127 and HPMC had a dual action of enhancing dissolution rate and inhibiting crystallization of the poorly aqueous soluble drug felodipine [135]. IBP as solid dispersions with poloxamer 188, poloxamer 407 (Pl F127) [136] and in combination with HPMC is reported to have enhanced bioavailability [137]. A possible explanation of this is that IBP-Pl F127 (1:10) solid dispersion systems might be completely miscible in the liquid state and immiscible in the solid state [138]. They crystallised out at once as micro-fine crystals from the liquid mixture, resulting in increased IBP surface area and enhanced dissolution rate [139, 140]. So, the improvement of solubility and the dissolution from the solid dispersions may be credited partially to the decrease in particle size in IBP crystalline state due to the presence of poloxamer 407 or Pl F127. In addition, a part of the drug might also have existed in a partial amorphous form [141]. Therefore, taking account of the evidences of solubility enhancement and growth inhibition role from available literature, Pl F127 was selected as a potential effective additive for the present study.

2.14.2 **Agglomeration inhibitor and stabilizer: HPMC**

Hydroxy propyl methyl cellulose (HPMC) is a large molecular non-ionic stabilizer and can adsorb onto IBP particles due to the interaction of the hydrophobic

(methoxyl) and hydrophilic (hydroxypropyl) groups (present in the polymeric chains (*Figure 2.12*b)) with the IBP surface [117]. Growth inhibition occurs based on the presence of a hydrodynamic boundary layer surrounding the crystal and aniso-tropic adsorption of the polymer on the growing crystal faces. Moreover, the non-adsorbed polymer molecules are not washed away but gather at the boundary region (*Figure 2.13*). Thus, provides higher resistance for drug molecules to diffuse through the barrier, perhaps resulting the growth inhibition. HPMC contains a large number of hydrogen bonding functional groups which is assumed to inhibit the crystal growth through habit modification [142].

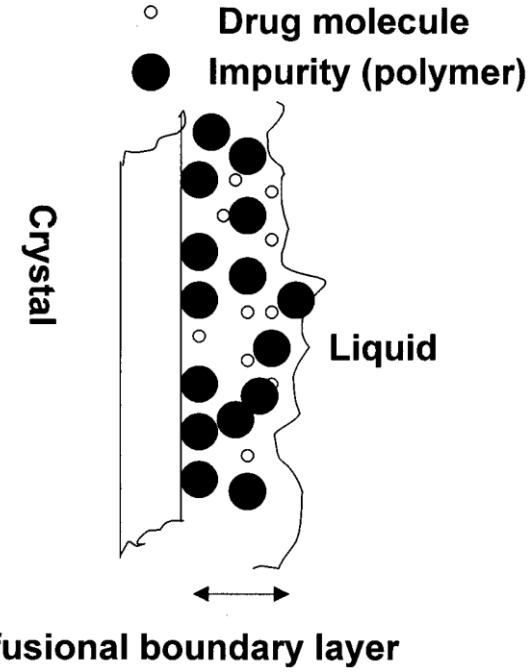

Figure 2.13 Schematic diagram showing the mechanism of growth inhibition and habit modification of crystals by polymers [142].

HPMC was successfully used as a stabilizer at a very low concentration (0.1%) dissolved in the anti-solvent phase due to its hydrogen bonding potential for IBP nanocrystal preparation in a cavi-precipitation process [115, 143]. Terebetski and co-workers investigated the physical role of HPMC in nucleation and crystal growth of IBP sodium by the dissolution method to assess the degree and extent of supersaturation [134]. It was shown that intermolecular hydrogen bonding between IBP and HPMC was driving supersaturation by delaying nucleation and crystal

growth of the thermodynamically stable crystalline free acid [134]. Another poorly water soluble drug, naproxen, was stabilised by HPMC and nanosuspensions were prepared by an optimised precipitation-ultrasonication process [144]. However, an increase in particle size was observed with an increase in HPMC concentration due to the deposition of concentric layers of HPMC on the drug surface [144]. It was also reported that the enhanced viscosity of the solution hindered the ultrasonic energy and obstructed the diffusion between the solvent and anti-solvent during precipitation, resulting in larger particle formation due to Ostwald ripening [144]. Therefore, the optimum HPMC concentration for the proposed anti-solvent crystallization (APC) of IBP was important to achieve the desired particle growth and agglomeration inhibition in the process.

2.14.3 **Cryoprotectant, carrier and bulking agent: D-mannitol**

D-Mannitol ($C_6H_8OH_6$) (Figure 2.12c), a hexahydric alcohol, has been largely used as a carrier and a bulking agent for freeze-dried pharmaceutical preparations [145]. Tee and Marriot, Steckel and Bolzen, and Saint-Lorant and Leterme reported its potential use as a carrier for aerosol delivery [146-148]. D-mannitol is also well known for its cryoprotective or lyoprotective properties [149] and as a bulking agent for the formulation, especially when the concentration of product for freeze drying is very low [150]. It has been chosen among other cryoprotectants because of its mucolytic property, as many lung diseases are characterised by the presence of thick stationary mucus in the airways [151]. Nanosuspension formulations or liquid dispersions have been converted to solid form by a lyophilization process. In order to protect the particles from freezing (cryoprotectants) or drying stress (lyoprotectants) [150], mannitol is incorporated at a constant concentration level (10%) [152] with liquid sample before freeze drying. The hypothesis of nanoparticle stabilization during the freezing step proposes that sugars isolate individual particles in the unfrozen fraction, thus avoiding aggregation for the period of freezing above glass transition temperature (Tg) [153]. The mechanism for stabilization of nanoparticles by lyoprotectants during the drying steps is explained by the water replacement hypothesis, which presumes the formation of hydrogen bonds between a lyoprotectant and the polar groups at the exterior of drug nanoparticles. These lyoprotectants preserve the intrinsic structures of nanoparticles by acting as water

replacements [154]. Figure 2.14 shows the nanosuspension samples freeze dried with and without mannitol.

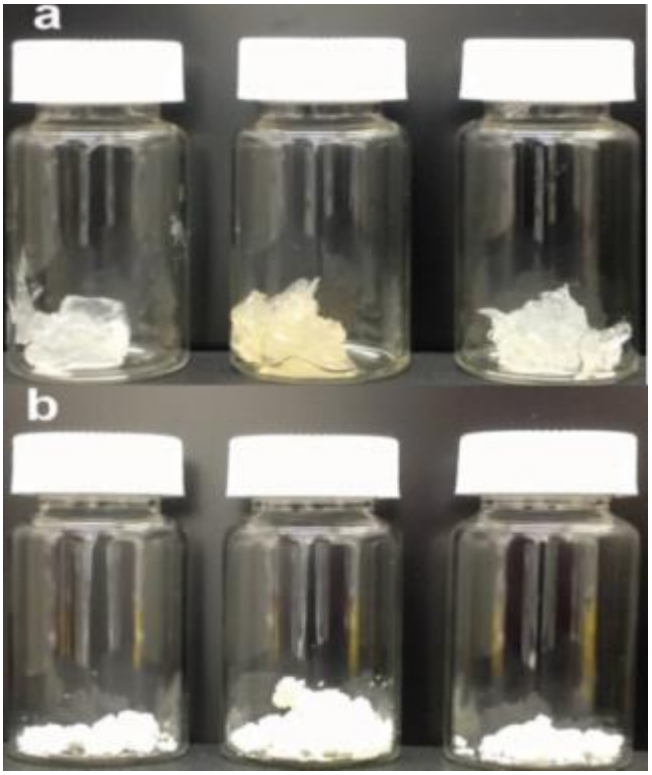

Figure 2.14 Physical state of drugs nanosuspension after freeze drying without mannitol (a) and with mannitol (b) [152].

Freeze dried nanosuspensions without mannitol appeared as off-white, fluffy and sheet-like materials, and large agglomerates were observed. Nanosuspensions with mannitol formed a powder easily redispersible in phosphate buffer solution (PBS) after manual shaking. Hence, mannitol acts as a carrier which prevents nanoparticle aggregation during the freeze drying process [152]. Although mannitol crystallises in different polymorphic forms (α, β or δ) depending on the concentration (relative to other components in the formulation) and freezing rate, no evidence of any effect of these mannitol polymorphs on drying/processing characteristics or product stability has been reported so far [145, 155]. Mannitol has been used as a matrix material for controlled crystallization of a poorly water soluble drug (fenofibrate) [155] and a cryoprotectant for curcumin-chitosan nanoparticle complex preparation in a spray freeze drying (SFD) process [156]. It has also been used successfully as a carrier for the DPI formulations of nucleic acid produced by a spray freeze drying process [157], and a hydrophobic drug budesonide containing freeze dried mannitol [133] to

enhance its aerosolization behaviour. The findings from the above studies suggest that D-mannitol can be used as an additive to recover the IBP nanoparticles in a freeze drying process and also can act as a potential carrier in the DPI formulation.

2.14.4 **Dispersive adjuvant: L-leucine**

L-leucine ($C_6H_{13}NO_2$) (*Figure 2.12* d), a hydrophobic amino acid, has been used as a dispersive adjuvant for DPI formulations. It is used because amino acids are additives that have been found to improve aerosol efficiency [158, 159]. Enhanced aerosolization performance of several drugs from DPIs by using L-leucine as dispersive agent among other amino acids has also been recorded [160-162]. A recent study demonstrated the enhanced dispersion of conjugated chitosan nanoparticles was ascribed to the amphiphilic setting of the L-leucine conjugate and hydrophobic cross-links formed on the nanoparticles' surface [163]. Addition of leucine was found to improve the flow and aerosolization properties of freeze dried mannitol [133]. Another investigation found a notable surface modification and substantial improvement in the flow properties of fine IBP powder after dry coating with L-leucine to use in an oral dosage form [164].

Feng and co-workers studied the effect of increasing L-leucine mass fraction in the DPI formulation of a model drug, specifically its effect on leucine crystallinity of microparticles, on powder density and on powder dispersibility [165]. L-leucine possess the ability to form hollow particles, and a change in particle morphology from solid spheres to hollow, rugose particles leads to the formation of low density particles and enhanced dispersibility of the DPI formulations [159, 166-168]. Due to the surfactant nature, leucine can also reduce the interparticulate adhesive forces and lessen the aerodynamic particle size [169, 170]. A study of the poorly water soluble drug budesonide demonstrated that leucine can be used in ethanol-water co-solvent systems to develop inhalable particles with great dispersibility and better manufacturability [171]. Therefore, from the available literature, it was evident that L-leucine would be a useful additive to the process of developing IBP as a dry powder inhaler formulation. However, it is also reported that high concentrations of l-leucine (i.e. above 50% w/w) have a negative effect on the long term drug stability [169].

2.15 MODEL DRUG: IBUPROFEN (IBP)

Ibuprofen (IBP), which is (±)-2-(p-isobutyl phenyl) propionic acid, belongs to class II of the Biopharmaceutics Classification System (BCS) of drugs, also known as non-steroidal anti-inflammatory drugs or NSAIDs [172-174]. *Figure 2.15* shows the molecular structure of IBP.

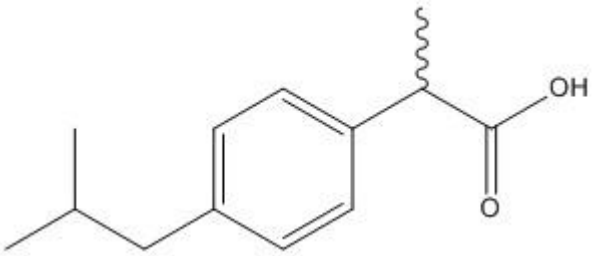

Figure 2.15. The molecular structure of IBP [28](Drawn using Chemdraw Pro 11).

IBP has a chiral carbon, and hence two different enantiomeric forms of IBP exist, with different biological effects. The *S*-enantiomer, which is the biologically active form, and the *R*-enantiomer, which has no biological activity, are partially converted into the *S*-form in the human organism [175] [176]. IBP is used in the therapy of rheumatism, dysmenorrhoea, headache, fever and arthritis. It is presented in a number of formulations such as oral suspensions, capsules, tablets, syrups, suppositories and creams, and transdermal patches are also under development [177].

Among all these IBP preparation products, the first five are subject to oral dosage forms which undergo gastrointestinal digestion and absorption and liver detoxification, and after a series of functional roles in the blood, circulation then activates its anti-inflammatory effect. The required dosage for this effect in an adult is 20 mg ~ 30 mg, whereas the provided dose is about ten times of this amount [174]. Moreover, it is also found that long-term usage of higher doses of IBP has the potential to cause hypertension and myocardial infarction, and there is an elevated risk of cancer mortality [3-5]. It was also found that pulmonary administration of IBP nanoparticles in mice requires a dose three to five times less than that for oral administration and has the same analgesic effect [118]. It is also documented that the onset of analgesia occurs at IBP plasma concentration between 6.8 and 10.1 μg/ml [178]. Hence, most of the literature suggests that peak plasma level of IBP from a 400 mg tablet lies between 17–36 μg/ml [179-182]. A nebulised oil-in-water nanoemulsion mist of IBP was developed with ideal properties for inhalation and

successful in-vitro drug release by the dissolution test [119]. However, in the case of both formulations, the cell toxicity tests revealed moderate effects from bio-incompatibility at an increased level of delivered drug concentration.

All types of oral dosage forms as well as oral formulations are associated with common adverse reactions. Some patients may also suffer from allergic nephritis, cystitis, kidney disease, renal papillary necrosis or renal failure, and bronchospasm [174]. In the case of topical products, there are no contra-indications or adverse reactions as for the oral medication, but poor sealing performance, production of secondary pollution and non-uniform administration cause tenderness as well as slowing the drug action [174]. Recently, research incorporating IBP in a gelatine based tissue adhesive found adverse effects on the bonding strength due to its reaction with the other adhesive components and increased crosslinking density [183].

As discussed earlier, the pulmonary route of administration is considered to be the most non-invasive route, because it bypasses the first stage of metabolism and is expected to eliminate most of the adverse drug reactions caused by oral drug administration. The route of drug delivery also offers the most efficacious drug action in the lowest dose (mostly 10–30 mg) and minimises the side effects caused by chronic use of higher drug doses.

Despite the fact that the IBP is the most commonly used therapeutic medicine, its poor solubility in aqueous solutions lessens the dissolution and absorption rates into the blood circulation [173]. A study has shown that the bioavailability of IBP increases two fold on a decrease of particle size from 150 μm to 30 μm [184]. The particles in dry powder inhaler formulations are to be less than 5μm, and such a particle size reduction in the formulation substantially enhances the dissolution rate as well as the bioavailability [64].

2.16 SOLUBILITY OF IBUPROFEN (IBP)

Ibuprofen (IBP) has poor water solubility and belongs to class II of the Biopharmaceutics Classification System (BCS). On the basis of their solubility and permeability through biological membranes, drugs can be categorized into four classes, as given by the Biopharmaceutical Classification System (BCS) (*Figure 2.16*).

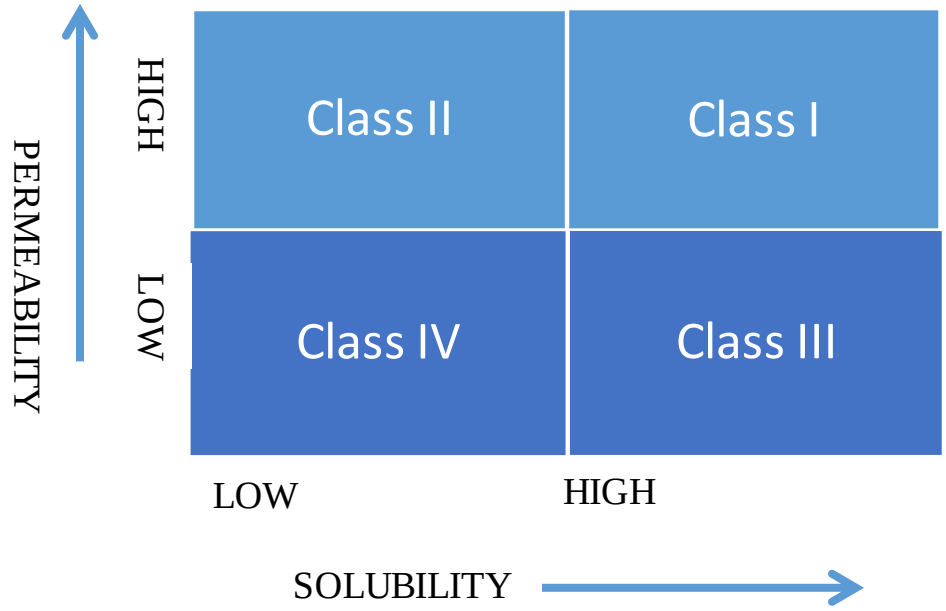

Figure 2.16 Biopharmaceutical classification (BCS) of drugs.

It is identified that poorly water soluble drugs are typically hydrophobic, having a better affinity penetrating more rapidly towards the lipophilic intestinal membrane. In spite of this, absorption of these drugs from the GI tract is unpredictable due to their poor solubility in water. Therefore, enhancement of the drug solubility from any dosage formulation is connected with the application of auxiliary substances to advance new technological possibilities [185].

Information on IBP solubility in aqueous solvents (especially low ethanol aqueous ones) is scarce, and results from the available studies are not in good agreement [116, 186-190]. For example, *Figure 2.17* shows the reported solubilities of IBP in pure water at 25°C arranged in order of increasing value. The value obtained in this study is also shown. There is considerable variability between the different data values.

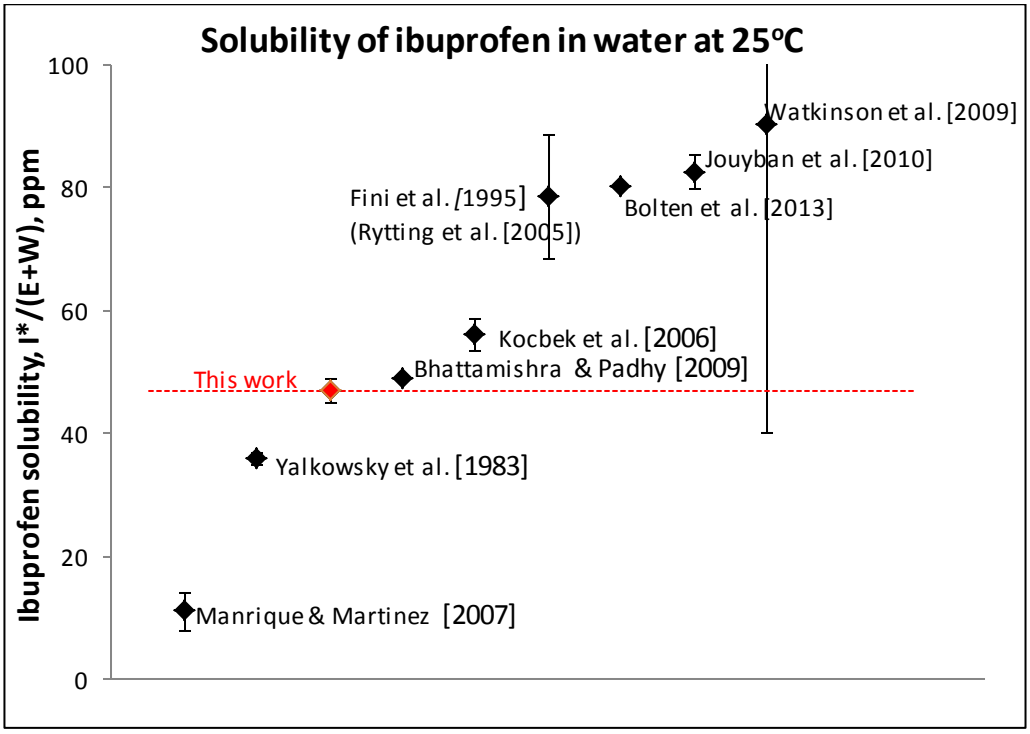

Figure 2.17 Reported solubilities of IBP in water at 25℃. Note that the Bolten et al. result is at 27℃, that of Yalkowsky et al. [190]. at 30 ℃ and Watkinson et al.[189] at 32 ℃. The Fini et al.[187] data was for the sodium salt in very dilute acid.

The poor aqueous solubility of IBP causes difficulties to determine its accurate solubility value in water; such as melting point alteration and temperature change due to the long term vigorous agitation in dissolution method. In *Figure 2.17* the methods for determining IBP aqueous solubilities were different in the reported works. The huge variability between the reported values are due to the errors associated with the differences in the adopted methods and conditions for the solubility determination. Manrique and Martinez [191], Yalkowsky (30 ℃) [190], Bhattamishra and Padhy (27 ℃) [29] and Kocbek [116] used the dissolution to equilibrium method but temperature condition differed in some cases from 2-7 ℃. Fini et. al. added the sodium salt of IBP in very diluted acid gradually into distilled water until it was saturated and equilibrium was achieved after a week of storage. Bhattamishra and Padhy [29], Jouyban [192] and Watkinson [189] used centrifugation to separate the IBP saturated solution sample for concentration determination. Bolten [172] determined the IBP solubility in water at 27 ℃ and used HPLC for the concentration determination. Whereas, Watkinson [189] determined

the IBP aqueous solubility at 32°C and used both HPLC and UV spectrophotometry for the concentration determination. Other researchers have used the UV spectrophotometry. Moreover, due to the very small amount of solute dissolving in aqueous solvents, the low solubility values show higher deviations in the derived data from other researchers. The variability in the available literature data for IBP solubility in pure water flag the need for extensive investigation on improving the current research in this area.

Figure 2.18 shows the available literature data for IBP solubility in aqueous ethanol.

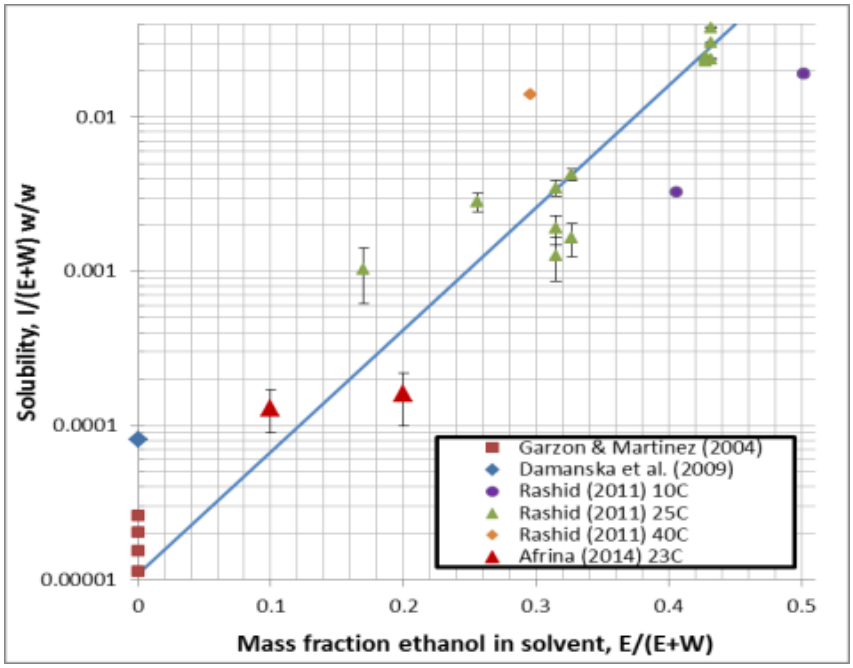

Figure 2.18 Prior solubility data for IBP in aqueous ethanol. The Garzon & Martinez [193] data are for 25, 30, 35 and 40°C.

The available solubility data in the low ethanol range was not sufficient to construct a phase diagram. Moreover, additives are to be used to control the particle size in the proposed method of precipitation crystallization. Hence, IBP solubility in the presence of the selected additives also needs to be investigated.

The outcomes of this investigation will be used to design and optimise the APC process for producing IBP crystals in nano/micrometer range for developing an efficient dry powder inhaler formulation.

2.17 CONCLUSION

This research proposes a new approach to developing IBP DPI formulation, using regular size particles produced by a controlled crystallization process. So far there is no work reported in the literature on IBP microcrystals to produce a DPI formulation, and thus it is anticipitated that the outcome of this project would be able to contribute to the development of a non-invasive DPI formulation with reduced cost and with better therapeutic benefit.

The limited literature shows some attempts have been made at a direct crystallization technique, using additives for producing respirable size crystals, but it appears that this technique has never been applied successfully. The present PhD project proposes to develop a new method of a controlled crystallization process for producing IBP of small size (< 5 μm) crystals for pulmonary delivery. This proposed work is expected to be of interest to pharmaceutical companies. In addition, it is anticipated that this project could result in novel intellectual property and appropriate protection will be sought through QUT Bluebox prior to any publication.

Chapter 3: Research Methods

3.1 INTRODUCTION

The materials and methodologies adopted to achieve the aims for this project are described in this chapter. The materials' sources and specifications are given at the beginning of the chapter. The equipment calibrations (UV spectrophotometry), method development and validations (solubility and particle preparation), and instruments to measure the characteristics of the formulations are outlined and described with the detailed methods and implementation of the study.

3.2 MATERIALS

3.2.1 **Model drug**

Ibuprofen (IBP) was used as the active pharmaceutical ingredient (API) in this study. USP grade IBP (Part no: 30-1192-1000GM) was purchased from Professional Compounding Chemists of Australia Pty Ltd (PCCA, Matraville, NSW 2036), as a high purity racemate of (R)/(S)-(±)-[2-(4-isobutyl-phenyl) propionic acid] with the empirical formula $C_{13}H_{18}O_2$ and molecular weight 206.27. It was used without further purification. *Figure 3.1* shows an SEM of the purchased IBP crystals with volume median size D[v,0.5] = 41 μm. The bar shown corresponds to 100 μm.

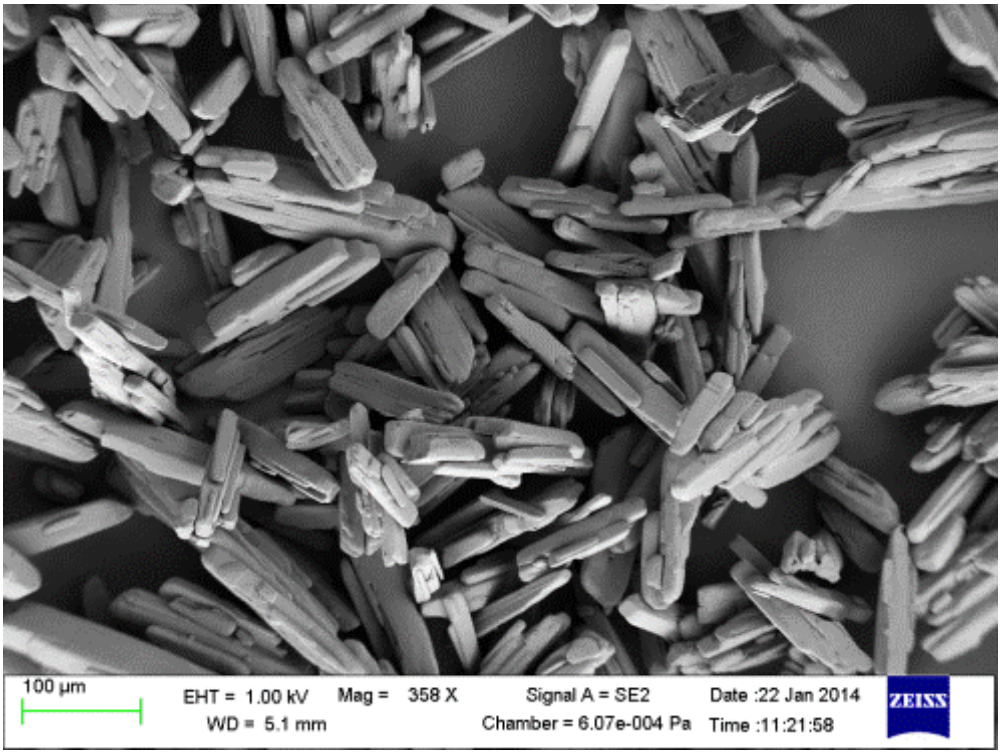

Figure 3.1. SEM of purchased IBP crystals.

3.2.2 **Additives**

A formulation additive is any component other than the active ingredient of the formulation. Some pharmaceutical excipients/additives used in this study for making inhalable particles are as follows:

Pluronic F127 (Pl F127)

Pluronic F127 (Pl F127) (*Figure 2.12*a) is a surfactant copolymer comprising a hydrophobic propylene oxide (PO) polymer block in the middle of two hydrophilic ethylene oxide (EO) polymer blocks. Pl F127 (Poloxamer 407 NF, Part no: 302637-500GM) was purchased from Professional Compounding Chemists of Australia Pty Ltd (PCCA, Matraville, NSW 2036).

Hydroxy propyl methyl cellulose (HPMC)

Hydroxy propy methyl cellulose (HPMC) (*Figure 2.12* b) is a large molecular non-ionic stabilizer. It was purchased from Sigma-Aldrich (Part no: 09963-100 G, Lot no: BCBG6002V).

D-mannitol ($C_6H_8OH_6$)

Mannitol (*Figure 2.12* c) is a hexahydric alcohol and has been largely used as a cryoprotectant and a bulking agent for freeze-dried pharmaceutical preparations

[145]. D-mannitol was purchased from Sigma-Aldrich (Part no: M4-125-500 g, Lot no: SLBJ5312V).

L-Leucine ($C_6H_{13}NO_2$)

L-leucine (*Figure 2.12* d), is a hydrophobic amino acid which has been used as dispersive adjuvant for DPI formulations [158]. L-leucine (Bioultra, ≥ 99.5%) was purchased from Sigma-Aldrich (Part no: 61819-100 G, Lot no: BCBM2322V).

3.2.3 **Chemicals and Solvents**

Spectrophotometric grade ethanol was purchased from Sigma-Aldrich and deionised/Millipore water is available in the laboratory.

3.3 METHODOLOGIES

3.4 UV SPECTROPHOTOMETRY

UV/Vis spectrophotometers use the UV (ultra violet) and visible regions of the spectrum. A spectrophotometer quantitatively measures the fraction of light at a given wavelength that is absorbed by a given solution.

According to the Beer-Lambert law, the absorbance Abs = ln (I_0/I_i) = k_S C , where I_i is the light intensity with the sample in the path and I_0 with no sample (solvent only), C is the solute molar concentration, and k_S is a co-efficient particular to each material and varies with the wavelength of the light and the cell path length. Thus it is necessary to select a suitable wavelength and path length and then determine the co-efficient k_S which can then be used to give the solute concentration in a solution. Concentrations units for this section on spectrophotometry are given as mass fraction IBP to total solution mass.

3.4.1 **Wavelength selection in UV spectrophotometer**

The wavelength was scanned by preparing different dilute IBP solutions in absolute ethanol. Though the scans showed maximum abs in 207 nm (*Figure 3.2*) and 262 nm (*Figure 3.3*), it was found in the literature that wavelengths of 221 [164, 194] and 264 nm [29, 152, 187, 195] show a good response to the low to high IBP concentration. The calibration plots in *Figure 3.4* for 264 nm & *Figure 3.6* for 221 nm have shown linear relationships (R^2=1) of IBP concentration with the absorbance value. In the wavelength of 264 nm, calibrations were performed for each of the solvents used for the solubility investigations. At 221 nm the calibration was done in

duplicate trials using 35% aqueous ethanol. In all cases the responses were linear confirming the accuracy of the analysis in the selected wavelengths. So, wavelength 221 nm [164, 194] was chosen for IBP assay in the in vitro aerosolization tests in the twin stage impinger due to its high sensitivity to detecting a low amount (0.3- 21 µg/mL) of the drug. The solubility measurement tests were done using 264 nm [29, 152, 187, 195] to minimise the dilution number in order to keep drug concentration (50 to 1500 ppm) within the limit of detection (*Figure 3.3*).

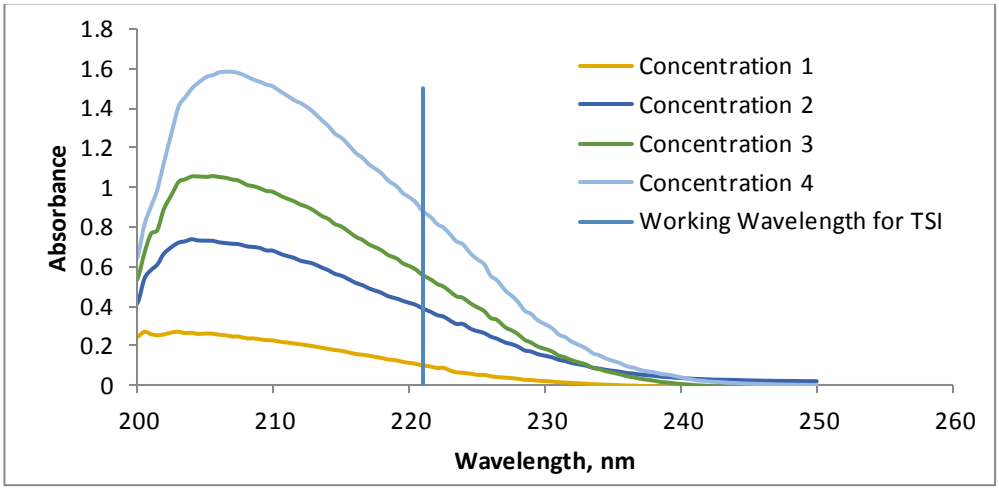

Figure 3.2 UV spectrophotometer wavelength scan with four different concentrations of IBP solutions in 35% w/w ethanol for identification at 221 nm.

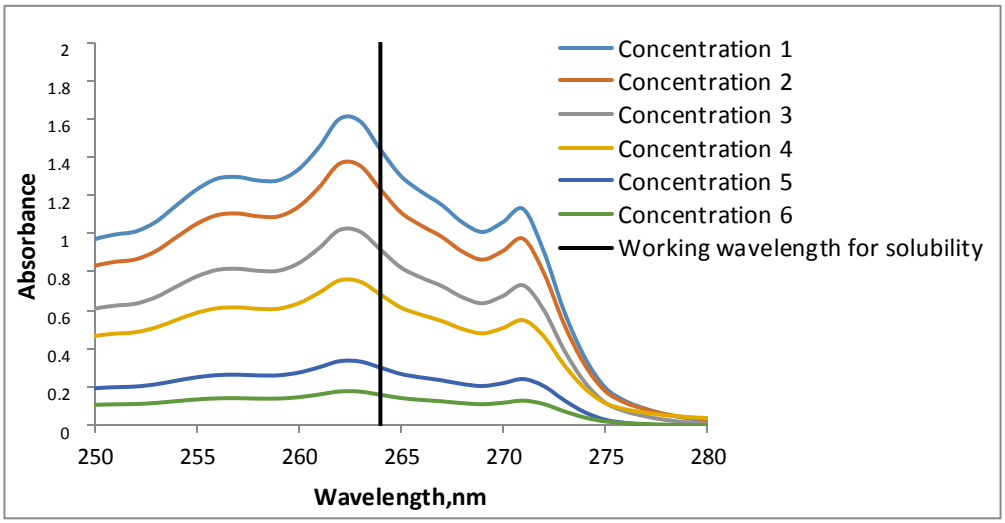

Figure 3.3. UV spectrophotometer wavelength scan with six different concentrations of IBP solutions in ethanol for identification at 264 nm.

3.4.2 **Calibration Method**

A Thermo Scientific Evolution Array UV-Visible spectrophotometer operated with VISIONcollect software (version 1.5, Build 7) was used in this study at a wavelength of 264 nm for the solubility tests. For IBP in aqueous ethanol, the concentration range of the spectrophotometer is 50 to 1500 ppm by wt. (mass fraction) IBP (absorbance from ~ 0.07 to 2). The spectrophotometer was calibrated against weighed solutions of ethanol (E), water (W) and IBP (I). All measurements were done using 10 mm square quartz cuvettes.

The calibration curves are illustrated in *Figure* 3.4, which indicates the linearity of the Beer-Lambert relation. However, the slope of the lines (the Beer-Lambert constant, ks) varies with the ethanol content (*Figure* 3.5), showing some interaction of the added ethanol with the IBP structure. The large errors in the low ethanol solutions were due to the very low solubilities and the resultant difficulties in getting a wide range of test results. The slope varies linearly with the ethanol content and the correlating equation is shown on *Figure 3.5* (with 95% uncertainties on the parameters). These slopes were used to determine the solubility of IBP in aqueous ethanol. The raw data is provided in Appendix A1 and Appendix A2.

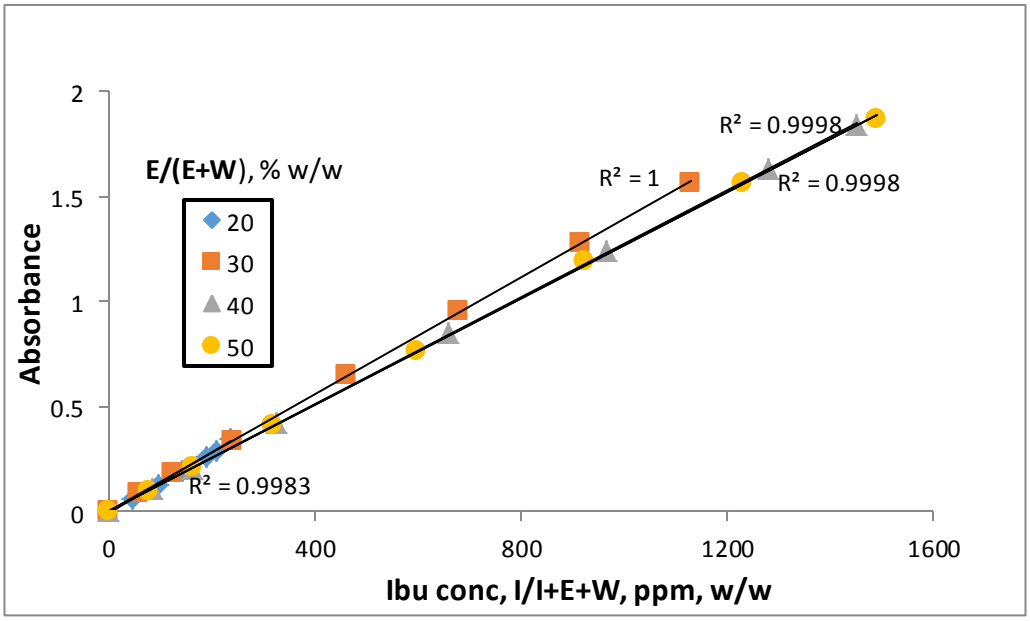

Figure 3.4 Linearity of Beer-Lambert law in calibration of the UV spectrophotometer. The data range for the 20% ethanol content is limited because of the low solubility. Values of R^2 for the correlations are also shown.

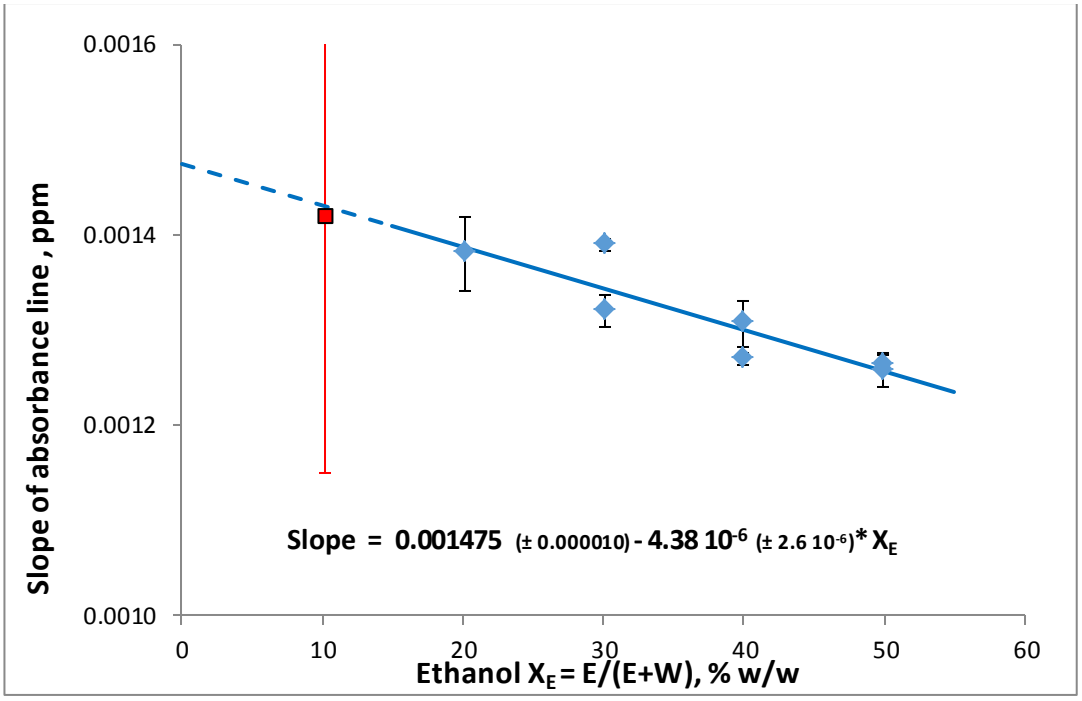

Figure 3.5 Calibration of UV spectrophotometer. Variation of slope ks with ethanol content.

Calibration at 221 nm for IBP DPI formulation assay after in vitro drug dispersibility test in Twin stage impinger: To determine the trace amount of drug content (< 1 µg) a calibration curve of IBP in 35% aqueous ethanol was constructed at 221 nm [164, 194] wavelength for its high sensitivity. The reproducible linear trends were established in the concentration range of 0.3- 21 µg/mL in volumetric method (*Figure* 3.6) from duplicate trials. The average slope (0.0405 ± <0.0001) of this calibration curves was used to determine the IBP drug content in the inhaler device, in stage 1 and stage 2 of the twin stage impinger (detailed in Section 3.16.1). The raw data is given in Appendix A3.

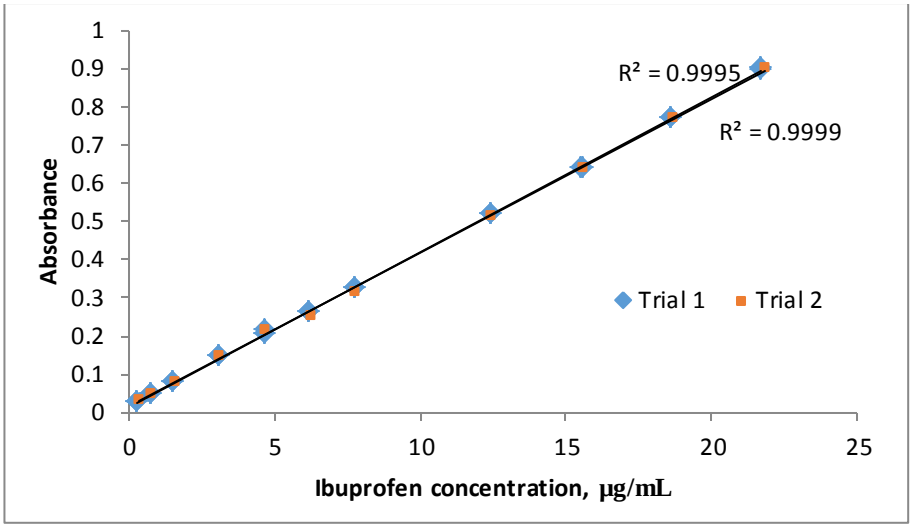

Figure 3.6 UV calibration curves for IBP concentration determination at 221 nm in 35% w/w ethanol solutions from duplicate trials. Values of R^2 for the correlations are also shown.

3.5 MEASUREMENT OF SOLUBILITY

Solubility studies were carried out by the dissolution of IBP particles to equilibrium into aqueous ethanol solvents in magnetically stirred Schott bottles in a water bath at constant temperature.

The water bath temperature was kept constant within ± 0.1 ºC of the desired temperatures (10, 25 and 40 ºC) and was checked with a calibrated glass thermometer. For an experiment, an excess amount of IBP was mixed with ~ 20 g of aqueous ethanol solvents of different composition. The experimental set up is shown in *Figure 3.7*.

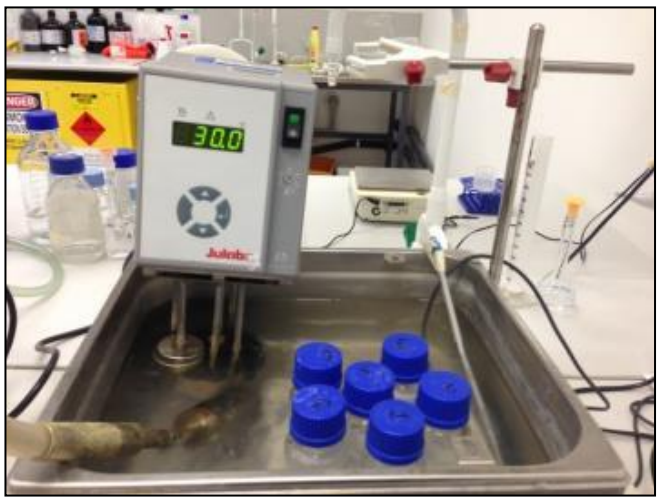

Figure 3.7 Schott bottles on stirrer plate in thermostatic water bath.

Figure 3.8 and *Figure 3.9* show the approach to equilibrium for several experiments (data is provided in Appendix A4 and A5). Equilibrium is reached within 30 minutes, so bottles were stirred with magnetic stirrers for at least 6 hours to ensure equilibrium. Then the bottles were left to settle in the bath and the supernatant from each bottle was filtered using preheated/pre-cooled syringes with 0.22 µm membranes, then diluted if necessary.

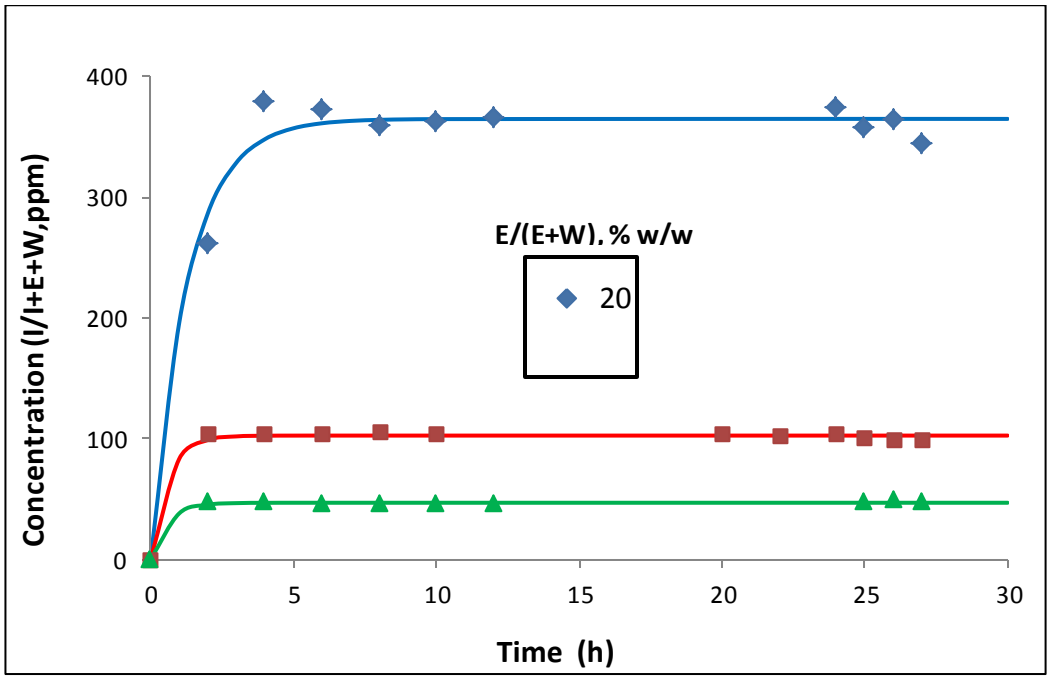

Figure 3.8 Approach to equilibrium for the dissolution of IBP in water and aqueous ethanol at 25 °C. Exponential curves have been fitted to the results.

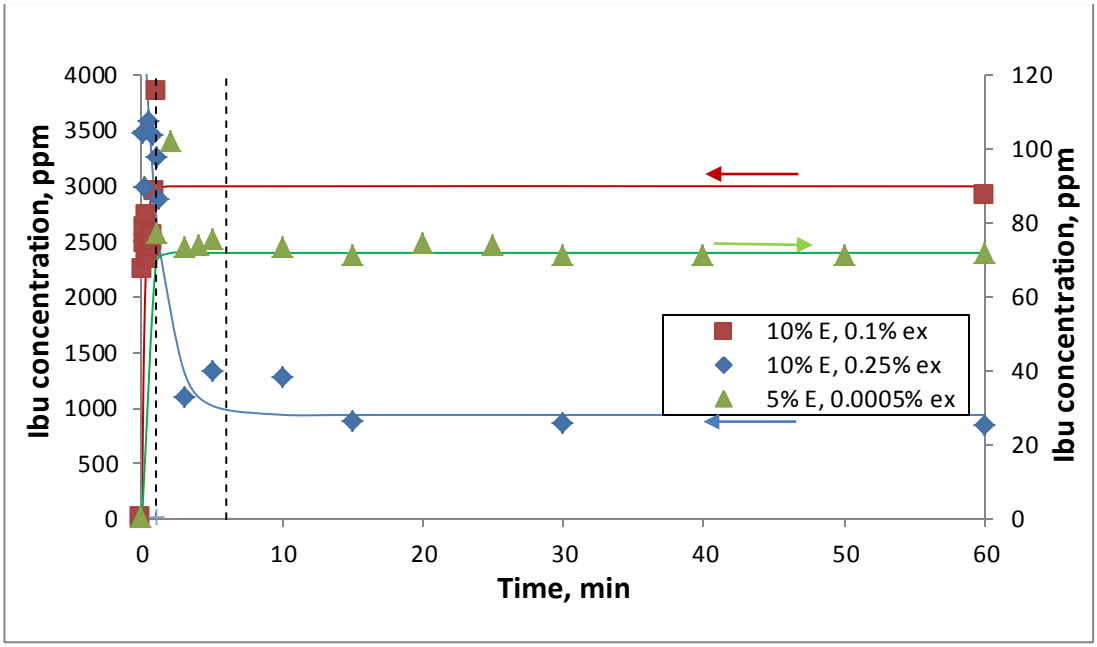

Figure 3.9 Investigation of equilibrium attainment for two dissolutions and one crystallization (falling curve) of IBP in aqueous ethanol with additives. The values for 10% E, 0.1% of each excipient (Pl F127 & HPMC)) have been multiplied by a factor of 6 to expand the scale for comparison.

The effect of additives on IBP solubility was investigated at 25°C. The concentration ranges used were 0 to 2% w/w HPMC/ (E+W), 0 to 2% w/w Pl F127/ (E+W), 0-1.6% w/w leucine/ (E+W), 0-18% w/w mannitol/(E+W), and 0 to 20% w/w E/(E+W). Unless otherwise indicated, concentrations are given as a mass ratio to the amount of solvent (E+W).

The supernatant from each bottle was filtered and diluted as necessary for quantification purposes. The diluted samples along with an appropriated standard calibrations were analysed on the UV spectrophotometer working at a wavelength of 264 nm [119, 152, 187, 195] and using 10 mm square **UV** quartz cuvettes [196]. Each experiment was done in triplicate.

3.5.1 **Preparation of HPMC solutions**

Solutions containing 5% w/w HPMC were prepared by adding HPMC powder to a weight of water required to make up to one tenth of the final weight. Vigorous agitation was used until the aggregates of powder were dissolved. The solutions was then refrigerated for 24 hours at 4°C to allow polymer hydration, made up to final weight and stored refrigerated for 72 hours prior to use [197]. The final solvents of

required concentration of additives were prepared by taking the weighed amount of Pl F127, leucine and mannitol powder, made up to the final weight with water/aqueous ethanol. They were magnetically stirred to dissolution.

3.6 NEAR-INFRARED SPECTROSCOPY

Near-infrared (NIR) spectroscopy is a technique with wide and varied applications in pharmaceutical analysis. The NIR spectral range extends from 780 nm to 2500 nm (from 12800 cm^{-1} to 4000 cm^{-1}) [198]. NIR spectroscopy has applications for chemical, physical and process analysis including the determination of absolute water content. In this work, a Cary series UV-Vis-NIR spectrophotometer (Cary 5000, Agilent technologies) was used for the determination of water in each phase after the phase separation of IBP in aqueous ethanol (>35% E/(E+W)) at 40°C. It is a double beam instrument operated by Cary WinUV software (version 6.1.0.1568).

3.7 PHASE SEPARATION

IBP in aqueous ethanol shown two liquid phases at certain concentration ((>35% E/(E+W)) at 40 °C [26]. This was checked using NIR in the present work. Excess amount of IBP was added in 40 and 50% E/ (E+W) solutions, stirred for 24 hours and allowed to settle in a 40 °C temperature controlled bath for 72 hours. Samples were collected from each layer. The IBP concentration was determined by the UV spectrophotometer as per the method described in Section 3.3. The water content was determined using an NIR spectrophotometer (Section 3.6) after diluting with ethanol as required. The ethanol content for each layer was determined by subtracting the measured IBP and water content value [199].

3.7.1 **Wavelength Selection**

The wavelength was scanned for eleven aqueous ethanol solvents (0-100% E/(E+W)) within the NIR spectral range using a quartz cuvette with a 1 mm optical path. Peaks were found in the wavelengths of 1446 nm, 1932 nm and 2310 nm (Scan spectrums shown in Appendix A6). The highest peak was typically shown at ~1932 nm wavelength and was considered as the best wavelength for determining water content. Other peaks might have resulted from the –OH group present in ethanol. Absolute ethanol was used as the reference.

3.7.2 **Calibration Method**

To determine the water content, 16 points were chosen to calibrate the NIR equipment. The calibration points were produced at a pre-determined concentration of water in ethanol (W/(E+W)), gravimetrically prepared on an analytical balance (with accuracy of ± 0.0001 g). The calibration curve is shown in *Figure 3.10*. The slope from this calibration line was used to calculate the water content using the Beer-Lambert relation. The raw data is given in Appendix A7.

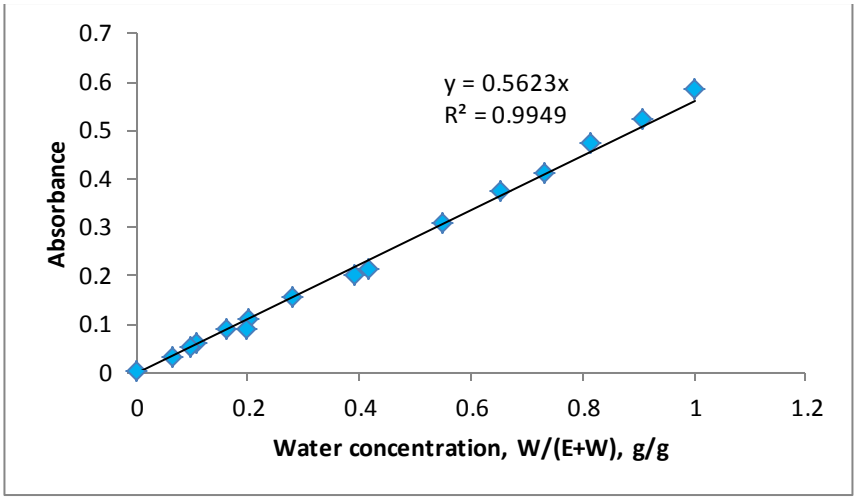

Figure 3.10 Calibration curve of NIR spectrophotometer at 1932 nm. Values of R^2 for the correlation is also shown.

3.8 PREPARATION OF IBP MICROCRYSTALS FOR INHALATION

This section will discuss the method of preparing IBP micro/nanocrystals for successful deep lung deposition. The method was the anti-solvent precipitation crystallization (APC) by co-solvent technique [28, 124, 152, 200, 201], optimized with respect to the significant variables identified from Plackett-Burman investigation (will be discussed in Chapter 5 Section 5.2).

This technique involves mixing of two different phases (*Figure 3.11***)**. The first phase (solvent phase) is ethanol with dissolved IBP (30-200 mg/g). The second phase (anti-solvent phase) where IBP is practically insoluble contains dissolved additives**.** The crystallizer is shown in *Figure 3.12* and shows the ultrasonic bath (Soniclean 750 HT), the cooler (Julabo, FT 200), the heating immersion circulator ED (Julabo) and the overhead stirrer (Lab Co.).

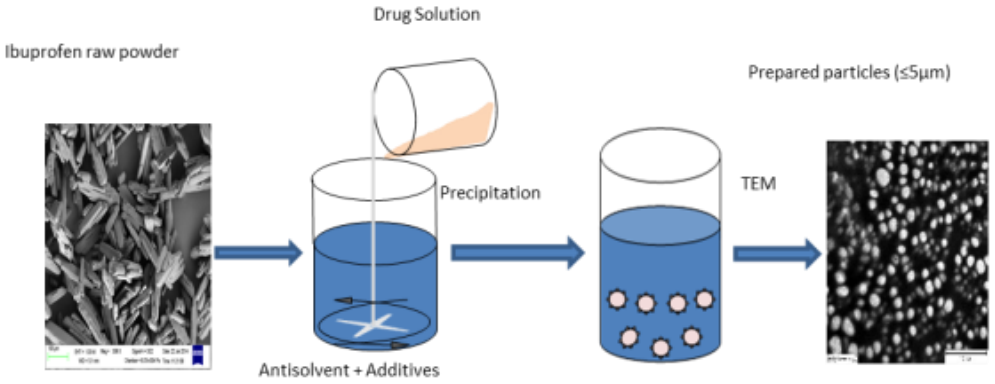

Figure 3.11 Anti-solvent precipitation crystallization (APC) process to make inhalable microparticles.

The additive solution was prepared by taking the weighed amount of powder of Pl F127, L-leucine, D-mannitol and 5% HPMC solution (prepared as described in the Section 3.5.1) made up to the final weight with water to give the additives in the concentration range HPMC **0.1-0.8%,** Pl F127 0-**1.8%,** leucine **0.9-1.3%** and mannitol **4.4-9%.** Mannitol acts as a carrier which prevents aggregation of particles during freeze drying [146-148, 152] and leucine is used for improving powder dispersibility [160-162].

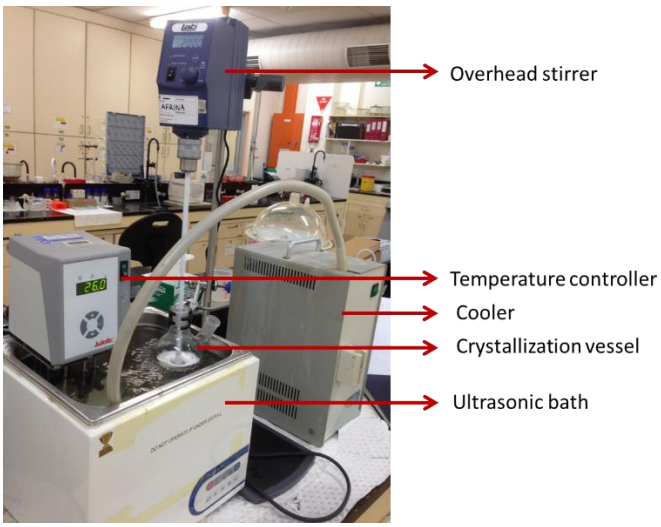

Figure 3.12 Crystallizer set up for anti-solvent precipitation crystallization (APC) preparing inhalable IBP particles.

Various process parameters *(Table 3.1)* including temperature, concentration and amount of polymers (HPMC and Pluronic F127), amount and concentration of mannitol, and stirring speed were varied to get the best size of the

micro/nanocrystals. These ranges were chosen based on the optimization experiments undertaken for each of the variables. The investigations for the optimum conditions are detailed in Chapter 5. The crystallization batch size range was chosen to be 10-50 g including the drug solution and the anti-solvent. The trial and error experiments showed that the particle size (< 5 µm) was better controlled in a small-scale batch (10 g). But considering the productivity of the process, the large-scale batches (50 g) were prepared with a maximum particle size (D[v,0.5]) of 20 µm. The solvent-antisolvent ratio and the range of stirring speed were chosen from the precipitation method used by Khan et. al [28]. The temperature range was selected from a series of experiments (section 5.3.1) where the smallest particle size D[v,0.5] = 7.14 µm was obtained at 25 °C. However, due to the ultrasound power during the process the temperature of the bath was increased to 30 °C producing particles with D[v,0.5] = 9.77 µm. Thus, the temperature range was chosen from 25 - 30 °C. The ultrasound duration range was 30 - 60 minutes where size of the particles was 8.4 - 6.4 µm (section 5.3.2). The minimum range (0.3 %) of drug concentration in organic phase was selected from Khan et. al [28] and the maximum range (2.0 %) was selected to get the maximum yield of particles. The maximum concentration of each additives were chosen based on their maximum solubility in the aqueous medium. The reason was to make sure they are in homogenous solution phase and not crystallizing out within the anti-solvent media.

Table 3.1 Anti-solvent precipitation crystallization (APC) process parameters and optimized range of conditions for preparing respirable IBP particles.

Process parameters	**Condition**
Batch size	10 – 50 g
Solvent-anti-solvent ratio (S/AS)	1 : 9 (fixed)
Stirring speed, rpm	600 – 1200
Temperature	25 - 30°C
Ultrasound application	50/60 Hz, Pulse swept power 180W
Duration of mixing	30 - 60 minutes
Drug concentration in organic phase	0.3-2%
Pl F127 concentration	0-1.8%
HPMC concentration	0-0.8%

Process parameters	Condition
Leucine concentration	0-1.5%
Mannitol concentration	0-9%

The drug solution was added into the antisolvent solution approximately at 1ml/s rate (maintained manually by hand and time recorded using a stopwatch). *Table 3.1* shows that the drug solution was one tenth of the anti-solvent solution. The very small volume of the drug solution was easier to add at a relatively constant rate manually by hand compared to the volume of the anti-solvent. Thus, the order of adding drug solution into the anti-solvent was chosen to maintain the addition rate relatively constant at all time.

3.8.1 **Isolation of dried particles**

The product of micro/nano crystal suspensions was centrifuged at 3500 rpm for 60 minutes in falcon tubes to remove dissolved additives. The excess liquid was discarded and the remainder was frozen using a deep freezer at -75 ºC for 24 hours. These frozen semisolids were the solid particles of IBP microcrystals present in the 10% aqueous ethanol crystallization media (<1ml, rationally containing HPMC, Pl F127, L-leucine and D-mannitol) which was converted into the semisolid state in a freezer at -75 ºC temperature, were freeze dried using a lyophilizer (Alpha 1-4 LD plus). The freeze drying was performed at a temperature of -55 °C and vacuum 1.0 mbar absolute for 24 – 96 hours, depending on the sample volume [144]. The duration of freeze drying was finalized by weighing the samples (n=5) once daily for four days. After freeze drying, the samples were kept over dried silica gel in the glass desiccator. Two samples were weighed once daily for 13 days to monitor any changes due to the moisture contents in the silica gel glass desiccator.

Figure 3.13 shows the weight variation plot of the samples in the freeze dryer (first four days) and silica gel glass desiccator (next eight days). The large error bars in the freeze dried samples are due to the batch-to-batch volume difference in five samples. The weight of the dried sample was stable after 36 hours of drying in the freeze dryer. The sample weight variation during storage in the silica gel glass desiccator remained within acceptable range (± 0.4 mg). The silica gel beads were freshly oven dried before using each time and replaced on time to make sure that the

humidity in the desiccator is maintained to approximately 0%. IBP melting point is about 75-77°C which was sensitive for an oven drying process. The melting process of IBP starts from 40-60°C for a normal oven drying process. Moreover, oven dried particles are found as hard solid cakes, which causes difficulties to get desired size particles for aerosolization. For the above reasons, the freeze drying process was chosen over the oven drying process.

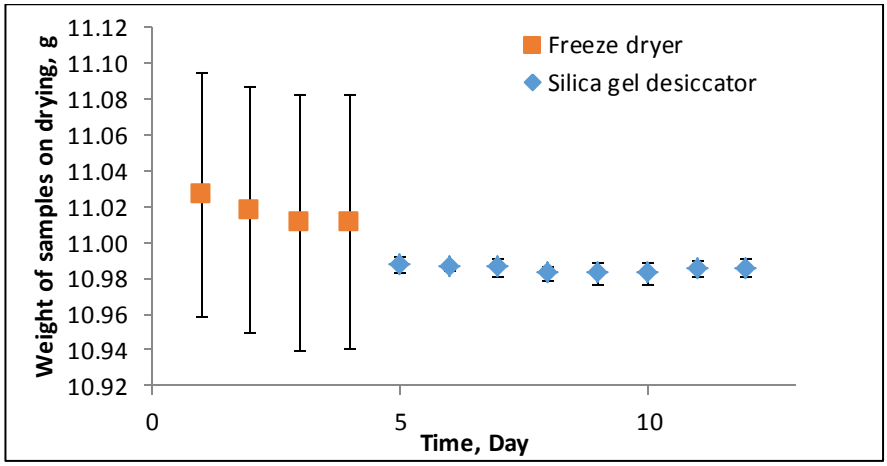

Figure 3.13 Sample weight variation on drying in freeze dryer and silica gel glass desiccator.

3.9 PARTICLE SIZE ANALYSIS

The particle size of the crystallized IBP was measured by the laser diffraction technique using a Malvern Mastersizer 3000 equipped with a small volume dispersion unit. Laser diffraction techniques are commonly used in crystallization studies, as they rapidly provide a volume based size distribution in terms of the convenient volume equivalent size of a particle. They determine particle sizes by measuring the intensities at different angles of forward light diffraction; smaller particles scatter at larger angles than larger ones do. Laser diffraction is a non-intrusive fast method, is simple to use, and measures a wide range of particle sizes. It is estimated that the relative error in the volume median diameter (VMD) calculated by the Malvern Mastersizer 3000 is ± 2% [202, 203]. Particle size measurements for the nanocrystals were done using the Zetasizer (NanoZS 90, Malvern Instruments, UK).

The suspending medium was saturated IBP solution prepared with equivalent composition to the final crystallization media at equilibrium. This medium was used

as the dispersant in the small volume (120 ml) dispersion unit stirring at 2000 rpm. Crystal suspensions were added dropwise until the obscuration reached the desired level.

The mass median diameter (MMD, D[v,0.5]) and volume mean diameter (Dv[4,3]) determined from the output of the laser diffraction particle sizing were used as the major size parameter to characterize the particle size distributions (PSD). The particle size distribution data was presented in the appendices C1-8 by tabulating the D[v,0.1], D[v,0.5] & D[v,0.9] data values. The particle size distribution data of the final formulations were given in Chapter 6 Table 6.3. Measurements were taken from three replicates of each of the formulations. The refractive index for IBP in *Table 3.2* was collected from the Malvern mastersizer refractive index guide [204].

Table 3.2 The optical parameter settings for size measurement by laser diffraction.

Material	**Refractive index**	**Absorption index**
IBP	1.43 [204, 205]	1.2
Dispersant	1.331[204]	NA

The absorption index was selected from the maximum value providing the lowest weighted residual (%). The trend of weighted residual vs absorption index simulated from calculations done by Mastersizer 3000 software (Mastersizer- v 3.10) is given in *Figure 3.14*. The selected value from the trend confirms the best suitability for the particle size distribution analysis.

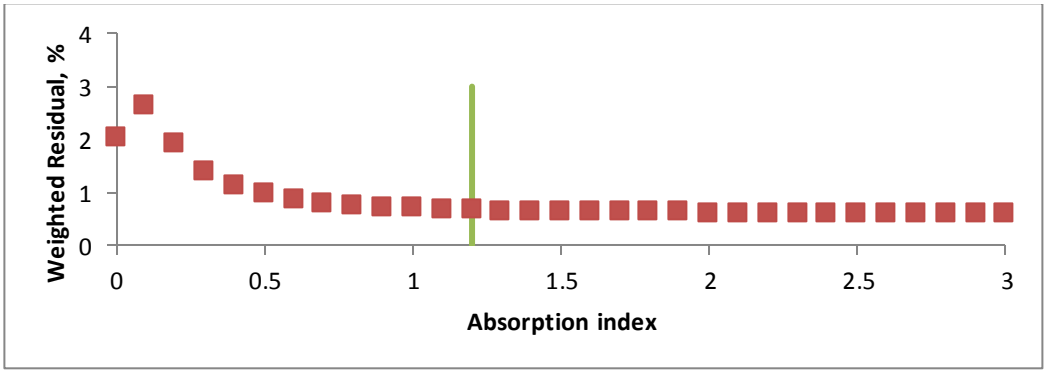

Figure 3.14 The trend of weighted residual vs absorbance index. The weighted residual remains substantially unchanged after an absorption index of 1.2.

3.10 MILL MICRONIZING METHOD

A McCrone Micronizing mill (serial no. 130803) was used to mill the raw IBP powder into inhalable size. Raw IBP powder was loaded (< 3 g) into the micronizer vessels with zirconia beads. Water with > 300 ppm of detergent (2 mL) was used as a fluid. Particle size was measured using Malvern Mastersizer 3000 at different time intervals until inhalable particle size was achieved by milling. Particles with the required size (~ 3 µm) were found after 12 hours of milling. *Figure 3.15* shows the size of particles at different durations of milling. The samples were then dried in an oven overnight at 40 °C.

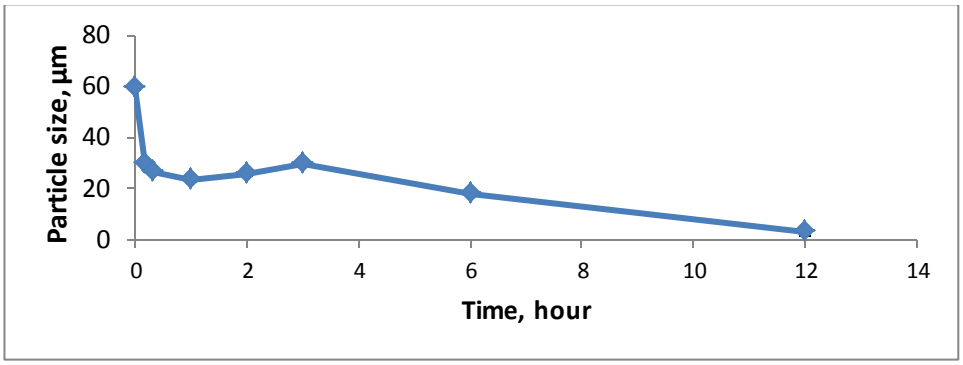

Figure 3.15 Duration of IBP particle size reduction to inhalable size using micronizing mill.

3.11 CRYSTAL IMAGE ANALYSIS

Scanning electron microscope (SEM) and transmission electron microscope (TEM) were used for the image analysis of IBP raw powder, wet and dry particles.

3.11.1 Scanning electron microscope (SEM)

A Zeiss Sigma scanning electron microscope was used to investigate the morphological properties (shape, size and surface) of the IBP crystals.

The sample preparation involved fixing the powder samples on to a metal stub with the aid of a double sided adhesive tape followed by coating for 180 seconds with a LEICA EM SCD005 gold coater. Scanning electron microscopy (SEM) was then carried out by loading the sample on SEM at 5 KV.

3.11.2 **Transmission electron microscope (TEM)**

A Jeol 1400 transmission electron microscope was used to investigate the morphological properties (shape, size and surface) of the IBP crystals.

Sample preparation for TEM involved deposition of a single drop of the sample suspension onto a 200 mesh copper grid coated with Formvar/Carbon (code no S162) followed by drying at ambient temperature. Images were then taken by loading the sample on the transmission electron microscope at 120 KV.

3.12 DENSITY MEASUREMENTS

Bulk density and tapped density of prepared powders were measured as described elsewhere [206]. IBP has a particle density of 1.110 g/cm^3 [207, 208].

3.12.1 **Bulk density**

The bulk density of a powder is defined as the ratio of the mass of an untapped powder sample to its volume, including the interparticulate void volume. Hence, the bulk density depends on both the density of powder particles and the spatial arrangement of particles in the powder bed [206].

The bulk density of the powder formulations was determined by measuring the volume of a known mass of powder sample in a dry, graduated cylinder (5 mL); the sample weighed with 0.1 per cent accuracy was gently introduced. Carefully the powder was levelled without compacting, and the unsettled apparent volume (V_0) to the nearest graduated unit was recorded. Three replications for each formulation were performed.

3.12.2 **Tapped density**

The tapped density is an increased bulk density achieved after mechanically tapping a receptacle containing the powder sample. Mechanical tapping is achieved by raising the cylinder and allowing it to drop, under its own mass, in a distance of 3.0 ± 0.2 mm using the Erweka tapped density tester [206]. After observing the initial powder volume and mass, the graduated (5 mL) measuring cylinder was mechanically tapped, and volume readings were taken until no further volume change was observed.

A 5 mL graduated cylinder was filled with a mass of 1.3 ± 0.3 g of powder sample. The initial particle volume (V_o) and the initial weight of the samples were

determined. Then the cylinder was secured in the support of the tapping apparatus, 100, 500 and 1250 taps on the same powder sample were carried out, and corresponding volumes V_{100}, V_{500} and V_{1250} were recorded to the nearest graduated unit. If the difference between V_{500} and V_{1250} was less than or equal to 0.1 mL, V_{1250} was considered as the tapped volume. If the difference between V_{500} and V_{1250} exceeded 0.1 mL, the increments of 1250 taps were repeated until the difference between successive measurements was less than or equal to 0.1 mL. Three replications for each formulation were performed.

3.13 POWDER COHESION AND FLOW MEASUREMENTS

The effectiveness of the drug particle deposition depends on the particle flow behaviour during inspiration. Free flowing powders overcome the cohesion and adhesion forces and increase drug deposition into the deep lungs. To ensure drug delivery from the DPI formulation, flowability of the prepared IBP crystals was determined using the angle of repose, Carr's index and the Hausner ratio.

3.13.1 **Angle of repose**

To form the angle of repose on a fixed base, a 5 mL beaker was used as a base (10 mm diameter) to retain the powder (250 ± 0.5 mg). The powder was poured through a funnel (40 mm diameter and 65 mm height). The funnel height was maintained at approximately 2 – 4 cm from the top of the powder pile which is formed in order to minimise the impact of falling powder on the tip of the cone. The angle of repose was determined by measuring the height of the cone of powder and calculating the angle of repose, α, from the following equation:

$$\tan(\alpha) = \frac{height}{0.5 \times base}$$

The degree of flowability is related to the angle of repose, presented in *Table 3.3*.

Table 3.3 Flow properties and corresponding angles of repose [209].

Flow Property	Angle of repose (degree)
Excellent	25-30
Good	31-35
Fair	36-40
Passable	41-45
Poor	46-55
Very poor	56-65
Very, very poor	> 66

3.13.2 **Carr's index and Hausner ratio**

In recent years the Carr's index and Hausner ratio have become the simple, fast, and most common methods of predicting powder flow properties. The Carr's index and the Hausner ratio are determined by measuring both the bulk volume and tapped volume of a powder (Section 3.12).

Basic methods for Carr's compressibility index and Hausner ratio: The basic procedure is to measure the unsettled apparent volume (V_0) and the final tapped volume, (V_f) of the powder after tapping the material until no further volume changes occur. The compressibility index and the Hausner ratio are calculated as follows:

$$Carr's\ Index = 100 \times \frac{V_o - V_f}{V_o}$$

$$Hausner\ Ratio = \frac{V_o}{V_f}$$

In this work, the Carr's compressibility index and Hausner ratio was calculated using measured values of bulk density (ρ_{bulk}) and tapped density (ρ_{tapped}) as follows:

$$Carr's\ Compressibility\ index = 100 \times \frac{\rho_{tapped} - \rho_{bulk}}{\rho_{tapped}}$$

$$Hausner\ Ratio = \frac{\rho_{tapped}}{\rho_{bulk}}$$

For the Carr's index and the Hausner ratio, the generally accepted scale of flowability is given in *Table 3.4* [206, 209]. The two quantities are related, Carr's index = 1 – 1/Hausner ratio.

Table 3.4 Scale of flowability [206, 209].

Carr's index (%)	Flow character	Hausner ratio
≤ 10	Excellent	1.00-1.11
11-15	Good	1.12-1.18
16-20	Fair	1.19-1.25
21-25	Passable	1.26-1.34
26-31	Poor	1.35-1.45
32-37	Very poor	1.46-1.59
> 38	Very, very poor	> 1.60

3.14 CRYSTALLINITY TEST

Crystallinity refers to the degree of structural order in a solid. In a crystal, the atoms or molecules are arranged in a regular, periodic manner. The degree of crystallinity of a drug has an effect on its bioavailability and on its physical and chemical stability. The experimental conditions (e.g. temperature, humidity) during the crystallization process might cause defects in the crystal lattice and decrease the degree of crystallinity, which could have a harmful effect on the drug's activity.

3.14.1 Differential scanning calorimetry (DSC)

Differential scanning calorimetry (DSC) experiments were carried out in a DSC Q100 from TA Instruments Explorer Q series. A small amount of sample (less than 6 mg) was enclosed in a hermetic aluminum pan. A liquid nitrogen cooling system was used in order to reach temperatures as low as - 42 °C.

Processed and unprocessed IBP samples were scanned from 10 °C to 110 °C, using a heating rate of 10°C/min. All samples were analysed in triplicate. The percent crystallinity is then determined using the following equation [210]:

$$\% \text{ Crystallinity} = [\Delta Hm - \Delta Hc] / \Delta Hm^{\circ} \times 100\%$$

The heats of melting, ΔHm, and cold crystallization, ΔHc, are determined by integrating the areas (J/g) under the peaks using TA instrument Analysis 2000 software. No cold crystallization exothermic peak was observed during the DSC experiment for IBP for both processed and unprocessed.

The term ΔHm° is a reference value and represents the heat of melting of the 100% crystalline IBP. Appendix A8 shows the DSC traces for determining the melting enthalpy of the raw IBP used in this work. It was found that the melting enthalpy of the raw IBP powder was 118.4 ± 7.3 J/g which is also in agreement with Nokhodchi and co-workers [194]. This value was used as the reference value to determine the percentage crystalline phase of IBP in the processed formulations with different compositions of additive.

3.14.2 **Powder X-ray diffraction (XRD)**

The crystallinities of the unprocessed and processed IBP were also evaluated using an X-ray powder diffractometer (XRD).

Samples were front pressed into low background quartz holders. Diffraction patterns were collected in θ/2θ geometry on a PANalytical X'Pert Pro diffractometer (Co Kα) using a W/Si parabolic mirror and 0.09° collimator before the point detector. A 0.25° fixed divergence slit, 10 mm mask, 1.4 mm incident antiscatter slit, and 0.04 rad pre and post diffraction Soller slits were used. Patterns were collected from 3 – 75°2θ at a step size of 0.02° for 1 hr. The sample was spun during data collection. An instrument function was determined from LaB_6 (SRM 660a). Phase identification was performed with Highscore Plus (V4.5, PANalytical) using the PDF4+ database (ICDD) and confirmed via Rietveld refinement with TOPAS (V5, Bruker). Quantitative phase analysis was performed using TOPAS (v5, Bruker) via the Rietveld method. An instrument function determined from LaB6 (NIST SRM 660a) was used to model the profile shape. A Lorentzian crystallite size term was refined for each phase to account for profile broadening. Refined terms included specimen displacement, scale factor for each phase, and unit cell parameters for each phase. The amount of pluronic in some samples was estimated by the degree of crystallinity method where the numerical area of each phase is used to determine abundances. The pluronic was accounted for by modelling a peak at c.a. 27° 2θ (most obvious feature not modelled) and designating it as the amorphous phase. HPMC phase

abundance could not be quantified as its concentration in the formulation was too low to identify in the XRD curves.

XRD patterns of both the processed and unprocessed IBP were compared to identify any alteration in their crystallinities.

3.15 DRUG LOADING DETERMINATION

Quantification of IBP content in the powder formulation was determined by UV spectrophotometer (Thermo Scientific Evolution Array) at a wavelength of 264 nm. Samples were prepared by dissolving 10-15 mg of powder formulation in 50% aqueous ethanol solvent system. Complete solution of IBP in the selected solvent system was confirmed from the predetermined solubility results. The calibration plot shown in Section 3.4.2 was used to quantify the IBP concentration in the samples. IBP loading in the formulation was quantified from the ratio of determined total IBP amount to the weight of the powder formulation taken, in percentage.

3.16 DRUG DISPERSIBILITY TESTING

The prepared IBP microparticles were subjected to an aerosolization test using a device, Rotahaler®.

3.16.1 Evaluation of aerosolization and in vitro drug deposition

The efficiency of the prepared dry powder inhaler in terms of aerosolization and in vitro drug deposition was investigated by a Twin Stage Impinger (TSI, Copley Scientific, Nottingham, UK) (*Figure 3.16*), using methodology described in the British Pharmacopoeia (TSI apparatus, Apparatus A, Glass Impinger, British Pharmacopoeia, 2014). A Rotahaler® (Glaxo Wellcome) was used as the DPI device and 35% aqueous ethanol (determined from the solubility analysis) was used as the collection liquid in the upper and lower stages of the apparatus. 7 mL of collection liquid was placed in stage-1 (S-1) of the apparatus and 30 mL in stage-2 (S-2). The airflow through the TSI was controlled by a vacuum pump (ERWEKA) using a calibrated flow meter (ERWEKA).

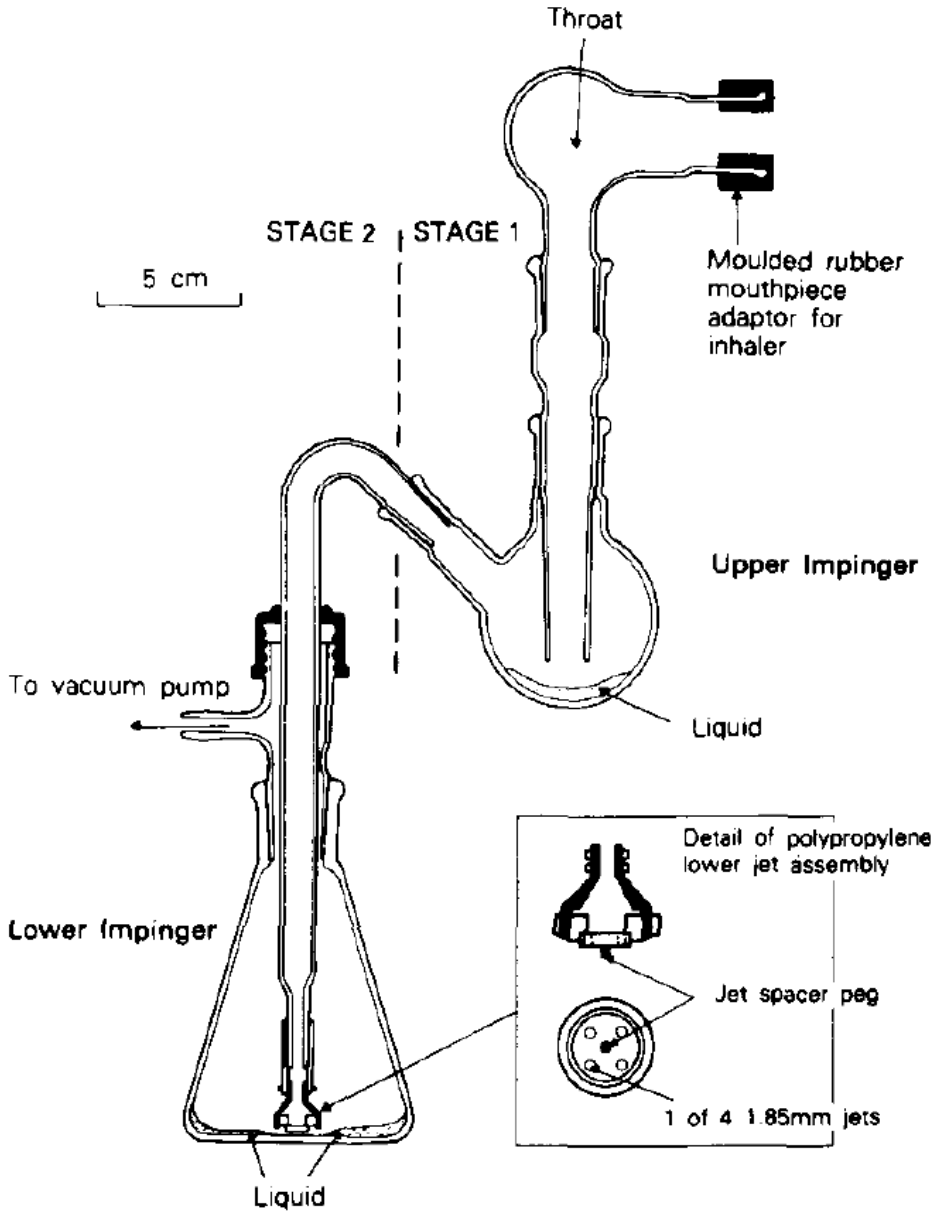

Figure 3.16 Diagrammatic representation of Twin Stage Impinger [211].

For each actuation, a size 3 hard gelatin capsule (Fawns and McAllan Pty Ltd. Australia) loaded with about 32 ± 1 mg [146, 148] powder formulation was inserted into the Rotahaler®, which was placed into a moulded mouthpiece attached to the TSI and then twisted to release the powder into the body of the device. The amount of 32 mg of powder formulation was used to ensure the minimum IBP concentration within the limit of detection in UV spectrophotometry. The liberated powder was drawn through the TSI at a flow rate of 60 L/min for 5 seconds. This procedure was repeated five times for each preparation.

After each run, the two stages of the impinger and the powder inhaler were washed separately with an appropriate ethanol solvent into volumetric flasks and the volume was adjusted to 100 ml. The amount of drug deposited in each stage was analysed by UV spectrophotometer at 221 nm (Section 3.4.2). The total amount of drug collected from the inhaler device, stage-1 (S1) and stge-2 (S2) are termed as the recovered dose (RD).

The emitted dose (ED) is defined as the fraction of recovered dose (RD) delivered from the inhalation device expressed as a percentage.

$$ED = \frac{S1 + S2}{RD} \times 100$$

The fine particle fraction (FPF) is defined as the fraction of recovered dose (RD) deposited in the stage-2 (S2) of TSI expressed as a percentage.

$$FPF = \frac{S2}{RD} \times 100$$

It was expected that DPI formulations of the prepared IBP crystals will be more efficient in delivering higher amount of drug (FPF%) into the deep lungs than the DPI formulations of the homogenised IBP drug particles.

3.17 *IN VITRO* DISSOLUTION TEST

A sample of pure IBP (12.5 mg) milled to 2.8 ± 0.1 µm volume median diameter (D[v,0.5]) and the processed formulations equivalent to 12.5 mg were subjected to dissolution studies. The USP paddle method (Pharma Test- DT 70) was adopted in 900 mL phosphate buffered saline (PBS) (pH 7.4) at 100 rpm and 37 °C for each sample. At the fixed time intervals of 2, 6, 10, 15, 20, 30, 60, 90 and 120 minutes, 5 mL aliquots of the release medium were withdrawn and the same amount replaced with the fresh PBS. The drug content in the withdrawn aliquot was analyzed in UV spectrophotometer at 221 nm. Percentage drug release versus time data were plotted to establish drug release profiles from the formulations based on three replications.

3.18 RAMAN SPECTROSCOPY

WItec alpha 300 series (system ID: 100-1200-736, configuration: Raman 532 nm) Raman instrument was used for spectral analysis of the individual components and scanning of the powder formulations. The purpose of the analysis was to identify

the additives and IBP drug component distinctively in the powder formulation from the Raman mapping. The samples were placed on a glass slide for running the spectrum of each of the components. A stainless-steel cup was filled with the formulation powder sample with a coverslip on the top for the confocal scans. The objective magnification of the lens was Zeiss 50×/0.7 and the laser power (THOR labs) used for each run was 10 mW. The scans were done with a spot size of 20/20 micron and step size of 41 with the integration time of 1s. The instrument was calibrated with pure silicon. IBP, Pl F127, HPMC and L-leucine spectrums were recorded using the commercial material as purchased. A D-mannitol spectrum was recorded after freeze drying the commercial material. The spectrum analysis and mapping of the powder components in the mixture were done using WITec control four and project four software.

3.19 CONCLUSION

Determination of IBP solubility by the dissolution method was validated by calibrating the UV spectrophotometer in the range of 0-50% aqueous ethanol solvents. The equilibrium of the IBP drug concentration was confirmed for each solvent system used. Method of preparing IBP particles in APC process was described. All the methods for the measurements of particle size, density, flow, crystallinity of prepared IBP particles and the milled IBP were demonstrated. A UV spectrophotometer was calibrated at 221 nm wavelength and the method was validated in duplicate to determine the drug dispersibility in the twin stage impinger. At least five capsules for each formulation were measured for the evaluation of in vitro aerosol performance of each formulation. Dissolution tests for the milled IBP and three selected formulations were performed in phosphate buffer media in triplicate runs.

Chapter 4: Solubility of ibuprofen in aqueous ethanol with additives

4.1 INTRODUCTION

The solubility of a compound is important in understanding the design and optimization of crystallization processes and drug delivery systems [29, 92, 191], especially in pre-formulation studies of new drugs and dosage forms [193, 212-214]. Ibuprofen (IBP) is a non-steroidal anti-inflammatory drug and is classified as a water insoluble compound (BCS Class II) [192, 215]. The non-random two-liquid (NRTL) and universal quasichemical (UNIQUAC) models [216, 217] for solubility prediction of seven pharmaceuticals (lovastatin, valsartan, paracetamol, budesonide, allopurinol, furosemide and sulfadiazine) have been useful for determining the crystallization yield per mass of single, binary and ternary solvent mixtures and estimating the optimum solvent mixture [218, 219]. The solubility prediction models were also used to distinguish the difference between two polymorphs of buspirone hydrochloride, as the Gibbs free energy difference can be obtained from the solubility data of two polymorphs [220]. This chapter will correlate the recemic IBP solubility in aqueous ethanol at 10, 25 and 40^{o}C by a single equation. Then the effect of the excipients on IBP solubility will be explained.

4.2 SOLUBILITY MEASUREMENT METHOD

Solubility studies were carried out using the method described in Chapter 3, section 3.5. For aqueous ethanol solvents, the IBP solubility was determined at 10, 25 and 40^{o}C. In Chapter 3, *Figure 3.8* and *Figure 3.9* show the approach to equilibrium for several experiments and indicated that solubility experiments should be continued for at least six hours to ensure equilibrium has been reached. Solubility by dissolution was performed by adding IBP to a chosen ethanol–water solvent (0 to 50% E/(E+W) by weight where E = ethanol and W = water). Solubility by crystallization was determined by the addition of an IBP in ethanol solution (0.112 g/g) into a stirred anti-solvent water making a chosen final ethanol composition 10 to 50% E/(E+W). The effect of HPMC, Pluronic F127, leucine and mannitol excipients on IBP solubility was investigated at 25°C. The concentration ranges used were 0 to

2% w/w HPMC/(E+W), 0 to 1.85% w/w Pl F127/(E+W), 0 to 1.5% w/w leucine/(E+W), 0-9% mannitol/(E+W) in 0 to 20% w/w E/(E+W) aqueous ethanol. Drug solubilities were determined in triplicate under each condition and the results are reported as the mean with estimated 95% uncertainties.

4.3 RESULTS AND DISCUSSIONS

Rashid et al. [221] measured the solubility of IBP in aqueous ethanol at high ethanol contents (> 50%, w/w E/(E+W) (where E = ethanol and W = water)) at 10, 25 and 40^{o}C. The present work [222] extends the study to the lower ethanol contents and also explores the effect of four excipients Pluronic F127, HPMC, L-leucine and D-mannitol on IBP solubility in water ethanol co-solvents. All those experiments were performed at least with triplicate samples. The error bars in the figures of this chapter are smaller than the used markers. The raw data given in the Table 4.1 and 4.2 and the appendixes (Appendix B1 and B2) corresponding to those figures includes the details of the sample number and the percentage errors.

4.3.1 **Solubility in aqueous ethanol without excipients**

Table 4.1 summarises the measured solubility results. *Figure 4.1* shows the present results for IBP solubility in aqueous ethanol without excipients at 10, 25 and 40 ^{o}C. Note that a log scale is used for the solubility. The majority were measured by the dissolution method, and those indicated (by a diamond) by the crystallization method. *Figure 4.2* combines the present results with the prior data of Rashid et al. [31] (for higher ethanol contents), showing an apparent consistency with the earlier data. Solubility is still shown as a mass ratio. *Figure 4.1* also shows solubility values obtained from crystallization (rather than dissolution) experiments. The crystallization results are in reasonable agreement, although, for unknown reasons, they are a little higher than the dissolution values. Note that the solubility in *Figure 4.2* covers nearly five orders of magnitude (from mass ratios of $3*10^{-5}$ in water to nearly 3 in ethanol).

Table 4.1 IBP solubility data in 0–50% aqueous ethanol solvents at 10, 25 and 40°C. The percentage errors are the estimated 95% uncertainties on the solubility values.

10°C			**25°C**			**40°C**		
E/(E+W) % w/w	**I*/(E+W) ppm w/w**	**% error**	**E/(E+W)% w/w**	**I*/(E+W) ppm w/w**	**% error**	**E/(E+W)% w/w**	**I*/(E+W) ppm w/w**	**% error**
0	41.1	0.4	0	45.5	2.6	0	88.4	5.9
10.18	65.1	2.2	5.16	71.0	2.5	10.44	216.7	3.8
20.16	124.4	4.7	10.07	102.4	1.5	20.57	1029	1.6
29.36	403.0	4.3	15.28	159.8	2.4	†29.92	6525	5.4
39.94	2165	3.9	19.94	284.7	0.7			
49.67	20410	2.8	20.85	367.3	1.8			
			30.1	1852	2.8			
			39.65	12470	3.6			
			50.19	67849.4	4			
			Solubility by crystallization					
			9.21	126.55	17.86			
			17.80	248.08	8.79			
			26.55	955.71	2.21			
			35.44	4934.75	0.64			

† *Above 34%, phase separation occurred.*

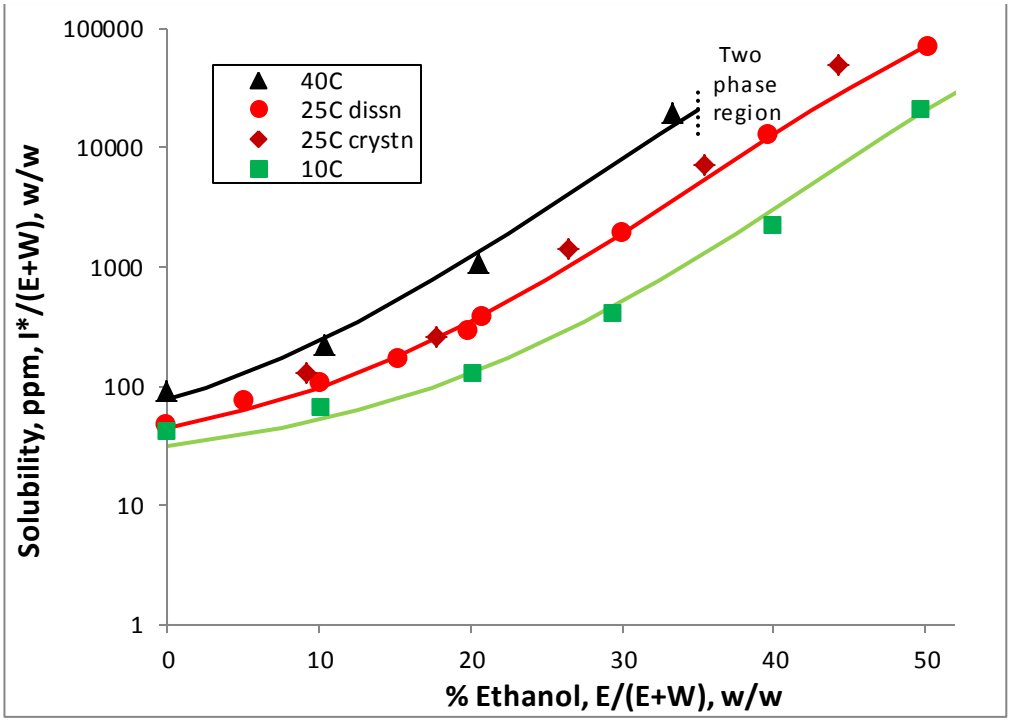

Figure 4.1 .Results for the solubility of IBP in aqueous ethanol (0-50%, E/ (E+W)) at 10, 25 and 40 °C. Errors are smaller than size of symbols.

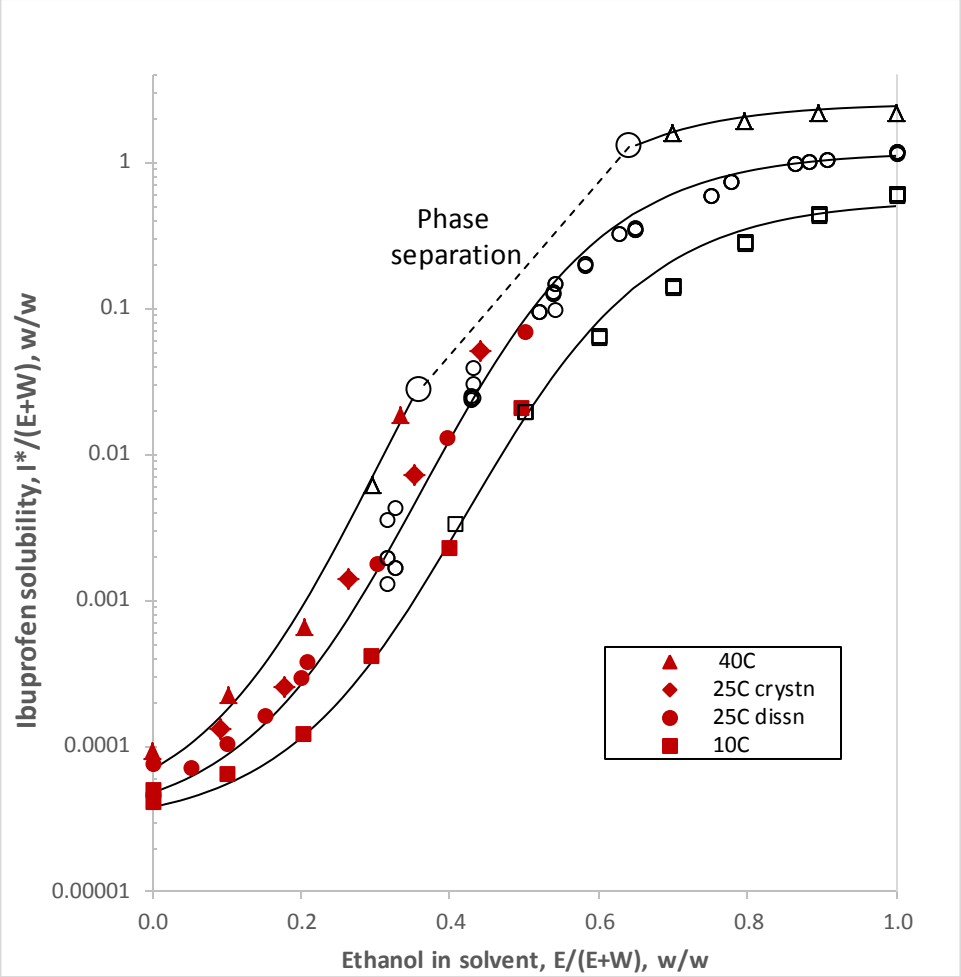

Figure 4.2 IBP solubility in aqueous ethanol (filled symbols), compared with results of Rashid et al. [31] (unfilled symbols).

The results in *Figure 4.2* have been fitted by the sigmoid relation,

$$\boldsymbol{log_{10}\ (Sol) = a + (b + e * (t - 25))/(1 + \exp[-(X_E - (c + f * (t - 25)))/ d])} \quad (4.1)$$

where **sol** = IBP solubility as mass ratio **I*/(E+W)** in ppm, **t** = temperature in ^{o}C and $\mathbf{X_E}$ = **E/(E+W)** is the ethanol content of the solvent as a solute free mass ratio. Here I* = IBP at equilibrium, E = ethanol and W = water. The parameters of the sigmoid were taken to be linear functions of temperature but only the two shown as functions of temperature were significant. The values of the parameters are shown in *Table 4.2* with their percentage uncertainty. The correlation fits an estimated 95% of the measured data within ± 42%.

Table 4.2 Values of parameters in correlation.

Parameters	Value	% uncertainty[1]
a	-4.56	3
b	4.63	4
c	0.36	7
d	0.12	20
e	0.02	75
f	0.004	70
GoF[2]		42%

[1] 95% uncertainty on parameter, as% .

[2] Goodness of fit to data, as%.

Figure 4.3 shows the goodness of fit of the experimental data to the correlation. The 42% error lines are shown. The biggest errors are those for Rashid et al. [31] for the lower ethanol contents where the evaporation to dryness measurement technique used becomes of limited accuracy. It is expected the correlation fits the true solubility within ± 10%.

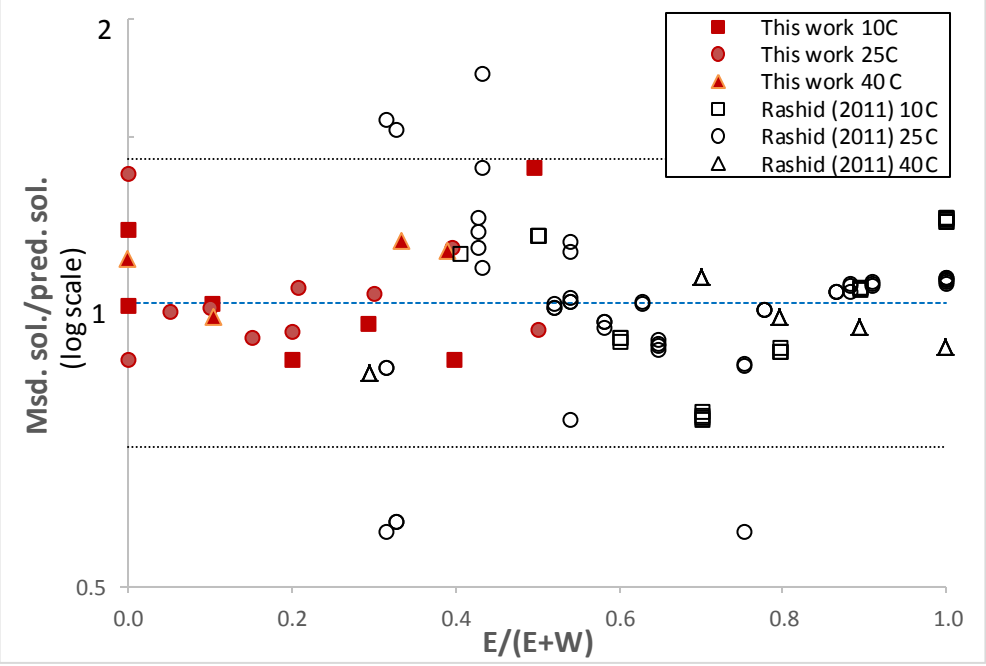

Figure 4.3 Goodness of fit of the solubility correlation to the data.

For low ethanol contents (< 50%) the data in *Figure 4.2* approximately follow a straight line (on a log scale) so the effect of ethanol on solubility is near exponential, i.e. the solubility doubles for each ~ 3% increase in ethanol content.

As demonstrated by Rashid et al. [31] and indicated on *Figure 4.1* and *Figure 4.2*, there is phase separation (three phases) for a range of solution concentrations at 40·°C (see section 4.3.2 below).

This measured solubility data will be used to design the crystallization conditions to produce fine (<5 μm) IBP crystals for DPI formulations. This solubility trend will also be used to select a suitable aqueous ethanol solvent to wash the drug formulation after in vitro drug dispersion tests using the twin stage impinger.

4.3.2 **Phase separation analysis at 40°C**

Phase separation was confirmed by Rashid et al. [31] at 40 °C when the ethanol in water percentage used is above 34% and below 63%. This phenomena was also reported by other literature [191, 223]. A brief experiment was undertaken to confirm these values which are in approximate agreement with Rashid's values. *Figure 4.4* shows these two liquid layers. The 30% E/(W+E) (a) does not show any liquid phase separation but the other two do. The interface between the two liquid layers (40 and 50% (E/E+W)) is clearly seen. IBP crystals are the densest species and they sink to sit in the bottom liquid layer.

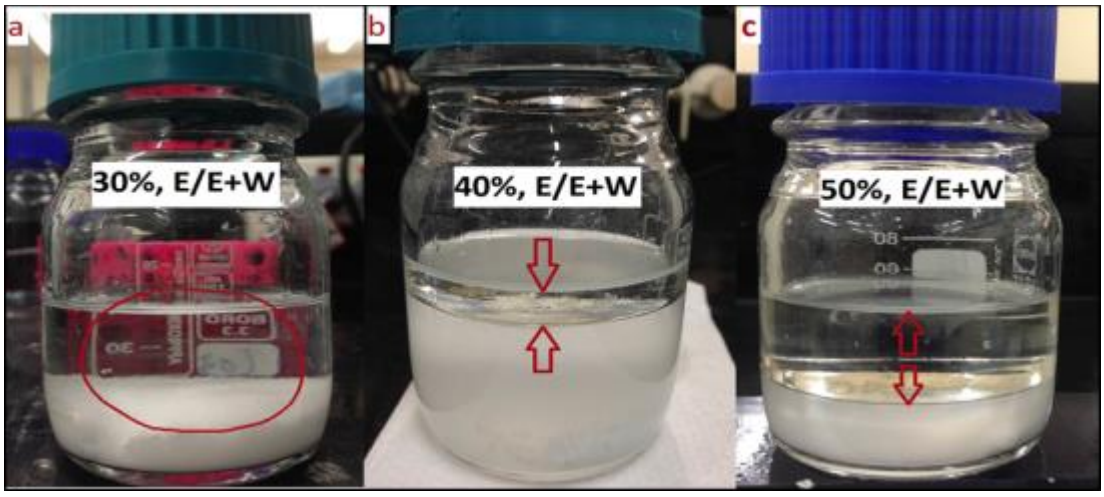

Figure 4.4: IBP induced phase separation with 40 & 50% E/(W+E) solvents at 40 ºC. 30% E/ (E+W) (a) does not show phase separation.

4.4 SOLUBILITY WITH ADDITIVES

The purpose of determining IBP solubilities with the additives was to find out the maximum limit of saturation for the crystallization process. So, only three points were chosen for the determination. As the purpose of finding out the saturation limit of IBP with additives was achieved, we attempted to increase the experimental points in the later Figures 4.9 and 4.10. But due to the time limitation it couldn't be increased for the other experiments. So, we leave the experiments for the trends of solubilities for future work.

4.4.1 **Effect of Pluronic F127 (Pl F127)**

The growth rate inhibition effect of Pl F127 on IBP APC is a phenomenon that is well established in previous studies [28, 117, 124]. Hence, Pl F127 was chosen by Khan [28], and in the present study, as the additive for producing fine IBP crystals (<5 μm). The effect of the additive on IBP solubility at low ethanol aqueous solvents was investigated for the APC process. The IBP solubility increased linearly with the concentration of Pl F127 at each of the three ethanol contents (*Figure 4.5*). The raw data is given in Appendix B2.

In ppm Pl F127 (% g/g solvent) units, the slopes of the lines in the units of *Figure 4.5* are 560 (± 4) for 0% E; 785 (± 5) for 10% E and 1520 (± 3) for 20% E. A correlation for the effect of Pl F127 on the solubility is

$$\boldsymbol{Sol = Sol_0 + (562 - 3.09 * [E] + 2.54 \times [E]^2)[Pl\,F127]} \quad \textbf{(4.2)}$$

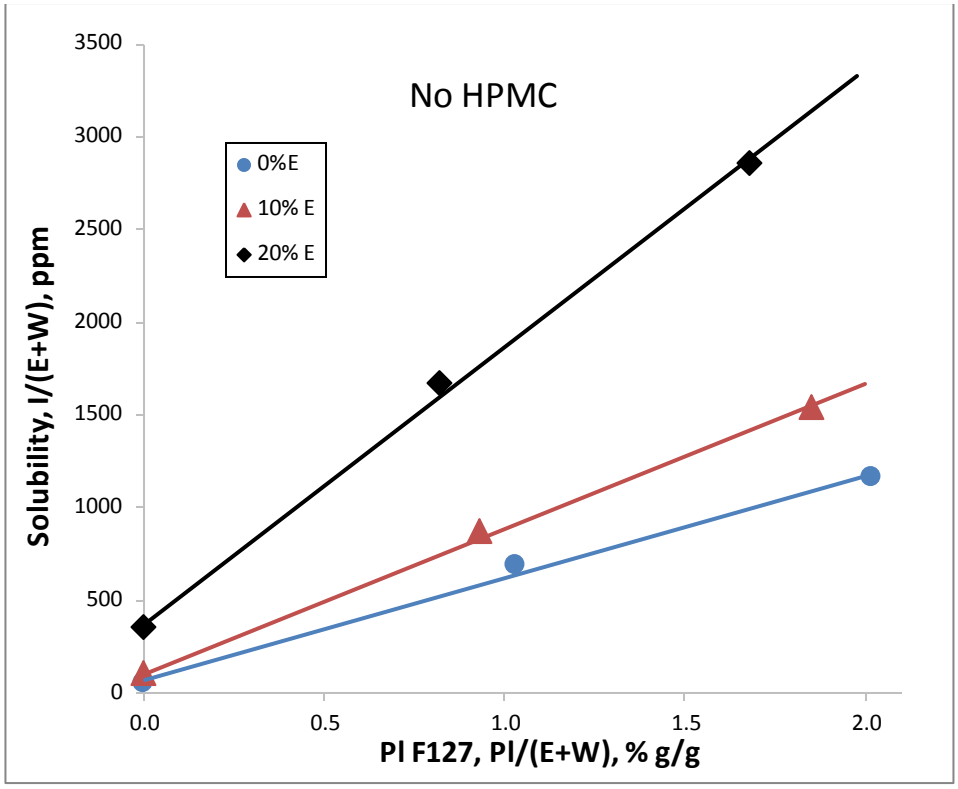

Figure 4.5 . Effect of Pl F127 on IBP solubility in aqueous ethanol at 25^{o}C.

A possible explanation for the trend might be the effects of the ethylene oxide (EO) and propylene oxide (PO) blocks in Pl F127. The hydrophobic core (PO) block acts a reservoir for the drug and the hydrophilic portion (EO) functions as interface between the aqueous medium and the drug [136]. As a nonionic surfactant Pl F127 molecules form monomolecular micelles with the drug at low concentration. However, these monomolecular micelles aggregate with each other at higher concentration (above the critical micelle concentration, typically ~ 0.7% Pl F127) [120, 136, 224]. Therefore, it was necessary to identify the optimum concentration of Pluronic F127 before using it in IBP precipitation.

When ethanol is present, the solubility increases but the relative effect of Pl F127 on the solubility falls slightly. A possible mechanism is that the proximate attraction of ethanol towards hydrophobic IBP suppresses the solubility enhancement effect of Pl F127. Verma et al., determined IBP solubility in 0.5% Pl F127 [117] and the value is in agreement with the linear correlation obtained in this work (*Figure 4.6*). In summary, the evidence from this study suggests that Pl F127 increases the IBP solubility linearly with its concentration in water and aqueous ethanol.

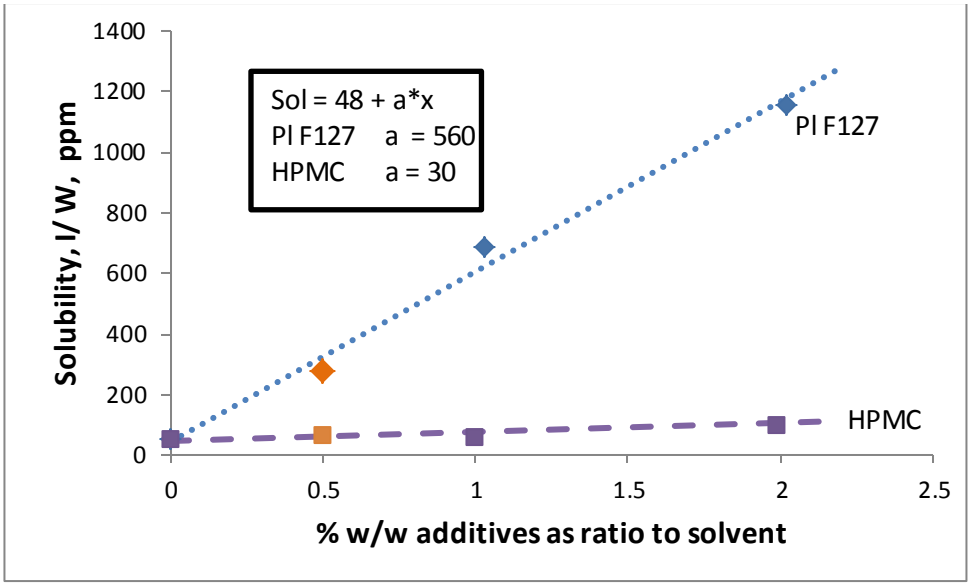

Figure 4.6.Solubility of IBP with Pluronic F127 and HPMC in the concentration range 0-2%. The orange points were reported by Verma et al. [117].

4.4.2 **Effect of HPMC**

Figure 4.7 shows the effect of HPMC on solubility in the absence of Pl F127. Again the results appear to be linear with the excipient concentration. At all ethanol contents the slope of the line is ~ 17 (± 4) ppm /HPMC (% g/g of solvent). This effect is far smaller (81 approx. one fiftieth) than the effect of Pl F127 (*Figure 4.5*). The raw data is given in Appendix B2.

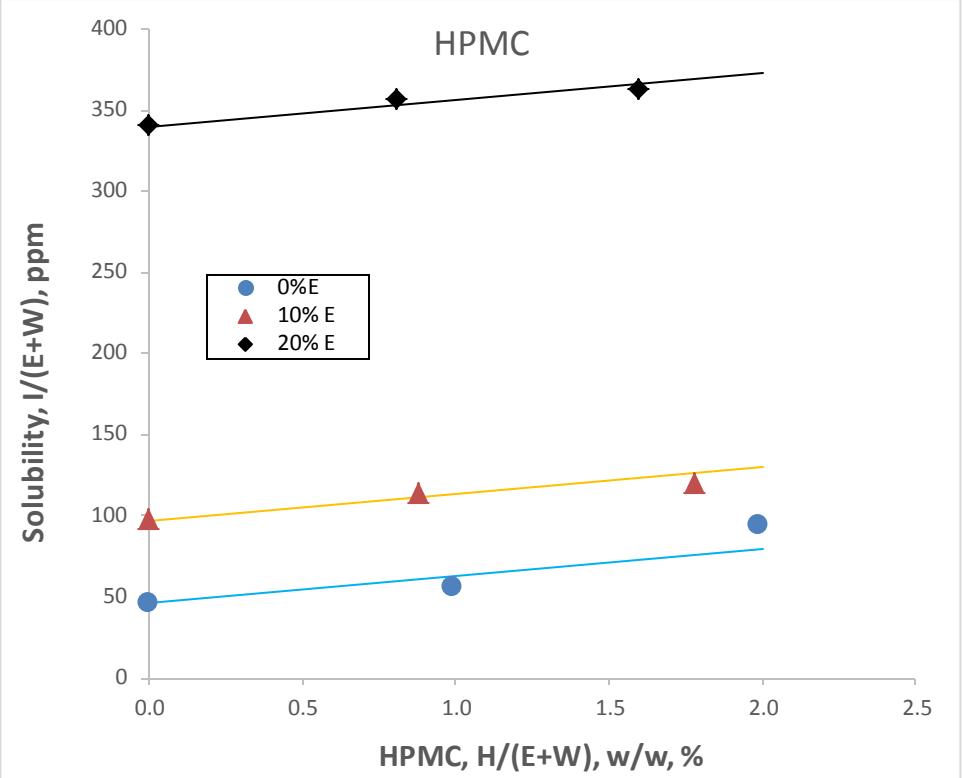

Figure 4.7. Effect of HPMC on IBP solubility in aqueous ethanol.

HPMCs are the substituted cellulosic polymers considered the most successful stabilizers for preparation of IBP suspensions [28]. Stabilization occurs by adsorbing onto the surface the IBP particles through the interaction of the hydrophobic methoxyl groups and hydrophilic hydroxypropyl groups present in the polymeric chain of HPMC [117]. It is also evident that the intermolecular hydrogen bonding between IBP and HPMC plays a role in prolonging supersaturation through nucleation inhibition, resulting in the stabilization of amorphous IBP particles [134]. Therefore, the APC process involving IBP suspension preparation requires using HPMC as a stabilizer to keep the fine IBP crystals non-aggregated in suspension during storage before drying. To identify the optimum quantity for use in precipitation, the effect of HPMC on IBP solubility was studied.

As a first approximation it might be assumed the effect of both excipients is the sum of the single effects, i.e.

$$\boldsymbol{Sol = Sol_0 + (562 - 3.09 * [E] + 2.54 * [E]^2) * [Pl\ F127] + 17 \times HPMC} \quad \boldsymbol{(4.3)}$$

where Sol is the IBP solubility (as I/(E+W) in ppm) in the presence of excipients, Sol_0 is that in the absence of excipients (as given by equation 4.1) and [E], [Pl F127] and [HPMC] are the concentrations of ethanol, Pl F127 and HPMC as % g/g to solvent.

Figure 4.8 plots the experimental solubility results against the Pl F127 concentration with ethanol HPMC contents as parameters. The results are grouped in terms of the nominal ethanol content. The lines show the values predicted by the correlation (Eqn. 4.3) for 0 and 2% HPMC. The data is in reasonable agreement with the correlation although the amount of data is limited. The solubility data is given in Appendix B2.

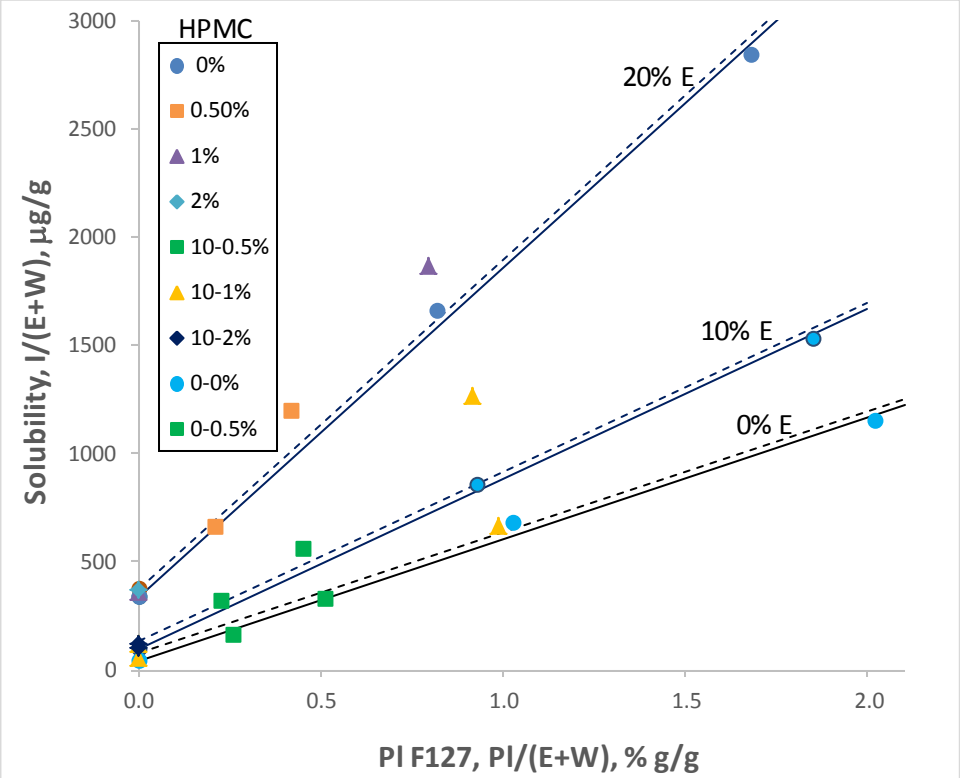

Figure 4.8. Solubility of IBP in mixtures of solvent and excipients. The solid lines are the predictions with no HPMC and the dotted lines with 2% HPMC. The first four entries in the legend are for 20% E. The last five are for HPMC and ethanol.

The purpose of using polymeric stabilizers is to deliver stability for IBP nanosuspensions on short term storage and to achieve successful formation of nanocrystals during particle production. The literatures suggests that HPMC and Pl F127 serve these purposes effectively [28, 117, 120, 137]. In this work the effect of excipient combinations on solubility were investigated at three levels of aqueous ethanol (0, 10, 20% w/w, E/(E+W)) and the concentration of the excipients was

varied up to 2%, w/w as (Pl F127+HPMC)/(E+W). It has been reported that the polarity of the solvent decreases as the amount of organic solvent increases, which favors the solute-solvent interaction, especially in case of a nonpolar drug molecule like IBP, and affects the function of nonionic polar excipients like HPMC and Pl F127 on solubility enhancement [28, 225]. However, the effect of the excipients in this work was found to increase IBP solubility by a factor of fourteen compared to the solubility determined in water-ethanol co-solvents alone.

4.4.3 **Effect of L-Leucine**

The effect of leucine on IBP solubility was investigated for three concentrations of leucine (0.5, 1.0, & 1.5%) in the crystallization media, which comprised HPMC (0.4%), Pl F127 (1.4%) and mannitol (5.2%) in 10% aqueous ethanol (All additive + 0.1 E/(E+W)) (*Figure 4.9*). To investigate the effect of leucine alone, IBP solubility was determined at four different concentrations of leucine in water and 10% ethanol solutions (0.1 E/(E+W)). In the 10% aqueous ethanol solvents with all additives, the IBP solubility was increased linearly with leucine concentration. For all ethanol contents the slope of the line is ~55 (± 2). This value was approximately three-fold of the HPMC and one-seventeenth of the Pl F127 effect on IBP solubility. The slope of the IBP solubility in the crystallization medium increased four times compared to that of leucine only solvents. It was also noticed that IBP solubility with ethanol compared to without ethanol did not increase significantly. The hydrophobic nature of both IBP and leucine [226] causes competition for the available ethanol. Thus, the drug solubility could not be enhanced as it was supposed to be in presence of ethanol in the solvent. Solubility data is given in Appendix B2.

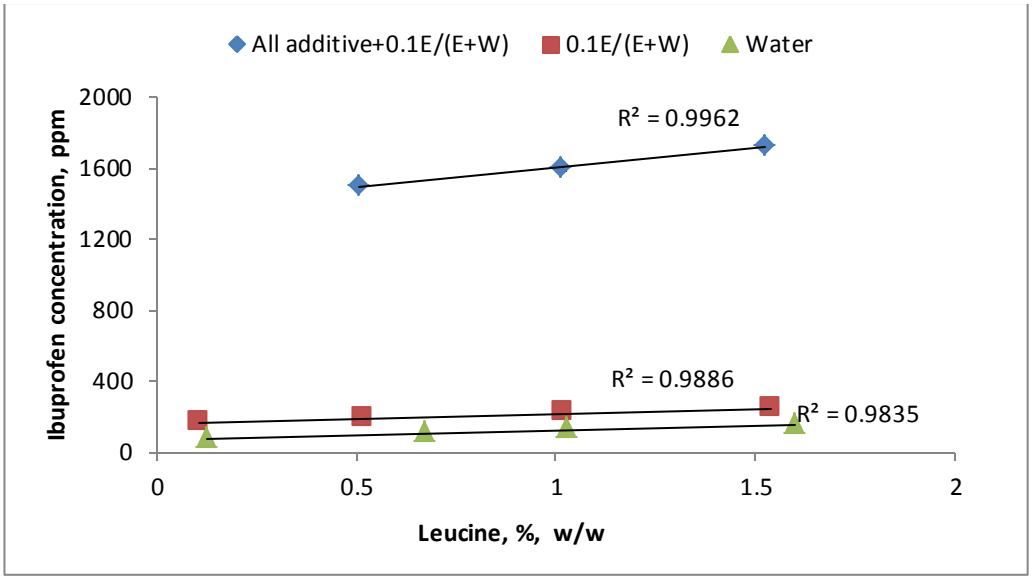

Figure 4.9. Effect of L- leucine on IBP solubility.

4.4.4 **Effect of Mannitol**

To investigate the effect of mannitol alone, the IBP solubility was determined at four different concentrations of mannitol with aqueous and 10% ethanol solutions (*Figure 4.10*). For mannitol as the only excipient the IBP solubility trend was stable. For the 10% ethanol the IBP solubility follows no specific trend but increased slightly due to the ethanol. A similar effect was found in the crystallization medium (all additives); again IBP solubility increased significantly compared with the other two solvents (water and 10% aqueous ethanol). Thus, the increased concentration of mannitol does not affect the IBP solubility in any solvent composition with solubility expressed as a mass ratio of IBP to solvent (E+W). A similar effect was observed in the solubility of other water insoluble drugs (Ursodeoxycholic acid, rofecoxib) [227, 228]. So, using this additive will not cause any fundamental change in the IBP mass ratio concentration during the APC. It will serve as an inert species to recover the prepared IBP fine particles after the freeze drying process. The effect of mannitol in IBP solubility was investigated using the crystallization media with three different concentrations of mannitol. Solubility data is given in Appendix B2.

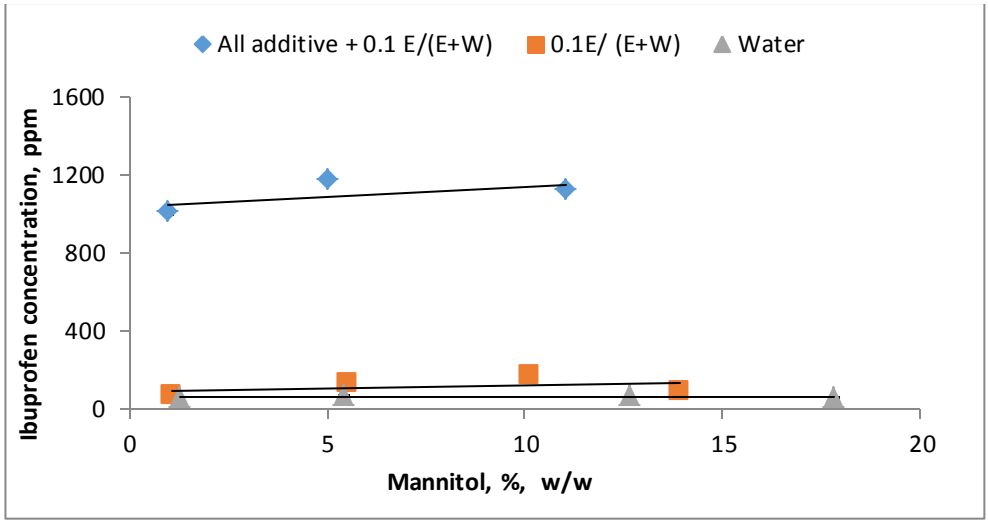

Figure 4.10. Effect of mannitol on IBP solubility.

4.5 CONCLUSIONS

The experimental solubility data of IBP was determined in aqueous ethanol solutions at 10, 25 and 40 °C. The solubility of IBP increases considerably with increasing ethanol contents and also increases with temperature. The experimental data at 25 °C was in good agreement with the prior data of Rashid et al. [31]. A correlation is given to fit all the measured data (without excipients) (*Figure 4.2*). This correlation can be used to select a suitable solvent for washing the IBP drug during the *in vitro* drug dispersion test using a twin stage impinger. The effect of the four excipients HPMC, Pl F127, mannitol and L-leucine in solubility enhancement was investigated first as single component and then in combinations. Pl F127 raises the IBP solubility considerably, with the increases depending on the ethanol content. HPMC has a smaller effect. The combined effect of both excipients appears to be additive. The effect of leucine was positive in increasing the IBP solubility linearly with concentration. Mannitol did not show any effects on the IBP solubility. The results allowed calculation of the minimum amount of initial drug to be used to precipitate IBP during the antisolvent precipitation crystallization to produce fine (<5 μm) IBP crystals for DPI formulations.

Chapter 5: Investigation of variables affecting ibuprofen particle size and morphology

5.1 INTRODUCTION

Chapter 5 involves the investigation of variables affecting the size of the ibuprofen (IBP) drug particles from an anti-solvent precipitation crystallization (APC) process. The experimental methods of the APC process and a Plackett-Burman design studying nine variables and screening for the most effective ones are discussed at the beginning of this chapter. Then the effects of individual excipients such as Pluronic F127 (Pl F127), HPMC (hydroxypropyl methyl cellulose), L-leucine and D-mannitol on the size of the particles' are discussed. A comparative study of the particle morphology is made in the presence and absence of the HPMC and Pl F127 polymers, using scanning electron microscope images of IBP particles. Then a comparative study on the particle size is made between particles prepared with four additives and without the leucine and mannitol. Thus, an optimized method for preparing IBP particles (<5) μm is established by characterizing the particle size, using a Malvern Mastersizer 3000, SEM and TEM.

5.2 EVALUATING THE SIGNIFICANT VARIABLES USING PLACKETT-BURMAN DESIGN

It was necessary to know which operating variables affected the product crystal size produced from the crash crystallization of IBP by the rapid addition of an ethanolic solution of IBP to an aqueous solution (containing excipients) in batch crystallizers. The product is desired to have an average size < 5 μm so the material can be used as an inhalable product. *Table 5.1* shows the variables suggested as possibly having an effect. The ranges in *Table 5.1* were chosen according to the Plackett-Burman design of experiments. These ranges were also chosen based on the trial and error experiments and the parameters were chosen from the references [28, 124, 152, 200, 201].

The crystallizer used for this experiment was shown in Chapter 3 *Figure 3.12*.

Table 5.1 Possible variables affecting the crystallization with high and low levels.

Variables	Name of Variables	+ values (High)	- Values (Low)
X_1	Stirring rate	2000 rpm	500 rpm
X_2	HPMC	1%	0.10%
X_3	Pluronic F127	2%	0.50%
X_4	Ethanol	10%	1%
X_5	Ibuprofen	0.005g/g E	1g/g E
X_6	Infusion rate	1000µl/s	100 µl/s
X_7	Ultrasound level	**ON**	**OFF**
X_8	Temperature	8-10°C	23-25°C
X_9	Batch size	100g	10g

5.2.1 **Plackett–Burman design**

A Plackett-Burman designed experiment [229] was considered appropriate as this gives a linear estimate of the effect of each variable with the smallest number of experiments. Each variable is investigated at a high (+) and low (-) level. Thus it is necessary to choose high and low levels for each variable. The choice should give values as far apart as possible to cover the near-full range of each variable, yet each condition should give a reasonable result (average product size say from 1 to 10 µm). Extreme size results will disturb the analysis. The high and low levels chosen are shown in *Table 5.1*. In retrospect some of the levels chosen were too extreme, but this was not known initially.

5.2.2 **Results**

An N = 16 Plackett-Burman pattern was chosen, so with the 9 variables above this results in 6 "dummy" variables (A-F) which will be used as a measure of reproducibility. The Plackett–Burman design is shown in *Table 5.2*, where the level of each variable is indicated by a 1 (high) or –1 (low). The experiments were

undertaken using these levels and the results (the volume median size of the product (D[v,0.5]) and the size spread (Span) are also shown on *Table 5.2*.

Table 5.2 Sixteen experiment Plackett–Burman design, with results.

Trials	X_1	X_2	X_3	X_4	X_5	X_6	X_7	X_8	X_9	A	B	C	D	E	F	D[v,0.5]µm	Span
1	1	1	1	1	-1	1	-1	1	1	-1	-1	1	-1	-1	-1	18.1	1.6
2	1	1	1	-1	1	-1	1	1	-1	-1	1	-1	-1	-1	1	12.4	2.9
3	1	1	-1	1	-1	1	1	-1	-1	1	-1	-1	-1	1	1	8.0	1.3
4	1	-1	1	-1	1	1	-1	-1	1	-1	-1	-1	1	1	1	7.8	1.3
5	-1	1	-1	1	1	-1	-1	1	-1	-1	-1	1	1	1	1	66.7	1.4
6	1	-1	1	1	-1	-1	1	-1	-1	-1	1	1	1	1	-1	9.2	1.5
7	-1	1	1	-1	-1	1	-1	-1	-1	1	1	1	1	-1	1	7.1	26.3
8	1	1	-1	-1	1	-1	-1	-1	1	1	1	1	-1	1	-1	7.1	17.0
9	1	-1	-1	1	-1	-1	-1	1	1	1	1	-1	1	-1	1	15.1	1.5
10	-1	-1	1	-1	-1	-1	1	1	1	1	-1	1	-1	1	1	223	0.8
11	-1	1	-1	-1	-1	1	1	1	1	-1	1	-1	1	1	-1	205	0.7
12	1	-1	-1	-1	1	1	1	1	-1	1	-1	1	1	-1	-1	5.6	3.2
13	-1	-1	-1	1	1	1	1	-1	1	-1	1	1	-1	-1	1	345	2.0
14	-1	-1	1	1	1	1	-1	1	-1	1	1	-1	-1	1	-1	8.8	4.2
15	-1	1	1	1	1	-1	1	-1	1	1	-1	-1	1	-1	-1	26.7	8.2
16	-1	-1	-1	-1	-1	-1	-1	-1	-1	-1	-1	-1	-1	-1	-1	5.81	2.0

The first point to note is that six of the experiments (nos 13, 10, 11, 5, 15, 9) gave average size results far outside the reasonable range. The first five of these results had a low level of stirring (500 rpm) which may not have been high enough to quickly mix in the added ethanolic solution or to keep the crystals suspended. Five of these six experiments (except for no. 5) also had the largest batch size, which reinforces the suggestion of inadequate mixing. Having an average size of 345 µm amongst other data around 5 µm will certainly greatly disturb the numerical analysis of the results. It is also noted that some of the product had multi-modal size

distributions resulting in large Spans (> 3) which would disrupt calculations for the effect of the variables on the size spread (Span).

5.2.3 **Analysis of Plackett-Burman results**

In spite of the above, it was decided to conclude the calculations for the Plackett–Burman results. *Table 5.3* shows the calculated effect of each variable. The effect of each variable is calculated by summing the product of the result (D[v,0.5]) and the signs in the column for that variable (*Table 5.2*). This is divided by N, the total number of experiments (= 16). The effect is the predicted change in the result (D[v,0.5]) for a change in the variable equal to half the difference between the high and low values shown in *Table 5.1*, with all other variables held constant. The very large values for the effect (e.g. -50 µm for stirring rate) shown in *Table 5.3* result from the very large sizes found in the experimental results, as described above. The sum of squares deviation for each variable (SSq) is the square of the effect multiplied by N. The degree of freedom (Dof) is 1 for each variable as there was only one change in its value. The numerical average of the sizes was 67.2 µm and its evaluation 'consumed' one degree of freedom, leaving 15 for the variables.

Table 5.3 Effect of variables and sum of squares.

Variable	Effect	SSq	Dof
Stirring rate	-50.31	40497	1
HPMC	-16.82	4526	1
Pl F127	-21.58	7451	1
Ethanol	1.49	35	1
Ibuprofen	-0.70	8	1
Infusion rate	14.96	3582	1
Ultrasound	43.65	30483	1
Temperature	8.63	1192	1
Batch size	45.26	32776	1
A	-23.03	8487	1
B	15.50	3844	1
C	24.51	9612	1
D	-17.82	5080	1
E	6.23	621	1
F	24.93	9941	1

Since the effects for the dummy variable (A–F) are just a measure of error, their sum of squares was combined (*Table 5.4*). This is shown as an ANOVA (Analysis of Variance) table. The mean sum of squares (MSSq), an estimate of the variance, is

obtained by dividing SSq by Dof. **F** is the ratio of the MSSq to that estimated for the error. At the 95% confidence level the critical **F** value (**F**[1,6]) is 5.99, so only one result (stirring rate) exceeds this and is a significant effect. Very low **F** values are shown in red.

Table 5.4 ANOVA table for all variables.

Variable	SSq	Dof	MSSq	F
Stirring rate	40497	1	40497	**6.46**
HPMC	4526	1	4526	0.72
Pl F127	7451	1	7451	1.19
Ethanol	35	1	35	0.01
Ibuprofen	8	1	8	0.00
Infusion rate	3582	1	3582	0.57
Ultrasound	30483	1	30483	**4.87**
Temperature	1192	1	1192	0.19
Batch size	32776	1	32776	**5.23**
Error	37586	6	6264	

The least significant variable (Ibuprofen) was then eliminated and its SSq treated as error and the ANOVA re-calculated. This was continued until all non-significant variables were removed. Finally only stirring rate, batch size and ultrasound were left as variables significantly affecting the product size (*Table 5.5*). At the 95% confidence level, the critical **F** value **(F**[1,12]) is 4.75, so all three remaining variables have a significant effect on product size.

Table 5.5 Final ANOVA.

Variable	SSq	Dof	MSSq	F
Stirring rate	40497	1	40497	**8.94**
Ultrasound	30483	1	30483	**6.73**
Batch size	32776	1	32776	**7.23**
Error	54381	12	4532	

The same was confirmed from the Pareto graph (*Figure 5.1*) in which it shows 90% of the standardized effect on D[v,0.5] was from the variables' stirring rate (X_1), batch size (X_9) and ultrasound (X_7).

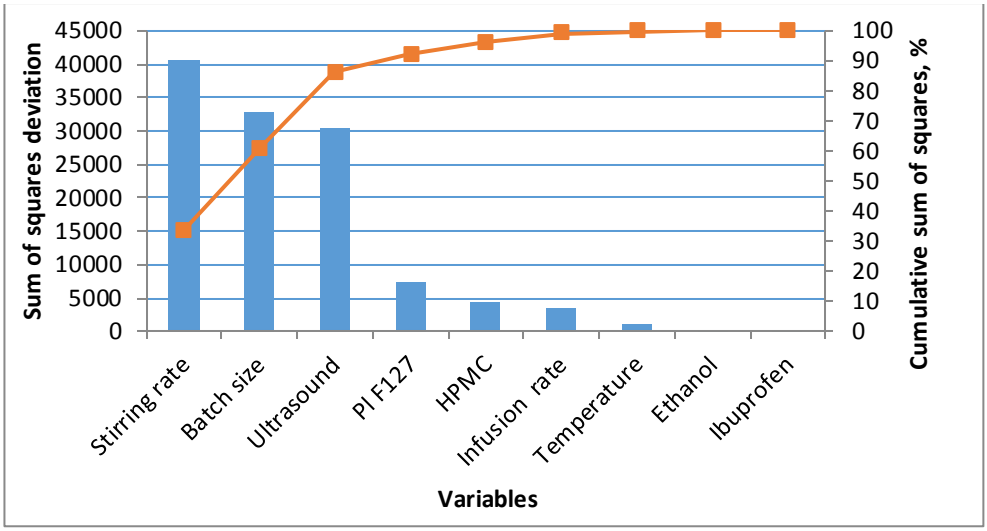

Figure 5.1 Pareto chart showing the effect of different factors on the volume median diameter (D[v,0.5]) of IBP particle based on the observations of the Plackett-Burman design.

5.2.4 **Final equation**

Finalising the Plackett–Burman analysis, the linear model fitting the data (in terms of -1, 1 coding for the variables) is,

$$\mathbf{D[v,0.5]_{pr} = 67\ (\pm\ 37) - 45\ (\pm\ 37)\ *St' + 45\ (\pm\ 37)\ *Ba' + 44\ (\pm\ 37)\ *Us'} \qquad \mathbf{(5.1)}$$

where $\mathbf{D[v,0.5]_{pr}}$ is the predicted product size, **St'** is the scaled stirring rate, **Ba'** the scaled batch size and **Us'** the scaled use of ultrasound. The value in brackets is the estimated 95% uncertainty on the coefficient. The dash symbol (') indicates scaled variables coded (-1, 1). This equation is readily coded into the variables with actual units using (from *Table 5.1*) St' = (St -1250)/750, Ba' = (Ba – 55)/45 and Us' = 2*Us -1, if ultrasound on = 1 and no ultrasound = 0, where the variables without dashes are in the original units shown in Table 1. Substituting gives,

$$\mathbf{D[v,0.5]_{pr} = 52}\ (\pm\ 40)\ \mathbf{- 0.067}\ (\pm\ 0.05)\ \mathbf{*St + 1.01}\ (\pm\ 08)\ \mathbf{Ba + 87.2}\ (\pm\ 75)\ \mathbf{*Us} \qquad \mathbf{(5.2)}$$

Thus a change in stirring rate from 500 to 1250 rpm would increase the volume median size of the product by 45 µm, which is not a useful result as the desired product size is < 10 µm.

This analysis used the volume median size of the product as the result. An analysis was also done using the log of this size as the result (to bring the larger sizes closer to the bulk of the results) but it gave similar conclusions.

5.2.5 **Conclusions**

Because of the range of variables chosen (particularly the stirring speed) a number of the results were out of range and the analysis was not very helpful.

It was decided not to repeat the Plackett–Burman experiment as considerable experience had been obtained undertaking the exercise. Instead it was decided to explore a number of the variables individually.

5.3 OPTIMIZATION OF THE PRECIPITATION PROCESS CONDITIONS

5.3.1 **Temperature**

The APC of IBP was undertaken in a constant temperature bath as described in Chapter 3, Section 3.8. The influence of the temperature on the resulting particle size was tested by increasing the temperature from 15 °C to 30 °C from individual batch crystallization. The smallest particle size was obtained at 25 °C temperature, as shown in *Figure 5.2*. The dried particles were resuspended in the saturated crystallization media for the size measurements in Malvern Mastersizer 3000. The investigation indicated 25 °C as the most suitable temperature to get inhalable size IBP particles. The raw data is given in Appendix C1.

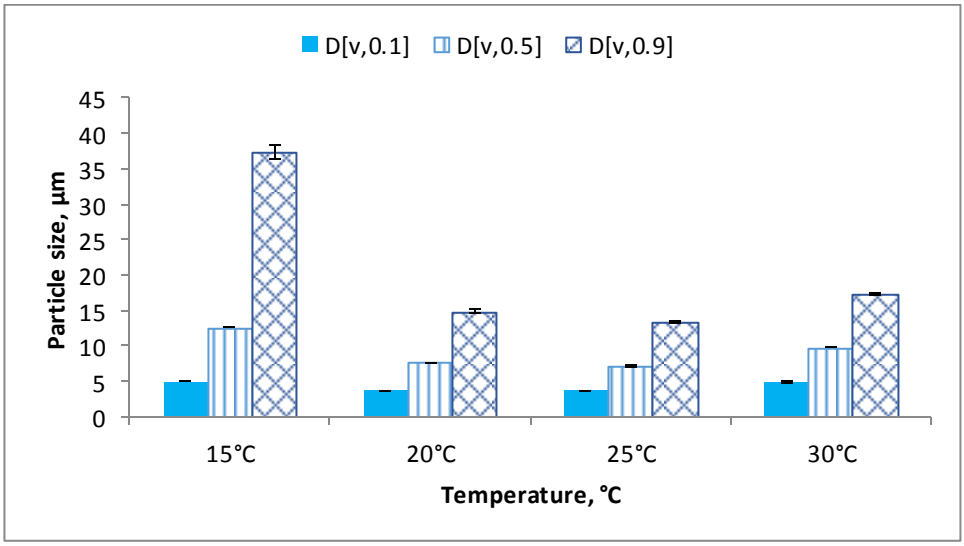

Figure 5.2 Effect of temperature of the precipitation process on particle size. Mean ± SD, n= 3.

5.3.2 **Ultrasound**

The Plackett-Burman design indicated that longer ultrasound duration will cause a larger particle size of IBP in the APC process. The indicated result contradicts the available studies [230, 231] which state that ultrasound aids in the production of small pure crystals with uniform size. However, a further investigation was performed by varying the ultrasound duration for the precipitation process and the effect on size was observed. *Figure 5.3* shows the particle size of IBP produced from individual batches using five different duration of ultrasound in the anti-solvent precipitation process. The raw data is given in Appendix C2.

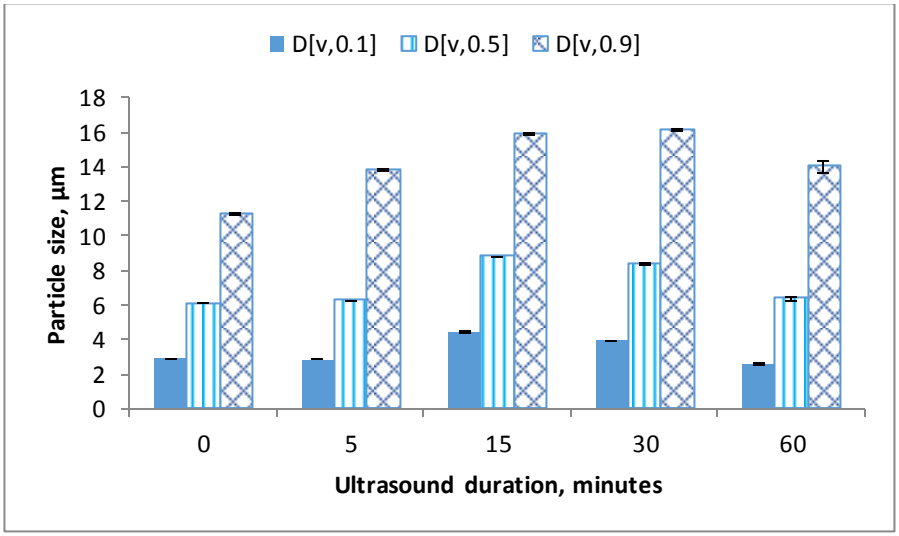

Figure 5.3 Effect of ultrasound duration on particle size in the APC process. Mean ± SD, n= 3.

Initially the particle size increased with ultrasound duration, but after 30 minutes duration the size decreased. A possible reason could be the large volume ultrasonic bath unit used for the study. The explanation from the literature states that a fixed wave ultrasonic in a larger unit produces weaker penetrating and reflecting waves, so vibration and cavitation at some points in the liquid are lower [231]. This results in fewer nuclei, and hence in larger crystals being formed [231]. The literature also suggests that short duration of the ultrasonic wave fails to blend the solution, whereas longer duration reduces crystal size under continuous sonication. The production of small crystals via continuous sonication throughout the duration of the process can facilitate productive nucleation at higher levels of supersaturation at the expense of crystal growth [232, 233]. However, in any event the optimum ultrasound duration needs to be determined. In our work the ultrasound application was

maintained for 30 minutes throughout the process of the APC. Ultrasound causes uncontrolled increase of temperature in the longer duration like 60 minutes. The results of the investigation on the temperature (section 5.3.1) effect on particle size in APC process have shown that uncontrolled temperature during crystallization adversely affects the size of the particles. Constant temperature is also an utmost condition to control the particle size in the APC process. Though, in the investigation particles were smaller at 60 minutes of ultrasound duration to maintain the constant temperature of the bath at 25 °C it was decided to run the ultrasound for 30 minutes.

5.3.3 **Mixing duration**

The particle growth equilibrium was considered the deciding factor to finalize the solvent-antisolvent mixing duration in the APC process. A single batch run was performed to estimate the particle size equilibrium attainment duration. Samples were collected at 1, 2, 3, 4, 5, 10, 15 and 20 minutes of mixing, and particle size was measured in the Malvern Mastersizer 3000 immediately after sample collection. *Figure 5.4* plots the particle size as volume median diameter against time in minutes. The raw data is given in Appendix C3.

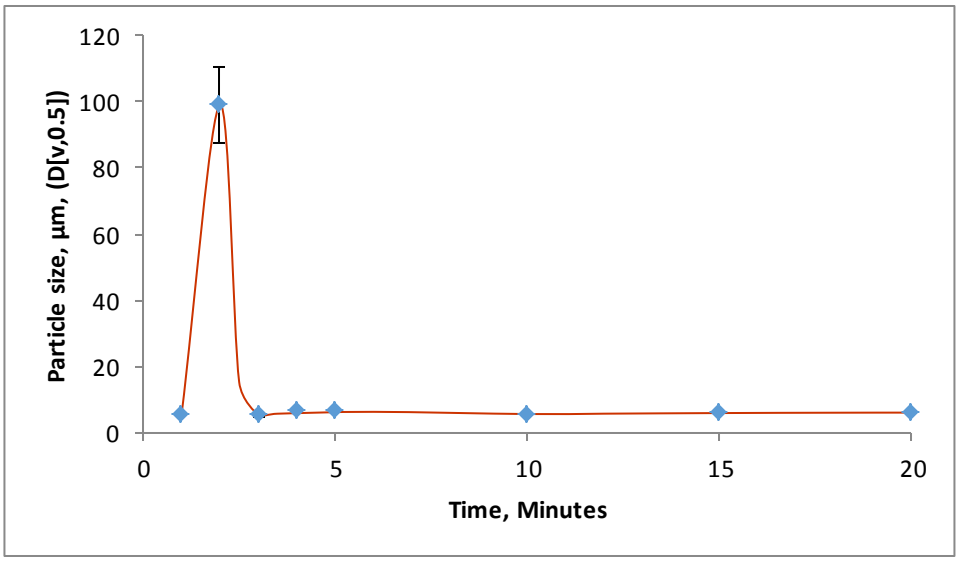

Figure 5.4 IBP Particle size vs time for a single batch in the APC process. Mean ± SD, n= 3.

The plot shows that in the second minute of mixing the particle size is abruptly increased. A possible explanation for this might be that the addition of solvent phase to antisolvent phase causes a very rapid supersaturation that leads to particle

aggregation initially. However, after two minutes of mixing time the particle size dropped down to 5.4 ± 0.6 µm and it remained constant at about 6.1 ± 0.5 µm for 20 minutes of mixing duration. Initial observation from this study suggests that the particle growth stopped after 5 minutes of solvent-antisolvent phase mixing. Therefore, the mixing duration for the APC process was considered to be a minimum of 20 minutes for preparing stable size IBP particles, as it should be continued fivefold the time taken for growth to stop.

5.4 OPTIMIZATION OF THE CRYSTALLIZATION COMPONENTS

5.4.1 IBP concentration in the solvent system

An alteration of the IBP concentration in the system had an effect on the final particle size obtained in the APC process. Five different IBP concentrations were investigated, 1.0%, 0.9%, 0.8%, 0.7% and 0.5%. The largest particle size was obtained for 1.0% and 0.5% IBP concentration. However, the volume median diameter (D[v,0.5]) of the particle size was 4.88 µm, obtained with 0.8% IBP concentration. Change away from this optimum drug concentration increased the particle size (*Figure 5.5*). However, the range of drug concentration for the particle preparation was from 0.3 – 2 % IBP (w/w). Because in the final particle preparation ultrasound was used during the APC process, which has not been used in the investigation for identifying optimum IBP % (w/w). The raw data is given in Appendix C4.

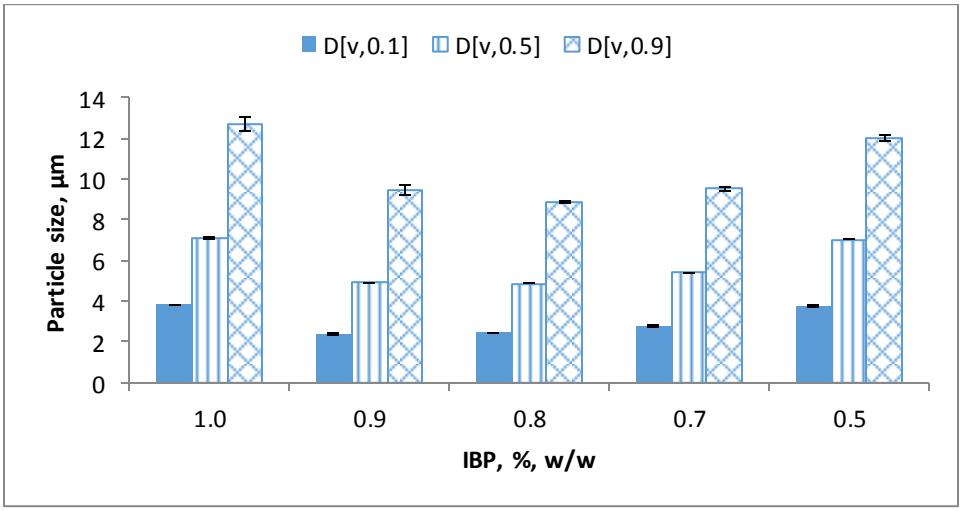

Figure 5.5 Effect of IBP concentration on the particle size obtained in the APC process. Mean ± SD, n= 3.

5.4.2 **Solvent-antisolvent ratio (S/AS ratio)**

The influence of the S/AS ratio on the resulting particle size was tested by increasing the ratio from 0.05, followed by 0.06, 0.08, and 0.09, up to 0.1 in individual batch crystallizations. The smallest particle size obtained was at a S/AS ratio of 0.08 (*Figure 5.6*). The volume median diameter (D[v,0.5]) of this sample was 4.88 µm (D[v,0.5]). A change in the S/AS ratio from this optimum level increased the particle size. The raw data is given in Appendix C5.

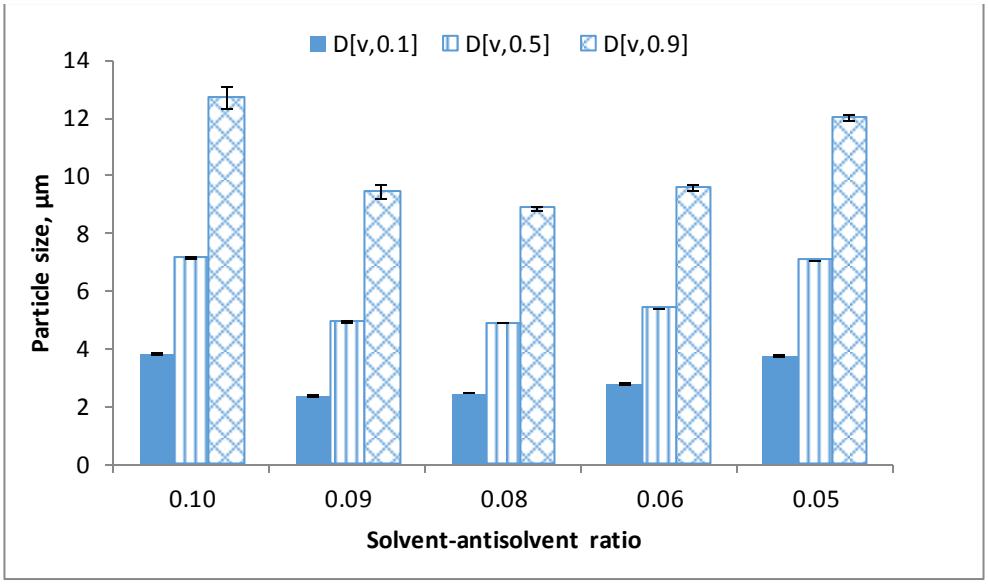

Figure 5.6 Effect of solvent-antisolvent ratio on particle size of IBP produced in the APC process. Mean ± SD, n= 3.

5.5 OPTIMIZATION OF THE ADDITIVE CONCENTRATION

As mentioned above, Pluronic F127 (Pl F127) was used to restrict crystal growth, HPMC to minimise agglomeration, mannitol as a vehicle and a bulking agent for recovering freeze-dried IBP crystals [145], and L-leucine as a dispersive adjuvant for DPI formulations to enhance aerosol efficiency [158, 159]. Additive optimization was very critical due to the presence of four different materials (Pluronic F127, HPMC, L-leucine and D-mannitol). In the investigation by Knox and co-workers, the crystal growth of paracetamol was strongly influenced by the solvent composition used in the anti-solvent precipitation crystallization [234]. Hence, several experiments were performed to identify the effect of each additive on the IBP crystal growth.

5.5.1 **Hydroxypropylmethyl cellulose (HPMC)**

The effect of HPMC on the particle size produced in an APC was investigated by running two series of experiments. *Table 5.6* shows the formulation table including the additive, ethanol, IBP concentrations, batch size and the volume median diameter (D[v,0.5]) of prepared particles from the respective batches.

Table 5.6 Formulation and results for the investigation of the HPMC effect on the particle size prepared in an APC process.

Formulation name	**Leucine, %, (w/w)**	**Mannitol,%, (w/w)**	**HPMC,%, (w/w)**	**Pl F127,%, (w/w)**	**Ethanol, %, (w/w)**	**IBP,%, (w/w)**	**Batch size, g**	**D[v,0.5] ± SD, n=5**
H1	0	0	0.0	1.7	10.0	0.3	10	4.4 ± 0.4
H2	0	0	0.2	1.7	10.0	0.3	10	3.7 ± 0.4
H3	0.2	0.9	0.0	0.9	9.9	3.0	101.1	7.9± 0.8
H4	0.2	0.9	0.5	0.9	9.9	3.0	101.7	7.5± 0.4

Formulations H1 and H2 were compared with each other with respect to the mean particle size obtained, where H1 is the control batch and H2 has both HPMC and pluronic F127. The batch size for H1 and H2 was 10.0 g and the IBP concentration was 0.3%. The volume median diameter (D[v,0.5]) obtained from H1 and H2 indicated a possible small reduction in particle size in the presence of HPMC. To ensure the same effect in presence of all other additives, Pl F127, L-leucine and D-mannitol, H3 and H4 formulations were compared. H3 formulation is the control formulation with no HPMC but with the other three additives and H4 is the formulation with all additives. The batch size for H3 and H4 was 100.0 (±1) g and the IBP concentration used was 3.0%. The particle volume median diameter (D[v,0.5]) comparison between H3 and H4 also showed particle size reduction in the presence of HPMC. Thus, taken together these results suggest that HPMC is useful to keep the particle size smaller during the APC of IBP, which also supports the hypothesis suggested by Verma et al. [117].

Several experiments were done to optimise HPMC concentration. *Figure 5.7* plots the volume median diameter (D[v,0.5]) of the particles produced in the APC process at different concentrations of HPMC. The raw data is given in Appendix C6.

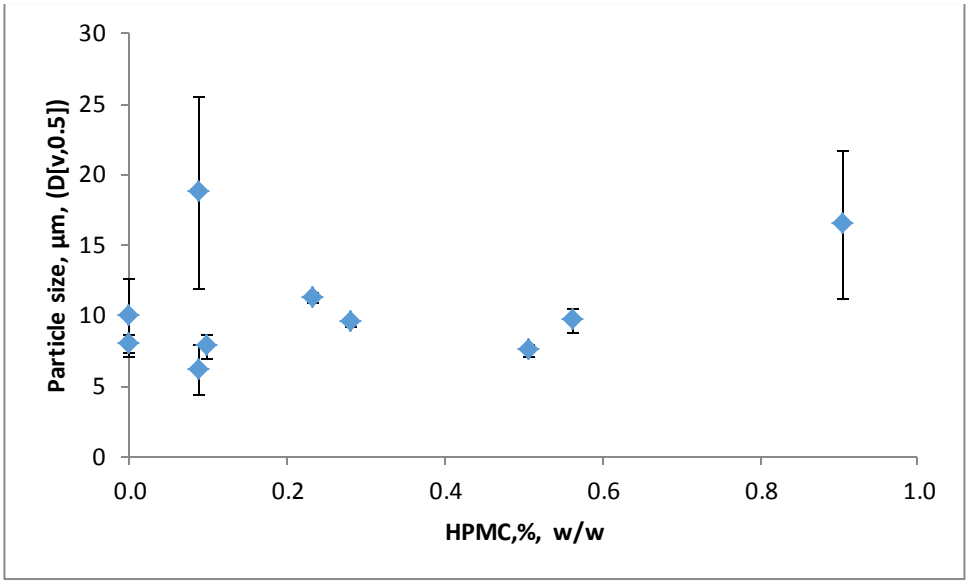

Figure 5.7 Effect of HPMC concentration on IBP particle size produced in the APC process. Mean ± SD, n= 3.

These results seem to indicate the optimum concentration would be 0.2% < HPMC < 0.6% for the smallest particle size. The outliers at 0.09% and 0.9% HPMC resulted as the initial IBP load for those experiments were 0.5 g and 8.8 g respectively, which was too extreme (too low or too high) to optimize the particle size. The decrease of particle size might be because agglomeration was less likely to occur due to the non-ionic nature of HPMC polymer. The probable mechanism might be the presence of a hydrodynamic boundary layer surrounding the crystal suspensions and the adsorption of the polymer molecules on the growing crystal faces, while HPMC also provides a steric hindrance to agglomeration and crystal growth [235, 236]. Hence, the drug-polymer system can be explained by hydrogen bonding between the drug molecules and the polymer with a profusion of hydroxyl groups. However, the increases in particle size with increase in HPMC concentration can be explained by the enhanced viscosity of the solution hindering the penetration of ultrasonic wave. Thus, during precipitation the diffusion between the solvent and anti-solvent phase is impeded, which results in larger particles, and the concentric layers of HPMC also cause particle size enlargement [144]. However, for formulations the HPMC concentration of 0.2-0.6% was expected to be the optimal range to sufficiently cover the crystal surface and provide steric repulsion between crystals.

5.5.2 **Pluronic F127 (Pl F127)**

The effect of Pl F127 on the particle size reduction of IBP particles in an APC has been reported by many researchers [28, 117, 124]. To determine the optimum concentration of Pl F127 for the lowest particles size, IBP particles were produced in an APC process by using Pl F127 concentrations of 0%, 0.7%, 1.3% and 2.0% in individual batches. All the other variables conditions and additive concentrations were maintained equally for all batches. Particles were prepared using the same method stated in Chapter 3, Section 3.8. *Figure 5.8* plots the particle sizes at the four different concentrations of Pl F127 from four individual batches. The raw data is given in Appendix C7.

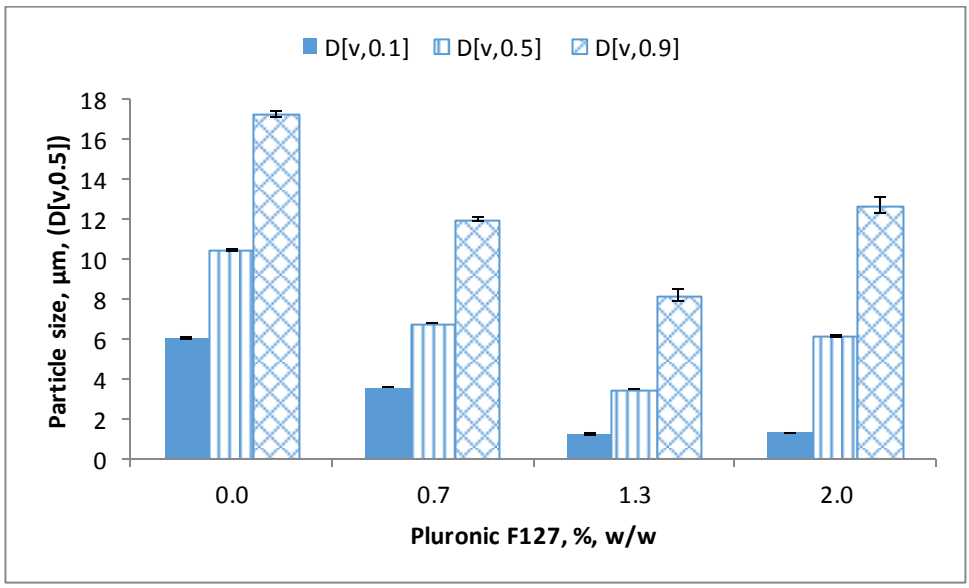

Figure 5.8 Effect of Pl F127 concentration on the size of IBP particles produced in an APC process. Mean ± SD, n= 3.

The particle size gradually decreases with an increase in Pl F127 concentrations up to 1.3%. Then there was an increase in particle size at 2.0% Pl F127. An explanation for this effect could be that above the critical micelle concentration of Pl F127, it tends to form micelles with each other. Then the drug molecules might agglomerate and produce larger particles. However, the smallest particles were produced at 1.3% of Pl F127 and the volume median diameter was 3.5 ± 0.3 µm. From the results of these experiments it was concluded that 1.3% Pl F127 would be the optimum concentration to get an inhalable size IBP particle in an APC process.

5.5.3 **L-leucine**

The effect of leucine concentration on the particle size was investigated by varying leucine concentrations (0%, 0.5%, 1.2% and 1.6%) with the same concentration of other additives and conditions in individual batches. Particles were prepared using the same method described in Chapter 3, Section 3.8. The dried particles were resuspended using crystallization medium before the size measurement in the Malvern Mastersizer 3000. *Figure 5.9* shows the particle size results for each concentration of leucine. The raw data is given in Appendix C8.

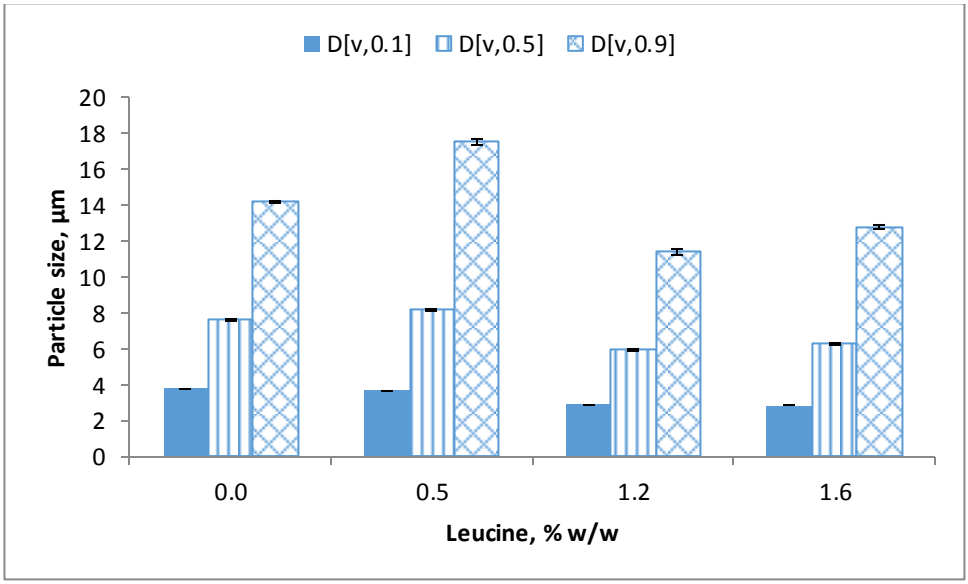

Figure 5.9 Effect of leucine concentration on the size of IBP produced in an APC process. Mean ± SD, n= 3.

The volume median diameter (D[v,0.5]) of all the powder formulations was within the range of 5-10 µm (Leucine 0%: 7.6 ± 0.2 µm, Leucine 0.5%: 8.2 ± 0.3 µm, Leucine 1.2%: 5.9 ± 0.8 µm, Leucine 1.5%: 6.3 ± 0.6 µm). No specific trend was observed from this investigation. Another study investigating different leucine concentration effects on the particle size observed a similar pattern [158]. However, the smallest particle size (though it may not be significant) in our investigation was found from 1.2% leucine concentration. Thus, the optimum concentration of leucine was taken to be 1.2% for getting the smallest product particle size.

5.5.4 **D-mannitol**

D-mannitol was used to recover the particles after freeze drying by acting as a bulking agent. After drying, the prepared IBP particles tend to form hard agglomerates which do not disperse easily while resuspended with a crystallization medium. To see the effect of mannitol on the size of prepared IBP particles, a control batch without mannitol was compared with a batch with mannitol. The particle size of the prepared particles from both batches was measured using the Malvern Mastersizer after drying and resuspending with crystallization medium. *Figure 5.10* shows the particle size distributions of the prepared IBP in both batches.

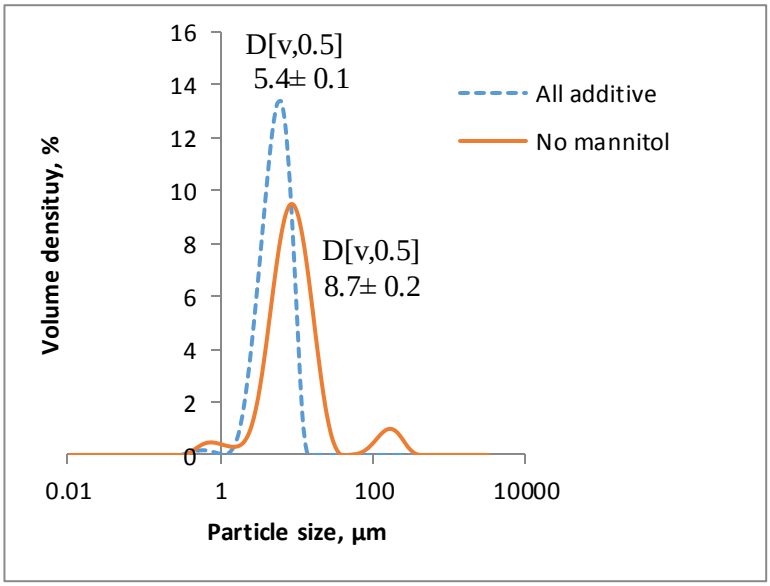

Figure 5.10 Effect of mannitol of the particle size of prepared IBP in APC process. Mean ± SD, n= 3.

The particle size distribution curve shown that D[v,0.5] of the prepared IBP particles in the absence of mannitol is larger than that of the particles prepared with mannitol. The size distribution curve for the no mannitol batch showed a small peak in the area of particles > 100 µm indicating the presence of large agglomerates. Therefore, it was confirmed that mannitol did not increase the IBP particle size during APC process and aids in particle dispersion after drying.

The experiment on local degree of supersaturation was attempted to determine the nucleation rate by sampling every 5 seconds up to 30 minutes and the concentration was observed in UV. But the local supersaturation was achieved within micro second

of adding the drug solution into the anti-solvent and the rate of nucleation could not be determined.

In chapter 2 section 2.11.1 the theory of controlling the local supersaturation in the APC process was discussed as per the available literature.

5.6 OPTIMIZED METHOD OF PRODUCING INHALABLE SIZE IBP USING HPMC AND PL F127 IN APC PROCESS

An optimized method of producing inhalable size IBP particles was established by using HPMC (0.4%) and Pl F127 (1.4%) as agglomeration and growth inhibitors. In this case the solvent and antisolvent phase was mixed together using magnetic stirrer at 750 rpm and continued for 20 minutes. The IBP concentration was 0.3% and batch size was 10.0 g. This batch was run in triplicate and the particle size of the wet crystal suspension of each batch was measured in the Malvern Mastersizer 3000. *Figure 5.11* presents the particle size distributions for three replicate batches.

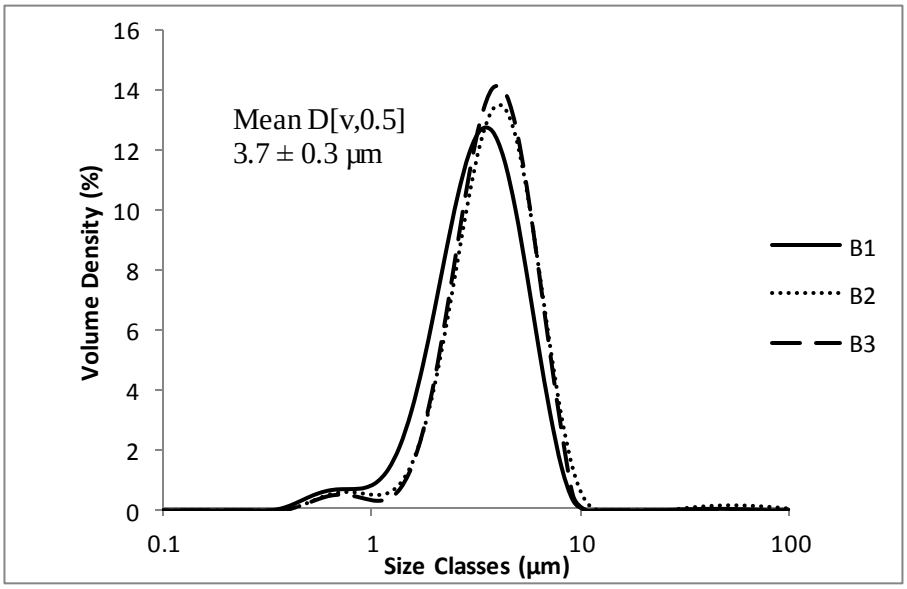

Figure 5.11 Reproducibility of particle size from three replicate batches of the optimized APC method of producing inhalable size IBP particles. Mean ± SD, n= 3.

The particle size distributions of the three batches were found to be in good agreement with each other and the mean particle size of the three batches was 3.7 ± 0.3 µm. This particle size was confirmed from the scanning electron microscope images of the particles at two different magnifications (*Figure 5.12*). The scale bars

of the images are shown. The images confirm the particle size obtained with the Malvern Mastersizer 3000.

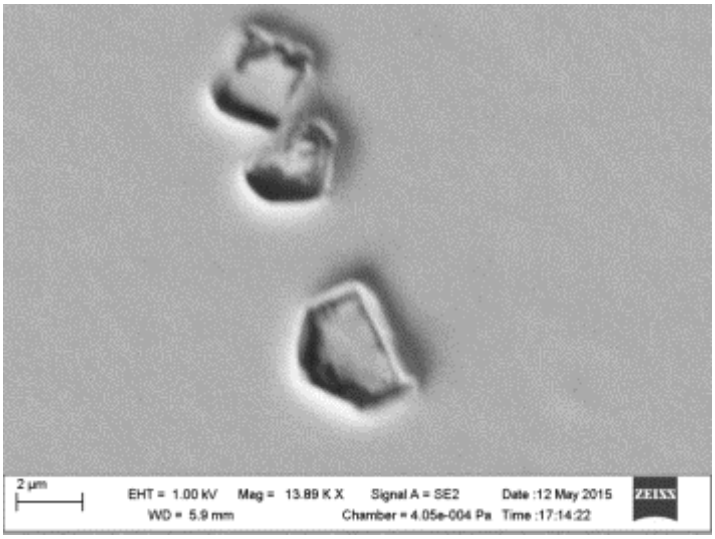

Figure 5.12 SEM image of the particles produced in an optimized APC process in presence of HPMC (0.4%) and Pl F127 (1.4%).

5.7 EFFECT OF HPMC AND PL F127 ON PARTICLE MORPHOLOGY

An experiment was executed to identify the effect of HPMC and Pl F127 on the particle morphology. Particles were prepared in an APC process using three different solvent-antisolvent ratios with and without HPMC and Pl F127 polymers. Then the prepared microparticle suspension samples were processed, as described in Chapter 3, Section 3.11.1, for the morphology investigation using a scanning electron microscope (SEM) after drying. It is seen from the SEM images in *Figure 5.13* that IBP crystals produced without polymers are isolated from each other and have a sharp chunky crystal shape. The crystals produced in the presence of HPMC and Pl F127 were a loosely agglomerated form and the shape and morphology of the crystals were slightly roughened compared with the crystals produced without polymers. No significant difference in the crystal size or morphology was observed with the ethanol concentration change in batches both with and without polymer. The investigation indicated that the presence of polymers has a potential agglomeration effect for the dry crystals. To overcome this problem it was necessary to introduce D-mannitol and L-leucine as additives during the APC process to acquire better particle flow and dispensability after drying.

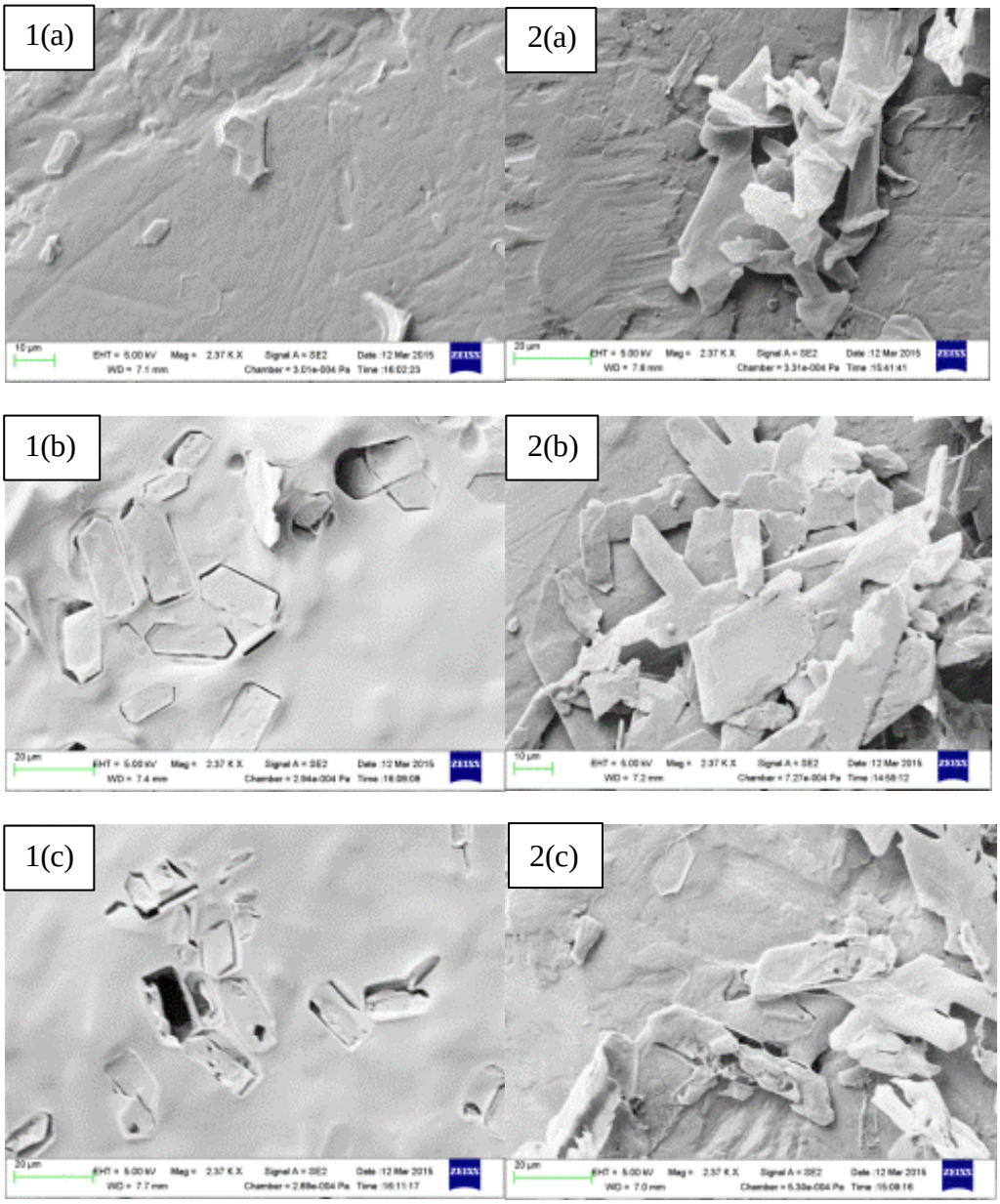

Figure 5.13 Scanning electron microscope images for the effect of HPMC and Pluronic F127 on the morphology of IBP particles produced in the APC process after drying. The SEM images 1(a),1(b) & 1(c) (on the left) represent particles produced without polymers at 5, 10 and 20 % w/w aqueous ethanol. The SEM images 2(a),2(b) & 2(c) (on the right) represent particles produced with polymers (0.5% HPMC+0.5% Pl F127) at 5, 10 and 20 % w/w aqueous ethanol.

5.8 EFFECT OF LEUCINE AND MANNITOL ON PARTICLE SIZE AND MORPHOLOGY

To overcome the particle aggregation and susceptible degradation of IBP particles after drying, mannitol as the bulking agent and leucine as a dispersive

adjuvant were incorporated in the antisolvent phase of the APC process. Hence, it was important to ensure the presence of leucine and mannitol does not increase the particle size and determine if any effect on the particle morphology exists. To answer these questions, particles produced with HPMC and Pl F127 were compared with the particles produced with HPMC, Pl F127, leucine and mannitol in terms of size and morphology both before and after drying. *Figure 5.14* shows the observations from the particle size measurements inform the Malvern Mastersizer 3000. *Figure 5.15* and *Figure 5.16* present the particle images from the scanning electron microscope and the transmission electron microscope.

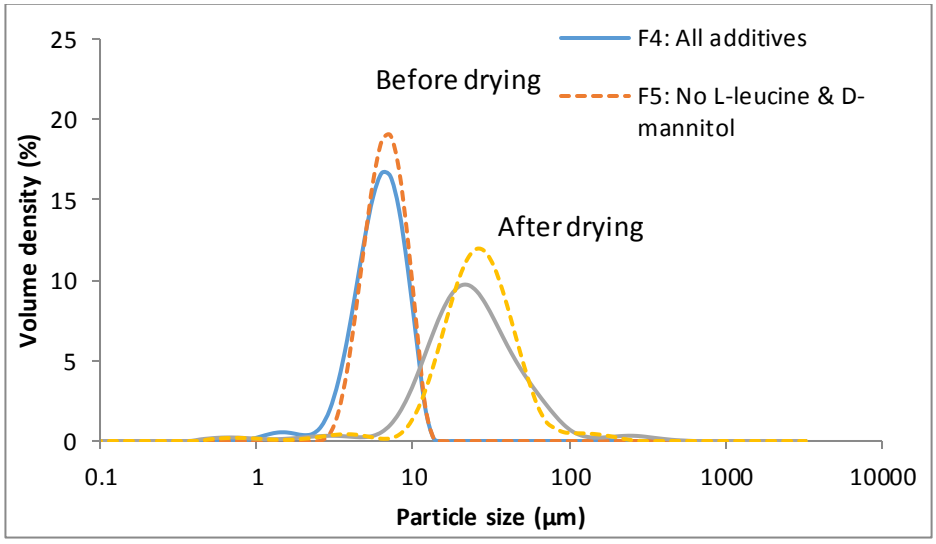

Figure 5.14 Effect of leucine and mannitol on the size of IBP particles produced in the APC process.

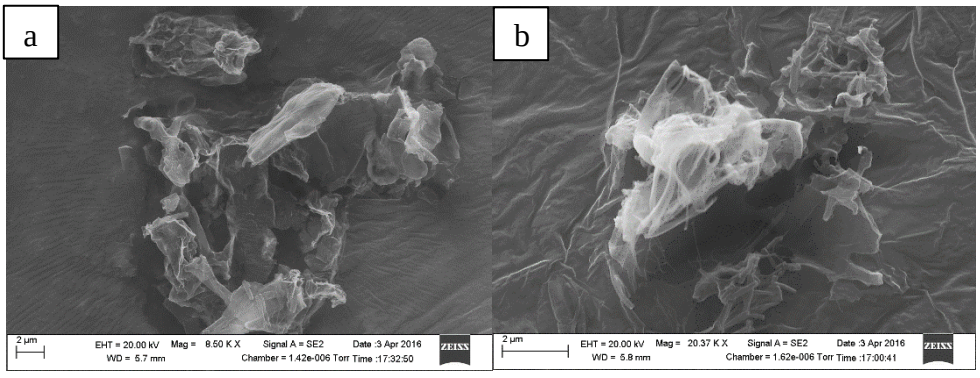

Figure 5.15 Effect of leucine and mannitol on the morphology of IBP particles produced in the APC process from the scanning electron microscope images; a) All additives; b) No L-leucine and D-mannitol.

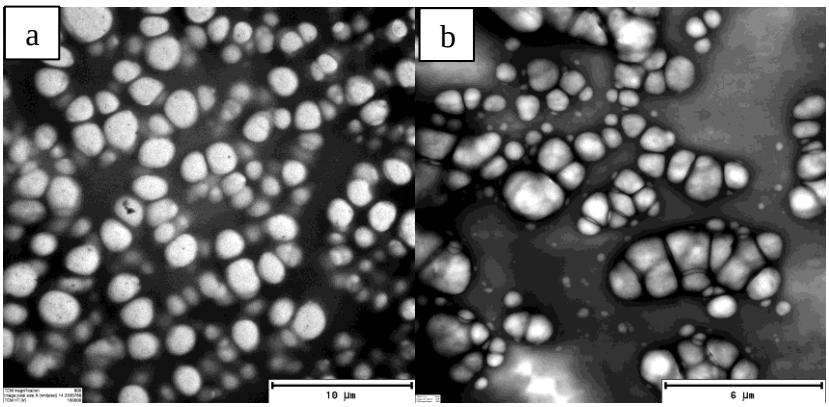

Figure 5.16 Effect of leucine and mannitol on the morphology of IBP particles produced in the APC process from the transmission electron microscope images; a) All additives; b) No L-leucine and D-mannitol.

The size distribution curves of the particles from both batches indicated no significant increase in particle size in the presence of leucine and mannitol. A parallel increase in the dried particle size distribution of both batches after one month of drying was observed. However, the particle size characteristics were found to be undisturbed due to the presence of leucine and mannitol with HPMC and Pl F127. The particle morphology characteristics were similar for both of the batches according to the images captured in SEM (*Figure 5.15)* and TEM (*Figure 5.16*). No size increase was observed from the image analysis either. The findings of the above investigation confirmed that leucine and mannitol did not interfere with the particle growth of morphology during the APC process.

5.9 OPTIMIZED METHOD OF PRODUCING INHALABLE SIZE IBP USING HPMC, PL F127, L-LEUCINE AND D-MANNITOL IN APC PROCESS

IBP particles were prepared by APC using HPMC (0.2%), Pl F127 (1.3%), leucine (1.2%) and mannitol (8.6%). The other method conditions and variables were maintained, as described in Section 5.6. The particle size of dried particles resuspended in the crystallization medium was measured using the nano zeta sizer (*Figure 5.17*) and the Malvern Mastersizer 3000 (*Figure 5.18*) with three replicate

batches. The particle size and morphology was also witnessed from the TEM images of the resuspended dried particles (*Figure 5.19*).

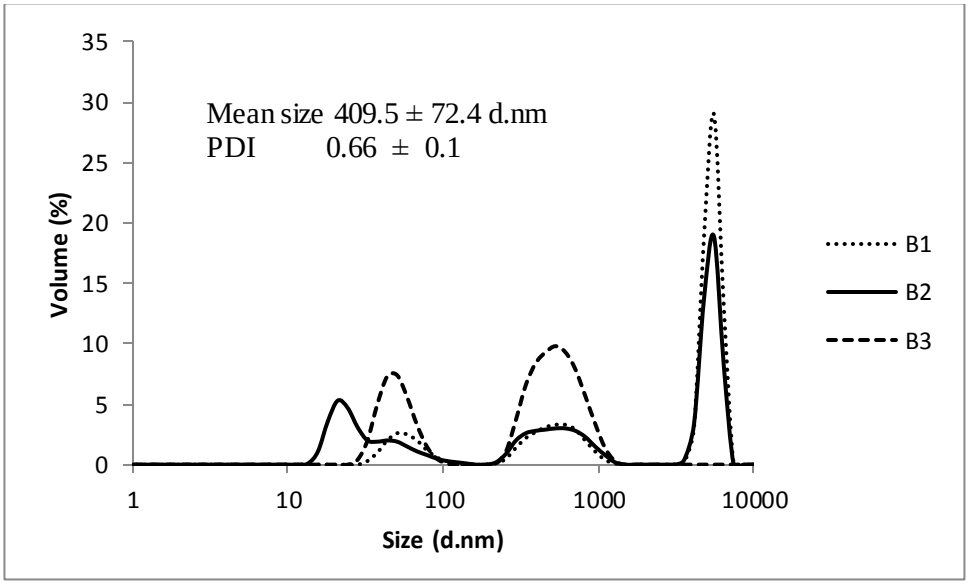

Figure 5.17 IBP particle size distribution in Zetasizer from three replicate batches (B1 to B3). Mean ± SD, n= 3.

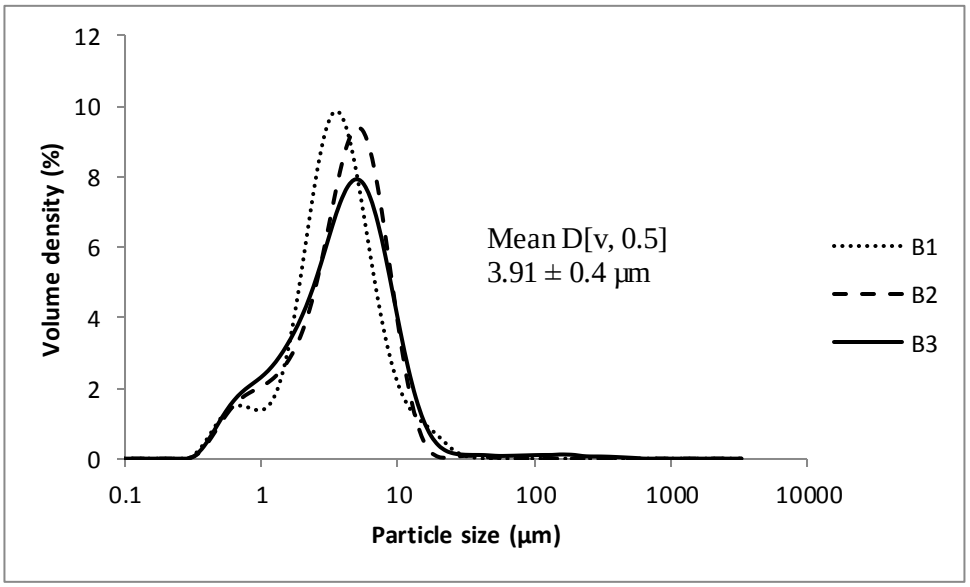

Figure 5.18 IBP particle size distribution in Malvern Mastersizer from three replicate batches (B1 to B3). Mean ± SD, n= 3.

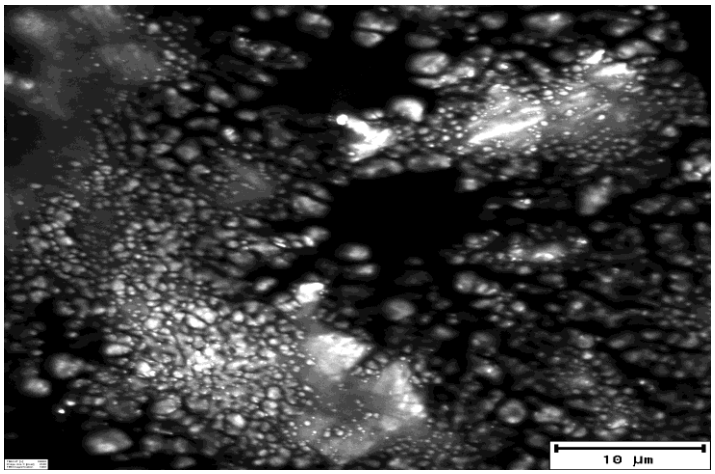

Figure 5.19 TEM image of the particles produced from APC process using HPMC, Pl F127, leucine and mannitol.

The particle size distribution curves from the nanoZetasizer showed multimodal distribution of particles. The peaks were found at approximate mean diameter of 5560, 500, 40 and 20 nm. The mean size of three replicate batches from the nanosizer was 410 ± 72 nm, with an average polydisperse index (PDI) of 0.66 ± 0.1. The size measurement results from Malvern Mastersizer 3000 showed a unimodal curve with a small bump in the nano size range (*Figure 5.18*). The mean D[v,0.5] of three replicate batches was 3.9 ± 0.4 µm. The size distributions curves for the same particles in both the nano Zetasizer and the Malvern Mastersizer indicated that the prepared IBP crystals from the APC process are a mixture of nano and micron size. The particle size distributions were slightly different due to the presence of particles with the size of both nano-meter covering 1.7 (±1) % and micro-meter 7.5 (±2) % range. The nano size particles have 1 % error, which are estimated 95% uncertainties on the amount of nanometer size particles from three batches. Whereas the micron size particles with 2% error are estimated 95% uncertainties on the amount of microparticles prepared from three batches. Though the estimated errors are within the acceptable limit it is significant enough to cause the appeared differences between the particle distribution curves of the three replicate batches. This phenomenon was supported from the particle images in the transmission electron microscope as well. However, the scale bar in the images also indicated that all the particles are below 5 µm in size (*Figure 5.19*). The results from the above findings

suggest that leucine and mannitol did not increase the particle size and morphology. The IBP particle size was within inhalable size range, as evident from the investigations above. Therefore, the optimized method for preparing inhalable size IBP particles by the APC process was validated. It was expected that the prepared IBP powder formulation will disperse successfully in the *in vitro* aerosolization test as the size requirements of the particles were fulfilled.

5.10 CONCLUSION

The Plackett-Burman design indicated ultrasound, stirring speed and the batch size as being the most significant variables for affecting the particle size of IBP produced in the APC process. Optimized level of temperature (25 °C), ultrasound (30 minutes), stirring duration (>20 minutes), IBP concentration, solvent/antisolvent ratio and the additive concentrations were determined to produce the best inhalable size IBP particles. HPMC and Pl F127 agglomerated IBP particles after drying and leucine and mannitol improved the particle flow with no increase in particle size. IBP particles with the D[v,0.5] of 3.7 ± 0.3 µm were prepared by using HPMC and Pl F127 from three replicated batches in the APC process. Finally, a method of producing a mixture of nano size (410 ± 72 nm, PDI 0.66 ± 0.1) and micron size (3.91 ± 0.4 µm) IBP particles using four additives HPMC (0.2%), Pl F127(1.3%), leucine (1.2%) and mannitol (8.6%) was optimized and validated. Therefore, a method of producing inhalable size IBP in APC process was established.

Chapter 6: Ibuprofen dry powder inhaler formulation development, characterization and efficiency evaluation

6.1 INTRODUCTION

This chapter demonstrates the dry powder inhaler (DPI) formulations prepared with different compositions of ibuprofen (IBP), leucine, mannitol, HPMC and Pl F127 and batch size. The formulations were prepared to compare the effect of batch size, IBP concentration, leucine concentration and Pl F127 concentration on the aerodynamic diameter, density, flow property, crystallinity and morphology of the prepared IBP particles. Finally, the efficiency of the DPI formulations was evaluated by testing the drug dispersibility using a Twin Stage Impinger. The dissolution rates of the prepared powders and the milled IBP were investigated to understand their solubility behaviour.

6.2 DPI FORMULATIONS OF THE PREPARED PARTICLES

To evaluate the efficiency of the processed IBP powder in an APC process, 14 DPI formulations were prepared based on different batch size of crystallization, initial IBP concentrations and the additive concentrations. The details of the methodology of preparing particles are given in Chapter 3 Section 3.8. *Table 6.1* represents the composition of all the DPI formulations. It is noted that the percentages of additives mentioned in the table are the percentages that were dissolved in the crystallization medium for the total batch size and are not the additive contents of the crystal product. The drug loading of each formulation was determined from the weighed amount of powder formulation (10-15 mg) dissolved in the suitable solvent system (50% aqueous ethanol).The concentrations of the drug in those formulations were measured using UV spectrophotometry at 264 nm wavelength. The method was described in Chapter 3, Section 3.15.

Table 6.1 Composition of the different formulations and the amount of additives.

Formulation name	Batch size, g	IBP* conc.%	Leucine*,%, (w/w)	Mannitol*,%, (w/w)	HPMC*,%, (w/w)	Pl F127*,%, (w/w)	Drug loading (%)
F1	10	1	1.3	4.5	0.4	1.8	72.7
F2	30	1	0.9	4.5	0.7	1.3	77.9
F3	100	1	0.9	4.5	0.7	1.3	90.3
F4	50	2	1	8.4	0.1	0.9	99.8
F5	50	2	0	0	0.1	0.9	100.0
F6	10	1	0.9	4.5	0.6	1.2	83.3
FPO	50	0.3	0.9	9.0	0.2	0	84.7
F7	10	0.3	0.9	9.0	0.2	1.2	53.2
F8	50	0.3	0.9	9.0	0.2	0.6	74.6
F9	50	0.3	0.9	9.0	0.2	1.8	43.9
FLO	50	0.3	0	9.0	0.2	1.2	83.9
F10	50	0.3	1.2	9.0	0.2	1.2	73.5
F11	50	0.3	1.5	9.0	0.2	1.2	52.7
FMO	50	0.3	0.9	0	0.2	1.2	99.9

*These are the percentages of drug/additives in total amount of crystallization batch size.

Each of the products from these formulations was characterized for density, flowability, particle size distribution, morphology, crystallinity and in vitro drug dispersibility. F1, F2, F3, F6 and F7 formulations had different batch sizes from the 50g. IBP concentration was varied from 0.3% in the formulations F1 to F6. The additive concentrations were 0.9% leucine, 9.0% mannitol, 0.2% HPMC and 1.2% Pluronic F127. These concentrations were varied as well.

The characterizations of the formulations and the milled raw IBP were performed by determining the density and flowability, particle size, morphology and crystallinity. The obtained results were used to investigate the correlation of these properties of the particles on the aerosol and dissolution performance of the prepared DPI formulations.

6.3 CHARACTERIZATION OF THE FORMULATIONS

Density measurements were done from the bulk and tapped density determinations, the flow property was measured by Carr's index, the Hausner ratio and angle of repose. Particle size was measured by dynamic light scattering in Malvern Mastersizer 3000. Particle morphology was investigated in SEM. Crystallinity of the formulations was investigated in DSC and XRD measurements.

6.3.1 **Density, angle of repose & flowability**

Powder bulk density and flowability are important parameters because they are closely related to the drug dispersibility. The estimation of the bulk density and tapped density (resulting in the Carr's index and Hausner ratio) and the angle of repose for estimating flowability are given in *Table 6.2*. The reference values and the scale of flowability of powders were discussed in Chapter 3, Section 3.13. Flowability of all the formulations given in *Table 6.1* was determined and the effect of the additive and drug concentration on it was observed from the obtained results. The purpose of preparing these formulations was to identify those formulations with an inhalable particle size and with a better flow property.

Table 6.2 Powder flow properties obtained from different formulations as [Mean ± SD, n=3]

Formulation	Bulk density (g/ml)	Tapped density (g/ml)	Carr's index (%)	Hausner ratio	Angle of Repose (°)	Flowability
F1	0.28 ± 0.02	0.36 ± 0.03	21.5 ± 0.3	1.27 ± 0.01	44.0 ± 0.1	Passable
F2	0.24 ± 0.03	0.28 ± 0.01	23.7 ± 1.0	1.31 ± 0.02	42.0 ± 1.7	Passable
F3	0.27 ± 0.04	0.35 ± 0.01	11.1 ± 1.0	1.12 ± 0.01	34.2 ± 1.8	Good
F4	0.29 ± 0.01	0.34 ± 0.01	13.2 ± 0.8	1.15 ± 0.01	33.9 ± 1.1	Good
F5	0.27 ± 0.03	0.35 ± 0.01	27.1 ± 0.8	1.37 ± 0.01	50.4 ± 0.2	Poor
F6	0.26 ± 0.01	0.30 ± 0.02	13.9 ± 0.7	1.16 ± 0.01	36.5 ± 1.3	Good
FPO	0.20 ± 0.02	0.29 ± 0.01	30.8 ± 0.7	1.44 ± 0.01	53.3 ± 0.4	Poor
F7	0.18 ± 0.05	0.26 ± 0.02	30.1 ± 0.6	1.43 ± 0.01	53.7 ± 1.1	Poor
F8	0.22 ± 0.03	0.34 ± 0.04	31.1 ± 0.4	1.45 ± 0.01	53.0 ± 0.7	Poor
F9	0.21 ± 0.02	0.32 ± 0.01	37.5 ± 0.7	1.60 ± 0.02	60.3 ± 1.4	Very poor
FLO	0.29 ± 0.001	0.36 ± 0.01	18.3 ± 0.6	1.22 ± 0.01	37.5 ± 0.4	Fair
F10	0.14 ± 0.01	0.16 ± 0.02	13.1 ± 1.0	1.15 ± 0.01	33.9 ± 2.0	Good
F11	0.18 ± 0.05	0.21 ± 0.03	26.9 ± 0.5	1.37 ± 0.01	53.3 ± 1.1	Poor
FMO	0.11± 0.01	0.13 ± 0.02	13.7 ± 0.5	1.16 ± 0.01	34.7 ± 1.9	Good
Milled IBP	0.13 ± 0.03	0.17 ± 0.05	22.7 ±1.0	1.29 ± 0.02	41.8 ± 0.5	Passable

Table 6.2 shows that formulations F3, F4, F6, F10 and FMO had good flow properties, F1, F2 and FLO were passable, and the rest were poor. Of those with good or passable flowabilities, F3, FPO and FMO formulations had a very large particle size (D[4,3] > 10 µm) which is not suitable for inhalation. F4, F5, F6, F7, F8, F9, F10, F11 and FLO formulations were suitable for inhalation as their aerodynamic diameter was smaller than 5 µm. However, the flow property for F5, F7, F8, F9 and F11 was not satisfactory for a DPI formulation. It was expected that the additive concentration might have a significant effect on the flow properties of the prepared IBP particles. The formulation F4 and F5 were prepared to compare the effect of L-leucine and D-mannitol on the flow properties. *Figure 6.1* presents the comparison between the flow properties of formulation F4 and F5, obtained from the Carr's index and angle of repose results. It is seen that the presence of L-leucine and D-mannitol in the formulations had good flow property, whereas without them the flow properties of the formulations were poor.

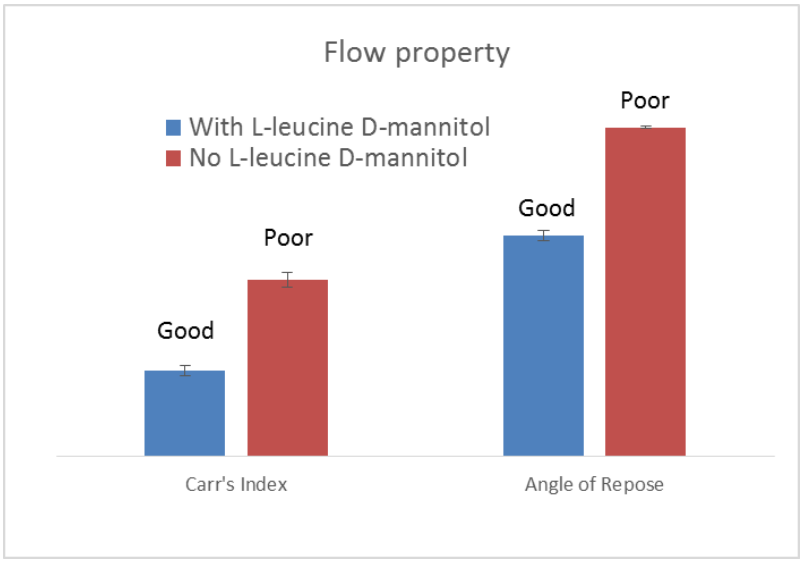

Figure 6.1 Effect of L-leucine and D-mannitol on the flow properties of the formulations. [Mean ± SD, n=3].

L-leucine is a well-accepted dispersive adjuvant for use in DPI formulations and it has been found to improve the powder flowability in several cases [133, 161, 164]. A recent study demonstrated that the enhanced dispersion of L-leucine conjugated chitosan nanoparticles was attributed to the amphiphilic environment of the L-

leucine. The mechanism stated that the hydrophobic domain of L-leucine would be at the surface when the formulation is dispersed in air and the hydrophilic domain would be at the surface in water during the delivery of the drug [163]. Hence, to see the leucine effect on flowability, in this work its concentration was increased gradually from 0%, through 0.9%, 1.2% to 1.5% in FLO, F7, F10 and F11 formulations respectively. However, no specific trend was observed in the flowability according to the values of Carr's index, Hausner ratio and angle of repose (as shown by the angle of repose plot *Figure 6.2*). Individually the F10 formulation shown the maximum flowability (lowest angle of repose) with 1.2% leucine and the lowest flowability were seen in F7 with 0.9% leucine.

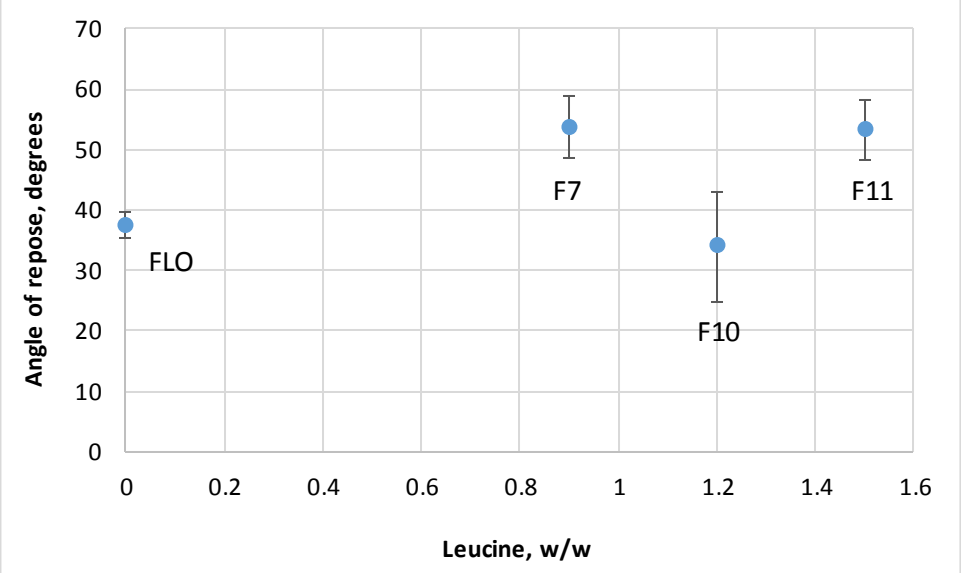

Figure 6.2 Effect of leucine concentration on particle flow. Here crystallization solution contains 0.3% IBP, 9.0% mannitol, 0.2% HPMC; 1.2% Pl F127; 50 g batch (except F7 at 10 g). [Mean ± SD, n=3, data from Table 6.2].

Surprisingly, FLO has no leucine but showed a better flowability than those of the formulations F7 and F11 (1.5% leucine). The literature suggests that, an optimal amount of leucine is critical to achieving the desired aerodynamic properties of the leucine coated particles, as excessive leucine decreases stability with no additional benefits [169]. Interestingly, an increase in the Pl F127 concentration in the formulations FPO, F8, F7 and F9, where concentration of PL F127 was increased from 0% to 0.6%, 1.2% and 1.8%, appeared to influence the flow ability negatively (*Figure 6.3*).

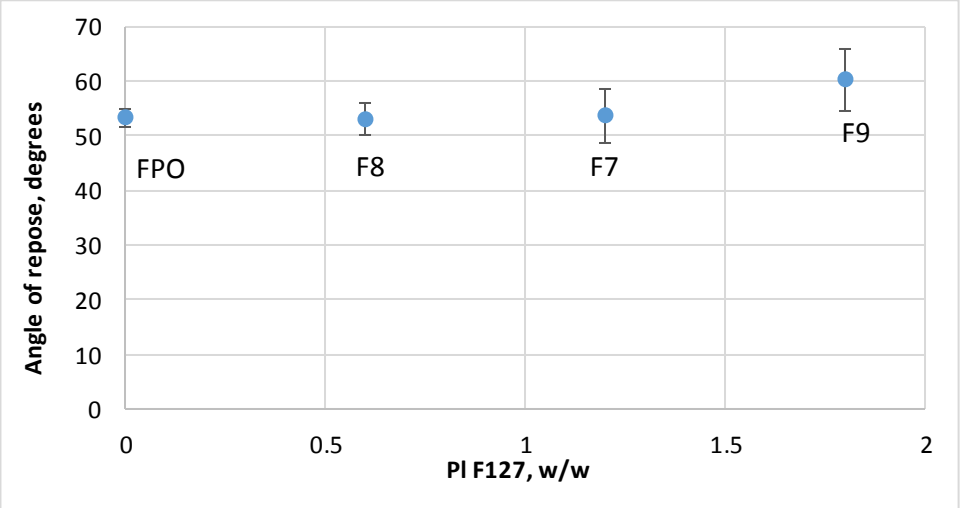

Figure 6.3 Effect of Pl F127 concentration on particle flow. Here, the crystallization solution contains 0.3% IBP; 9.0% mannitol; 0.2% HPMC; 0.9% leucine; 50 g batch (except F7 at 10 g). [Mean ± SD, n=3, data from Table 6.2]

The possible reason would be the decreased particle size with increasing Pl F127 concentration, as the literature suggests that flowability increases significantly with increase in particle size [24]. The literature also shows that the drug particle owns a partial amorphous form due to the presence of Pl F127 [141], which might have influenced the powder flow negatively. This will be discussed in Section 6.3.4. Therefore, based on the flowability results, it was expected that F4, F6 and F10 formulations would be more appropriate candidates for the drug dispersibility tests.

6.3.2 **Particle size & aerodynamic diameter**

The particle size distributions were measured from three replicate samples of each formulation. The volume mean diameter (D[4,3]) was used to determine the aerodynamic diameter (D_{ae}) using the following equation:

$$D_{ae} = D_{eq}\sqrt{\rho_p}\chi$$

where ρ_p is the tapped densities as determined and given in *Table 6.2* and χ is the dynamic shape factor, defined as the ratio of the drag force on the particle to the drag force on the spherical equivalent particle at the same velocity [22, 50, 55-57, 156, 237-240]. The average D_{eq} was the volume mean diameter (D[4,3]) as given *Table 6.3* calculated from at least three replicate runs from the particle size distribution curves. The volume percentage (w/w) of particles < 6 µm (effective cut-off diameter (ECD)=6.4 µm [211]) was directly determined from the frequency and

undersize curves of the respective formulations using Malvern Mastersizer v3.10 software.

Table 6.3 Particle sizes for the various IBP DPI formulations (units µm [Mean ± SD, n=3).

Formulation	D[v,0.1],	D[v,0.5],	D[v,0.9],	D[4,3]	D_{ae}	*<6 µm (%)
F1	2.9 ± 0.1	6.9 ± 0.1	20.4 ± 2.9	9.6 ± 0.8	5.7 ± 0.1	8.2 ± 0.1
F2	3.5 ± 0.1	8.5 ± 0.1	18.0 ± 0.2	9.7 ± 0.1	5.2 ± 0.1	6.9 ± 0.1
F3	4.6 ± 0.1	17.1±0.5	47.9 ± 1.4	22.0 ± 0.4	13.1 ± 0.1	3.5 ± 0.1
F4	3.3 ± 0.6	6.2 ± 0.2	9.3 ± 0.3	6.3 ± 0.2	3.7 ± 0.1	14 ± 0.3
F5	4.2 ± 0.3	7.2 ± 0.5	11.3 ± 1.5	7.5 ± 0.5	4.4 ± 0.1	15.4 ± 0.4
F6	2.9 ± 0.5	5.9 ± 0.8	10.7 ± 1.6	6.5 ± 1.1	3.6 ± 0.1	9.6 ± 0.1
FPO	6.1 ± 0.1	11 ± 0.6	18.7 ± 1.3	12.34 ± 1.2	6.7 ± 0.1	6.1 ± 0.1
F7	1.1 ± 0.1	3.9 ± 0.4	9.0 ± 0.9	5.1 ± 0.9	2.6 ± 0.1	4.8 ± 0.1
F8	3.7 ± 0.1	6.8 ± 0.1	11.9 ± 0.1	7.4 ± 0.1	4.3 ± 0.1	10.5 ± 0.1
F9	1.3 ± 0.1	6.1 ± 0.1	12.8 ± 0.3	6.7 ± 0.1	3.8 ± 0.1	7.8 ± 0.2
FLO	3.2 ± 0.1	6.1 ± 0.1	10.1 ± 0.3	6.6 ± 0.6	4.0 ± 0.1	12.6 ± 0.4
F10	1.4 ± 0.2	6.4 ± 0.3	12.9 ± 0.5	7.1 ± 0.2	2.9 ± 0.1	8.1 ± 0.1
F11	1.2 ± 0.0	5.4 ± 0.6	11.8 ± 0.7	6.4 ± 0.4	2.9 ± 0.1	7.8 ± 0.2
FMO	3.7 ± 0.1	8.7 ± 0.1	28.2 ± 1.2	20.9 ± 1.3	7.4 ± 0.2	26.1 ± 1.2
Milled IBP	1.2 ± 0.1	2.8 ± 0.1	4.45 ± 0.2	2.8 ± 0.1	1.2 ± 0.1	99.7 ± 0.5

* Effective cut-off diameter (ECD), 6.4 µm [211]

The effect of batch size was noticeable (*Figure 6.4*) in the F6 (10g), F2 (30 g) and F3 (100g) formulations. It shows an increase of D[4,3] from 6.52 ± 1.07 µm (F6), 9.73 ± 0.11 µm (F2) and 22.0 ± 0.41 (F3) µm of the particles prepared in 10, 30 g and 100 g batch sizes respectively. It means increased particle size was observed with increased batch size. Figure 6.4 limits only three points because we were not interested to proceed with the experiments where particle size was more than 6.4 µm.

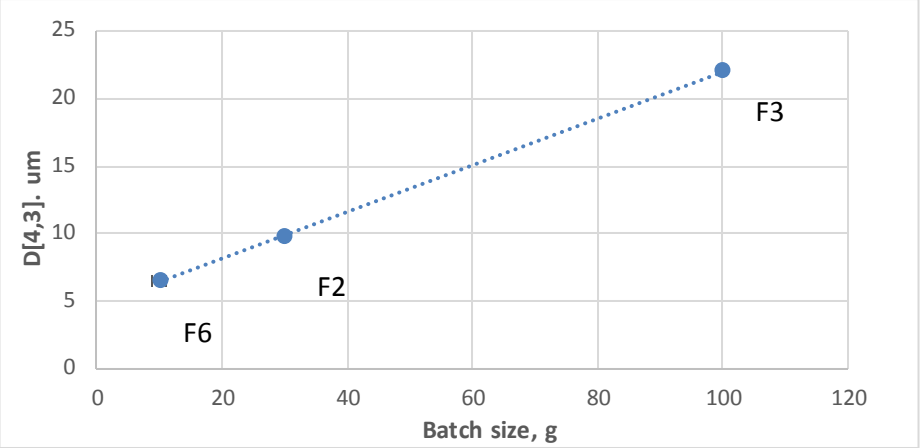

Figure 6.4 Effect of batch size on particle size produced in APC process. Crystallizaton solution contains 1.0% IBP; 4.5% mannitol; 0.7% HPMC; 1.3% Pl F127;0.9% leucine. [Mean ± SD, n=3, data from Table 6.3]

This effect of batch size on particle size was also identified in the Plackett-Burman investigation (demonstrated in Chapter 5 Section 5.2). Usually the batch size makes no difference and is fundamental in scaling up to industrial scale. It may be the mechanics of addition of the alcohol solution which does not scale [99, 241].

The concentration of leucine and Pl F127 did not show any specific trend on the particle size of the formulations. *Figure 6.5* shows the plot of particle aerodynamic diameter of the formulations with increasing concentration of Pl F127.

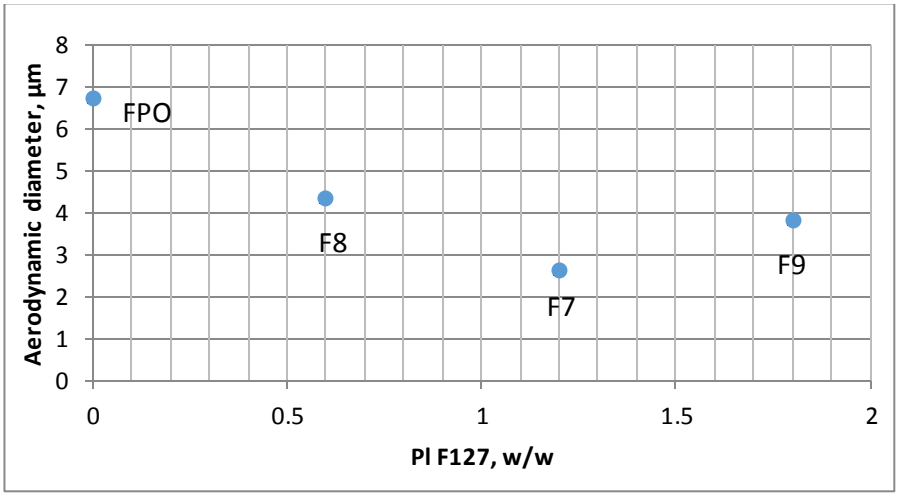

Figure 6.5 Effect of Pl F127 concentration on particle aerodynamic diameter. Here, the crystallization solution contains 0.3% IBP; 9.0% mannitol; 0.2% HPMC; 0.9% leucine; 50 g batch (except F7 at 10 g). [Mean ± SD, n=3, data from Table 6.3]

The aerodynamic diameter of the particles decreased linearly until 1.2% Pl F127 (F7) concentration in the formulations. But for an unknown reason, the aerodynamic diameter increased in the formulation F9, having 1.8% of Pl F127 concentration. It was seen (see Section 5.5) that mannitol and PL F127 aids in reducing particle size. FPO and FMO are the formulations without Pl F127 and D-mannitol respectively, and particles grew larger in these formulations due to their absence. It has been explained in Chapter 2, Section 2.14.3, that mannitol prevents nanoparticle aggregation during the drying process. The hypothesis of nanoparticle stabilization during the freeze drying step proposes that sugars isolate individual particles in the unfrozen fraction, thereby preventing aggregation during freezing above glass transition temperature, Tg. In this case, the transition of the substance into a glass is not required for this effect and the spatial separation of particles within the unfrozen fraction is sufficient to prevent aggregation [153]. As a result, the particle size remains stable with no further growth due to aggregation after the drying step. Therefore, bearing in mind the limit of an aerodynamic diameter of 1-5 μm for successful lung delivery [16-18, 49, 50], the formulations F4, F5, F6, F7, F8, F9, F10, F11 and FLO were chosen to be tested for the aerosol performance.

6.3.3 **Particle Morphology**

The particle morphology of the formulations was investigated by scanning with the electron microscope (SEM). *Figure 6.6* represents the SEM images of raw IBP, milled raw IBP and all the formulations. The dried powder formulation was sprinkled on an aluminium metal stub and gold coated, following the method described in Section 3.11.1.

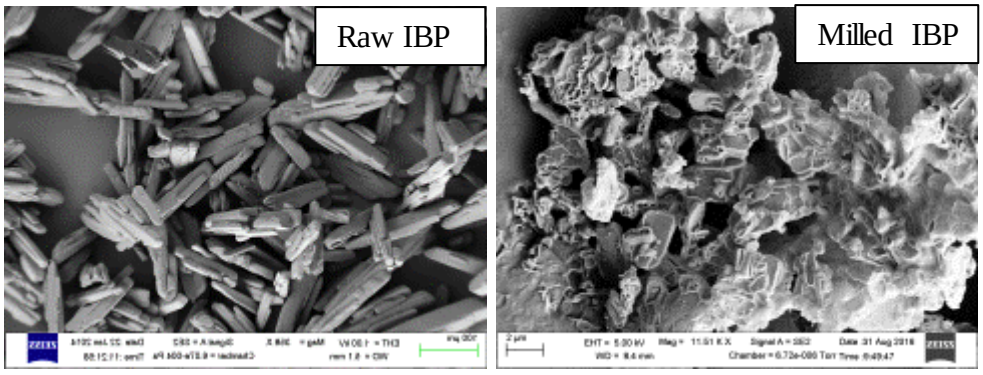

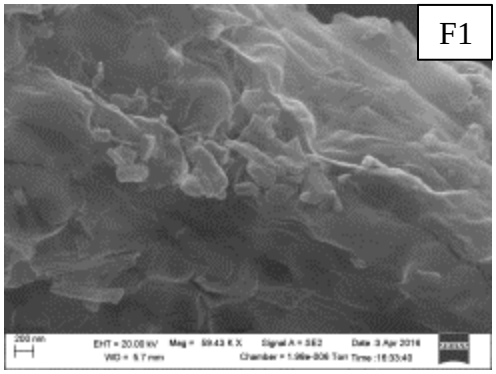
F1

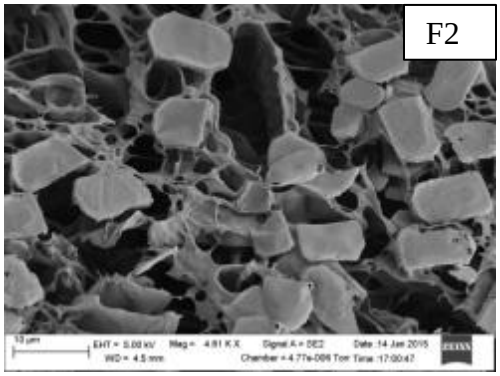
F2

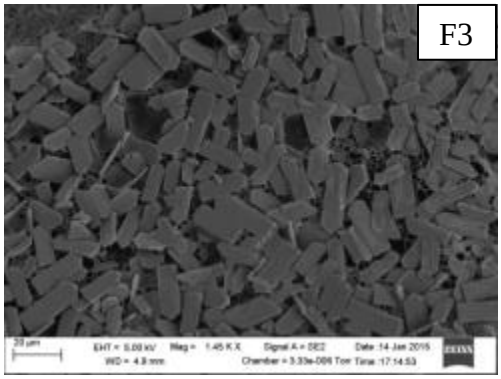
F3

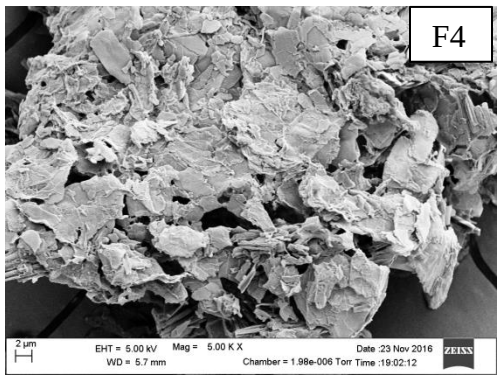
F4
2 µm
EHT = 5.00 kV
Mag = 5.00 K X
Date :23 Nov 2016
WD = 5.7 mm
Chamber = 1.98e-006 Torr Time :19:02:12
ZEISS

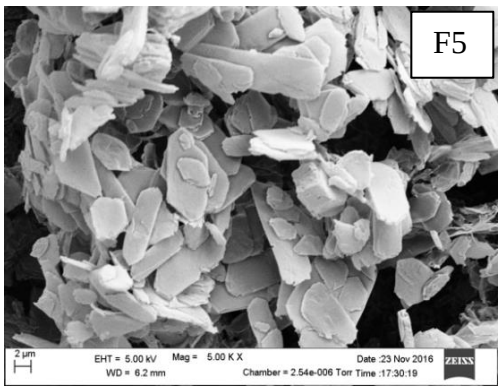
F5
2 µm
EHT = 5.00 kV
Mag = 5.00 K X
Date :23 Nov 2016
WD = 6.2 mm
Chamber = 2.54e-006 Torr Time :17:30:19
ZEISS

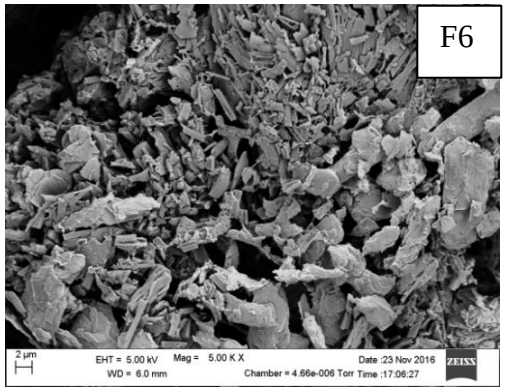
F6
2 µm
EHT = 5.00 kV
Mag = 5.00 K X
Date :23 Nov 2016
WD = 6.0 mm
Chamber = 4.66e-006 Torr Time :17:06:27
ZEISS

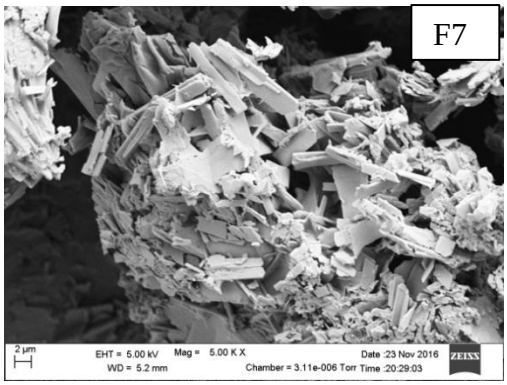
F7
2 µm
EHT = 5.00 kV
Mag = 5.00 K X
Date :23 Nov 2016
WD = 5.2 mm
Chamber = 3.11e-006 Torr Time :20:29:03
ZEISS

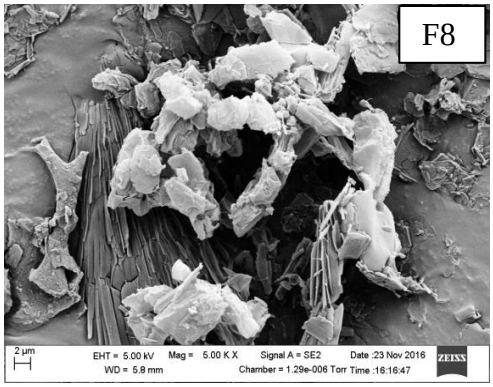
F8
2 µm
EHT = 5.00 kV
Mag = 5.00 K X
Signal A = SE2
Date :23 Nov 2016
WD = 5.8 mm
Chamber = 1.29e-006 Torr Time :16:16:47
ZEISS

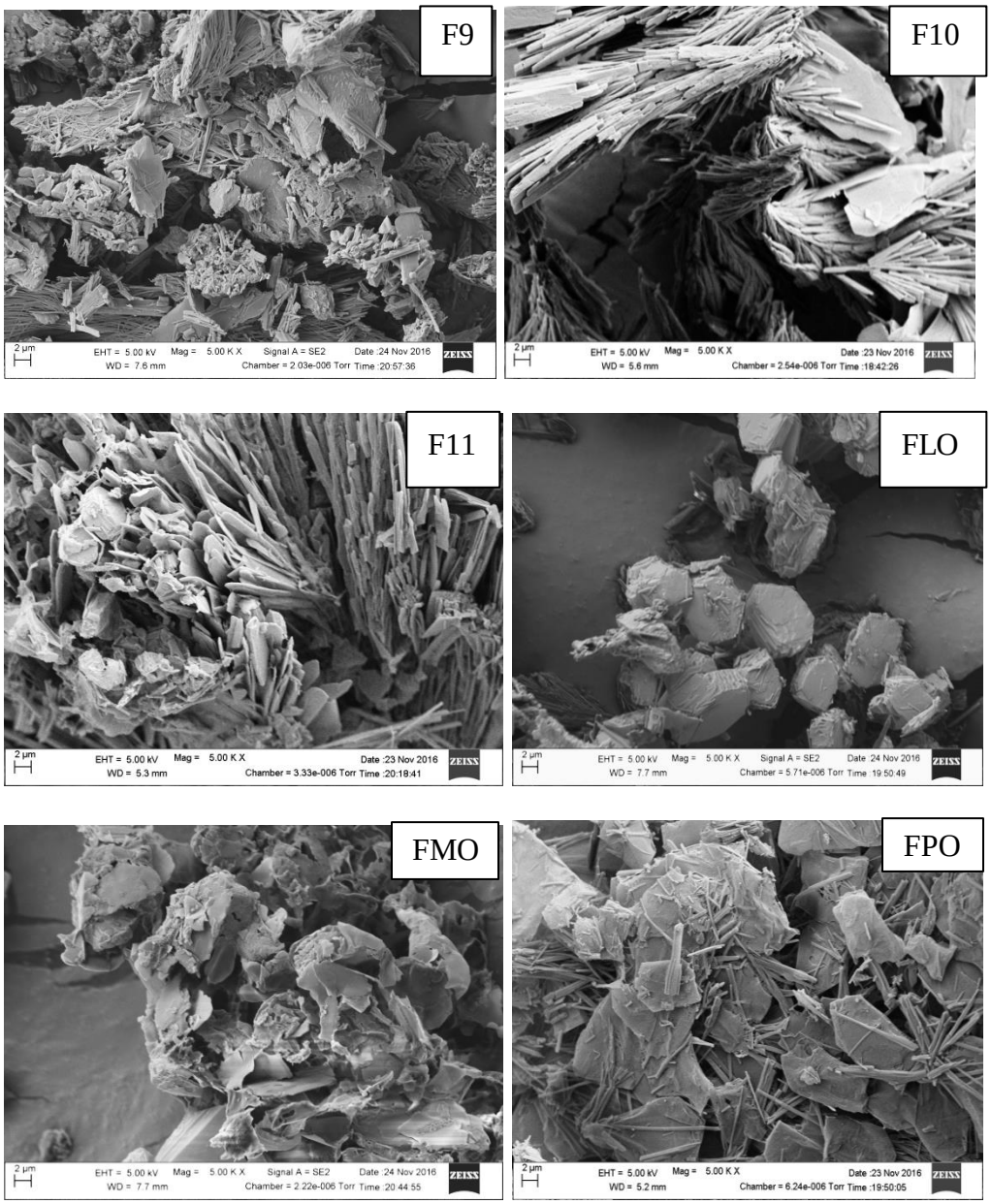

Figure 6.6 Particle morphology of the raw and milled IBP and formulations F1, F2, F3, F4, F5, F6, F7, F8, F9, F10, F11, FLO, FMO and FPO in scanning electron microscopy (Magnification: 5.00 K X).

The crystal habit of IBP depends on the crystallization conditions such as the solvent type and presence of additives [133, 207, 242]. *Figure 6.6* shows that the commercial raw IBP is needle-shaped, whereas the formulation particles crystallized in presence of additives are platelike (*Figure 6.6* : F2 & F3), chunky (FMO) or irregular shapes (milled IBP, F1, F4, F5,F6, F7, F8, F9, F10, F11, FPO and FLO). The different crystal habits and shapes could be the function of the different IBP concentration and the additive composition and concentration. The formulations with platelike crystal

shape were mostly with high IBP concentrations, which was 1% for F2 & F3 formulations. Leucine and Pl F127 concentrations during the crystallization process of F1 particles were higher than for the others which may have had more additives on the surface of IBP particles causing shape irregularity and roughness. In the case of formulation F5, the crystallization was carried out in the absence of leucine and mannitol, which resulted in different morphology, with the crystals having rough surfaces comprising flat-shaped IBP particles sticking together to make bigger particles. As the SEM images here represent the dried form of formulation, it is very likely the particles in F5 formulation aggregated and agglomerated into large irregular shapes due to drying without the presence of leucine and mannitol. The morphology of the formulations F6, F7, F9, F10, F11, FPO and FLO with low IBP concentration (0.3%) seems to be the loose agglomerate of IBP particles adhering to each other. As the drug concentration was comparatively low during crystallization in the presence of all additives, there was no distinguishable difference. The particle size also appears to be changed in the formulations with low IBP and high additive concentrations. However, in the case of FMO, the IBP particles are seen clearly in the tight agglomerated form of chunky shaped crystals. This indicates that mannitol influences the particles to be agglomerated either tightly or loosely after drying. The needle shaped crystal habit of the particles with no Pl F127 formulation (FPO) indicated that Pl F127 does influence the crystal habit of the treated IBP particles. However, the IBP particle morphology was significantly influenced by both the additive composition and concentration. Hence, the best additive concentration and composition would possibly be identified from the aerosol performance of the respective formulations.

6.3.4 **Crystallinity**

Particles of the same organic compound that have different shapes could have different polymorphic forms [133]. Therefore, crystallinity of the raw IBP powder, milled IBP powder, additives and the DPI formulations was examined using differential scanning calorimetry (DSC) and X-ray diffraction (XRD). *Table 6.4* shows the melting peak temperature, enthalpy and the percentage of crystalline material present in the formulations obtained from DSC runs. The percentage of crystallinity is then determined using the following equation [210]:

$$\% \text{ Crystallinity} = \Delta Hm / \Delta Hm^{\circ} \times 100\%$$

The heat of melting, ΔHm, was determined by integrating the areas (J/g) under the peaks using TA instrument Analysis 2000 software. The term ΔHm° is a reference value and represents the heat of melting of 100% crystalline IBP. It was found that the melting enthalpy of the raw IBP powder was 118.4 ± 7.3 J/g which is also in agreement with Nokhodchi and co-workers [194]. This value was used as the reference value to determine the percentage crystalline phase of IBP in the processed formulations with different compositions of additive.

Table 6.4 DSC data obtained for various formulations [mean ± SD, n=3]

Formulation	**Peak (°C)**	**Enthalpy (jg^{-1})**	***Crystalline IBP (%)**
*Pure IBP	77.1 ± 0.5	118.4 ± 7.3	100
Milled IBP	74.2 ± 0.7	111.8 ± 0.9	94.7 ± 0.9
F1	74.6 ± 0.3	40.02 ± 6.8	33.8 ± 5.7
F2	76 ± 1.4	75.4 ± 6.5	63.7 ± 5.5
F3	77.1 ± 0.1	84.8 ± 3.3	71.6 ± 2.8
F4	76.3 ± 0.4	117.4 ± 2.0	99.1 ± 1.7
F5	76.5 ± 0.8	113.3 ± 4.7	95.7 ± 4.0
F6	76.0 ± 0.5	61.2 ± 5.2	51.7 ± 4.4
FPO	77.1 ± 0.9	63.7 ± 4.6	53.7 ± 3.9
F7	75.0 ± 0.4	30.6 ± 2.8	25.8 ± 2.4
F8	76.3 ± 1.3	75.6 ± 4.1	63.7 ± 3.4
F9	74.6 ± 0.3	13.0 ± 1.1	11.0 ± 1.0
FLO	75.4 ± 1.2	65.1 ± 2.4	55.0 ± 2.1
F10	75.6 ± 0.4	47.4 ± 1.5	40.0 ± 1.3
F11	75.3 ± 0.3	34.5 ±1.4	29.1 ± 1.2
FMO	78.0 ± 3.8	83.2 ± 7.4	70.3 ± 6.2
HPMC	55.5 ± 0.8	243.8 ± 1.2	0
Pl F127	77.5 ± 0.4	134.1 ± 2.3	0
Mannitol	165.9 ± 0.5	303.3 ± 1.4	0
Leucine	>300	Not determined	0

DSC can be used to determine the polymorphic composition of pharmaceutical powders, if two or more polymorphs are present and if the transition temperatures are known. As can be seen in *Table 6.4*, in all the formulations (including the milled IBP) an endothermic peak commenced in the range of 74–78 °C. These transition temperature results are in agreement (within ± 2.0 °C) with the previous reports which suggest that IBP exists as a stable crystalline solid exhibiting a typical melting range of 75–77 °C [242]. *Figure 6.7* (a) shows the melting point for pure IBP,

HPMC, Pl F127, mannitol and leucine. *Figure 6.7* (b) shows the DSC curves for raw and milled IBP and all the prepared formulations.

(a)

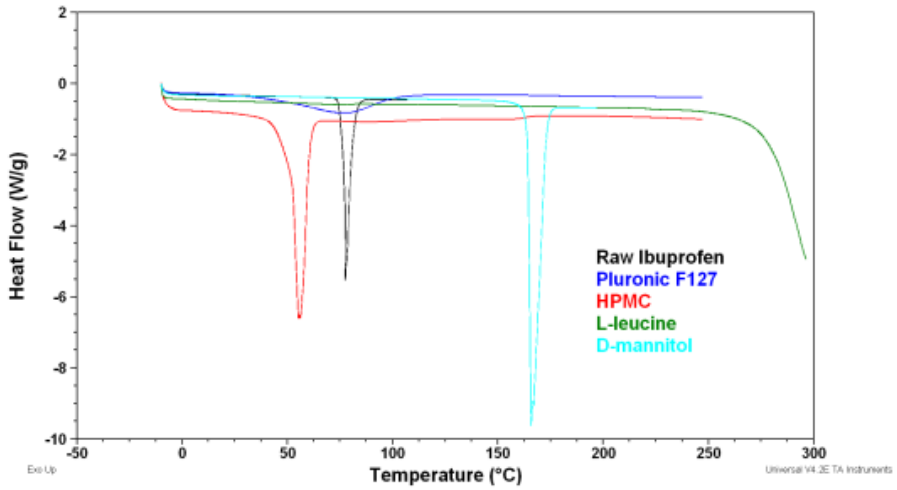

(b)

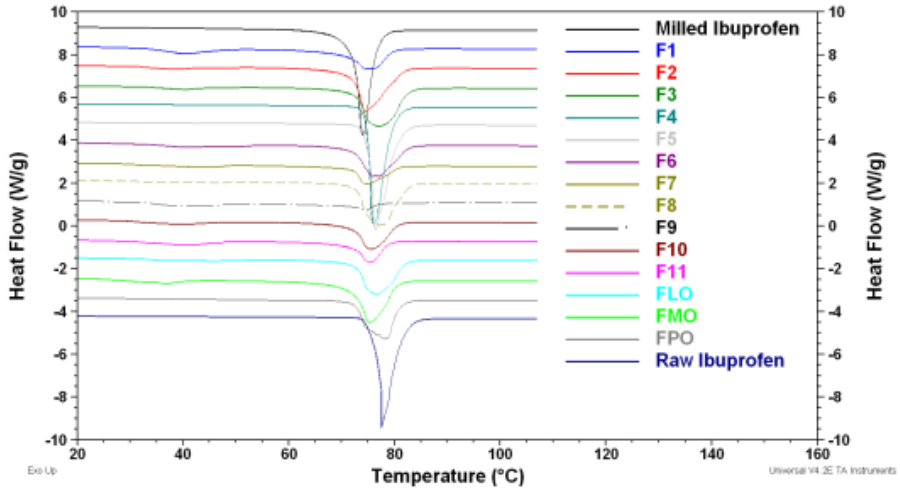

Figure 6.7 DSC curves for (a) Pluronic F127, HPMC, L-leucine, D-mannitol, raw IBP; (b) milled IBP, F1, F2, F3, F4, F5. F6, F7, F8, F9, F10, F11, FPO, FLO, FMO and raw IBP.

In *Figure 6.7* (a) only HPMC had shown a sharp peak before the melting point of the pure IBP drug. Pl F127 also shows a small peak at a similar melting range to pure IBP. The melting point for mannitol was much higher than for pure IBP. The leucine melting point could not be detected as it was out of the range of the instrument calibration (>300 °C). The additive melting peaks confirmed that the presence of

mannitol and leucine would not interfere with the pure IBP melting peak identification in DSC, but HPMC and Pl F127 could. *Figure 6.7* (b) shows the endothermic peaks for all the formulations, within the melting point range for crystalline IBP. The height of the peak was changed with respect to the IBP content present in the formulation. The low IBP concentration formulations have shown a smaller peak than the formulations containing high IBP concentration. For certain formulations with a low concentration of IBP and high HPMC, the melting peak for HPMC also appeared at 55 °C. The peak for Pl F127 might have overlapped with IBP, as both have a similar melting point (*Table 6.4*). However, to ensure IBP does not exist in other polymorphs, all the formulations and additives were examined by XRD. *Figure 6.8* presents the XRD patterns of pure IBP and all the additives. *Figure* 6.9 presents the XRD patterns for all the formulations compared with the raw IBP and milled IBP powder.

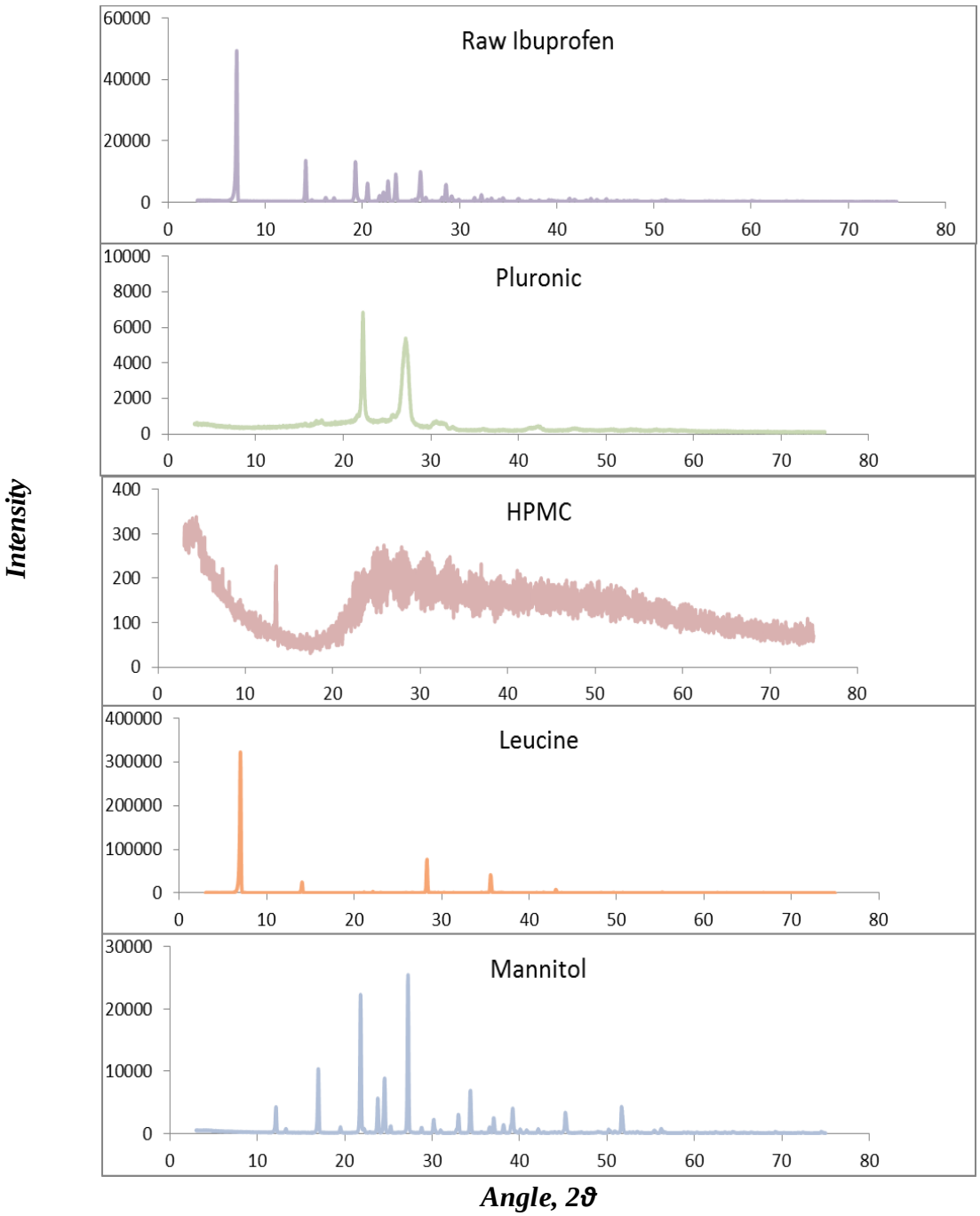

Figure 6.8. XRD patterns of raw IBP, pluronic F127, HPMC, leucine and mannitol.

The XRD patterns of the raw additives (*Figure 6.8*) shows that HPMC is an amorphous compound showing one small intensity peak at around 13° two theta angles, and Pl F127 shows two peaks though it was partly in an amorphous phase. Leucine and mannitol show complete crystalline phases with sharp peaks on several angles. The XRD patterns of the independent additives will help to identify the peaks which are not due to the IBP crystalline phase in the formulations.

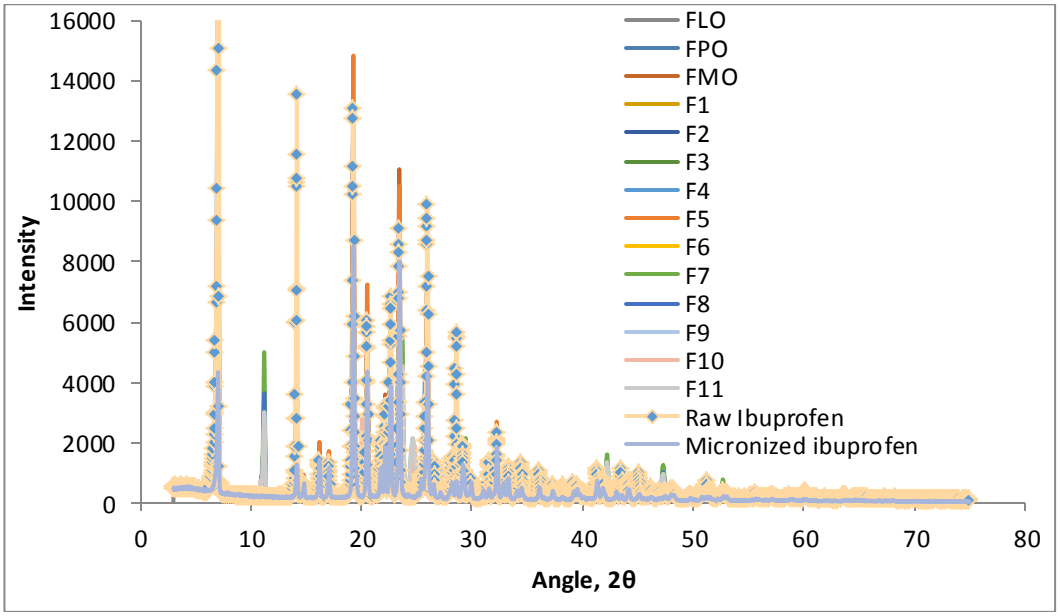

Figure 6.9 XRD of raw IBP, milled IBP and DPI formulations of crystallized IBP.

Figure 6.9 presents XRD patterns for all the formulation compared with the XRD pattern of pure IBP. It can be seen that all the formulations show peaks in the similar angle point as to the pure IBP. The concern about the polymorphic change in the milled IBP due to the high energy milling process could be addressed from the DSC and XRD analysis results. As can be seen in *Table 6.4*, for the milled IBP powder, endothermic peak commenced at 74.2 ± 0.7 °C and for the raw IBP it was at 77.1 ± 0.5 °C. These transition temperature results are in agreement (within ± 2.0 °C) with the previous reports which suggest that IBP exists as a stable crystalline solid with no polymorphic change exhibiting a typical melting range of 75–77 °C [242]. *Figure 6.10* shows the comparison between the XRD patterns of raw and milled IBP. The micronized IBP had shown peaks at the same angle points to that of the raw IBP. This investigation confirmed that micronized particles did not produce polymorphs due to the high energy milling process.

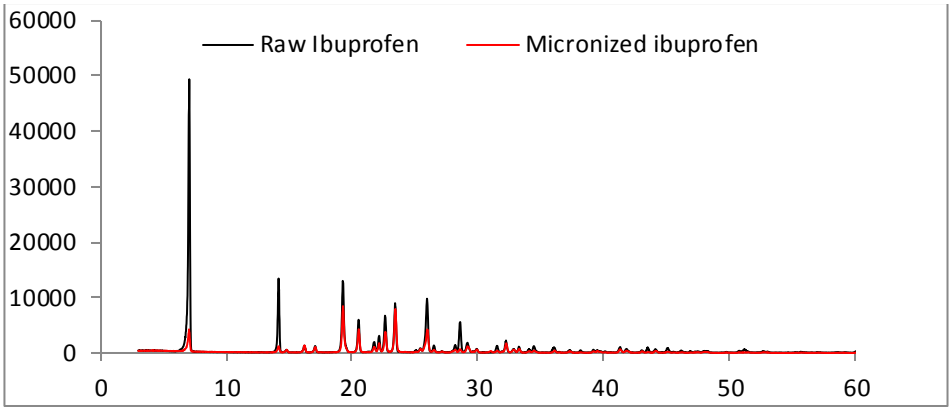

Figure 6.10 XRD patterns for raw and milled IBP showing no polymorphic change due to the milling process.

The peaks other than the IBP points were due to the presence of mannitol which can be confirmed by looking at the XRD pattern of the FMO formulation (*Figure 6.13*). *Figure 6.11* presents the XRD patterns of formulations FLO, F7 and F11 where L-leucine concentration is increased from 0- 1.5%. The XRD pattern of F11 shows that higher concentration of L-leucine produces a higher amorphous phase. *Figure 6.12* presents the XRD patterns of formulations with increasing concentration of Pl F127. The smallest peak intensity was seen for the formulation F9 with the highest Pl F127 concentration. The possible reason could be due to the small particle size or the presence of an amorphous phase as a function of Pl F127 [92, 101, 194, 240].

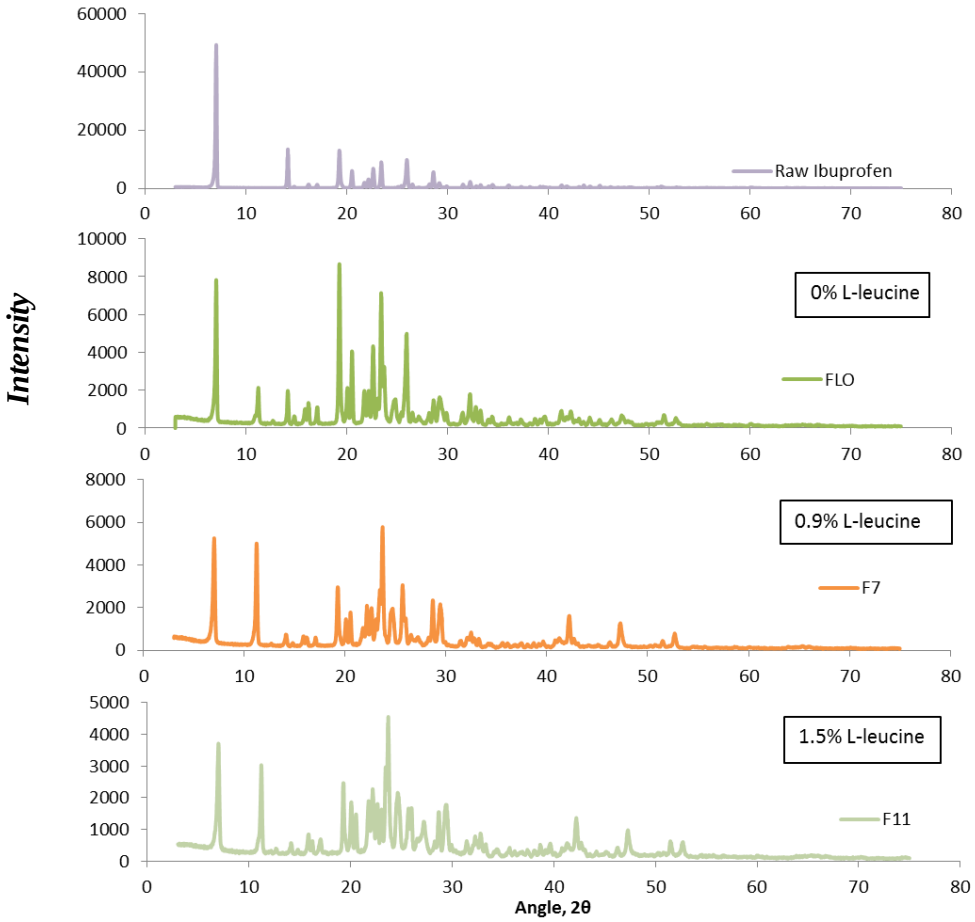

Angle, 2ϑ

Figure 6.11 XRD patterns of formulations with increasing concentration of L-leucine; and raw IBP.

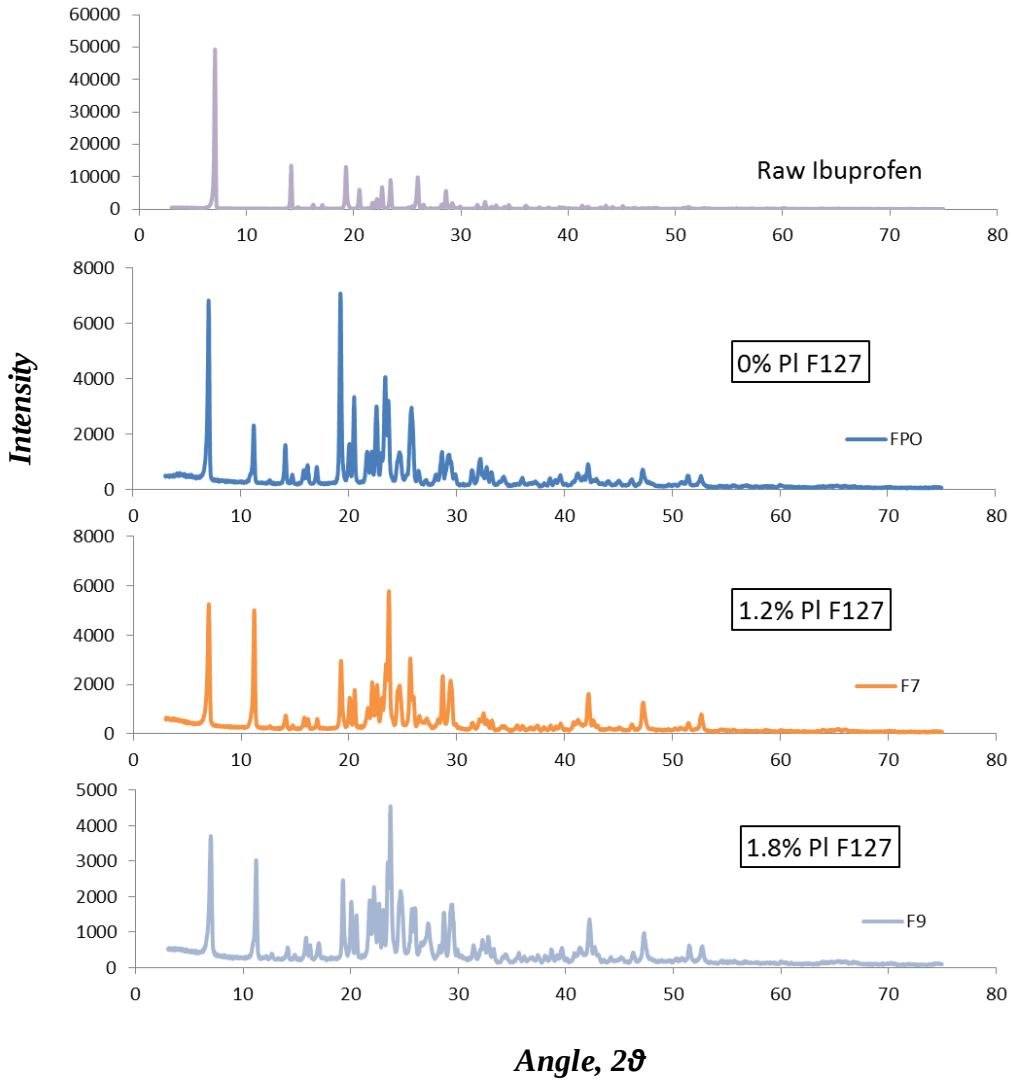

Figure 6.12 XRD patterns of formulations with increasing concentration of Pl F127 and raw IBP.

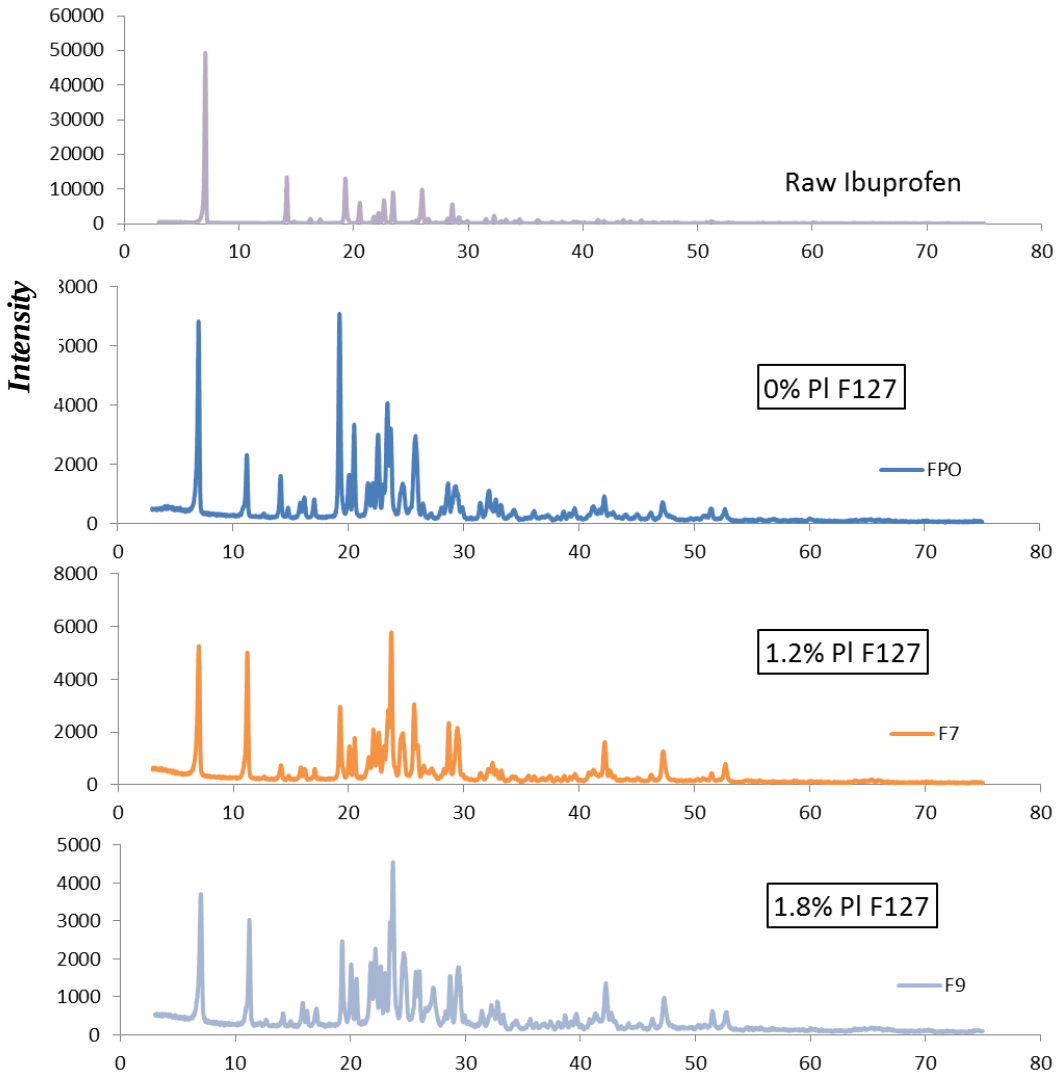

Figure 6.13 XRD patterns of raw IBP, mannitol, formulation with mannitol (F7) and formulation without mannitol (FMO). Mannitol was encountered with a signature peak at angle 52° 2θ (shown in red circle), which was absent for the formulation FMO but present in the formulation F7.

FMO does not contain mannitol in its formulation composition and did not show any peaks on the points raw mannitol has shown in *Figure 6.13*. This indicates that mannitol was present in the final formulations in crystalline form. *Table 6.5* shows that mannitol exists in two polymorphic forms (alpha and delta). It is to be noted that although mannitol crystallizes in different polymorphic forms (α, β or δ) depending on the concentration (relative to other component in the formulation) and freezing rate, no evidence of any effect of these mannitol polymorphs on the

drying/processing characteristics or product stability has been reported so far [145, 155]. However, XRD profiles for all the formulations of treated IBP were similar to the untreated raw IBP powder (shown with diamond markers in *Figure 6.9*) at the same angles, demonstrating that the crystal structure of treated IBP had not changed. The DSC curves of all the treated IBP formulations also demonstrated sharp peaks in the melting point range of raw IBP particles. Therefore, it could be confirmed that IBP remain isomorphic in the formulations after being treated in the APC process, but the amorphous content of the drug increased due to the presence of the additives. The interaction between the IBP particles and the additives in the APC process caused no change in the crystal structure of the IBP drug. Moreover, the XRD patterns of milled IBP were similar with the raw IBP powder indicating that no polymorphic change caused by the milling process.

The amount of Pl F127 in some samples was estimated by the degree of crystallinity method, where the numerical area of each phase is used to determine abundances. The Pl F127 was accounted for by modelling a peak at about 27 °2θ (most obvious feature not modelled) and designating it as the amorphous phase. HPMC phase abundance could not be quantified, as its concentration in the formulation was too low to identify in the XRD curves. *Table 6.5* presents the data calculated from the XRD curves of the dry powder formulations. The results could be used to get an approximate percentage of the IBP and the additive concentration in the crystalline phase in the dry powder formulations.

Table 6.5 IBP and the additive phase abundance from area and weight percentages from XRD curves of the DPI formulations.

Sample	Phase abundance from area %					Phase abundance from weight %			
	IBP	Pl F127	delta-D-Mannitol	alpha-D-Mannitol	L-Leucine	IBP	delta-D-Mannitol	alpha-D-Mannitol	L-Leucine
F9	29.1	4.0	36.2	19.6	11.2	30.8	39.7	21.5	8.0
F11	29.1	4.0	36.2	19.6	11.2	48.6	20.1	21.1	10.3
F7	37.0	1.9	40.5	11.6	9.0	37.9	44.4	11.5	6.2
F10	46.6	1.7	18.5	18.9	14.3	56.8	32.9	4.5	5.8
FLO	68.7	1.0	13.7	16.6		69.3	14.1	16.6	-
F6	73.0	1.6	19.4	-	6.0	74.8	21.1	-	4.1
FMO	94.8	1.3	-	-	3.9	97.7	-	-	2.3

Figure 6.14 presents the comparison of the IBP content percentage from XRD and DSC data. It shows that F9 and F11 contain the lowest IBP content due to the presence of a high percentage of Pl F127 and L-leucine during the particle preparation. Pl F127 and L-leucine increase the dissolution of IBP linearly (demonstrated in Chapter 4, Sections 4.4.1 & 4.4.3) causing loss of IBP particles with the discarded solution after crystallization, during the isolation of the particles by centrifugation. The maximum IBP content in FMO also shows that absence of mannitol has a significant effect on the IBP drug content percentage in the final formulation.

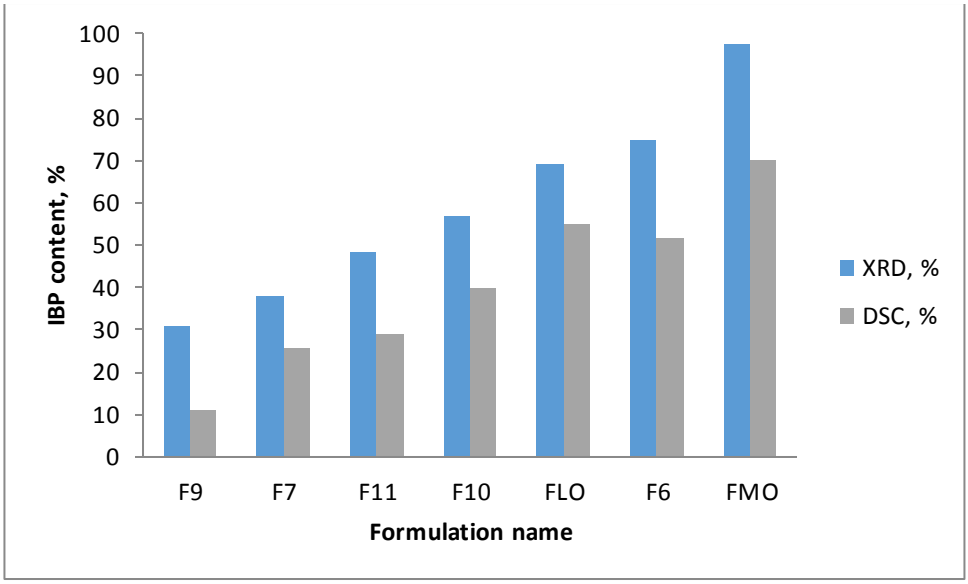

Figure 6.14 IBP crystalline content percentage comparison between the formulations obtained from the XRD and DSC data.

Interestingly, the DSC data for IBP content percentage was lower but in a reasonable parallel trend with the results obtained from XRD data. This relationship indicates that the calculated results might be useful to estimate relative drug percentages in the crystalline phase of the dry formulations.

6.4 AEROSOL PERFORMANCE IN TWIN STAGE IMPINGER (TSI)

The aerosol performances of the formulations of the milled and prepared IBP particles were investigated using the TSI (details in Chapter 3, Section 3.16). The raw IBP powder (D [v,0.5] = 41 µm) was milled using a micronizer which reduced

the mean particle size to 2.8 ± 0.1 µm (details of procedure in Chapter 3, Section 3.10) which was used as control, to compare the dispersibility behaviour with the prepared formulations. *Table 6.6* shows the TSI results of all the formulations tested. The amount of IBP per capsule that is deposited in the lower stage of the TSI after aerosolization at 60 l/min (effective cut-off diameter (ECD), 6.4 µm [211]) was considered to be the fine particle dose (FPD). The recovered dose (RD) was defined as the total quantity of drug recovered per capsule after each actuation, while the emitted dose (ED) was that emitted from the inhaler device into the TSI (by loss of weight of inhaler). The percentage emission was calculated as the percentage of emitted dose to total recovered dose. Fine particle fraction (FPF) was the ratio of FPD to RD, while dispersibility was the percentage of FPD to ED [146].

Table 6.6 Deposition of IBP in a TSI after aerosolization from dry powder formulations containing additives via a Rotahaler® at 60 ± 5 l/min [Mean ± SD, n=5]

Formulation	RD (%)	ED (%)	Dispersibility (%)	FPF (%)	FPD (µg)
Milled IBP	89.0 ± 3.9	73.8 ± 1.2	16.0 ± 1.2	11.8 ± 0.9	3424.8 ± 346.6
F4	80.1 ± 3.2	51.1 ± 1.3	4.2 ± 0.4	2.1 ± 0.2	553.8 ± 42.3
F5	76.3± 1.6	39.3 ± 0.4	4.0 ± 0.1	1.6 ± 0.04	387.3 ± 6.3
F6	64.2± 2.3	69.4 ± 2.4	4.0 ± 0.4	2.8 ± 0.1	574.0 ± 15.4
F7	65.3± 1.7	50.4 ± 1.5	2.5 ± 0.2	1.6 ± 0.1	332.3 ± 16.0
F8	69.3± 3.0	58.5 ± 0.1	2.1 ± 2.0	1.2 ± 0.1	272.1 ± 11.8
F9	33.6± 1.1	68.6 ± 2.7	0.5 ± 0.1	0.4 ± 0.1	38.7 ± 10.3
FLO	60.7± 1.8	67.7 ± 1.4	2.1 ± 0.1	1.4 ± 0.1	283.4 ± 11.2
F10	55.9± 2.8	67.1 ± 2.9	3.4 ± 0.1	2.3 ± 0.1	413.8 ± 9.8
F11	44.2± 2.7	62.9 ± 2.5	1.6 ± 0.2	1.0 ± 0.1	140.2 ± 8.1

Formulations F4 and F5 were prepared to investigate the contribution of leucine and mannitol to the overall physicochemical properties of the formulation. Formulation F5 was prepared without leucine and mannitol and characterized for its aerosolization efficiency. The flowability of F4 (good) was better than F5 (poor) (*Figure 6.2*); the aerodynamic diameter of the F4 particles was smaller than that of F5, and the percentage of crystalline IBP in F4 was higher than the F5 formulation. All these results indicated that presence of leucine and mannitol in the F4

formulation lowered the aerodynamic diameter of the particle and improved the flow properties, resulting in better FPF. The aerosolization test results of F4 and F5 show 2.1% and 1.6% FPF respectively, indicating increase of drug dispersibility due to the presence of leucine and mannitol in F4. A study by Feng et. al. revealed that the crystallinity of leucine in the microparticles relates to a change in particle morphology which decreases powder density and enhances the dispersibility [165]. L-leucine possess the ability to form hollow particles, and a change in particle morphology from solid spheres to hollow, rugose particles leads to the formation of low density particles and enhanced dispersibility of the DPI formulations [159, 166-168]. The hollow particles were observed from SEM images of the formulations (F4, F6, F9, F10, F11) shown in *Figure 6.6*. On the other hand, the particles in the the SEM image of formulation F5 (no L-leucine) did not show the hollow feature in their appearance. *Figure 6.15* plots the FPF % of the formulations F4 and F5 against their aerodynamic diameter, which clearly supports the above statements. However, to determine the significance of the results, errors were estimated as the 95% uncertainties on the mean values of the FPF% of F4 and F5. Using the t-test the 95% uncertainties of F4 was 13.1 % and F5 was 3.9% which indicated the significance of the increase in FPF% of F4 is negligible.

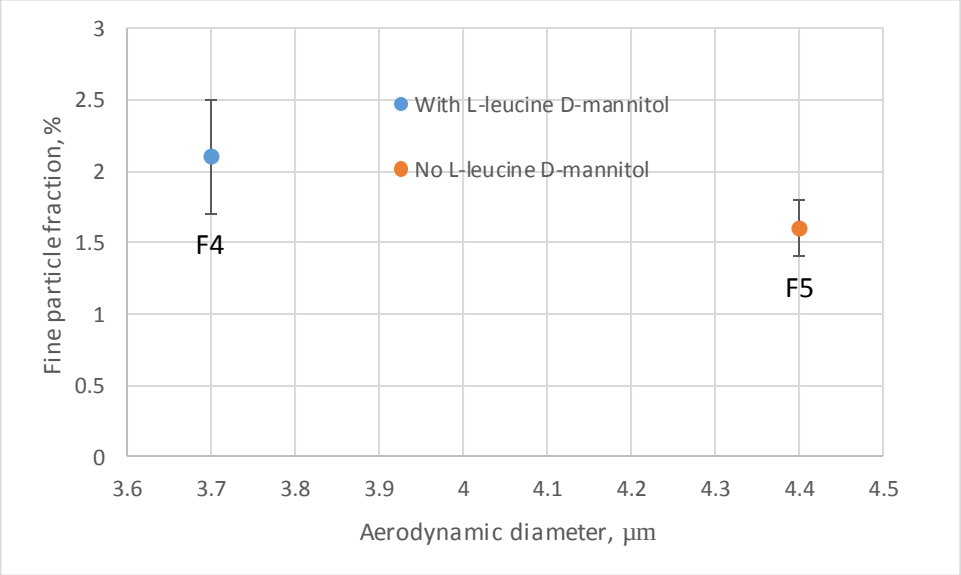

Figure 6.15 Aerodynamic diameter vs fine particle fraction (FPF) comparison between formulations with (F4) and without (F5) L-leucine and D-mannitol. [Mean ± SD, n=5, data from Table 6.6]

Maximum drug dispersibility was achieved from the F6 formulation, which is 2.8%. The particles of F6 formulation achieved a good flow property with an aerodynamic diameter of 3.6 ± 0.05 µm. However, the percentage of IBP crystalline of F6 was lower than for F4 and F5. A possible explanation would be the higher drug and lower Pl F127 concentration used in F4 and F5 compared to F6. As was seen earlier, Pl F127 influences the production of more amorphous particles in the APC process. Hence, a better controlled aerodynamic diameter and flowability of the F6 formulation increased the percentage of FPF. The FPF percentage of the formulations was increased with the increase in crystalline content percentage obtained from the XRD and DSC results. *Figure 6.16* presents the nearly linear trend of FPF % increase with the IBP crystalline content in the formulations.

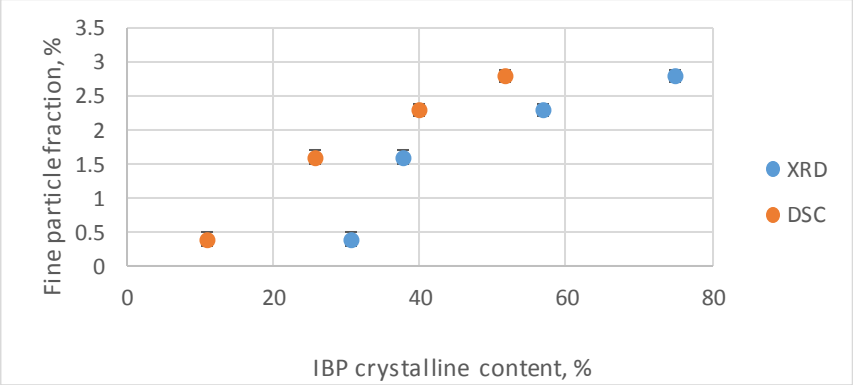

Figure 6.16 Relationship between IBP crystalline content (determined in XRD and DSC) and fine particle fraction (TSI) percentage of the formulations. [Mean ± SD, n=5, data from Table 6.6]

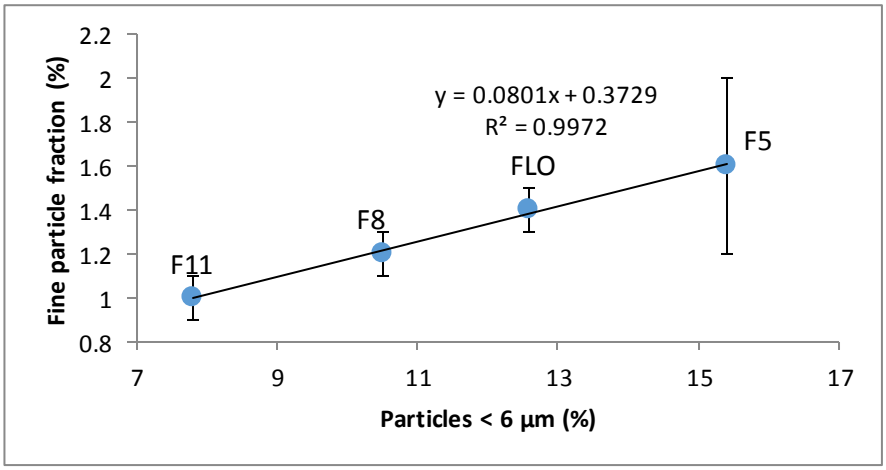

Figure 6.17 Linear relationship between the % particles < 6 µm and the % FPF in the formulations F5, FLO, F8 and F11. [Mean ± SD, n=5, data from Table 6.6]

A linear trend was observed between the percentage of particle < 6 µm size and FPF % in the formulations F5, FLO, F8 and F11 (*Figure 6.17*). The lowest FPF % of the formulation F9 indicated that a high concentration of Pl F127 resulted in very poor particle properties leading to a very low drug dispersibility. It is also to be noted that F9 had shown the lowest percentage of IBP crystalline particles in the DSC investigation. It has been reported by many researchers that a higher loss in the capsule and device retention for a DPI formulation occurs due to the cohesive nature of amorphous powders, lower Gibbs free energy [86, 243, 244] or electrostatic charges [245]. Pl F127 is a non-ionic surfactant widely used as a growth inhibitor in the APC process which integrates onto the surface of IBP particles. Pl F127 also enhances IBP solubility significantly (discussed in Section 4.4.1) thus slowing IBP precipitation and perhaps resulting in the production of low crystalline and highly amorphous IBP particles in the APC process. Therefore, increased Pl F127 concentration decreased the percentage of crystalline IBP in the formulations, perhaps resulting in a low percentage of FPF. The second lowest drug dispersion was from the formulation with highest leucine concentration (F11), having an aerodynamic diameter of 2.95 ± 0.02 µm but a poor flow property and a low percentage of crystalline IBP present in the formulation. This also might have lowered the percentage of FPF. Taking all the results together, the composition of formulation F6 showed best aerosol performance among all formulations prepared in the APC process. The percentage of FPF from the milled IBP powder was much higher than that of the formulations prepared in the APC process. For pulmonary drug delivery, the drug powder should have a narrow particle size distribution and a mean particle size of 5 µm with almost no particles larger than 10 µm [76]. The particle size distribution of milled IBP (*Table 6.3*) achieved the above criteria, which caused high IBP dispersibility in the aerosolization test. Another possible explanation for this might be that the absence of additives and no antisolvent precipitation produced a low amorphous content of IBP (as seen in the crystallinity results from the DSC), eventually increasing the FPF compared to the formulation prepared in the APC process using the additives. Moreover, the rough and corrugated surface of the milled IBP might have aided in the higher dispersibility [246, 247]. This phenomenon was evidenced in a study of enhancing powder aerosol performance of

particles with corrugated surfaces [248], due to the reduction of contact area and increasing the separation distance between the particles [249].

Finally, it should be noted that, although it is quite feasible to achieve particles with narrow size distribution with controlled solution crystallization process, some key disadvantages are to eliminate the residual solvents and absolute drying of the material which may result powder caking and declined powder dispersibility [22, 99].

6.5 DISSOLUTION STUDIES

Dissolution studies for the milled raw IBP powder and the prepared formulation powders F4, F6 and F10 were performed to compare drug release rates in phosphate buffer saline at 37°C. The first three formulations ranking on the drug dispersibility performance test were selected for the dissolution studies and compared with the performance of milled raw IBP powder. *Figure 6.18* presents the dissolution release profiles of the milled raw IBP powder and the formulations F4, F6 and F10, respectively. The formulation compositions for F4, F6 and F10 are different with respect to the initial drug load and the additive concentration. F4 contains 2% initial IBP and the additive concentrations are 1% L-leucine, 8.4% D-mannitol, 0.1% HPMC and 0.9% Pl F127. The composition of F6 includes 1% initial IBP and the additive concentrations are 1.2% L-leucine, 4.5% D-mannitol, 0.6% HPMC and 1.2% Pl F127. Finally, F10 contains 0.3% initial IBP and the additive concentrations are 1.2% L-leucine, 9% D-mannitol, 0.2% HPMC and 1.2% Pl F127.

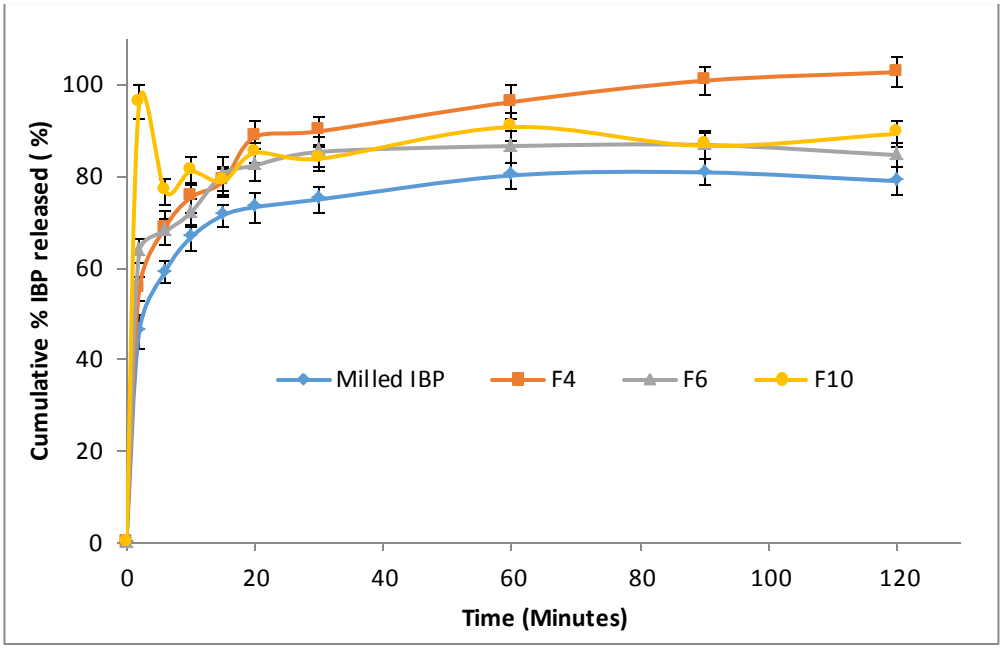

Figure 6.18 In vitro dissolution of milled raw IBP powder and formulations prepared in APC process. [Mean ± SD, n=3, data from Table 6.7]

Table 6.7 Dissolution release data for milled pure IBP powder and formulations (F4, F6 and F10) prepared in APC process versus time. [Mean ± SD, n=3]

Time (Minutes)	**Cumulative % IBP release (%)**			
	Milled IBP	**F4**	**F6**	**F10**
0	0	0	0	0
2	46.2 ± 1.7	55.4 ± 1.4	63.6 ± 1.7	96.1 ± 3.7
6	59.1 ± 1.4	68.7 ± 2.5	67.9 ± 2.0	76.6 ± 2.1
10	66.6 ± 1.9	75.4 ± 2.6	72.0 ± 2.1	81.0 ± 2.5
15	71.5 ± 1.8	78.8 ± 2.1	80.4 ± 2.9	78.8 ± 2.5
20	73.3 ± 2.4	88.6 ± 3.0	82.4 ± 2.9	85.1 ± 1.8
30	75.0 ± 2.1	89.8 ± 2.7	85.3 ± 2.9	83.8 ± 2.1
60	80.2 ± 2.3	96.2 ± 3.7	86.6 ± 3.0	90.8 ± 2.7
90	80.9 ± 2.3	100.9 ± 3.0	86.9 ± 2.7	86.7 ± 2.6
120	79.0 ± 2.6	102.7 ± 3.4	84.6 ± 2.2	89.3 ± 2.4

Dissolution studies revealed that the milled pure IBP release rate was slower than the prepared formulations (*Table 6.7*). In the first two minutes, drug release rate from

milled IBP, F4, F6 and F10 were 46.2 ± 1.7%, 55.4 ± 1.4%, 63.6 ± 1.7% and 96.1 ± 3.7% respectively. The results indicated that the prepared formulation dissolution rate is faster than the milled pure IBP. Among the prepared formulations, F10 released the maximum percentage of drug content (96.1 ± 3.7%) in the first two minutes. The possible reason could be the presence of a higher content of additives (Pl F127 1.2%, L-leucine 1.2%, D-mannitol 9.0% and HPMC 0.2%) and very low initial drug load (0.3%) in the composition of the formulation F10. The formulations with the higher initial IBP and lower additive concentrations have shown a comparatively lower dissolution rate in the first two minutes. The dissolution profiles of the pure milled IBP and the prepared formulations indicated that the presence of the hydrophilic polymeric additives in the formulations strongly promotes drug wettability by reducing the interaction among the hydrophobic IBP particles. On the other hand, the relatively higher cohesive forces with the milled pure IBP could potentially influence the overall dissolution negatively [250]. The maximum release from milled pure IBP was 81 ± 2.3%, whereas from the prepared formulations F4, F6 and F10 were 102 ± 3.4%, 87 ± 2.7% and 96 ± 3.7% respectively. In Chapter 4 we demonstrated that the solubility profile of IBP with additives was significantly higher than the solubility of raw IBP in water. Therefore, it can be concluded that the prepared formulations are better than the milled IBP in terms of the dissolution release rate. A faster dissolution rate of the formulations is expected to provide a better bioavailability than that of milled IBP powder.

A recent in vivo study for IBP after inhalation revealed that the inhalation dose is four to five orders of magnitude less than the orally delivered one that gives the same analgesic action [251]. Hence, the peak plasma level of IBP is found in the literature to be within 17-36 µg/mL (typically from 400 mg tablet administered orally after ~1 hour) [179-182]. The dissolution test results and the FPD of the prepared formulations (554 µg, 574.0 µg & 413.8 µg from the formulations F4, F6 and F10, respectively) indicate the future potential to improve the IBP drug delivery by lowering the dose and increasing the bioavailability. Our predicted calculation indicates the available IBP plasma concentration would be approximately 17 µg/mL (predicted from the obtained FPD and dissolution rate of the prepared formulations (F4, F6 & F10)) from a single puff of a 32 mg dose of the prepared DPI formulations. If the prediction is proven true in future (from an in vivo study), the

prepared formulations are expected to provide the same analgesic effect as a 400 mg tablet but with approximately a 10 times smaller dose.

6.6 RAMAN MAPPING FOR POWDER FORMULATION

The particle morphology was investigated using Raman spectroscopy to identify each component individually and the arrangements of the drug particle with the additives materials in the powder formulation mixture of F6. *Figure 6.19* shows the images extracted by mapping each component from their Raman spectrum and analysed by the WItec Project four software. The images revealed that IBP drug particles are covered by the additives used specially the Pl F127 was mostly seen on the surface of IBP drug particles. It was also visible that the IBP drug particles are surrounded by the D-mannitol extensively. The Raman images also showed presence of very trace amount of HPMC and L-leucine. *Figure 6.19* (a) shows the usual appearance of F6 powder formulation whereas *Figure 6.19* (b) presents the appearance of the F6 powder formulation in the second stage of TSI after in vitro aerosolization test.

(a)

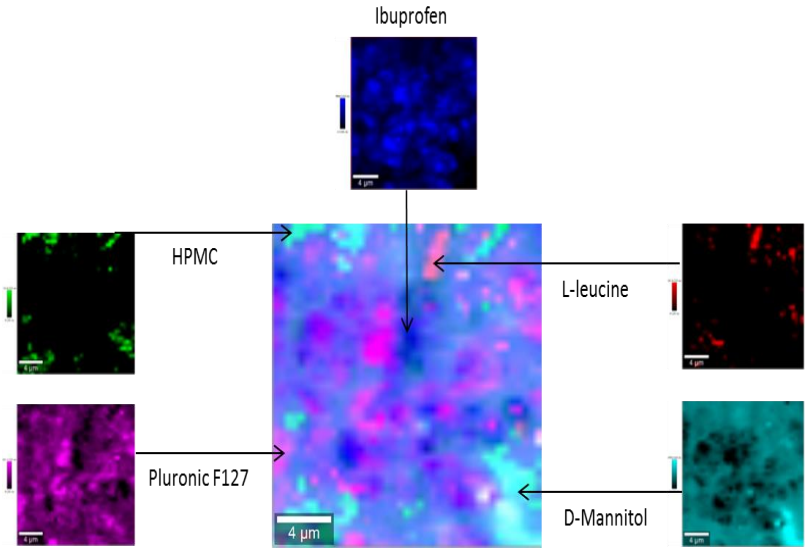

(b)

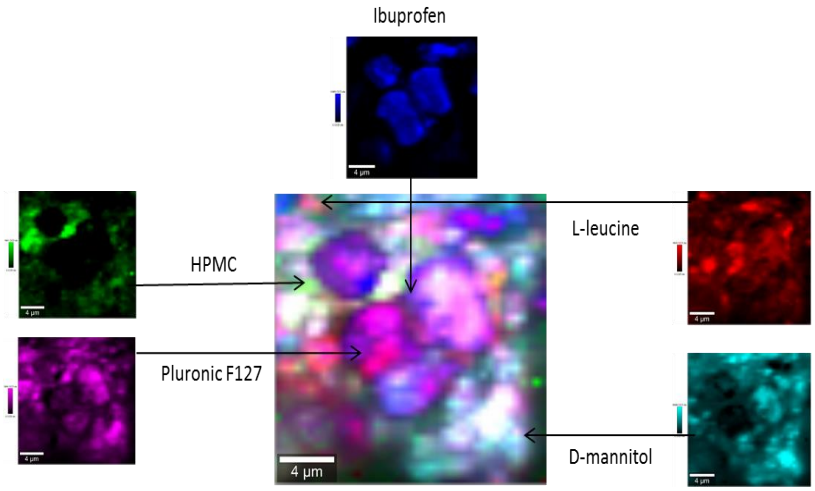

Figure 6.19 Raman images of F6 powder formulation mixture (a) Before in vitro aerosolization test, (b) in stage 2 of TSI after in vitro aerosolization test.

The difference between two images indicated that IBP drug particles are deagglomerated from the mixture of additives after impaction in TSI though the additives are still present. The interaction between IBP and Pl F127, HPMC and L-leucine found similar in both images whereas the attachment of the IBP particles with the D-mannitol shown to be apart slightly. The Raman investigation also confirmed that presence of the additives with the IBP particle will have a significant effect on the drug dispersibility test of the powder formulations.

6.7 CONCLUSION

This chapter has compared the characteristics of the formulations with respect to the composition, batch size and additive concentrations in their preparation. The presence of leucine and mannitol in the formulations improved the flowability, lowered the particle aerodynamic diameter, and showed higher FPF of IBP from DPI formulations. Among all the parameters, a narrow aerodynamic diameter of particles and high percentage of crystalline IBP phase in the formulation positively influenced the drug dispersibility. The FPF % of the milled IBP was much higher than that of the prepared formulations due to achieving narrow particle size distribution, high IBP content, and rough and corrugated particle surface. However, the dissolution tests revealed that the rate of dissolution of milled IBP is slower than that of the prepared formulations (as compared with F4, F6 and F10) which indicates that the prepared powders would provide better bioavailability of IBP.

Chapter 7: Conclusion and future directions

7.1 SUMMARY & CONCLUSION

This research proposes a new approach to developing IBP DPI formulation using regular size particles produced by a controlled crystallization process. So far there is no work reported in the literature on IBP microcrystal to produce a DPI formulation, and thus the outcome of this project is expected to enable the development of a non-invasive DPI formulation with reduced cost and with better therapeutic benefit. The limited literature shows some attempts have been made at a direct crystallization technique using additives for producing respirable size crystals, but it appears that this technique has never been applied successfully. The present PhD project proposes to develop a new method of controlled crystallization process for producing IBP small size (~5 μm) crystals for pulmonary delivery.

IBP solubility determination by the dissolution method was undertaken in the range of 0-50% aqueous ethanol solvents. Attainment of equilibrium of the IBP drug concentration was confirmed for each solvent system used.

The UV spectrophotometer was calibrated at 264 nm for the solubility measurements and at 221 nm wavelength to measure the drug dispersibility in the twin stage impinger. The experimental solubility data of IBP in aqueous ethanol solutions was determined at 10, 25 and 40 °C. The solubility of IBP increases considerably with increasing ethanol contents and also increases with temperature. The experimental data at 25 °C was in good agreement with the prior data of Rashid et al. [31]. A correlation is given to fit all the measured data. This correlation was used to select a suitable solvent for washing the IBP drug during the in vitro drug dispersion test using the twin stage impinger. The effectiveness of the four excipients HPMC, Pl F127, mannitol and leucine in solubility enhancement was investigated first as single component and then in combinations. Pl F127 raises the IBP solubility considerably, with the increases depending on the ethanol content. HPMC has a smaller effect. The effect of leucine was certainly positive in increasing the IBP solubility linearly with concentration. Mannitol did not show any trend of affecting the IBP solubility. The

combined effect of all excipients appears to be additive. The results allowed calculation of the minimum amount of initial drug to be used to precipitate IBP during particle preparation in precipitation crystallization in order to produce fine (<5 µm) IBP crystals for dry powder inhaler formulations.

A Plackett-Burman design was used to attempt to optimize the variables for the anti-solvent precipitation crystallization (APC) process of producing inhalable IBP particle. The experiment indicated ultrasound, stirring speed and batch size as most significant variables for the particle size of IBP produced in the APC process. However, optimization of the variables was not successful in the Plackett-Burman design and the effect of individual variables was studied. Optimized level of temperature (25 °C), ultrasound (30 minutes), stirring duration (>20 minutes), IBP concentration, solvent/antisolvent ratio and the additive concentrations needed to produce inhalable size IBP particles were determined. HPMC and Pl F127 agglomerated IBP particles after drying, and leucine and mannitol, improve the particle flow with no increase in particle size. IBP particles with the volume median diameter (D[v,0.5]) of 3.7 ± 0.3 µm were prepared by using HPMC and Pl F127. Finally, a method of producing a mixture of nano size (410 ± 72 nm, PDI 0.66 ± 0.10) and micron size (3.9 ± 0.4 µm) IBP particles using four additives—HPMC (0.2%), Pl F127(1.3%), leucine (1.2%) and mannitol (8.6%)—was optimized and validated. A method of producing inhalable size IBP by an APC process was established.

DPI formulations were developed with respect to the composition, batch size and drug and additive concentrations, and characterized for the density, size, flow and crystallinity. It was seen that the presence of leucine and mannitol in the formulation improved the flowability, lowered the particle aerodynamic diameter, and showed a higher percentage of FPF in the drug dispersibility test. A trend of decrease in the percentage of crystalline IBP phase was observed, with an increase in Pl F127 concentration in the formulations, which also decreased the drug dispersibility in the TSI test. Among all the parameters, the narrow aerodynamic diameter of particles and high percentage of crystalline IBP phase in the formulation positively influenced the drug dispersibility in the aerosolization test. The milled IBP had shown higher dispersibility than the prepared IBP particles in the APC process. It is assumed that

the surface roughness and corrugation of the milled IBP particles, narrow particle size distribution and the 100% drug content delivery increased the FPF significantly.

The dissolution tests results revealed that the dissolution rate of the prepared powder is faster than the milled IBP powder. The prepared particles (F10) achieved 96% of dissolution in the first two minutes of drug delivery. On the other hand, the maximum dissolution of milled IBP was 80% after two hours of drug delivery. The faster dissolution rate of the prepared particles is expected to provide better bioavailability than the raw milled IBP. A recent in vivo study for IBP after inhalation revealed that the inhalation dose is four to five orders of magnitude less than the orally delivered one that gives the same analgesic action [251]. Hence, the peak plasma level of IBP from the literature is found to be within 17-36 µg/mL [179-182]. The dissolution test results and the FPD of the prepared formulations (554 µg, 574.0 µg & 413.8 µg from the formulations F4, F6 and F10, respectively) indicate the future potential to improve IBP drug delivery by lowering the dose and also increasing the bioavailability.

The solubility correlation of IBP in aqueous ethanol systems developed in this work would be very useful for the pre-formulation investigation of IBP in other dosage forms as well. Solubility enhancement in the presence of the additives (especially Pl F127) certainly has the potential to overcome the bioavailability issues caused by the poor water solubility of IBP. The IBP solubility trend in aqueous ethanol with Pl F1127, HPMC, L-leucine and D-mannitol is the first novelty of this research. It is expected that this work would contribute to advancing new technological possibilities in the enhancement of the drug's solubility for any dosage formulation.

The second novelty of this research is the one step process of producing inhalable size IBP particles without further high shear milling. This outcome is expected to contribute to precise and predictive control of vital physicochemical properties like solubility of the active pharmaceutical ingredients (APIs) and pharmaceutical excipients in pharmaceutical formulation development for improving the in vivo delivery, storage stability, and manufacturability of drug substances.

The effects of Pl F127, HPMC, L-leucine and D-mannitol on the crystallinity of the IBP and their relationship to the drug's dispersibility have not been investigated prior to this study. The knowledge obtained from this work will contribute to further

studies on the use of these excipients in the formulation and for the prediction of possible stability problems during storage.

7.2 LIMITATIONS AND FUTURE DIRECTION

IBP is usually administered as tablets. This project looks at the feasibility of administering IBP pneumatically into the lungs, which is expected to be more effective and efficient in terms of bioavailability. Our work was limited to *in vitro* studies of the drug dispersibility into the lungs. To achieve the actual effectiveness of the prepared formulations, *in vivo* lung dispersibility tests would be an important future approach. This is a very general recommendation for the future direction of this research.

The solubility studies of IBP in water ethanol co-solvents produced correlations which can calculate the IBP solubility in water-ethanol co-solvents at different temperatures (10, 25 and 40 °C). However, in the case of the solubility studies of IBP with additives, the experimental points were limited to the required conditions to produce inhalable IBP particles. IBP solubility investigations with the selected additives at a wider range of concentrations would be useful to establish a correlation for further pre-formulation studies for developing new IBP dosage forms.

The DPI formulations prepared in this work have shown a considerably low fine particle fraction, though the fine particle dose amount was at a satisfactory level. However, developing interactive mixtures of the prepared IBP particles in an APC process with lactose or any other suitable carrier might enhance the fine particle fraction of the DPI formulations.

Finally, performing a stability test of the developed formulations would be a valuable added feature to this research work in the future. As seen from the crystallinity characterizaization, Pl F127 and L-leucine caused loss of IBP from the dry powder formulations. Though mannitol is a very useful additive for pharmaceutical formulations, its hygroscopicity often creates problems of stability. Thus, a long term stability investigation would provide appropriate answers to the efficiency of the developed formulation.

References

1. Ballester M, Nembrini C, Dhar N, Titta A, Piano C, Pasquier M, et al. Nanoparticle conjugation and pulmonary delivery enhance the protective efficacy of ag85b and cpg against tuberculosis. Vaccine. 2011;29:6959-66.
2. Alhanout K, Brunel JM, Dubus JC, Rolain JM, Andrieu V. Suitability of a new antimicrobial aminosterol formulation for aerosol delivery in cystic fibrosis. Journal of Antimicrobial Chemotherapy. 2011;66:2797-800.
3. Forman JP, Stampfer MJ, Curhan GC. Non-narcotic analgesic dose and risk of incident hypertension in us women. Hypertension. 2005;46:500-7.
4. Chan AT, Manson JE, Albert CM, Chae CU, Rexrode KM, Curhan GC, et al. Nonsteroidal antiinflammatory drugs, acetaminophen, and the risk of cardiovascular events. Circulation. 2006;113:1578-87.
5. Daugherty SE, Berndt SI, Purdue M, Huang W-y. Abstract b93: Nonsteroidal anti-inflammatory drugs and all-cause mortality, cancer mortality, and cardiovascular mortality in the prostate, lung, colorectal, and ovarian cancer screening trial. Cancer Prevention Research. 2012;5:B93.
6. Gradon L, Sosnowski TR. Formation of particles for dry powder inhalers. Advanced Powder Technology. 2013.
7. Shoyele SA, Slowey A. Prospects of formulating proteins/peptides as aerosols for pulmonary drug delivery. International Journal of Pharmaceutics. 2006;314:1-8.
8. Timsina MP, Martin GP, Marriott C, Ganderton D, Yianneskis M. Drug delivery to the respiratory tract using dry powder inhalers. International Journal of Pharmaceutics. 1994;101:1-13.
9. Weibel E. Morphometry of the human lung: The state of the art after two decades. Bulletin européen de physiopathologie respiratoire. 1979;15:999.
10. Lee H-K, Kwon J-H, Park S-H, Kim C-W. Insulin microcrystals prepared by the seed zone method. Journal of Crystal Growth. 2006;293:447-51.
11. Wolff RK, Dorato MA. Toxicologic testing of inhaled pharmaceutical aerosols. Critical Reviews in Toxicology. 1993;23:343-69.
12. Emami J, Hamishehkar H, Najafabadi AR, Gilani K, Minaiyan M, Mahdavi H, et al. Particle size design of PLGA microspheres for potential pulmonary drug delivery using response surface methodology. Journal of Microencapsulation. 2009;26:1-8.
13. Sakagami M. In vivo, in vitro and ex vivo models to assess pulmonary absorption and disposition of inhaled therapeutics for systemic delivery. Advanced Drug Delivery Reviews. 2006;58:1030-60.
14. Kho K, Hadinoto K. Optimizing aerosolization efficiency of dry-powder aggregates of thermally-sensitive polymeric nanoparticles produced by spray-freeze-drying. Powder Technology. 2011;214:169-76.
15. Tsapis N, Bennett D, Jackson B, Weitz DA, Edwards DA. Trojan particles: Large porous carriers of nanoparticles for drug delivery. Proceedings of the National Academy of Sciences of the United States of America. 2002;99:12001-5.
16. Rasenack N, Steckel H, Müller BW. Preparation of microcrystals by in situ micronization. Powder Technology. 2004;143-144:291-6.
17. Service RF. Hijacking a cell's chemical paths to make new antibiotics. Science. 1997.

18. Shoyele SA, Cawthorne S. Particle engineering techniques for inhaled biopharmaceuticals. Advanced Drug Delivery Reviews. 2006;58:1009-29.
19. Islam N, Gladki E. Dry powder inhalers (DPIs)—a review of device reliability and innovation. International Journal of Pharmaceutics. 2008;360:1-11.
20. Islam N, Stewart P, Larson I, Hartley P. Effect of carrier size on the dispersion of salmeterol xinafoate from interactive mixtures. Journal of Pharmaceutical Sciences. 2004;93:1030-8.
21. Steckel H, Mueller BW. In vitro evaluation of dry powder inhalers i: Drug deposition of commonly used devices. International Journal of Pharmaceutics. 1997;154:19-29.
22. Ragab DM, Rohani S. Particle engineering strategies via crystallization for pulmonary drug delivery. Organic Process Research and Development. 2009;13:1215-23.
23. Andreou J, Stewart P, Morton D. Short-term changes in drug agglomeration within interactive mixtures following blending. International Journal of Pharmaceutics. 2009;372:1-11.
24. Liu LX, Marziano I, Bentham AC, Litster JD, White ET, Howes T. Effect of particle properties on the flowability of ibuprofen powders. International Journal of Pharmaceutics. 2008;362:109-17.
25. Muzzio FJ, Shinbrot T, Glasser BJ. Powder technology in the pharmaceutical industry: The need to catch up fast. Powder Technology. 2002;124:1-7.
26. Rashid MA. Crystallization engineering of ibuprofen for pharmaceutical formulation [PhD Thesis]. Brisbane, Australia: University of Queensland; 2011.
27. Waltersson J, Lundgren P. The effect of mechanical comminution on drug stability. Acta Pharmaceutica Suecica. 1985;22:291-300.
28. Khan S, Matas Md, Zhang J, Anwar J. Nanocrystal preparation: Low-energy precipitation method revisited. Crystal Growth Design. 2013;13:2766-77.
29. Bhattamishra S, Padhy R. Estimation of ibuprofen solubilization in cationic and anionic surfactant media: Application of the micelle binding model. Indian Journal of Chemical Technology. 2009;16:426-30.
30. Newman SP, Busse WW. Evolution of dry powder inhaler design, formulation, and performance. Respiratory medicine 2002;96:293-304.
31. Rashid A, White ET, Howes T, Litster JD, Marziano I. Effect of solvent composition and temperature on the solubility of ibuprofen in aqueous ethanol. Journal of Chemical & Engineering Data. 2014;59:2699-703.
32. Reid DJ, Pham NT. Emerging therapeutic options for the management of copd. Clinical Medicine Insights: Circulatory. 2013;7:7-15, 9 pp.
33. Behara SRB, Longest PW, Farkas DR, Hindle M. Development and comparison of new high-efficiency dry powder inhalers for carrier-free formulations. Journal of Pharmaceutical Sciences. 2014;103:465-77.
34. Patton JS. Mechanisms of macromolecule absorption by the lungs. Advanced Drug Delivery Reviews. 1996;19:3-36.
35. Haghi M, Ong HX, Traini D, Young P. Across the pulmonary epithelial barrier: Integration of physicochemical properties and human cell models to study pulmonary drug formulations. Pharmacology & therapeutics. 2014;144:235-52.
36. Fehrenbach H. Alveolar epithelial type ii cell: Defender of the alveolus revisited. Respiratory Research. 2001;2:1-20.
37. Thiriet M. Cell and tissue organization in the circulatory and ventilatory systems: Springer; 2011.
38. Nicod LP. Lung defences: An overview. European Respiratory Review. 2005;14:45-50.

39. Hamm H, Fabel H, Bartsch W. The surfactant system of the adult lung: Physiology and clinical perspectives. The Clinical Investigator. 1992;70:637-57.
40. Samet JM, Cheng PW. The role of airway mucus in pulmonary toxicology. Environmental Health Perspectives. 1994;102:89-103.
41. Effros RM, Mason GR. Measurements of pulmonary epithelial permeability in vivo. American Review of Respiratory Disease. 1983;127:S59-S65.
42. Schneeberger EE, Lynch RD. The tight junction: A multifunctional complex. American Journal of Physiology - Cell Physiology. 2004;286:C1213-C28.
43. Chandar N, Viselli S. Cell and molecular biology: Lippincott Williams & Wilkins; 2012.
44. Foth H. Role of the lung in accumulation and metabolism of xenobiotic compounds — implications for chemically induced toxicity. Critical Reviews in Toxicology. 1995;25:165-205.
45. Rejman J, Oberle V, Zuhorn IS, Hoekstra D. Size-dependent internalization of particles via the pathways of clathrin- and caveolae-mediated endocytosis. Biochemical Journal. 2004;377:159-69.
46. Matsukawa Y, Lee VHL, Crandall ED, Kim K-J. Size-dependent dextran transport across rat alveolar epithelial cell monolayers. Journal of Pharmaceutical Sciences. 1997;86:305-9.
47. Hastings RH, Folkesson HG, Matthay MA. Mechanisms of alveolar protein clearance in the intact lung. American Journal of Physiology - Lung Cellular and Molecular Physiology. 2004;286:L679-L89.
48. Adjei A, Garren J. Pulmonary delivery of peptide drugs: Effect of particle size on bioavailability of leuprolide acetate in healthy male volunteers. Pharm Res. 1990;7:565-9.
49. Fernández Tena A, Casan Clarà P. Deposition of inhaled particles in the lungs. Archivos de Bronconeumología (English Edition). 2012;48:240-6.
50. Carvalho TC, Peters JI, Williams RO, III. Influence of particle size on regional lung deposition: What evidence is there? International Journal of Pharmaceutics. 2011;406:1-10.
51. Gonda I. Targeting by deposition. Drugs and the pharmaceutical sciences. 1992;54:61-82.
52. Gonda I. Particulate interactions in dry powder formulations for inhalation. Elsevier B.V; 2004. p. 509-.
53. Newman S, Anderson P. Respiratory drug delivery: Essential theory and practice: Respiratory Drug Delivery Online; 2009.
54. Azhdarzadeh M, Olfert JS, Vehring R, Finlay WH. Effect of electrostatic charge on oral-extrathoracic deposition for uniformly charged monodisperse aerosols. Journal of Aerosol Science. 2014;68:38-45.
55. Telko MJ, Hickey AJ. Dry powder inhaler formulation. Respiratory Care. 2005;50:1209-27.
56. El-Sherbiny IM, Smyth HDC. Biodegradable nano-micro carrier systems for sustained pulmonary drug delivery: (i) self-assembled nanoparticles encapsulated in respirable/swellable semi-ipn microspheres. International Journal of Pharmaceutics. 2010;395:132-41.
57. Du J, El-Sherbiny IM, Smyth HD. Swellable ciprofloxacin-loaded nano-in-micro hydrogel particles for local lung drug delivery. AAPS PharmSciTech. 2014;15:1535-44.
58. De Boer AH, Gjaltema D, Hagedoorn P, Frijlink HW. Characterization of inhalation aerosols: A critical evaluation of cascade impactor analysis and laser diffraction technique. International Journal of Pharmaceutics. 2002;249:219-31.
59. Yang Y, Cheow WS, Hadinoto K. Dry powder inhaler formulation of lipid-polymer hybrid nanoparticles via electrostatically-driven nanoparticle assembly onto microscale carrier particles. International Journal of Pharmaceutics. 2012;434:49-58.

60. Tuli R, . Studies on the surface properties of biodegradable polymer carriers in respiratory delivery of drug from dry powder inhaler formulations [PhD Thesis]. Brisbane, Australia: Queensland University of Technology.; 2012.
61. Jaafar-Maalej C, Andrieu V, Elaissari A, Fessi H. Assessment methods of inhaled aerosols: Technical aspects and applications. Expert Opinion on Drug Delivery. 2009;6:941-59.
62. Pilcer G, Vanderbist F, Amighi K. Correlations between cascade impactor analysis and laser diffraction techniques for the determination of the particle size of aerosolised powder formulations. International Journal of Pharmaceutics. 2008;358:75-81.
63. Freedman T. Medihaler therapy for bronchial asthma; a new type of aerosol therapy. Postgraduate Medicine. 1956;20:667-73.
64. Stegemann S, Kopp S, Borchard G, Shah VP, Senel S, Dubey R, et al. Developing and advancing dry powder inhalation towards enhanced therapeutics. European Journal of Pharmaceutical Sciences. 2013;48:181-94.
65. Labiris NR, Dolovich MB. Pulmonary drug delivery. Part ii: The role of inhalant delivery devices and drug formulations in therapeutic effectiveness of aerosolized medications: Physiological factors affecting the effectiveness of inhaled drugs. British Journal of Clinical Pharmacology. 2003;56:600-12.
66. de KJP, van dMTW, Coenegracht PMJ, Tromp TFJ, Frijlink HW. Effect of an external resistance to airflow on the inspiratory flow curve. International Journal of Pharmaceutics. 2002;234:257-66.
67. Janssens W, VandenBrande P, Hardeman E, De LE, Philps T, Troosters T, et al. Inspiratory flow rates at different levels of resistance in elderly copd patients. European Respiratory Journal. 2008;31:78-83.
68. Virchow JC, Crompton GK, Dal NR, Pedersen S, Magnan A, Seidenberg J, et al. Importance of inhaler devices in the management of airway disease. Respiratory Medicine. 2008;102:10-9.
69. Hammerlein A, Muller U, Schulz M. Pharmacist-led intervention study to improve inhalation technique in asthma and copd patients. Journal of Evaluation in Clinical Practice,. 2011;17:61-70.
70. Taburet A-M, Schmit B. Pharmacokinetic optimization of asthma treatment. Clinical Pharmacokinetics. 1994;26:396-418.
71. Israelachvili JN. Intermolecular and surface forces. San Diego: Academic Press; 1991.
72. Kaialy W, Alhalaweh A, Velaga SP, Nokhodchi A. Effect of carrier particle shape on dry powder inhaler performance. International Journal of Pharmaceutics. 2011;421:12-23.
73. Wong J, Kwok PCL, Noakes T, Fathi A, Dehghani F, Chan H-K. Effect of crystallinity on electrostatic charging in dry powder inhaler formulations. Pharmaceutical Research. 2014;31:1656-64.
74. Briggner LE, Buckton G, Bystrom K, Darcy P. The use of isothermal microcalorimetry in the study of changes in crystallinity induced during the processing of powders. International Journal of Pharmaceutics. 1994;105:125-35.
75. Ticehurst MD, Basford PA, Dallman CI, Lukas TM, Marshall PV, Nichols G, et al. Characterization of the influence of micronization on the crystallinity and physical stability of revatropate hydrobromide. International Journal of Pharmaceutics. 2000;193:247-59.
76. Rohani S. Applications of the crystallization process in the pharmaceutical industry. From Frontiers of Chemical Engineering in China 2010;4:2-9.
77. Kubavat HA, Shur J, Ruecroft G, Hipkiss D, Price R. Influence of primary crystallisation conditions on the mechanical and interfacial properties of micronised budesonide for dry powder inhalation. International Journal of Pharmaceutics. 2012;430:26-33.

78. Shur J, Kubavat HA, Ruecroft G, Hipkiss D, Price R. Influence of crystal form of ipratropium bromide on micronisation and aerosolisation behaviour in dry powder inhaler formulations. Journal of pharmacy and pharmacology. 2012;64:1326-36.
79. Kaialy W, Nokhodchi A. Treating mannitol in a saturated solution of mannitol: A novel approach to modify mannitol crystals for improved drug delivery to the lungs. International Journal of Pharmaceutics. 2013;448:58-70.
80. Kaialy W, Larhrib H, Ticehurst M, Nokhodchi A. Influence of batch cooling crystallization on mannitol physical properties and drug dispersion from dry powder inhalers. Crystal Growth Design. 2012;12:3006-17.
81. Kaialy W, Larhrib H, Martin GP, Nokhodchi A. The effect of engineered mannitol-lactose mixture on dry powder inhaler performance. Pharmaceutical Research. 2012;29:2139-56.
82. Zeng XM, Martin GP, Marriott C, Pritchard J. The use of lactose recrystallised from carbopol gels as a carrier for aerosolised salbutamol sulphate. European Journal of Pharmaceutics and Biopharmaceutics. 2001;51:55-62.
83. Tuli RA, Dargaville TR, George GA, Islam N. Polycaprolactone microspheres as carriers for dry powder inhalers: Effect of surface coating on aerosolization of salbutamol sulfate. Journal of Pharmaceutical Sciences. 2012;101:733-45.
84. Kaialy W, Hussain T, Alhalaweh A, Nokhodchi A. Towards a more desirable dry powder inhaler formulation: Large spray-dried mannitol microspheres outperform small microspheres. Pharmaceutical Research. 2014;31:60-76.
85. Chawla A, Taylor KMG, Newton JM, Johnson MCR. *Production of spray-dried salbutamol sulfate for use in dry powder aerosol formulation*. International Journal of Pharmaceutics. 1994;108:233-40.
86. Buckton G, Darcy P, Greenleaf D, Holbrook P. The use of isothermal microcalorimetry in the study of changes in crystallinity of spray-dried salbutamol sulphate. International Journal of Pharmaceutics. 1995;116:113-8.
87. Kaerger JS, Price R. Processing of spherical crystalline particles via a novel solution atomization and crystallization by sonication (saxs) technique. Pharmaceutical Research. 2004;21:372-81.
88. Manish M, Harshal J, Anant P. Melt sonocrystallization of ibuprofen: Effect on crystal properties. European Journal of Pharmaceutical Sciences. 2005;25:41-8.
89. Lee M-J, Kwon J-H, Shin J-S, Kim C-W. Microcrystallization of α-lactalbumin. Journal of Crystal Growth. 2005;282:434-7.
90. Kwon J-H, Lee B-H, Lee J-J, Kim C-W. Insulin microcrystal suspension as a long-acting formulation for pulmonary delivery. European Journal of Pharmaceutical Sciences. 2004;22:107-16.
91. Murnane D, Martin GP, Marriott C. Dry powder formulations for inhalation of fluticasone propionate and salmeterol xinafoate microcrystals. Journal of Pharmaceutical Sciences. 2009;98:503-15.
92. Rasenack N, Steckel H, Muller BW. Micronization of anti-inflammatory drugs for pulmonary delivery by a controlled crystallization process. Journal of Pharmaceutical Sciences. 2003;92:35-44.
93. Steckel H, Rasenack N, Muller BW. In-situ-micronization of disodium cromoglycate for pulmonary delivery. European Journal of Pharmaceutics and Biopharmaceutics. 2003;55:173-80.
94. Bakhbakhi Y, Charpentier PA, Rohani S. Experimental study of the gas process for producing microparticles of beclomethasone-17,21-dipropionate suitable for pulmonary delivery. International Journal of Pharmaceutics. 2006;309:71-80.

95. Ikegami K, Kawashima Y, Takeuchi H, Yamamoto H, Momose D-I, Saito N, et al. In vitro inhalation behavior of spherically agglomerated steroid particles with carrier lactose. Advanced Powder Technology. 2000;11:323-32.
96. Yang Z, Hu T, Le Y, Liu M, Shen Z, Chen J. Preparation of ultrafine sumatriptan succinate for dry powder inhalation via reactive crystallization and its evaluation. Huagong Jinzhan. 2008;27:1412-6.
97. Chiou H, Li L, Hu T, Chan H-K, Chen J-F, Yun J. Production of salbutamol sulfate for inhalation by high-gravity controlled antisolvent precipitation. International Journal of Pharmaceutics. 2007;331:93-8.
98. Balducci AG, Cagnani S, Sonvico F, Rossi A, Barata P, Colombo G, et al. Pure insulin highly respirable powders for inhalation. European Journal of Pharmaceutical Sciences. 2014;51:110-7.
99. Ragab D, Rohani S, Samaha MW, El-Khawas FM, El-Maradny HA. Crystallization of progesterone for pulmonary drug delivery. Journal of Pharmaceutical Sciences. 2010;99:1123-37.
100. Chen J-F, Wang Y-H, Guo F, Wang X-M, Zheng C. Synthesis of nanoparticles with novel technology: High-gravity reactive precipitation. Industrial & Engineering Chemistry Research. 2000;39:948-54.
101. Hu T, Chiou H, Chan H-K, Chen J-F, Yun J. Preparation of inhalable salbutamol sulphate using reactive high gravity controlled precipitation. Journal of Pharmaceutical Sciences. 2008;97:944-9.
102. Muhammad SAFS, Oubani H, Abbas A, Chan HK, Kwok PCL, Dehghani F. The production of dry powder by the sonocrystallisation for inhalation drug delivery. Powder Technology. 2013;246:337-44.
103. Ter Horst JH, Schmidt C, Ulrich J. 32 - fundamentals of industrial crystallization a2 - rudolph, peter. Handbook of crystal growth (second edition). Boston: Elsevier; 2015. p. 1317-49.
104. Dirksen JA, Ring TA. Fundamentals of crystallization: Kinetic effects on particle size distributions and morphology. Chemical Engineering Science 1991;46:2389-427.
105. Chan H-K, Kwok PCL. Production methods for nanodrug particles using the bottom-up approach. Advanced Drug Delivery Reviews. 2011;63:406-16.
106. Mullin JW. Crystallization (4th edition). Elsevier.
107. Myerson A. Handbook of industrial crystallization: Butterworth-Heinemann; 2002.
108. Ostrowska K, Kropidlowska M, Katrusiak A. High-pressure crystallization and structural transformations in compressed r,s-ibuprofen. Crystal Growth Design. 2015;15:1512-7.
109. Shankland N, Florence AJ, Cox PJ, Sheen DB, Love SW, Stewart NS, et al. Crystal morphology of ibuprofen predicted from single-crystal pulsed neutron diffraction data. Chemical Communications. 1996:855-6.
110. Cano H, Gabas N, Canselier JP. Experimental study on the ibuprofen crystal growth morphology in solution. Journal of Crystal Growth. 2001;224:335-41.
111. McConnell JF. The 2-(4-isobutylphenyl) propionic acid. Ibuprofen or prufen. Crystal Structure Communications 1974;3:73-5.
112. Leising G, Resel R, Stelzer F, Tasch S, Lanziner A, Hantich G. Physical aspects of dexibuprofen and racemic ibuprofen. Journal of Clinical Pharmacology. 1996;36:3S-6S.
113. Freer AA, Bunyan JM, Shankland N, Sheen DB. Structure of (s)-(+)-ibuprofen. Acta Crystallogr, Sect C: Crystal Structure Communications. 1993;C49:1378-80.
114. Montes A, Litwinowicz AA, Gradl U, Gordillo MD, Pereyra C, Martinez de la Ossa EJ. Exploring high operating conditions in the ibuprofen precipitation by rapid expansion of supercritical solutions process. Industrial & Engineering Chemistry Research. 2014;53:474-80.

115. Sinha B, Müller RH, Möschwitzer JP. Systematic investigation of the cavi-precipitation process for the production of ibuprofen nanocrystals. International Journal of Pharmaceutics. 2013;458:315-23.
116. Kocbek P, Baumgartner S, Kristl J. Preparation and evaluation of nanosuspensions for enhancing the dissolution of poorly soluble drugs. International Journal of Pharmaceutics. 2006;312:179-86.
117. Verma S, Gokhale R, Burgess DJ. A comparative study of top-down and bottom-up approaches for the preparation of micro/nanosuspensions. International Journal of Pharmaceutics. 2009;380:216-22.
118. Onischuk AA, Tolstikova TG, Sorokina IV, Zhukova NA, Baklanov AM, Karasev VV, et al. Analgesic effect from ibuprofen nanoparticles inhaled by male mice. Journal of Aerosol Medicine and Pulmonary Drug Delivery. 2009;22:245-53.
119. Nesamony J, Shah IS, Kalra A, Jung R. Nebulized oil-in-water nanoemulsion mists for pulmonary delivery: Development, physico-chemical characterization and in vitro evaluation. Drug Development and Industrial Pharmacy. 2014;40:1253-63.
120. Wu L, Zhang J, Watanabe W. Physical and chemical stability of drug nanoparticles. Advanced Drug Delivery Reviews. 2011;63:456-69.
121. Montes A, Gordillo MD, Pereyra C, De los Santos DM, Martínez de la Ossa EJ. Ibuprofen–polymer precipitation using supercritical co2 at low temperature . The Journal of Supercritical Fluids. 2014;94:91-101.
122. Matteucci ME, Hotze MA, Johnston KP, Williams RO. Drug nanoparticles by antisolvent precipitation: Mixing energy versus surfactant stabilization. Langmuir. 2006;22:8951-9.
123. Rasenack N, Mueller BW. Dissolution rate enhancement by in situ micronization of poorly water-soluble drugs. Pharmaceutical Research. 2002;19:1894-900.
124. Vetter T, Mazzotti M, Brozio J. Slowing the growth rate of ibuprofen crystals using the polymeric additive pluronic f127. Crystal Growth Design. 2011;11:3813-21.
125. Gao L, Zhang D, Chen M. Drug nanocrystals for the formulation of poorly soluble drugs and its application as a potential drug delivery system. Journal of Nanoparticle Research. 2008;10:845-62.
126. Douroumis D, Fahr A. Nano- and micro-particulate formulations of poorly water-soluble drugs by using a novel optimized technique. European Journal of Pharmaceutics and Biopharmaceutics. 2006;63:173-5.
127. Zhang J-Y, Shen Z-G, Zhong J, Hu T-T, Chen J-F, Ma Z-Q, et al. Preparation of amorphous cefuroxime axetil nanoparticles by controlled nanoprecipitation method without surfactants. International Journal of Pharmaceutics. 2006;323:153-60.
128. Zhong J, Shen Z, Yang Y, Chen J. Preparation and characterization of uniform nanosized cephradine by combination of reactive precipitation and liquid anti-solvent precipitation under high gravity environment. International Journal of Pharmaceutics. 2005;301:286-93.
129. Kipp JE. The role of solid nanoparticle technology in the parenteral delivery of poorly water-soluble drugs. International Journal of Pharmaceutics. 2004;284:109-22.
130. Xie S, Poornachary SK, Chow PS, Tan RBH. Direct precipitation of micron-size salbutamol sulfate: New insights into the action of surfactants and polymeric additives. Crystal Growth Design. 2010;10:3363-71.
131. Zhang X-Y, Fevotte G, Zhong L, Qian G, Zhou X-G, Yuan W-K. Crystallization of zinc lactate in presence of malic acid. Journal of Crystal Growth. 2010;312:2747-55.
132. Kestur US, Lee H, Santiago D, Rinaldi C, Won Y-Y, Taylor LS. Effects of the molecular weight and concentration of polymer additives, and temperature on the melt crystallization kinetics of a small drug molecule. Crystal Growth Design. 2010;10:3585-95.

133. Kaialy W, Nokhodchi A. The use of freeze-dried mannitol to enhance the in vitro aerosolization behaviour of budesonide from the aerolizer®. Powder Technology. 2016;288:291-302.
134. Terebetski JL, Michniak-Kohn B. Combining ibuprofen sodium with cellulosic polymers: A deep dive into mechanisms of prolonged supersaturation. International Journal of Pharmaceutics. 2014;475:536-46.
135. Basalious EB, El-Sebaie W, El-Gazayerly O. Application of pharmaceutical qbd for enhancement of the solubility and dissolution of a class ii bcs drug using polymeric surfactants and crystallization inhibitors: Development of controlled-release tablets. AAPS PharmSciTech. 2011;12:799-810.
136. Newa M, Bhandari KH, Li DX, Kwon T-H, Kim JA, Yoo BK, et al. Preparation, characterization and in vivo evaluation of ibuprofen binary solid dispersions with poloxamer 188. International Journal of Pharmaceutics. 2007;343:228-37.
137. Park Y-J, Kwon R, Quan QZ, Oh DH, Kim JO, Hwang MR, et al. Development of novel ibuprofen-loaded solid dispersion with improved bioavailability using aqueous solution. Archives of Pharmacal Research. 2009;32:767-72.
138. Vasil'ev MV. Classification of diagrams of state of binary metallic systems by the force of interatomic reactions. Zh Fiz Khim. 1964;38:871-7.
139. Passerini N, Albertini B, Gonzalez-Rodriguez ML, Cavallari C, Rodriguez L. Preparation and characterization of ibuprofen-poloxamer 188 granules obtained by melt granulation. European Journal of Pharmaceutical Sciences. 2002;15:71-8.
140. Seo A, Holm P, Kristensen HG, Schaefer T. The preparation of agglomerates containing solid dispersions of diazepam by melt agglomeration in a high shear mixer. International Journal of Pharmaceutics. 2003;259:161-71.
141. Newa M, Bhandari KH, Oh DH, Kim YR, Sung JH, Kim JO, et al. Enhanced dissolution of ibuprofen using solid dispersion with poloxamer 407. Archives of Pharmacal Research. 2008;31:1497-507.
142. Raghavan S, Trividic A, Davis A, Hadgraft J. Crystallization of hydrocortisone acetate: Influence of polymers. International Journal of Pharmaceutics. 2001;212:213-21.
143. Iervolino M, Raghavan SL, Hadgraft J. Membrane penetration enhancement of ibuprofen using supersaturation. Journal of Pharmaceutical Sciences. 2000;198:229-38.
144. Mishra B, Sahoo J, Dixit PK. Formulation and process optimization of naproxen nanosuspensions stabilized by hydroxy propyl methyl cellulose. Carbohydrate Polymers. 2015;127:300-8.
145. Schwegman JJ, Hardwick LM, Akers MJ. Practical formulation and process development of freeze-dried products. Pharmaceutical Development and Technology. 2005;10:151-73.
146. Tee SK, Marriott C, Zeng XM, Martin GP. The use of different sugars as fine and coarse carriers for aerosolised salbutamol sulphate. International Journal of Pharmaceutics. 2000;208:111-23.
147. Steckel H, Bolzen N. Alternative sugars as potential carriers for dry powder inhalations. International Journal of Pharmaceutics. 2004;270:297-306.
148. Saint-Lorant G, Leterme P, Gayot A, Flament MP. Influence of carrier on the performance of dry powder inhalers. International Journal of Pharmaceutics. 2007;334:85-91.
149. Lee MK, Kim MY, Kim S, Lee J. Cryoprotectants for freeze drying of drug nano-suspensions: Effect of freezing rate. Journal of Pharmaceutical Sciences.98:4808-17.
150. Abdelwahed W, Degobert G, Stainmesse S, Fessi H. Freeze-drying of nanoparticles: Formulation, process and storage considerations. Advanced Drug Delivery Reviews. 2006;58:1688-713.

151. Flume PA, Aitken ML, Bilton D, Agent P, Charlton B, Forster E, et al. Optimising inhaled mannitol for cystic fibrosis in an adult population. Breathe. 2015;11:39-48.
152. Yadollahi R, Vasilev K, Prestidge CA, Simovic S. Polymeric nanosuspensions for enhanced dissolution of water insoluble drugs. Journal of Nanomaterials. 2013:170201, 11 pp.
153. Allison SD, Molina MC, Anchordoquy TJ. Stabilization of lipid/DNA complexes during the freezing step of the lyophilization process: The particle isolation hypothesis. Biochim Biophys Acta. 2000;1468:127-38.
154. Abdelwahed W, Degobert G, Fessi H. Investigation of nanocapsules stabilization by amorphous excipients during freeze-drying and storage. European Journal of Pharmaceutics and Biopharmaceutics. 2006;63:87-94.
155. de Waard H, Grasmeijer N, Hinrichs WLJ, Eissens AC, Pfaffenbach PPF, Frijlink HW. Preparation of drug nanocrystals by controlled crystallization: Application of a 3-way nozzle to prevent premature crystallization for large scale production. European Journal of Pharmaceutical Sciences. 2009;38:224-9.
156. Yu H, Teo J, Chew JW, Hadinoto K. Dry powder inhaler formulation of high-payload antibiotic nanoparticle complex intended for bronchiectasis therapy: Spray drying versus spray freeze drying preparation. International Journal of Pharmaceutics. 2016;499:38-46.
157. Liang W, Kwok PCL, Chow MYT, Tang P, Mason AJ, Chan H-K, et al. Formulation of ph responsive peptides as inhalable dry powders for pulmonary delivery of nucleic acids. European Journal of Pharmaceutics and Biopharmaceutics. 2014;86:64-73.
158. Otake H, Okuda T, Hira D, Kojima H, Shimada Y, Okamoto H. Inhalable spray-freeze-dried powder with l-leucine that delivers particles independent of inspiratory flow pattern and inhalation device. Pharm Res. 2016;33:922-31.
159. Lechuga-Ballesteros D, Charan C, Stults CLM, Stevenson CL, Miller DP, Vehring R, et al. Trileucine improves aerosol performance and stability of spray-dried powders for inhalation. Journal of Pharmaceutical Sciences. 2008;97:287-302.
160. Begat P, Price R, Harris H, Morton DAV, Staniforth JN. The influence of force control agents on the cohesive-adhesive balance in dry powder inhaler formulations. KONA Powder and Particle Journal. 2005;23:109-21.
161. Chew NYK, Shekunov BY, Tong HHY, Chow AHL, Savage C, Wu J, et al. Effect of amino acids on the dispersion of disodium cromoglycate powders. Journal of Pharmaceutical Sciences. 2005;94:2289-300.
162. Begat P, Morton DAV, Shur J, Kippax P, Staniforth JN, Price R. The role of force control agents in high-dose dry powder inhaler formulations. Journal of Pharmaceutical Sciences. 2009;98:2770-83.
163. Muhsin MD, George G, Beagley K, Ferro V, Wang H, Islam N. Effects of chemical conjugation of l-leucine to chitosan on dispersibility and controlled release of drug from a nanoparticulate dry powder inhaler formulation. Molecular Pharmaceutics. 2016;13:1455-66.
164. Qu L, Zhou Q, Denman JA, Stewart PJ, Hapgood KP, Morton DAV. Influence of coating material on the flowability and dissolution of dry-coated fine ibuprofen powders. European Journal of Pharmaceutical Sciences. 2015;78:264-72.
165. Feng AL, Boraey MA, Gwin MA, Finlay PR, Kuehl PJ, Vehring R. Mechanistic models facilitate efficient development of leucine containing microparticles for pulmonary drug delivery. International Journal of Pharmaceutics. 2011;409:156-63.
166. Lucas P, Anderson K, Potter UJ, Staniforth JN. Enhancement of small particle size dry powder aerosol formulations using an ultra low density additive. Pharmaceutical Research. 1999;16:1643-7.

167. Lähde A, Raula J, Kauppinen EI. Simultaneous synthesis and coating of salbutamol sulphate nanoparticles with l-leucine in the gas phase. International Journal of Pharmaceutics. 2008;358:256-62.
168. Wang L, Zhang Y, Tang X. Characterization of a new inhalable thymopentin formulation. International Journal of Pharmaceutics. 2009;375:1-7.
169. Ibrahim BM, Jun SW, Lee MY, Kang SH, Yeo Y. Development of inhalable dry powder formulation of basic fibroblast growth factor. International Journal of Pharmaceutics. 2010;385:66-72.
170. Islam N, Tuli RA, George GA, Dargaville TR. Colloidal drug probe: Method development and validation for adhesion force measurement using atomic force microscopy. Advanced Powder Technology. 2014;25:1240-8.
171. Boraey MA, Hoe S, Sharif H, Miller DP, Lechuga-Ballesteros D, Vehring R. Improvement of the dispersibility of spray-dried budesonide powders using leucine in an ethanol-water cosolvent system. Powder Technology. 2013;236:171-8.
172. Bolten D, Lietzow R, Tuerk M. Solubility of ibuprofen, phytosterol, salicylic acid, and naproxen in aqueous solutions. Chemical Engineering & Technology. 2013;36:426-34.
173. Bakhbakhi Y, Alfadul S, Ajbar A. Precipitation of ibuprofen sodium using compressed carbon dioxide as antisolvent. European Journal of Pharmaceutical Sciences. 2013;48:30-9.
174. Yang J, inventor; Hubei South Ocean Medicine Products Co., Ltd., Peop. Rep. China . assignee. Ibuprofen medical formulation and its preparation method patent CN1919188A. 2007.
175. Adams SS, Bresloff P, Mason CG. Pharmacological differences between the optical isomers of ibuprofen: Evidence for metabolic inversion of the (-)-isomer. Journal of Pharmacy and Pharmacology 1976;28:256-7.
176. Rainsford KD. Ibuprofen: A critical bibliographic review: CRC Press; 2003.
177. Gee CM, Watkinson AC, Nicolazzo JA, Finnin BC. The effect of formulation excipients on the penetration and lateral diffusion of ibuprofen on and within the stratum corneum following topical application to humans. Journal of Pharmaceutical Sciences. 2014:Ahead of Print.
178. Mehlisch DR, Sykes J. Ibuprofen blood plasma levels and onset of analgesia. International Journal of Clinical Practice. 2013;67:3-8.
179. Albert KS, Gernaat CM. Pharmacokinetics of ibuprofen. The American Journal of Medicine. 1984;77:40-6.
180. Jones K, Seymour RA, Hawkesford JE. Are the pharmacokinetics of ibuprofen important determinants for the drug's efficacy in postoperative pain after third molar surgery? British Journal of Oral and Maxillofacial Surgery. 1997;35:173-6.
181. Wood DM, Monaghan J, Streete P, Jones AL, Dargan PI. Fatality after deliberate ingestion of sustained-release ibuprofen: A case report. Critical Care. 2006;10:R44.
182. Collier PS, D'Arcy PF, Harron DW, Morrow N. Pharmacokinetic modelling of ibuprofen. British Journal of Clinical Pharmacology. 1978;5:528-30.
183. Cohen B, Shefy-Peleg A, Zilberman M. Novel gelatin/alginate soft tissue adhesives loaded with drugs for pain management: Structure and properties. Journal Of Biomaterials Science-Polymer Edition. 2014;25:224-40.
184. Obidchenko YA, Khuchua NS, Abramovich RA, Savochkina AY, Karamyan AS, Barsegyan SS, et al. Preparation of micronized ibuprofen substance and assessment of its bioavailability. Pharmaceutical Chemistry Journal. 2013;47:382-6.
185. Jachowicz R, Nürnberg E, Pieszczek B, Kluczykowska B, Maciejewska A. Solid dispersion of ketoprofen in pellets. International Journal of Pharmaceutics. 2000;206:13-21.

186. Bolten D, Lietzow R, Türk M. Solubility of ibuprofen, phytosterol, salicylic acid, and naproxen in aqueous solutions. Chemical Engineering & Technology. 2013;36:426-34.
187. Fini A, Fazio G, Feroci G. Solubility and solubilization properties of non-steroidal anti-inflammatory drugs. International Journal of Pharmaceutics. 1995;126:95-102.
188. Rytting E, Lentz K, Chen X-Q, Qian F, Venkatesh S. Aqueous and cosolvent solubility data for drug-like organic compounds. The AAPS Journal. 2005;7:E78-E105.
189. Watkinson RM, Herkenne C, Guy RH, Hadgraft J, Oliveira G, Lane ME. Influence of ethanol on the solubility, ionization and permeation characteristics of ibuprofen in silicone and human skin. Skin Pharmacology and Physiology. 2009;22:15-21.
190. Yalkowsky SH, Valvani SC, Roseman TJ. Solubility and partitioning vi: Octanol solubility and octanol–water partition coefficients. Journal of Pharmaceutical Sciences. 1983;72:866-70.
191. Manrique J, Martinez F. Solubility of ibuprofen in some ethanol + water cosolvent mixtures at several temperatures. Latin American Journal of Pharmacy. 2007;26:344-54.
192. Jouyban A, Soltanpour S, Acree WE, Jr. Solubility of acetaminophen and ibuprofen in the mixtures of polyethylene glycol 200 or 400 with ethanol and water and the density of solute-free mixed solvents at 298.2 k. Journal of Chemical & Engineering Data. 2010;55:5252-7.
193. Garzon LC, Martinez F. Temperature dependence of solubility for ibuprofen in some organic and aqueous solvents. Journal of Solution Chemistry. 2004;33:1379-95.
194. Nokhodchi A, Homayouni A, Araya R, Kaialy W, Obeidat W, Asare-Addo K. Crystal engineering of ibuprofen using starch derivatives in crystallization medium to produce promising ibuprofen with improved pharmaceutical performance. RSC Advances. 2015;5:46119-31.
195. Wahbi AA, Hassan E, Hamdy D, Khamis E, Barary M. Spectrophotometric methods for the determination of ibuprofen in tablets. Pakistan Journal of Pharmaceutical Sciences. 2005;18:1-6.
196. Silva KGH, Xavier FH, Jr., Farias IEG, Silva AKA, Caldas NJA, Souza LCA, et al. Stationary cuvette: A new approach to obtaining analytical curves by uv-vis spectrophotometry. Phytochemical Analysis. 2009;20:265-71.
197. Bajwa GS, Sammon C, Timmins P, Melia CD. Molecular and mechanical properties of hydroxypropyl methylcellulose solutions during the sol:Gel transition. Polymer. 2009;50:4571-6.
198. Vannucci M, Sha N, Brown PJ. Nir and mass spectra classification: Bayesian methods for wavelet-based feature selection. Chemometrics and Intelligent Laboratory Systems. 2005;77:139-48.
199. Campbell FC. Theorem of le châtelier and the clausius-clapeyron equation. Phase diagrams - understanding the basics. USA: ASM International; 2012.
200. Thorat AA, Dalvi SV. Liquid antisolvent precipitation and stabilization of nanoparticles of poorly water soluble drugs in aqueous suspensions: Recent developments and future perspective. Chemical Engineering Journal. 2012;181–182:1-34.
201. Dalvi SV, Dave RN. Analysis of nucleation kinetics of poorly water-soluble drugs in presence of ultrasound and hydroxypropyl methyl cellulose during antisolvent precipitation. International Journal of Pharmaceutics. 2010;387:172-9.
202. Bs iso 13320-1:1999: Particle size analysis. Laser diffraction methods. General principles. British Standards Institute; 2000.
203. Malvern. Increased dynamic range and resolution with the mastersizer 3000 particle size analyzer In: Malvern, editor. Extending the capabilities of laser diffraction particle size and size distribution measurements: Malvern Instruments Limited; 2016.

204. Malvern. Sample dispersion and refractive index guide [User Manual]. England: Malvern Instruments Limited 2007 [April 2007:[1-44]. Available from: http://www.malvern.com/en/support/resource-center/user-manuals/MAN0396EN.aspx.
205. Saritha D, Bose PSC, Nagaraju R. Formulation and evaluation of self emulsifying drug delivery system (sedds) of ibuprofen. International Journal of Pharmaceutical Sciences and Research. 2014;5:3511+.
206. Pharmacopoeia B. Bulk density and tapped density of powders. British pharmacopoeia. Appendix XVII S.2016.
207. Nokhodchi A, Amire O, Jelvehgari M. Physico-mechanical and dissolution behaviours of ibuprofen crystals crystallized in the presence of various additives. Daru: journal of Faculty of Pharmacy, Tehran University of Medical Sciences. 2010;18:74.
208. Adeleke I, Okafor I, Alebiowu G. Studies on the micromeritic properties of ibuprofen microcapsules. The Pacific Journal of Science and Technology. 2012;13:469-72.
209. Lakshmi MGP, Prabha MS, Manikiran SS, Rao NR. Formulation and evaluation of pulsatile salubutamol sulphate tablet in capsule pulsatile release device for asthma. European Journal of Biomedical and Pharmaceutical Sciences 2014;1:125-48.
210. Sichina WJ. Dsc as problem solving tool: Measurement of percent crystallinity of thermoplastics. wwwperkinelmercom.
211. Hallworth G, Westmoreland D. The twin impinger: A simple device for assessing the delivery of drugs from metered dose pressurized aerosol inhalers. Journal of pharmacy and pharmacology. 1987;39:966-72.
212. Machatha SG, Bustamante P, Yalkowsky SH. Deviation from linearity of drug solubility in ethanol/water mixtures. International Journal of Pharmaceutics. 2004;283:83-8.
213. Ojha N, Prabhakar B. Advances in solubility enhancement techniques. International Journal of Pharmaceutical Sciences Review and Research. 2013;21:351-8.
214. Wang S, Zhang P, Song Z, Du Y, Qu Y. Solution thermodynamics of s-ibuprofen n-octyl-d-glucamine salt in ethanol-water cosolvent mixtures. Fluid Phase Equilibria. 2014;372:69-75.
215. Kawabata Y, Wada K, Nakatani M, Yamada S, Onoue S. Formulation design for poorly water-soluble drugs based on biopharmaceutics classification system: Basic approaches and practical applications. International Journal of Pharmaceutics. 2011;420:1-10.
216. Fang Z, Zhang L, Mao S, Rohani S, Ulrich J, Lu J. Solubility measurement and pre diction of clopidogrel hydrogen sulfate polymorphs in isopropanol and ethyl acetate. The Journal of Chemical Thermodynamics. 2015;90:71-8.
217. Mirmehrabi M, Rohani S, Perry L. Thermodynamic modeling of activity coefficient and prediction of solubility: Part 2. Semipredictive or semiempirical models. Journal of Pharmaceutical Sciences. 2006;95:798-809.
218. Sheikholeslamzadeh E, Chen C-C, Rohani S. Optimal solvent screening for the crystallization of pharmaceutical compounds from multisolvent systems. Industrial & Engineering Chemistry Research. 2012;51:13792-802.
219. Sheikholeslamzadeh E, Rohani S. Solubility prediction of pharmaceutical and chemical compounds in pure and mixed solvents using predictive models. Industrial & Engineering Chemistry Research. 2012;51:464-73.
220. Sheikhzadeh M, Rohani S, Taffish M, Murad S. Solubility analysis of buspirone hydrochloride polymorphs: Measurements and prediction. International Journal of Pharmaceutics. 2007;338:55-63.
221. Rashid A, White T, Howes T, Litster J, Marziano I. Racemic ibuprofen solubility in ethanol and aqueous ethanolic mixtures. Chemeca 2008: Towards a Sustainable Australasia. 2008:1393.

222. Afrose A, White T, Howes T, George G, Rashid A, Islam N, editors. A controlled crystallization technique for producing ibuprofen fine crystals for developing an efficient dry powder inhaler (DPI) formulation. IHBI Inspires 2014 19-20 November 2014; Gold Coast, Qld.
223. Jbilou M, Ettabia A, Guyot-Hermann AM, Guyot JC. Ibuprofen agglomerates preparation by phase separation. Drug Development and Industrial Pharmacy. 1999;25:297-305.
224. Jones M-C, Leroux J-C. Polymeric micelles – a new generation of colloidal drug carriers. European Journal of Pharmaceutics and Biopharmaceutics. 1999;48:101-11.
225. Filippa MA, Gasull EI. Ibuprofen solubility in pure organic solvents and aqueous mixtures of cosolvents: Interactions and thermodynamic parameters relating to the solvation process. Fluid Phase Equilibria. 2013;354:185-90.
226. Nozaki Y, Tanford C. Solubility of amino acids and two glycine peptides in aqueous ethanol and dioxane solutions. Establishment of a hydrophobicity scale. The Journal of biological chemistry. 1971;246:2211-17.
227. Okonogi S, Yonemochi E, Oguchi T, Puttipipatkhachorn S, Yamamoto K. Enhanced dissolution of ursodeoxycholic acid from the solid dispersion. Drug Development and Industrial Pharmacy. 1997;23:1115-21.
228. Desai KH, Kulkarni AR, Agnihotri SA, Gudasi KB, Aminabhavi TM. Solubility enhancement of rofecoxib in water in the presence of hydrophilic polymers, surfactants, co-solvents, and small molecules at 310.15 k. Indian Journal of Chemistry. 2006;45A:1667-9.
229. Plackett RL, Burman JP. The design of optimum multifactorial experiments. Biometrika. 1946;33:305-25.
230. Gandhi P, Patil S, Aher S, Paradkar A. Ultrasound-assisted preparation of novel ibuprofen-loaded excipient with improved compression and dissolution properties. Drug Development and Industrial Pharmacy. 2016:1-11.
231. Luque de Castro MD, Priego-Capote F. Ultrasound-assisted crystallization (sonocrystallization). Ultrasonics Sonochemistry. 2007;14:717-24.
232. Li H, Wang J, Bao Y, Guo Z, Zhang M. Rapid sonocrystallization in the salting-out process. Journal of Crystal Growth. 2003;247:192-8.
233. Ruecroft G, Hipkiss D, Ly T, Maxted N, Cains PW. Sonocrystallization: The use of ultrasound for improved industrial crystallization. Organic Process Research & Development. 2005;9:923-32.
234. Knox M, Trifkovic M, Rohani S. Combining anti-solvent and cooling crystallization: Effect of solvent composition on yield and meta stable zone width. Chemical Engineering Science. 2009;64:3555-63.
235. Raghavan SL, Trividic A, Davis AF, Hadgraft J. Crystallization of hydrocortisone acetate: Influence of polymers. International Journal of Pharmaceutics. 2001;212:213-21.
236. Zimmermann A, Millqvist-Fureby A, Elema MR, Hansen T, Müllertz A, Hovgaard L. Adsorption of pharmaceutical excipients onto microcrystals of siramesine hydrochloride: Effects on physicochemical properties. European Journal of Pharmaceutics and Biopharmaceutics. 2009;71:109-16.
237. Hassan M, Lau R. Effect of particle shape on dry particle inhalation: Study of flowability, aerosolization, and deposition properties. AAPS PharmSciTech. 2009;10:1252-62.
238. Chow AHL, Tong HHY, Chattopadhyay P, Shekunov BY. Particle engineering for pulmonary drug delivery. Pharmaceutical Research. 2007;24:411-37.
239. Gradon L, Sosnowski TR. Formation of particles for dry powder inhalers. Advanced Powder Technology. 2014;25:43-55.
240. Yang Z-Y, Le Y, Hu T-T, Shen Z, Chen J-F, Yun J. Production of ultrafine sumatriptan succinate particles for pulmonary delivery. Pharmaceutical Research. 2008;25:2012-8.

241. Bakhbakhi Y, Charpentier PA, Rohani S. Experimental study of the gas process for producing microparticles of beclomethasone-17,21-dipropionate suitable for pulmonary delivery. Journal of Pharmaceutical Sciences. 2006;309:71-80.
242. Garekani HA, Sadeghi F, Badiee A, Mostafa SA, Rajabi-Siahboomi AR. Crystal habit modifications of ibuprofen and their physicomechanical characteristics. Drug Development and Industrial Pharmacy. 2001;27:803-9.
243. Ward GH, Schultz RK. Process-induced crystallinity changes in albuterol sulfate and its effect on powder physical stability. Pharmaceutical Research. 1995;12:773-9.
244. Raula J, Thielmann F, Kansikas J, Hietala S, Annala M, Seppälä J, et al. Investigations on the humidity-induced transformations of salbutamol sulphate particles coated with l-leucine. Pharmaceutical Research. 2008;25:2250-61.
245. Elajnaf A, Carter P, Rowley G. The effect of relative humidity on electrostatic charge decay of drugs and excipient used in dry powder inhaler formulation. Drug Development and Industrial Pharmacy. 2007;33:967-74.
246. Adi H, Traini D, Chan H-K, Young PM. The influence of drug morphology on the aerosolisation efficiency of dry powder inhaler formulations. Journal of Pharmaceutical Sciences. 2008;97:2780-8.
247. Tan BMJ, Chan LW, Heng PWS. Improving dry powder inhaler performance by surface roughening of lactose carrier particles. Pharmaceutical Research. 2016;33:1923-35.
248. Chew NYK, Chan H-K. Use of solid corrugated particles to enhance powder aerosol performance. Pharmaceutical Research. 2001;18:1570-7.
249. Chew NYK, Tang P, Chan H-K, Raper JA. How much particle surface corrugation is sufficient to improve aerosol performance of powders? Pharmaceutical Research. 2005;22:148-52.
250. Pattnaik S, Swain K, Rao JV, Talla V, Prusty KB, Subudhi SK. Polymer co-processing of ibuprofen through compaction for improved oral absorption. RSC Advances. 2015;5:74720-5.
251. Onischuk AA, Tolstikova TG, An'kov SV, Baklanov AM, Valiulin SV, Khvostov MV, et al. Ibuprofen, indomethacin and diclofenac sodium nanoaerosol: Generation, inhalation delivery and biological effects in mice and rats. Journal of Aerosol Science. 2016;100:164-77.

Appendices

Appendix A

Title

Appendix A1: Shows the concentration and absorbance data of IBP in different composition of water and ethanol mixture from three trials at a wavelength of 264 nm (Refer to Figure 3.4and Figure 3.5).

0.1% aqueous ethanol		0.2% aqueous ethanol		0.3% aqueous ethanol		0.4% aqueous ethanol		0.5% aqueous ethanol	
IBP conc, I/I+E+W, ppm	Abs	IBP conc, I/I+E+W, ppm	Abs	IBP conc, I/I+E+W, ppm	Abs	IBP conc, I/I+E+W, ppm	Abs	IBP conc, I/I+E+W, ppm	Abs
49.7	0.1	63.7	0.1	647.7	0.9	313.5	0.4	166.1	0.2
59.9	0.2	97.3	0.1	1258.2	1.7	626.3	0.8	341.7	0.5
95.8	0.2	125.6	0.2	1590.3	2.2	939.2	1.3	636.0	0.9
119.0	0.3	51.3	0.1	976.7	1.4	1236.9	1.7	1013.8	1.4
305.9	0.3	97.3	0.2	1291.0	1.8	1568.5	2.1	1333.7	1.8
48.5	0.1	188.6	0.3	1649.9	2.3	82.7	0.1	1642.6	2.2
59.9	0.2	218.8	0.3	86.8	0.1	169.9	0.2	181.1	0.2
97.1	0.2	245.9	0.4	173.0	0.2	342.6	0.5	341.0	0.5
121.6	0.3	99.4	0.2	340.0	0.5	635.0	0.9	674.4	0.9
307.7	0.3	147.5	0.2	668.3	0.9	940.0	1.3	963.5	1.3
48.8	0.1	194.4	0.3	978.3	1.4	1247.1	1.7	1346.8	1.8
60.8	0.1	221.3	0.3	1315.9	1.8	623.7	0.9	373.7	0.5
96.8	0.2	244.9	0.4	1643.7	2.2	934.8	1.3	736.5	1.0
122.0	0.3	199.0	0.3	1610.1	2.2	1244.8	1.7	1056.8	1.4
52.0	0.1	223.4	0.3	599.4	0.8	86.9	0.1	1413.9	1.9
		244.1	0.4	900.0	1.2	179.8	0.3	166.1	0.2
				148.5	0.2	315.9	0.4	341.7	0.5
						1262.5	1.7	636.0	0.9
						305.2	0.4	1013.8	1.4
						611.2	0.9	1333.7	1.8
						909.2	1.3	1642.6	2.2
						1212.7	1.7	315.7	0.4
						907.8	1.3	616.3	0.8
						1212.6	1.7	920.8	1.2
						77.0	0.1	1236.1	1.6

0.1% aqueous ethanol		0.2% aqueous ethanol		0.3% aqueous ethanol		0.4% aqueous ethanol		0.5% aqueous ethanol	
IBP conc, I/I+E+W, ppm	**Abs**	**IBP conc, I/I+E+W, ppm**	**Abs**	**IBP conc, I/I+E+W, ppm**	**Abs**	**IBP conc, I/I+E+W, ppm**	**Abs**	**IBP conc, I/I+E+W, ppm**	**Abs**
						158.6	0.2	317.7	0.4
						310.8	0.4	636.0	0.8
						608.9	0.8	939.1	1.2
						914.9	1.4	1242.5	1.6
								317.5	0.4
								1218.8	1.7

Appendix A2: Slopes of calibration lines with error estimates (Refer to Figure 3.5).

% E	slope	95% error	as%
10.15	0.00142	0.00027	19
20.13	0.001380	0.000038	2.8
30.10	0.001321	0.000016	1.2
30.10	0.001389	0.000006	0.5
39.94	0.001270	0.000007	0.5
39.94	0.001307	0.000024	1.9
49.85	0.001258	0.000017	1.3
49.85	0.001264	0.000012	1.0

Appendix A3: Shows the concentration and absorbance data of IBP in 35% w/w ethanol solution from two trials at a wavelength of 221 nm (Refer to Figure 3.6).

Trial 1		**Trial 2**	
IBP conc, µg/mL	**Absorbance**	**IBP conc, µg/mL**	**Absorbance**
0.3	0.03	0.4	0.03
0.8	0.05	0.8	0.05
1.6	0.08	1.6	0.08
3.1	0.15	3.1	0.15
4.7	0.20	4.7	0.21
6.2	0.26	6.2	0.25
7.8	0.32	7.8	0.32
12.4	0.51	12.5	0.51
15.5	0.64	15.6	0.64
18.6	0.77	18.7	0.77
21.7	0.90	21.8	0.90

Appendix A4: Shows time and concentration data of IBP in water, 10% and 20% aqueous ethanol for equilibrium investigation at 25 °C. (Refer to Figure 3.8)

0% aqueous ethanol		**10% aqueous ethanol**		**20% aqueous ethanol**	
Time, h	**IBP conc, I/I+E+W, ppm**	**Time, h**	**IBP conc, I/I+E+W, ppm**	**Time, h**	**IBP conc, I/I+E+W, ppm**
0	47.52	0	0	0	0
2	47.17	2	103.4	2	263
4	46.34	4	103.1	4	384
6	45.93	6	104.1	6	378
8	45.79	8	105.5	8	364
10	45.79	10	103.6	10	367
12	45.79	20	103.6	12	370
25	47.17	22	102.2	24	379
26	48.28	24	103.1	25	362
27	46.97	25	100.5	26	369
		26	98.8	27	349
		27	98.7	46	377

Appendix A5: Shows time and concentration data of IBP in water, 10% and 20% aqueous ethanol for equilibrium investigation at 25°C. (Refer to Figure 3.9)

5% ethanol, .0005% excipients		**10% ethanol, 0.1% excipients**		**10% ethanol, 0.25% excipients**	
Time, mins	**IBP conc, I/I+E+W+Ex, ppm**	**Time, mins**	**IBP conc, I/I+E+W+Ex, ppm**	**Time, mins**	**IBP conc, I/I+E+W+Ex, ppm**
0	0	0.08	372.72	0.08	3471.06
1	76.62	0.17	413.25	0.25	2967.53
2	101.8	0.25	435.45	0.5	3567.19
3	72.93	0.33	454.55	0.75	3438.75
4	73.7	0.42	387.04	1	3252.73
5	75.23	0.50	388.25	1.25	2861
10	73.07	0.58	407.14	3	1077.17
15	71.05	0.67	407.28	5	1323.93
20	74.04	0.75	414.66	10	1255.36
25	73.49	0.83	422.77	15	858.44
30	70.91	0.92	490.34	30	847.03
40	70.63	1.00	640.23	60	822.95
50	70.84	60.00	483.38		
60	71.54				

Appendix A6: NIR spectrophotometer wavelength scan with eleven different concentrations of aqueous ethanol. The legend indicates the fraction of water in the sample.

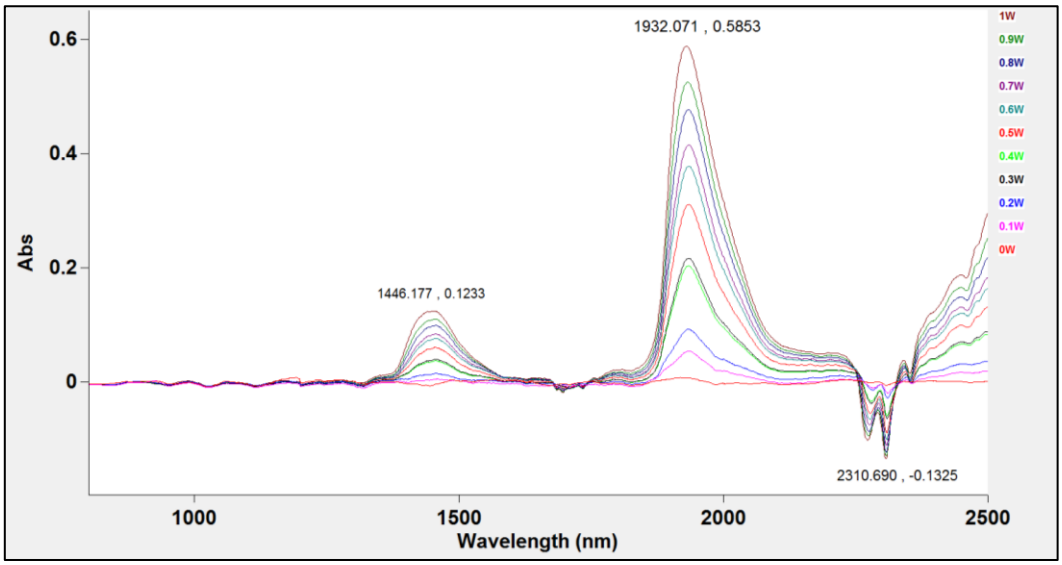

Appendix A7: Shows the concentration and absorbance data of water in ethanol solution from at least two trials at a wavelength of 1932 nm (Refer to Figure 3.10).

Water conc. W/(E+W), g/g	**Absorbance**	**Water conc. W/(E+W), g/g**	**Absorbance**
0.00	0.00	0.39	0.20
0.06	0.03	0.42	0.21
0.11	0.06	0.55	0.30
0.16	0.08	0.65	0.37
0.20	0.11	0.73	0.41
0.28	0.15	0.81	0.47
0.10	0.05	0.91	0.52
0.20	0.09	1.00	0.58

Appendix A8: Determining the melting enthalpy from DSC curves of raw IBP in triplicate.

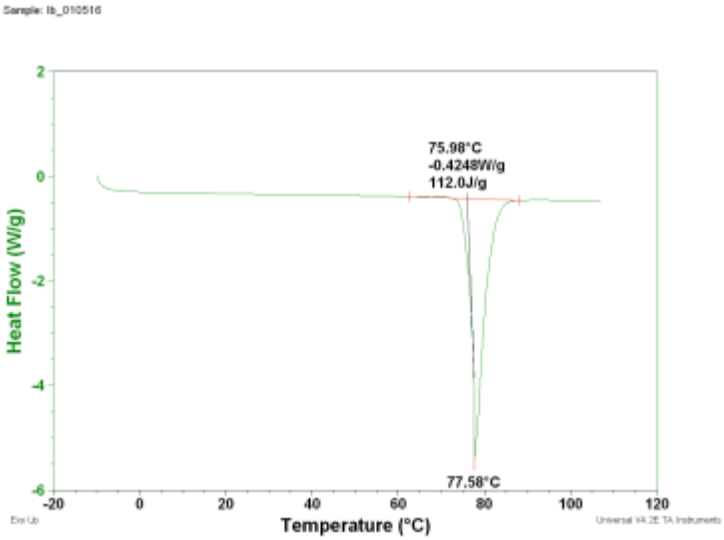

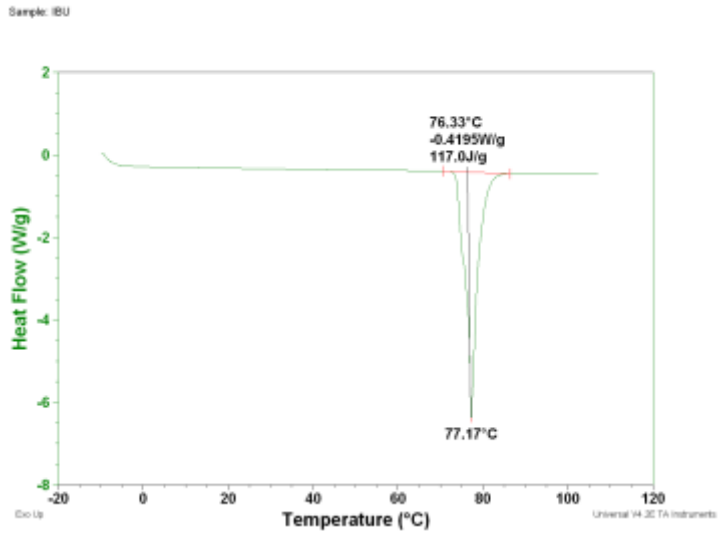

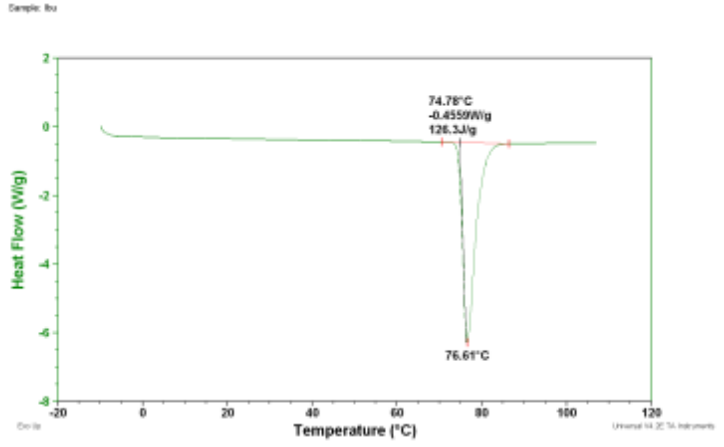

Appendix B

Appendix B1: Shows IBP solubility raw data in 0- 50% aqueous ethanol solvents at 10, 25 and 40°C. Here XE represents the percentage of ethanol in water in weight basis of the solvents and the solubility values are given with 95% uncertainties in ppm. (Refer to Figure 4.1).

XE (% wt. basis)	Sample No.	10°C		25°C		40°C	
		Absorbance	Solubility, I/I+E+W, ppm	Absorbance	Solubility, I/I+E+W, ppm	Absorbance	Solubility, I/I+E+W, ppm
0	1	0.06	40.9	0.07	46.3	0.13	84.7
	2	0.06	40.6	0.07	45.9	0.13	86.7
	3	0.06	40.7	0.07	45.8	0.14	91.6
	4	0.06	40.8	0.07	45.8	0.13	90.6
	5			0.06	42.3		
	6			0.07	47.2		
	7			0.07	48.3		
	8			0.07	47.0		
	9			0.07	46.3		
5.16	1			0.10	67.6		
	2			0.10	69.0		
	3			0.11	72.7		
	4			0.11	72.5		
	5			0.10	71.6		
	6			0.10	71.4		
	7			0.11	72.3		
10	1	0.09	65.3	0.15	103.3	0.32	223.7
	2	0.09	64.9	0.15	103.1	0.31	215.7
	3	0.09	66.3	0.15	104.1	0.31	216.1
	4	0.09	62.9	0.15	105.5	0.30	211.2
	5	0.09	63.0	0.15	103.6		
	6	0.09	65.7	0.15	103.6		
	7			0.15	102.2		
	8			0.15	103.1		
	9			0.14	100.5		
	10			0.14	98.8		
	11			0.14	98.7		
15	1			0.22	155.3		
	2			0.23	161.4		
	3			0.23	164.0		
	4			0.24	169.3		
	5			0.22	156.4		
	6			0.22	156.2		
	7			0.22	155.9		
	8			0.23	159.9		
	9						

XE (% wt. basis)	Sample No.	10°C		25°C		40°C	
		Absorbance	Solubility, I/I+E+W, ppm	Absorbance	Solubility, I/I+E+W, ppm	Absorbance	Solubility, I/I+E+W, ppm
19.94	1			0.40	285.6		
	2			0.40	287.2		
	3			0.39	283.5		
	4			0.40	286.4		
	5			0.39	284.2		
	6			0.39	283.0		
	7			0.40	287.8		
	8			0.39	280.0		
20	1	0.17	125.8	0.53	375.9	1.41	1013.8
	2	0.17	125.7	0.52	375.9	1.44	1034.7
	3	0.17	125.8	0.50	361.9	1.44	1037.3
	4	0.16	118.4	0.51	364.7	1.43	1031.4
	5			0.51	368.2		
	6			0.52	376.9		
	7			0.50	360.2		
	8			0.51	366.9		
	9			0.48	347.3		
	10			0.52	375.3		
30	1	0.53	392.8	1.51	1804.0	2.82	17845.2
	2	0.53	394.5	1.47	1747.5	2.92	20400.7
	3	0.54	404.7	1.46	1848.9	2.72	19263.0
	4	0.56	416.5	1.59	1897.8	2.43	18775.1
	5			1.58	1883.9		
	6			1.58	1880.1		
	7			1.50	1899.3		
40	1	2.76	2126.9	1.73	13022.4	0.99	59938.2
	2	2.62	2017.5	1.71	12913.9	0.77	55603.5
	3	2.73	2100.4	1.74	12208.5	0.86	60725.5
	4	2.86	2200.8	1.72	12447.5	0.87	54349.5
	5	3.00	2305.7	1.70	11912.3		
	6	2.85	2195.0	1.67	12326.8		
	7	2.87	2206.6				
50	1	0.51	20125.5	0.99	65248.4	2.1	241494.5
	2	0.63	20530.2	1.05	69578.9	2.1	302580.8
	3	0.66	20251.5	1.07	69307.9	2.1	283079.7
	4	0.64	20931.4	1.01	65687.5	1.5	275315.5
	5			1.10	69424.4		

Appendix B2: IBP solubility in 0%, 10% and 20% aqueous ethanol solvents at 25°C. The errors shown for the solubility values are the 95% probable for the mean (Refer to Figure 4.5,Figure 4.6,Figure 4.7,Figure 4.8, Figure 4.9 & Figure 4.10).

Solvent composition					**IBP solubility, ppm**
Leucine, L/(E+W), w/w,%	**Mannitol, M/(E+W), w/w,%**	**HPMC, HP/(E+W),w/w,%**	**Pl F127, Pl/(E+W),w/w,%**	**Ethanol, E/(E+W), w/w,%**	
Intrinsic solubility (water)					45.55 ± 0.05
0.51	5.32	0.42	1.43	11.15	1496.17 ± 0.05
1.02	5.20	0.43	1.41	11.12	1599.04 ± 0.08
1.52	5.22	0.42	1.55	10.75	1725.76 ± 0.04
0.11	0.00	0.00	0.00	11.21	164.34 ± 0.07
0.52	0.00	0.00	0.00	11.21	185.32 ± 0.05
1.02	0.00	0.00	0.00	11.21	221.62 ± 0.10
1.54	0.00	0.00	0.00	11.21	243.19 ± 0.12
0.13	0.00	0.00	0.00	0.00	74.52 ± 0.11
0.67	0.00	0.00	0.00	0.00	112.99 ± 0.04
1.03	0.00	0.00	0.00	0.00	129.56 ± 0.02
1.60	0.00	0.00	0.00	0.00	155.19 ± 0.06
0.98	0.98	0.39	1.37	0.00	1007.21 ± 0.05
0.98	5.04	0.39	1.37	0.00	1173.15 ± 0.03
1.00	11.04	0.40	1.40	0.00	1124.01 ± 0.02
0.00	1.08	0.00	0.00	10.02	59.65 ± 0.08
0.00	5.51	0.00	0.00	10.02	127.95 ± 0.08
0.00	10.14	0.00	0.00	10.02	166.54 ± 0.06
0.00	13.95	0.00	0.00	10.02	88.47 ± 0.03
0.00	1.30	0.00	0.00	0.00	55.32 ± 0.11
0.00	5.44	0.00	0.00	0.00	65.81 ± 0.04
0.00	12.66	0.00	0.00	0.00	60.69 ± 0.06
0.00	17.82	0.00	0.00	0.00	58.40 ± 0.06
0.49	0.51	0.00	0.00	0	330.46 ± 0.01
0.46	0.45	0.00	0.00	9.40	562.42 ± 0.06
0.39	0.42	0.00	0.00	20.23	1195.52 ± 0.04
0.22	0.26	0.00	0.00	0	161.32 ± 0.01
0.22	0.23	0.00	0.00	9.95	321.42 ± 0.03
0.21	0.21	0.00	0.00	17.84	658.23 ± 0.07
0.96	0.99	0.00	0.00	0	663.80 ± 0.04
0.85	0.92	0.00	0.00	10.11	1260.58 ± 0.04

Solvent composition					IBP solubility, ppm
Leucine, L/(E+W), w/w,%	**Mannitol, M/(E+W), w/w,%**	**HPMC, HP/(E+W),w/w,%**	**Pl F127, Pl/(E+W),w/w,%**	**Ethanol, E/(E+W), w/w,%**	
0.77	0.80	0.00	0.00	19.85	1859.76 ± 0.01
0	1.03	0.00	0.00	0	680.58 ± 0.05
0	0.93	0.00	0.00	10.06	857.49 ± 0.06
0	0.82	0.00	0.00	20.07	1662.20 ± 0.01
0	2.02	0.00	0.00	0	1152.19 ± 0.01
0	1.85	0.00	0.00	10.06	1534.14 ± 0.07
0	1.68	0.00	0.00	19.6	2847.70 ± 0.06
0.99	0	0.00	0.00	0	55.09 ± 0.06
0.88	0	0.00	0.00	9.17	112.37 ± 0.02
0.81	0	0.00	0.00	19.66	355.96 ± 0.05
1.99	0	0.00	0.00	0	92.66 ± 0.07
1.78	0	0.00	0.00	10.52	119.48 ± 0.01
1.60	0	0.00	0.00	19.82	362.58 ± 0.03

Appendix C

Appendix C1: Data representing the effect of temperature of the precipitation process on particle size, Mean ± SD, n= 3 (Refer to Figure 5.2).

Particle size	**Temperature (°C)**			
(µm)	**15°C**	**20°C**	**25°C**	**30°C**
D[v,0.1]	4.93 ± 0.01	3.65 ± 0.03	3.72 ± 0.01	4.92 ± 0.07
D[v,0.5]	12.6 ± 0.05	7.61 ± 0.02	7.14 ± 0.01	9.77 ± 0.04
D[v,0.9]	37.3 ± 0.97	14.9 ± 0.32	13.4 ± 0.10	17.4 ± 0.17

Appendix C2: Data representing the effect of ultrasound duration on particle size in the APC process, Mean ± SD, n= 3 (Refer to Figure 5.3).

Particle size	**Ultrasound duration (Minutes)**				
(µm)	**0**	**5**	**15**	**30**	**60**
D[v,0.1]	2.92 ± 0.01	2.86 ± 0.01	4.44 ± 0.06	3.93 ± 0.02	2.62 ± 0.07
D[v,0.5]	6.11 ± 0.02	6.27 ± 0.01	8.8 ± 0.01	8.4 ± 0.04	6.4 ± 0.12
D[v,0.9]	11.3 ± 0.08	13.8 ± 0.07	15.9 ± 0.08	16.1 ± 0.05	14 ± 0.39

Appendix C3: Data representing IBP Particle size vs time for a single batch in the APC process, Mean ± SD, n= 3 (Refer to Figure 5.4).

Time, Minutes	**Particle size, µm, (D[v,0.5])(± SD)**
1	5.47 ± 0.38
2	99.1 ± 11.30
3	5.39 ± 0.59
4	6.55 ± 0.03
5	6.78 ± 0.03
10	5.6 ± 0.46
15	5.95 ± 0.26
20	6.04 ± 0.33

Appendix C4: Data representing the effect of IBP concentration on the particle size obtained in the APC process, Mean ± SD, n= 3 (Refer to Figure 5.5).

Particle size	**IBP concentration, %, (w/w)**				
(µm)	1.0	0.9	0.8	0.7	0.5
D[v,0.1]	3.82 ± 0.04	2.39 ± 0.04	2.47± 0.01	2.79 ± 0.03	3.76 ± 0.06
D[v,0.5]	7.13± 0.03	4.92 ± 0.03	4.88 ± 0.01	5.39 ± 0.01	7.05 ± 0.02
D[v,0.9]	12.7 ± 0.36	9.43 ± 0.25	8.86 ± 0.07	9.56 ± 0.10	12 ± 0.13

Appendix C5: Data representing the effect of IBP concentration on the particle size obtained in the APC process, Mean ± SD, n= 3 (Refer to Figure 5.6).

Particle size	**Solvent-antisolvent ratio**				
(µm)	**0.10**	**0.09**	**0.08**	**0.06**	**0.05**
D[v,0.1]	3.82 ± 0.04	2.39 ± 0.04	2.47± 0.01	2.79 ± 0.03	3.76 ± 0.06
D[v,0.5]	7.13± 0.03	4.92 ± 0.03	4.88 ± 0.01	5.39 ± 0.01	7.05 ± 0.02
D[v,0.9]	12.7 ± 0.36	9.43 ± 0.25	8.86 ± 0.07	9.56 ± 0.10	12 ± 0.13

Appendix C6: Data representing the effect of HPMC concentration on IBP particle size produced in the APC process, Mean ± SD, n= 3 (Refer to Figure 5.7).

HPMC, % (w/w)	**Particle size, D[v,0.5], (µm)**
0.9	16 ± 5.3
0.1	19 ± 6.9
0.1	6 ± 1.8
0.1	8 ± 0.8
0.2	11 ± 0.3
0.6	10 ± 0.9
0.3	9 ± 0.3
0.5	7 ± 0.4
0.0	10 ± 2.6
0.0	8 ± 0.8

Appendix C7: Data representing the effect of Pl F127 concentration on the size of IBP particles produced in an APC process, Mean ± SD, n= 3 (Refer to Figure 5.8).

Particle size	**Pluronic F127 concentration, %, (w/w)**			
(µm)	**0.0**	**0.7**	**1.3**	**2.0**
D[v,0.1]	6.06 ± 0.05	3.59 ± 0.03	1.22 ± 0.03	1.29 ± 0.01
D[v,0.5]	10.5 ± 0.04	6.77 ± 0.01	3.49 ± 0.01	6.14 ± 0.02
D[v,0.9]	17.3 ± 0.16	12 ± 0.08	8.19 ± 0.28	12.7 ± 0.41

Appendix C8: Data representing the effect of leucine concentration on the size of IBP produced in an APC process, Mean ± SD, n= 3 (Refer to Figure 5.9).

Particle size	**L-leucine concentration, %, (w/w)**			
(µm)	**0.0**	**0.5**	**1.2**	**1.6**
D[v,0.1]	3.82 ± 0.01	3.66 ± 0.01	2.9 ± 0.01	2.86 ± 0.02
D[v,0.5]	7.62 ± 0.01	8.16 ± 0.02	5.94 ± 0.05	6.3 ± 0.04
D[v,0.9]	14.2 ± 0.07	17.5 ± 0.17	11.4 ± 0.13	12.8 ± 0.06